UNCLASSIFIED

DEPARTMENT OF DEFENSE
UNITED STATES OF AMERICA

AD NUMBER

AD-513 618

CLASSIFICATION CHANGES

TO **UNCLASSIFIED**

FROM **CONFIDENTIAL**

AUTHORITY

OCA; Jul 31, 1982

THIS PAGE IS UNCLASSIFIED

UNCLASSIFIED

DEPARTMENT OF DEFENSE
UNITED STATES OF AMERICA

AD NUMBER

AD-513 618

NEW LIMITATION CHANGE

TO **DISTRIBUTION STATEMENT - A**

Approved for public release;
distribution is unlimited.

LIMITATION CODE: 1

FROM **DISTRIBUTION STATEMENT - B**

LIMITATION CODE: 3

AUTHORITY

AFRPL; Feb 5, 1986

THIS PAGE IS UNCLASSIFIED

[redacted]

SECURITY MARKING

The classified or limited status of this report applies to each page, unless otherwise marked. Separate page printouts MUST be marked accordingly.

THIS DOCUMENT CONTAINS INFORMATION AFFECTING THE NATIONAL DEFENSE OF THE UNITED STATES WITHIN THE MEANING OF THE ESPIONAGE LAWS, TITLE 18, U.S.C., SECTIONS 793 AND 794. THE TRANSMISSION OR THE REVELATION OF ITS CONTENTS IN ANY MANNER TO AN UNAUTHORIZED PERSON IS PROHIBITED BY LAW.

NOTICE: When government or other drawings, specifications or other data are used for any purpose other than in connection with a definitely related government procurement operation, the U.S. Government thereby incurs no responsibility, nor any obligation whatsoever; and the fact that the Gov[redacted]mulated, furnished, or in any way supplied the said drawings, specifications, or other data is not to be regarded by implication or otherwise as in any manner licensing the holder or any other person or corporation, or conveying any rights or permission to manufacture, use or sell any patented invention that may in any way be related thereto.

[redacted]

AFRPL-TR-70-86 VOLUME I

AD513618

INJECTOR/CHAMBER SCALING FEASIBILITY PROGRAM (U)

DESIGN AND SHORT DURATION TESTING
VOLUME I

D D C
RECEIVED
FEB 5 1971

G.A.VOORHEES,JR
B. G. MORTON

TRW SYSTEMS GROUP
ONE SPACE PARK • REDONDO BEACH • CALIFORNIA

TECHNICAL REPORT AFRPL-TR-70-86 VOLUME I

JULY 1970

SEE INSIDE FRONT COVER FOR PATENT SECRECY ORDER NOTICE

[redacted]

AIR FORCE ROCKET PROPULSION LABORATORY
AIR FORCE SYSTEMS COMMAND
UNITED STATES AIR FORCE
EDWARDS, CALIFORNIA

[illegible]

[redacted]

THIS DOCUMENT CONTAINS INFORMATION AFFECTING THE NATIONAL DEFENSE OF THE UNITED STATES WITHIN THE MEANING OF THE ESPIONAGE LAWS, TITLE 18, U.S.C., SECTION 793 AND 794, THE TRANSMISSION OF WHICH IN ANY MANNER TO AN UNAUTHORIZED PERSON IS PROHIBITED BY LAW.

REPRODUCTION QUALITY NOTICE

This document is the best quality available. The copy furnished to DTIC contained pages that may have the following quality problems:

- Pages smaller or larger than normal.
- Pages with background color or light colored printing.
- Pages with small type or poor printing; and or
- Pages with continuous tone material or color photographs.

Due to various output media available these conditions may or may not cause poor legibility in the microfiche or hardcopy output you receive.

☐ If this block is checked, the copy furnished to DTIC contained pages with color printing, that when reproduced in Black and White, may change detail of the original copy.

PATENT SECRECY ORDER

The subject matter in this document contains information which is the subject matter of patent applications on which the United States Patent Office has issued secrecy orders. These secrecy orders are superimposed on the usual secrecy regulations which are in force with respect to military contractors' activities. Information under patent secrecy orders must not be disclosed to unauthorized persons.

By statute, violation of a Secrecy Order is punishable by a fine not to exceed $10,000 and/or imprisonment for not more than two years.

NOTICE

When U.S. Government drawings, specifications or other data are used for any purpose other than a definitely related Government procurement operation, the Government thereby incurs no responsibility nor any obligation whatsoever and the fact that the Government may have formulated, furnished or in any way supplied the said drawings, specifications, or other data, is not to be regarded by implication or otherwise, or in any manner licensing the holder or any other person or corporation, or conveying any rights or permission to manufacture, use or sell any patented invention that may in any way be related thereto.

[redacted]

FOREWORD

(U) This final technical report is in two volumes; Volume I covers all work performed in Task I of Contract F04611-68-C-0085, "Injector/Chamber Scaling Feasibility Program." The Task I phase of the program covered the period from 8 July 1968 to 1 September 1969. The report was prepared by G. A. Voorhees, Jr., Program Manager, Applied Technology Department of the Technology Laboratory. Bruce Heckert of the Applied Technology Department served as Program Manager during the initial three months of the program. Richard Williams was responsible for data reduction. The program was carried out under the direction of Dr. Harland L. Burge, Department Manager, Applied Technology Department.

(U) Air Force technical direction was provided by M. F. Powell.

(U) This technical report has been reviewed and is approved.

Roy A. Silver
Project Engineer
Air Force Rocket Propulsion Laboratory

ABSTRACT

(U) The results of the Task I phase of an injector/chamber scaling feasibility program are presented. During the fourteen month program, covering the period from 8 July 1968 to 1 September 1969, the feasibility of scaling the TRW Systems coaxial injector design to the 250,000 lb_f thrust level was demonstrated. A total of forty-one injector development test firings were made using eight injector configurations. Three chamber lengths were evaluated with a single injector configuration. Satisfactory performance was achieved with the longest chamber tested. Injector dynamic stability was demonstrated in numerous stability rating tests employing both pulse-guns and non-directional bombs. Three demonstration injectors were designed and fabricated and two of these injectors were subjected to checkout firings in preparation for Task II testing.

Contents

Page

1. INTRODUCTION AND SUMMARY

1.1 INTRODUCTION 1-1
1.2 PROGRAM SUMMARY 1-1
    1.2.1 Task I Injector/Chamber Development. 1-2
    1.2.2 Task II Ablative Chamber Evaluation. 1-3
    1.2.3 Injector Development Testing 1-2
    1.2.4 Design and Fabrication - Demonstration Injector. . . 1-3
    1.2.5 Demonstration Injector Testing 1-3
    1.2.6 Scaling Summary 1-3

2. ENGINE DESIGN AND FABRICATION

2.1 GENERAL 2-1
    2.1.1 Design Philosophy 2-1
    2.1.2 Combustion Stability 2-2
    2.1.3 Scaling 2-3
2.2 250,000 LB_F THRUST STATIC TEST ENGINE DESIGN 2-11
    2.2.1 Engine Operation 2-16
2.3 COMPONENT DESIGN - DEVELOPMENT INJECTOR 2-16
    2.3.1 Fuel Orifice 2-18
    2.3.2 Pintle Tip Assembly 2-20
2.4 COMPONENT DESIGN - DEMONSTRATION INJECTOR 2-41
    2.4.1 Pintle Tip Assembly 2-46
2.5 COMPONENT DESIGN - THRUST CHAMBER 2-53
    2.5.1 Combustion Chamber 2-53
    2.5.2 Thrust Mount 2-57
    2.5.3 Instrumentation Ports 2-57
2.6 ACQUISITION COSTS 2-57
    2.6.1 Development Hardware 2-57
    2.6.2 Demonstration Injectors 2-61

3. TEST RESULTS

3.1 SUMMARY 3-1
    3.1.1 Facility Checkout Firings 3-1
    3.1.2 Development Injector Firings 3-3
    3.1.3 Demonstration Injector Firings 3-7

CONFIDENTIAL UNCLASSIFIED

CONTENTS (Cont'd)

Page

3.2 DATA REDUCTION PROCEDURES 3-9
3.3 TEST HARDWARE 3-9
3.4 DETAILED TEST RESULTS 3-11

3.4.1 Facility Checkout Firings 3-11
3.4.2 Development Injector Firings 3-14
3.4.3 Demonstration Injector Firings 3-48
3.4.4 Injector Hydraulic Tests 3-63

4. SCALING

4.1 GENERAL 4-1

4.2 SCALING VERIFICATION 4-1

4.2.1 Momentum Correlation 4-1
4.2.2 Throttling 4-2
4.2.3 Effect of Chamber Length 4-2

4.3 DESIGN AND FABRICATION 4-3

4.3.1 General 4-3
4.3.2 Fabrication 4-9

4.4 COST AND WEIGHTS 4-10
4.5 COMBUSTION PERFORMANCE 4-12
4.6 COMBUSTION STABILITY 4-14

5. CONCLUSIONS 5-1

6. REFERENCES 6-1

APPENDIX A - FACILITY CHECKOUT ENGINE DESIGN

APPENDIX B - THERMAL ANALYSIS OF 250,000 LB_F THRUST HEAT-SINK ENGINE CONFIGURATION

APPENDIX C - DATA REDUCTION PROCEDURES

APPENDIX D - TASK I INJECTOR/CHAMBER DESIGN CRITERIA

Total Pages: 226

CONFIDENTIAL

UNCLASSIFIED

LIST OF FIGURES

Figure	Title	Page
2-1	Injector Element Schematic Diagram (U)	2-2
2-2	Comparison of Stability Modes (U)	2-4
2-3	Correlation of Performance with Length (U)	2-10
2-4	X404446 250,000 Lbf Thrust Development Engine Assembly (U)	2-12
2-5	250,000 Lbf Thrust Test Engine - Stress Analysis Regions (U)	2-15
2-6	X403829 250,000 Lbf Thrust Development Injector Assembly (U)	2-17
2-7	250,000 Lbf Thrust Development Injector Assembly (U)	2-18
2-8	250,000 Lbf Thrust Development Injector Centerbody (U)	2-18
2-9	250,000 Lbf Thrust Injector Fuel Jacket Assembly (U)	2-20
2-10	250,000 Lbf Thrust Injector Pintle Tip Assemblies (U)	2-21
2-11	Initial Oxidizer and Fuel Orifice Rings (U)	2-22
2-12	X403831 Ring, Oxidizer Orifice 250,000 Lbf Development Static Test Injector (U)	2-23
2-13a	X403831-1 Oxidizer Orifice Ring (U)	2-24
2-13b	X403666-7 Oxidizer Orifice Ring (U)	2-24
2-14	Predicted Injection Pressure Losses (O1/F1) (U)	2-27
2-15	Modification "A" to X403831-1 (U)	2-29
2-16	Predicted Injection Pressure Losses (O1A/F2 - O1B/F2)(U)	2-29
2-17	Modification "B" to X403831-1 (U)	2-29
2-18	Oxidizer Orifice Ring (O2) (U)	2-30
2-19	Predicted Injection Pressure Losses (O2/F2) (U)	2-33
2-20	X404408-2 Pintle Tip Assembly (U)	2-33
2-21	X404047 Oxidizer Orifice Ring (O3) (U)	2-34
2-22	X404047-1 Oxidizer Orifice Ring (O3) (U)	2-35
2-23	Predicted Injection Pressure Loss (U)	2-37
2-24	X403946 Oxidizer Orifice Ring No. 4 (U)	2-38
2-25	Predicted Injection Pressure Loss (U)	2-39
2-26	X404408-4 Pintle Tip Assembly (U)	2-39
2-27	X404408-5 Pintle Tip Assembly Showing X404480-1 Back Oxidizer Ring (U)	2-41
2-28	X404108-1 Oxidizer Orifice Ring (O6) (U)	2-42
2-29	X404056 250,000 Lbf Thrust Demonstration Injector Assembly (U)	2-45
2-30	Demonstration Injector During Final Assembly (U)	2-46
2-31	X404280-1 Pintle Tip Assembly (U)	2-47
2-32	X404693-1 Oxidizer Orifice Ring (U)	2-48
2-33	X403646 250,000 Lbf Thrust Development Chamber Assembly (U)	2-54
2-34	X403646-1 Thrust Chamber Assembly (Grano Steel) (U)	2-55
2-35	Modification 1 and 2 to X403646-1 (U)	2-56
2-36	X404053 Instrumentation Assembly, 250,000 Lbf Development Engine (U)	2-58
2-37	X404097 Thermocouple Locations, Development Chamber (U)	2-59
3-1	Specific Impulse Efficiency - Test Firings 2-10 (U)	3-2
3-2	Combustion Efficiency - Test Firings 2-10 (U)	3-2

LIST OF FIGURES (Cont'd)

Figure	Title	Page
3-3	Measured Thrust - Development Injector Firings (U)	3-4
3-4	Specific Impulse Efficiency - Baseline Chamber (U)	3-5
3-5	Combustion Efficiency - Baseline Chamber (U)	3-5
3-6	Effect of Chamber Length on Specific Impulse Efficiency (U)	3-6
3-7	Effect of Chamber Length on Combustion Efficiency (U)	3-6
3-8	Nozzle Efficiency - Demonstration Injector Firings (U)	3-8
3-9	Specific Impulse Efficiency - Demonstration Injector (U)	3-8
3-10	Combustion Efficiency - Demonstration Injector Firings (U)	3-9
3-11	Measured Thrust - Facility Checkout Firings (U)	3-12
3-12	Specific Impulse Efficiency - Facility Checkout Firings (U)	3-13
3-13	Combustion Efficiency - Facility Checkout Firings (U)	3-13
3-14	Nozzle Efficiency - Function of Mixture Ratio (U)	3-15
3-15	Nozzle Efficiency - Function of Nozzle Stagnation Pressure (U)	3-15
3-16	Fuel Injector Conductance - Facility Checkout Firings (U)	3-16
3-17	Facility Checkout Injector - Photo showing cocked weir (U)	3-16
3-18	Oxidizer Injector Conductance - Facility Checkout Firings (U)	3-17
3-19	Measured Thrust - Test Series 1 and 2 (U)	3-18
3-20	Specific Impulse Efficiency - Test Series 1 and 2 (U)	3-19
3-21	Combustion Efficiency - Test Series 1 and 2 (U)	3-19
3-22	Nozzle Efficiency, Test Series 1 and 2 - Function of Mixture Ratio (U)	3-21
3-23	Nozzle Efficiency, Test Series 1 and 2 - Function of Nozzle Stagnation Pressure (U)	3-21
3-24	Fuel Injector Conductance, Test Series 1 (U)	3-22
3-25	Oxidizer Injector Conductance, Test Series 1 and 2 (U)	3-22
3-26	Specific Impulse Efficiency - Function of $(\Delta P_r)^{0.5}(\mu)^{0.4}$ (U)	3-22
3-27	Measured Thrust, Test Series 3 (U)	3-24
3-28	Specific Impulse Efficiency - Test Series 3 (U)	3-25
3-29	Combustion Efficiency - Test Series 3 (U)	3-25
3-30	Nozzle Efficiency - Test Series 3 (U)	3-26
3-31	Fuel Injector Conductance - Test Series 3 (U)	3-26
3-32	Oxidizer Injector Conductance - Test Series 3 (U)	3-27
3-33	Specific Impulse Efficiency - Function of $(\Delta P_r)^{0.5}$ $(\mu)0.4$ (U)	3-27
3-34	Measured Thrust - Test Series 4 (U)	3-29
3-35	Specific Impulse Efficiency - Test Series 4 (U)	3-30
3-36	Combustion Efficiency - Test Series 4 (U)	3-30
3-37	Nozzle Efficiency - Test Series 4 (U)	3-31
3-38	Nozzle Efficiency - Test Series 4 (U)	3-31
3-39	Fuel Injector Conductance - Test Series 4 (U)	3-32

LIST OF FIGURES (Cont'd)

Figure	Title	Page
3-40	Oxidizer Injector Conductance - Test Series 4 (U)	3-32
3-41	Specific Impulse Efficiency, Test Series 4, Function of $(\Delta P_r)^{0.5} (\mu)^{0.4}$ (U)	3-34
3-42	Measured Thrust - Test Series 5 (U)	3-34
3-43	Specific Impulse Efficiency, Test Series 5 (U)	3-35
3-44	Combustion Efficiency, Test Series 3/5 (U)	3-35
3-45	Combustion Efficiency, Test Series 5 - Effect of Chamber Length (U)	3-36
3-46	Nozzle Efficiency, Test Series 5 - Effect of Nozzle Divergence Angle (U)	3-36
3-47	Nozzle Efficiency, Test Series 5 - Effect of Chamber Length (U)	3-38
3-48	Nozzle Efficiency, Test Series 5 - Effect of Chamber Length (U)	3-38
3-49	Fuel Injector Conductance, Test Series 5 (U)	3-39
3-50	Oxidizer Injector Conductance, Test Series 5 (U)	3-39
3-51	Specific Impulse Efficiency, Test Series 5, Function of $(\Delta P_r)^{0.5} (\mu)^{0.4}$ (U)	3-40
3-52	Combustion Efficiency, Test Series 6 (U)	3-40
3-53	Nozzle Efficiency, Test Series 6 (U)	3-42
3-54	Fuel Injector Conductance, Test Series 6 and 7 (U)	3-42
3-55	Oxidizer Injector Conductance, Test Series 6 (U)	3-42
3-56	Combustion Efficiency, Test Series 7 (U)	3-43
3-57	Nozzle Efficiency, Test Series 7 (U)	3-43
3-58	Measured Thrust, Test Series 8 (U)	3-45
3-59	Specific Impulse Efficiency, Test Series 8 (U)	3-45
3-60	Nozzle Efficiency, Test Series 8 (U)	3-46
3-61	Combustion Efficiency, Test Series 8 (U)	3-46
3-62	Fuel Injector Conductance, Test Series 8 (U)	3-47
3-63	Oxidizer Injector Conductance, Test Series 8 (U)	3-47
3-64	Measured Thrust, Test Series 9 (U)	3-49
3-65	Efficiency, Test Series 9 (U)	3-49
3-66	Specific Impulse Efficiency, Test Series 9, Function of $(\Delta P_r)^{0.5} (\mu)^{0.4}$ (U)	3-50
3-67	Injector Conductance, Test Series 9 (U)	3-50
3-68	Measured Thrust, Test Firings 72-77 (U)	3-52
3-69	Nozzle Efficiency, Test Firings 72-77 (U)	3-53
3-70	Specific Impulse Efficiency, Test Firings 72-77 (U)	3-53
3-71	Combustion Efficiency, Test Firings 72-77 (U)	3-53
3-72	Fuel Injector Conductance, Test Firings 72-77 (U)	3-54
3-73	Fuel Line Conductance, S/N 001 Injector (U)	3-54
3-74	Fuel Manifold Conductance, Test Firings 72-77 (U)	3-55
3-75	Oxidizer Injector Conductance, Test Firings 72-77 (U)	3-55
3-76	Specific Impulse Efficiency-Durability Firing No.78 (U)	3-57
3-77	Fuel Injector Conductance-Durability Firing No.78 (U)	3-57
3-78	Fuel Side Conductance as a Function of Time, Durability Firing No. 78 (U)	3-58
3-79	Measured Thrust - Test Firings 90-93 (U)	3-59

LIST OF FIGURES (Cont'd)

Figures	Title	Page
3-80	Specific Impulse Efficiency, Test Firings 90-93 (U)	3-59
3-81	Combustion Efficiency, Test Firings 90-93 (U)	3-61
3-82	Measured Thrust, Test Firings 98-100 (U)	3-61
3-83	Nozzle Efficiency, Test Firings 98-100 (U)	3-62
3-84	Specific Impulse Efficiency Test Firings 98-100 (U)	3-62
3-85	Combustion Efficiency, Test Firings 98-100 (U)	3-62
3-86	Fuel Injector Conductance, Test Firings 98-100 (U)	3-64
3-87	Fuel Line Conductance, Test Firings 98-100 (U)	3-64
3-88	Oxidizer Injector Conductance, Test Firings 98-100 (U)	3-64
3-89	Water Flow of Oxidizer Ring 01B @ 100% (U)	3-65
3-90	Injection Pressure Loss, 01B/F2 (U)	3-65
3-91	Water Flow of Demonstration Injector S/N 002 @ 100% (U)	3-66
3-92	Injection Pressure Loss, S/N 002 Demonstration Injector (U)	3-67
4-1	Preliminary Design, 3500K lbf Thrust (Sea Level) Engine (U)	4-4
4-2	Preliminary Design, 387K lbf Thrust (Vacuum) Engine (U)	4-5
4-3	Preliminary Design, 57.8K lbf Thrust (Vacuum) Engine (U)	4-6
4-4	Approximate Thrust Chamber Dimensions (U)	4-7
4-5	Predicted Combustion Efficiency of 3000K Engine (U)	4-13

LIST OF TABLES

Table	Title	Page
2-1	Static Test Engine Design Parameters (U)	2-13
2-2	Static Test Engine Stress Analysis (U)	2-14
2-3	Description of Fuel and Oxidizer Orifice Rings Used In Task I Injector Development (U)	2-19
2-4	Initial Oxidizer Orifice Ring Characteristics (U)	2-25
2-5	Measurement of X403831-1 Oxidizer Orifice Ring (U)	2-26
2-6	Characteristics of Oxidizer Orifice Ring 2 (U)	2-31
2-7	X404107 "A" Oxidizer Orifice Ring Measurements (U)	2-32
2-8	Characteristics of Oxidizer Orifice Rings 3 and 4 (U)	2-35
2-9	X404047 "A" Oxidizer Orifice Ring Measurements (U)	2-36
2-10	X403946 "A" Oxidizer Orifice Ring Measurements (U)	2-40
2-11	Characteristics of Oxidizer Orifice Rings 4 and 6 (U)	2-43
2-12	X404108 Oxidizer Orifice Ring Measurements (06) (U)	2-44
2-13	Characteristics of X404693-1 Oxidizer Orifice Ring (U)	2-49
2-14	X404693-1 Ring, Oxidizer Orifice S/N 001 (U)	2-50
2-15	X404693-1 Ring, Oxidizer Orifice S/N 002 (U)	2-51
2-16	X404693-1 Ring, Oxidizer Orifice S/N 003 (U)	2-52
2-17	Development Hardware Acquisition Costs (U)	2-60
2-18	Demonstration Hardware Acquisition Costs (U)	2-61
3-1	Test Hardware Configurations (U)	3-10
4-1	Preliminary Cost and Weight Data for Three Point Design Engine Sizes (U)	4-11

NOMENCLATURE

F	thrust, lb_f
P	pressure, psia
ϵ	area ratio
O/F	mixture ratio
O	oxidizer
F	fuel, throat
I_{sp}	specific impulse
η	efficiency
C^*	characteristic velocity
A	area
UW	unit width = $\pi D_p/N$, in
D_p	diameter of pintle, in.
N	number of elements
W_p	width of primary orifice, in.
t_{fsh}	fuel sheet thickness, in.
ΔP	pressure differential
$\dot{Q}$	volumetric flow rate, ft^3/sec
$\dot{W}$	propellant flow rate, lb/sec
g_o	conversion factor, $lbm\text{-}ft^2/lbf\text{-}ft\text{-}sec^2$
D	diameter, inches
L^*	characteristic length, inches
K	conductance
KIJCF	fuel injector conductance
KIJCO	oxidizer injector conductance
C_f	thrust coefficient
KLF	fuel line conductance

NOMENCLATURE (Cont'd)

C_d	discharge coefficient
β	correction factor
μ	mixture ratio (lb_m oxidizer/lb_m fuel)
ρ	propellant density
γ	specific heat ratio
ΔP_r	pressure differential ratio ($\Delta P_{io}/\Delta P_{if}$)

Subscripts

e	exit
c	chamber
ot	total oxidizer injection orifices
op	primary oxidizer injection orifices
os	secondary oxidizer injection orifices
i	injection
o	oxidizer, or stagnation
f	fuel
t	throat, total

SECTION 1

INTRODUCTION AND SUMMARY

1.1 INTRODUCTION

(U) In-depth systems studies of various means of minimizing the cost of launch vehicles have been conducted by the Air Force over the past several years. These studies have shown that a system based upon a low cost liquid fueled propulsion system (sometimes referred to as a "big dumb booster") offers a very attractive solution to the problem. The key technological aspect of the concept hinges upon the ability to develop at modest cost a thrust chamber assembly (injector/chamber) which exhibits the following characteristics:

- Low Cost Manufacture - commercial tolerances and manufacturing processes, low cost ablative materials
- Scaleability - to minimize development cost for multi-million pound thrust levels
- Dynamic Stability - to minimize typical trial and error development of stable injectors which has plagued large liquid fueled engines
- Performance - adequate to accomplish the mission

(U) The TRW Systems approach to the solution of this critical technology area was to demonstrate the feasibility of scaling the single element coaxial injector/ablative thrust chamber concept successfully utilized in the Lunar Module Descent Engine (LMDE) from the 10,000 lbf thrust level to the 250,000 lbf thrust level. Under the requirements of this contract, F04611-68-C-0085, Injector/Chamber Scaling Feasibility Program, TRW Systems designed and fabricated low-cost injector/chamber hardware for test and evaluation at the AFRPL High-Thrust Test Facility, 1-56. The program consisted of two tasks: (1) Task I - 250,000 lbf thrust injector/chamber development; and (2) Task II - 250,000 lbf thrust long duration ablative chamber evaluation.

(U) In Task I, TRW Systems furnished the AFRPL a contractor-owned thrust chamber assembly (LMDE engine design scaled to 250,000 lbf thrust level) for the purpose of facility checkout. TRW Systems also designed and fabricated a development injector and heat-sink combustion chamber to investigate the effects of variations in critical geometric and hydraulic parameters on combustion performance. The development injector incorporated replaceable fuel orifice rings and oxidizer pintle tip assemblies. The final demonstration injector configuration was defined after only 41 full scale test firings. This is significant in the fact that TRW fabricated 3 identical injectors for the subsequent long duration ablative material evaluation tests using commercial manufacturing processes and commercial tolerance practices.

(U) In Task II, three different candidate low cost ablative material systems were evaluated in 250,000 lbf thrust chamber hardware.

(U) This report is in two volumes. Volume I describes all accomplishments during the Task I phase of the program covering the period of 8 July 1968 to 1 September 1969. Volume II describes the results of the Task II phase of the program covering the period of 11 December 1968 to 3 February 1970.

1.2 PROGRAM SUMMARY

(U) The TRW Systems experimental low-cost pressure fed engine demonstrated the following:

- An inherently stable and scalable injector design which minimizes the development costs.
- Engine metal components fabricated from low-carbon steels using commercial fabrication methods.
- Low-cost ablative liner materials and fabrication techniques.

The ability to design, fabricate and test these flight configured engines within the scope of the program demonstrates the feasibility of the minimum cost design approach to designing rocket vehicles.

1.2.1 Task I Injector/Chamber Development

(U) Task I consisted of forty-one short duration test firings with the development heat sink hardware. Performance, heat transfer, and stability data were obtained. Three different length combustion chambers (36, 48 and 60 inches) were tested to determine the effect of length on engine performance. These tests were conducted using a single element coaxial injector operated at eight different fuel to oxidizer settings. The TRW injector design minimizes the number of injector builds normally associated with engine development programs because of its simple construction which accommodates interchangeable oxidizer rings and fuel gap adjustments.

(C) The maximum specific impulse efficiency measured was 89.5 percent in the 60-inch long ($L/D = 1.54$ and $L^* = 120$ inches) heat-sink combustion chamber. Increasing the combustion chamber length from 36 inches to 60 inches resulted in an engine performance increase of approximately 4 percent. Data indicates that higher performance can be achieved by modest increases in combustion chamber length.

(C) A total of 21 stability rating tests, using both pulse-guns and non-directional bombs, were made with the various injector configurations. The induced chamber pressure disturbances were all damped to within 10 percent of the original chamber pressure within 10-37 milliseconds, once again providing that the centrally located, coaxial injector is dynamically stable.

(C) The nominal combustion performance (ηC^*) for six of the eight injector settings was essentially the same (within the accuracy of the data). The remaining two settings incorporated changes in the ratio of primary to secondary flow rates and oxidizer orifice entrance flow dynamics. These

(C) changes resulted in lower performance than the original six injector configurations. Because of the desire to continue into Task II, no further injector changes were made to improve performance. The final demonstration injector setting for Task II was selected from the test base of 41 injector firings.

(C) Fourteen additional checkout firings were made with the S/N 001 and S/N 002 demonstration injectors. The S/N 001 demonstration injector was test-fired in the 60 inch chamber (L* = 120 inches) both with and without a turbulence ring. The turbulence ring resulted in a performance increase of approximately 1-1/2 percent. The S/N 002 demonstration injector was test-fired in the same chamber without the turbulence ring.

(U) The S/N 001 demonstration injector also was subjected to a test firing of 10 seconds duration to check injector durability. A heat sink thrust chamber was lined with a low-cost gypsum-phenolic insulation at the AFRPL for this firing. Most of the insulation was either ablated or ejected during the initial five seconds of the firing. As a result, the convergent and throat sections of the heat-sink chamber were eroded during the latter half of the firing. No erosion of the oxidizer orifice ring or the ablative pintle tip was encountered.

1.2.2 Task II Ablative Chamber Evaluation

(U) Three ablative lined thrust chamber assemblies were designed and tested. Four S/N 001 injector checkout tests were also conducted during Task II. Performance agreed with the S/N 001 and 002 checkout tests.

(U) A number of low-cost fabrication techniques were evaluated. Tape wrapping over a male mandrel, and hand lay-up of standard ablative materials in conjunction with a low-pressure cure cycle appear applicable for fabricating large ablative components but would require expensive tooling. Casting of room temperature curing ablators is a feasible technique for producing large ablative components without the use of expensive tooling. The high pressure molding of interlocking panels appears to be a practical technique. The joint design and secondary bonding of the molded panels to the shell become the critical and expensive parts of the ablative component.

(U) The material selections for the three ablative chambers were based upon results of subscale test programs conducted at both the AFRPL and TRW Systems. Cost-effectiveness studies were made of chamber liners using the most promising materials. Final material selections were based on the cost-effectiveness studies, fabrication processes adaptable to larger size ablative liners, and new material technology.

(U) The configuration 1 ablative liner consisted of a tape-wrapped MX-2600 (silica-phenolic) throat insert, an MX-2600 (silica-phenolic) exit cone liner layed up in a rosette pattern, and an MXA-150 (asbestos-phenolic) chamber liner which was layed-up parallel-to-surface. The exit cone and chamber sections were cured in place at 100 psi while the throat insert was cured in an autoclave at 100 psi, machined and secondarily bonded into the pressure shell using an epoxy adhesive. The chamber internal configuration consisted of an L* of 89 inches, a chamber length to diameter ratio of 1.56 and a contraction ratio of 1.80. This chamber design demonstrated an engine life of 66 seconds.

(U) The configuration 2 ablative liner consisted of a cast Dow-Corning 93-104 filled-silicone rubber throughout the chamber. The liner was cast in three sections; the throat-exit cone, the dome section, and the cylindrical chamber section using internal plaster molds and sheet metal/plywood mandrels. The cast chamber was cured at room temperature. The chamber internal configuration consisted of an L* of 104 inches, a chamber length to diameter ratio of 1.44 and a contraction ratio of 2.07. The demonstrated engine life for this design was 98 seconds.

(U) The configuration 3 ablative liner consisted of a tape-wrapped MX-2600 (silica-phenolic) throat insert, an MXA-150 (asbestos-phenolic) exit cone liner and a cast Ironsides Resin DP5-161 chamber liner. The exit cone was fabricated from compression molded MXA-150 segments which were secondarily bonded into the pressure shell. The DP5-161 chamber section was cast in two sections, the dome and cylindrical chamber section, using internal plaster molds and sheet metal/plywood mandrels. The cast chamber section was cured at room temperature. The internal configuration of the combustion chamber was identical to the configuration 1 ablative liner. The demonstrated engine life for this design was 83 seconds.

(U) The average weight of the three engine assemblies is estimated to be 5290 pounds with the lightest engine being the configuration 2 design (5030 pounds). The injector assemblies weighed 1500 pounds each, the thrust chamber pressure vessels weighed 2850 pounds each and the ablative liners weighed from 680 pounds to 1130 pounds.

(C) The demonstrated specific impulse for the three ablative engine firings was 88 ± 0.5 percent of the theoretical value at the nominal design mixture ratio of 2.60 O/F. The maximum performance measured was 89 percent at a mixture ratio of 2.50.

(C) The test program proved the feasibility of a minimum cost design with minimal engine development required. The heat-sink thrust chamber tests determined the effect of thrust chamber length (i.e., chamber stay time) on combustion performance for a given injector. Using this relationship with the ablative engines' delivered performance indicates an ability to deliver 92% specific impulse by increasing the chamber length to diameter ratio to 1.68. Acceptable ablative performance may be achieved with the Fiberite MX-2600 (silica-phenolic tape or broadgoods) used for the chamber liner, throat insert, and nozzle exit-cone.

SECTION 2

ENGINE DESIGN AND FABRICATION

2.1 GENERAL

(U) The TRW low-cost, pressure-fed engine design consists of two major assemblies - a centrally located, coaxial injector and an ablatively cooled thrust chamber. The engine uses low-cost storable propellants (N_2O_4/UDMH) which are compatible with conventional materials of construction. The engine is designed with a minimum of "precision" tolerances such that industrial fabrication techniques may be used to fabricate both the injector and thrust chamber shell. Low-cost ablative-type thrust chamber liners, capable of being fabricated by low-cost techniques, are used to protect the chamber shell during the engine firing duration.

(U) The Task I Design and Fabrication effort consisted of the design and fabrication of three major items. These items were as follows:

1) 250,000 lb_f Thrust Development Injector
2) 250,000 lb_f Thrust Heat-Sink Chamber
3) 250,000 lb_f Thrust Demonstration Injectors

The 250,000 lb_f thrust development injector was designed to accept replaceable fuel and oxidizer orifice rings in order to expedite testing of various injector configurations. The heat-sink combustion chamber had numerous pulse-gun and bomb bosses for conducting stability rating tests. Three demonstration injectors were fabricated. The fuel and oxidizer orifice design was based on the tests results achieved with the development injector.

2.1.1 Design Philosophy

(U) It has been recognized that the propellant injector is the critical component in the overall determination of engine performance, combustion stability, and thrust chamber durability. For many years TRW Systems has been conducting analytical and experimental investigations of the combustion process from the standpoint of performance, stability and thrust chamber durability. These efforts have led to TRW Systems selection of the coaxial injector concept as the most suitable basic design for meeting these engine requirements.

(U) The basic design simplicity of the coaxial injector results in reduced development and production costs while maintaining high component reliability. Since most of the fabrication consists of turning operations and electrical discharging machining (EDM), the part-to-part reproduction is excellent and the scraprate reduced when compared with designs requiring a large number of precision drilling operations.

(U) The basic injector concept permits adjusting both the fuel and oxidizer injection flow areas, either separately or simultaneously, thus providing increased flexibility during the early development phases of a program.

(U) This feature permits a more rapid injector optimization. A schematic diagram of the injector element is shown in Figure 2-1. The coaxial injector design is predicated upon obtaining a mechanical interlock of the propellants which forces liquid phase mixing to occur.

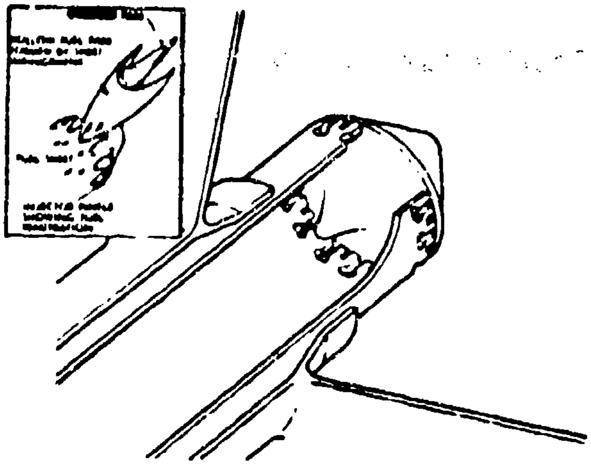

Figure 2-1. Injector Element Schematic Diagram (U)

(U) The oxidizer is metered and directed radially outward as individual streams from the central pintle. The fuel is injected as a hollow cylindrical sheet which intercepts the oxidizer streams as shown in Figure 2-1, with part of the fuel impinging the oxidizer stream and part of it penetrating between the oxidizer orifices. The geometry of the interaction system is selected on the basis of required performance and wall environment.

(U) The injection parameters for this injector which have shown a dominating influence on injector performance in previous work are as follows:

1. Ratio of oxidizer to fuel injection momentum
2. Ratio of secondary oxidizer flow to primary orifice flow
3. Number, size and shape of oxidizer orifices
4. Elemental spacing of oxidizer orifices
5. Location of secondary oxidizer orifices
6. Injection pressure level.

(U) Variation of these parameters are used to control both performance and wall environment.

2.1.2 Combustion Stability

(U) The injector design directly affects overall dynamic stability, performance, and thrust chamber durability. Realization of these design goals is not possible unless the injector can be made to operate in a dynamically stable manner.

(U) The centrally located, coaxial injector design has proven its inherent dynamic stability in thousands of tests on engines ranging from small RCS thrustors to the present 250,000 $\mathrm{lb_f}$ thrust pressure-fed engine. Non-directional bombs and radial and tangentially oriented pulse guns have been utilized to rate the injector dynamic stability. High frequency response pressure transducers are used to record the pressure disturbances.

(U) The tangential, radial, and longitudinal modes are of concern, with the tangential modes being most important. The TRW Systems centrally located, coaxial injector provides a fundamental approach to the theoretical elimination of these acoustic modes of instability.

(U) Examination of the anti-nodes of various acoustic vibrational modes shows the location of possible abnormally high energy release zones which could result in sustaining combustion instability. Figures 2-2a, 2-2b and 2-2c show a comparison between distributed injection and centralized injection. The figures show that the location of abnormally high energy releases in a chamber can have a dominant effect on whether or not the engine will be dynamically stable.

(U) Figure 2-2a compares a distributed injector and centrally located injector response during a tangential disturbance. Stable operation is indicated by the solid line while the energy release pattern resulting from a large pressure pulse at one side of the injector is shown as a dashed line. The zone of the maximum energy release rate in the distributed injection system moves generally toward the injector face (source of propellants) thus sustaining the instability.

(U) In the centrally located injector the zone of maximum energy release must again move toward the incoming propellants to increase the combustion rate above its normal value. The maximum energy release zone moves toward the injector and inward toward the chamber axis, or nodal location. It is apparent that, under these conditions, the energy is released closer to the pressure node and becomes ineffective in sustaining the spinning or tangential pressure front.

(U) Similar arguments can be offered in support of the stability of the centrally located injector to both the first radial and first longitudinal modes of instability.

2.1.3 Scaling

(U) Past experience has demonstrated the scalability of the centrally located coaxial injector over a wide range of thrust levels. This is accomplished through the use of simple geometrical scaling techniques. Of primary importance in scaling the coaxial injector is the maintenance of hydraulic similarity at the impingement point. The oxidizer orifice configuration is essentially photographically scaled. In making gross scaling changes it has been necessary only to make minimal changes to achieve the desired performance and chamber compatibility. The scaling criteria used in designing the 250,000 lbf (vacuum) thrust injector and combustion chamber are given in the following paragraphs.

2.1.3.1 Mixing

(U) It has been long recognized that high injector performance requires maximum use of the kinetic energy of jet interaction. To assure that peak performance will occur, it is necessary to optimize the injection hydraulics. It has been found that control of basic momentum considerations results in peak performance (Reference 2) for the hypergolic propellant combinations under consideration, i.e., where liquid phase reactions are considered to be of major importance.

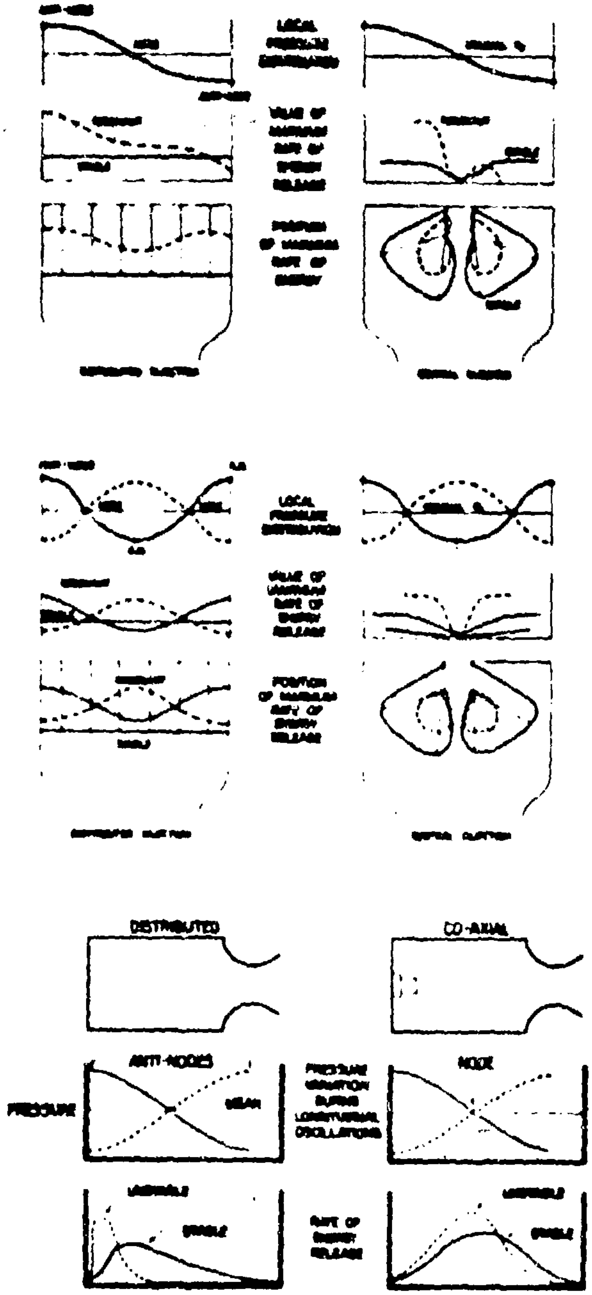
LOCAL
DISTRIBUTED
CO-AXIAL
ANTI-NODES
NODE
PRESSURE
MEAN
PRESSURE VARIATION DURING LONGITUDINAL OSCILLATIONS
UNSTABLE
STABLE
RATE OF ENERGY RELEASE

(a) First Tangential

(b) First Radial

(c) First Longitudinal

Figure 2-2. Comparison of Stability Modes (U)

(U) A highly effective approach to control of momentum interaction is obtained through an examination of the gross dynamics of interaction of the fuel and oxidizer streams. Initially, maximum mixing can be achieved only by optimum use of available momentum forces. Using this approach, Rupe at JPL (Reference 3) arrived at a criteria for two impinging round streams for maximum mixing which is given as

$$\frac{\rho_f V_f^2 d_f}{\rho_o V_o^2 d_o} = 1 \qquad (2\text{-}1)$$

(U) Reibling at JPL (Reference (4)) reports that all of the criteria for optimum propellant mixing in impinging jet injection elements can be expressed in the form

$$\left[a_2/a_1\right]_{\text{Max } \eta_m} = k \left[\left(\rho_1/\rho_2\right) R^2\right]^b \qquad (2\text{-}2)$$

where:

R = ratio of mass flow rate of liquid 2 to liquid 1 i.e., mixture ratio

ρ = liquid density

a = cross-sectional area of an individual orifice

η_m = mixing efficiency

or in terms of oxidizer and fuel

$$\left[a_{ox}/a_f\right]_{\text{Max } \eta_m} = k \left[\left(\rho_f/\rho_o\right)\left(\dot{W}_o/\dot{W}_f\right)^2\right]^b \qquad (2\text{-}3)$$

The coefficient k is a unique function of the ratio of the number of streams of one fluid to the other fluid (n_f/n_o); b is relatively insensitive to changes in (n_f/n_o) with a nominal value of 0.7.

(U) Experimental programs at TRW employing the coaxial injector element indicates that a modification of Equation (2-3) after Reibling, to account for side interaction of the fuel sheet with the oxidizer filaments and differences in discharge coefficients, results in acceptable correlation of the test data. The modified correlating parameter is given by

$$k' \left(\rho_f/\rho_o\right)^{0.2} \mu^{0.4} \Delta P_r^{0.5} = 1.0 \qquad (2\text{-}4)$$

where:

ρ = liquid density

μ = mixture ratio $(\dot{W}_o/\dot{W}_f)$

$\Delta P_r = \Delta P_o/\Delta P_f$

for maximum mixing efficiency, and k' is determined empirically.

(U) Injection parameters which have been shown important in prior work include the following:

- Ratio of oxidizer to fuel injection momentum
- Fuel and oxidizer orifice pressure drop level
- Number of oxidizer orifices
- Shape of oxidizer orifices
- Setback of oxidizer secondary orifice
- Spacing between oxidizer orifices
- Percentage of oxidizer secondary flow
- Ratio of pintle diameter to chamber diameter

The various orifice parameters are shown in the following sketch.

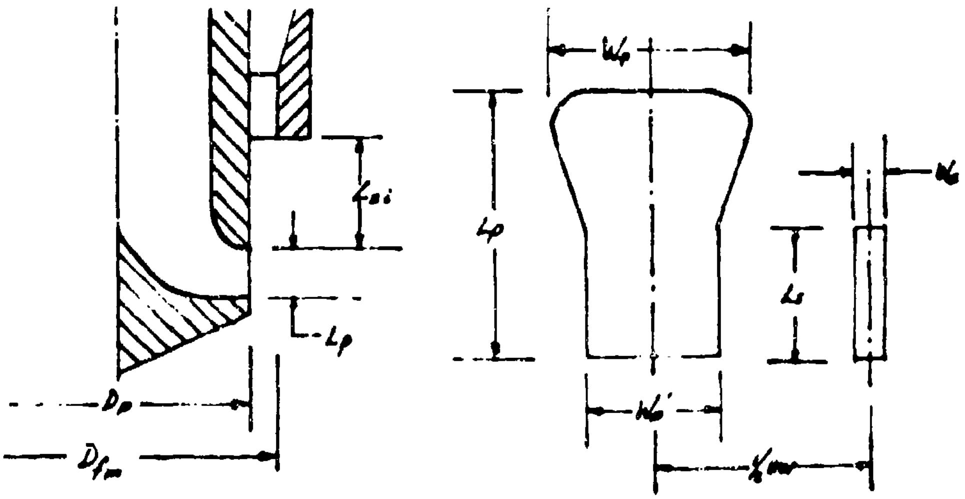

D_p = pintle diameter

D_{fm} = fuel metering orifice diameter

L_{si} = length of fuel stream to impingement

L_p = length of primary oxidizer orifice

W_p = major width of primary oxidizer orifice

W_p' = minor width of primary oxidizer orifice

L_s = length of secondary orifice

W_s = width of secondary orifice

(U) Injector configurations with 30, 32, 36, 38, 42, 48 and 60 primary oxidizer orifices have been tested previously. Most of these configurations were tested also with secondary oxidizer orifices. In configurations employing primary oxidizer orifices only, insufficient spacing between individual orifices $[UW - (W_p + W_s)]$ precludes adequate penetration of the fuel sheet, while a spacing which is too great allows excessive penetration of the fuel sheet. In both cases performance is lowered and in the latter case (fuel rich central core) the chamber wall zone would normally be oxidizer rich resulting in excessive erosion of the ablative chamber liner. The basic approach which was developed in the LMDE program is the addition of secondary oxidizer orifices between primary orifices at a predetermined setback $(L_p - L_s)$ and with an area approximately 10 percent of the total oxidizer injection area.

(U) The selection of the central pintle tube assembly diameter, D_p, is based on consideration of: (1) fuel sheet thickness at the design injection velocity, (2) resulting pintle tube circumference from the standpoint of length available for locating the oxidizer injection orifices and (3) ratio of fuel sheet thickness $[1/2\ (D_p - D_{fm})]$ to spacing between primary oxidizer orifices $(UW - W_p)$.

(U) Only the first six of the eight injector parameters were varied in this program. The percentage of oxidizer secondary flow was nominally 10 percent of the total flow (8 to 11. percent), while the ratio of pintle diameter to chamber diameter was invariant (0.327).

(U) Only two injectors with more than 36 elements (02 and 06 with 48 elements) were tested during the injector development phase. The shape of the oxidizer orifices were not varied significantly. The spacing between orifices was varied from 50 percent of unit width to 33 percent of unit width.

2.1.3.2 Vaporization

(U) For geometrically similar injection elements the effective mean size droplet (r_m) is a function of the total mass flow through the orifice and the injection velocity. The vaporization of these propellant droplets, and subsequent reaction, is a function of the chamber diameter and chamber length. Using LMDE experience the chamber configuration required to vaporize and complete the combustion of the injected propellants is given by

$$\text{Chamber diameter (I.D.)},\ \sqrt{2}\ D_t = D_c$$

$$\text{Chamber length,} = 1.45\ D_c = L_c \text{ where}$$

the length is measured between the impingement plane and the throat. The chamber convergence angle is selected as 30° and the throat radius of curvature is 0.5 D_t.

(U) An analytical combustion efficiency analysis using one-dimensional vaporization rate-limited combustion model computer programs described in References 5 and 6 was performed in support of the experimental program. Additional data from a company-funded 50,000 lbf program was used to verify the chamber scaling approach.

(U) The scaling approach involved correlating the mass median drop radius, r_m, standard deviation, σ, and number of drop groups (which characterize the spray at the initial station) with the measured combustion efficiency. The variation of volume mean drop diameter, d_{30}, was correlated by

$$\frac{d_j}{d_{30}} = 2.64\sqrt{d_j V_j} + 0.97\, d_j \left| V_{gas} - V_j \right| \qquad (2\text{-}5)$$

For a constant injection velocity and the assumption that $\left| V_{gas} - V_j \right| \approx 0$

$$d_{30} \sim (d_j)^{1/2} \qquad (2\text{-}6)$$

or in terms of injected flow rates

$$d_{30} \sim (\dot{m})^{1/4} \qquad (2\text{-}7)$$

It is further assumed that:

$$r_m \sim d_{30} \sim (\dot{m})^{1/4} \qquad (2\text{-}8)$$

or

$$r_{m_2} = r_{m_1} (\dot{m}_2/\dot{m}_1)^{1/4} \qquad (2\text{-}9)$$

(U) Equation 2-9 was used to scale drop size (and number flux distribution) from a know condition (r_{m_1}, $\dot{m}_1$) to the new condition.

(U) The mass median drop radius, r_m, also is related to two primary injector parameters, specifically injector pressure drop, ΔP and number of primary and secondary orifices, n, as follows:

(U) $$\dot{m} = \rho V_j (\pi/4) d_j^2 n \qquad (2\text{-}10)$$

or $$d_j \sim \sqrt{\frac{\dot{m}}{V_j n}} \qquad (2\text{-}11)$$

Substitution of 2-11 in equation 2-5 (with $\left| V_{gas} - V_j \right| \approx 0$) leads to

$$d_{30} \sim \frac{\dot{m}^{1/4}}{(V_j)^{3/4}(n)^{1/4}} \qquad (2\text{-}12)$$

Substituting the following relationship into equation (2-12)

$$\Delta P \sim V_j^2 \qquad (2\text{-}13)$$

results in

$$r_m \sim \frac{\dot m^{1/4}}{(\Delta P)^{3/8}\ (n)^{1/4}} \qquad (2\text{-}14)$$

or

$$r_m\ (\dot m_2,\ \Delta P_2,\ n_2) = r_m\ (m_1,\ \Delta P_1,\ n_1) \left(\frac{\dot m_2}{m_1}\right)^{1/4} \left(\frac{n_1}{n_2}\right)^{1/4} \left(\frac{\Delta P_1}{\Delta P_2}\right)^{3/8} \qquad (2\text{-}15)$$

Equation (2-15) describes how the mass median drop size changes with the flow rate (i.e., thrust level), injector pressure drop, and number of orifice.

(C) The one-dimensional vaporization rate-limited combustion model previously discussed was used to correlate the initial 250,000 lbf thrust test results with mass median drop size. Several drop sizes were input to the computer program with the first 250,000 lbf thrust chamber configuration tested (Lc = 36 inches, ϵ_c = 2.23 and L* = 70 inches). The experimental test results obtained during these tests (11 through 32) correlated with a mass median drop radius of 109μ (microns). Knowing that the $\dot m_1$, ΔP_1, and n_1 for the 250,000 lbf thrust engine result in a mass median drop radius ($\bar r_{m1}$) of 109μ, equation 2-15 was used to calculate the drop size ($\bar r_{m2}$ of 75μ) for the 50,000 lbf thrust engine ($\dot m_2$, P_2, and n_2). The vaporization rate-limited combustion model was then used to calculate the relationship between performance and chamber length for both the 250,000 lbf thrust engine (109μ) with 50,000 lbf thrust engine (75μ). These computed relationships are shown in Figure 2-3 along with experimental test results. The agreement between the performance computed from the combustion model and the actual experimental test results for both the 50,000 lbf and 250,000 lbf thrust engines demonstrates the capability of equation 2-15 to predict the injector characterization drop size for various engine sizes and the capability of the combustion model to determine the effect of chamber length on combustion performance for a given injector.

2.1.3.3 Application of Scaling Criteria to Original 250,000 lbf TCA

(U) The original 250,000 lbf thrust injector/chamber configuration (Appendix A) which was fired at the 50,000 lbf thrust level in 1967 and then used for facility checkout of 1-56, was based on values of injection parameters scaled from the LMDE injector. Thus, the pintle diameter is given by

$$D_p \simeq 0.4\sqrt{\dot W_t} \qquad (2\text{-}16)$$

and results in a pintle diameter of 12.75 inches. The number of oxidizer elements (primary orifices plus secondary orifices) is 36 which is identical to the LMDE injector. The oxidizer orifice spacing (W_p/UW) of approximately 0.40 is identical to that of the LMDE injector. The orifice shape, secondary oxidizer orifice setback and percentage of secondary oxidizer flow are also approximately the same as the LMDE injector.

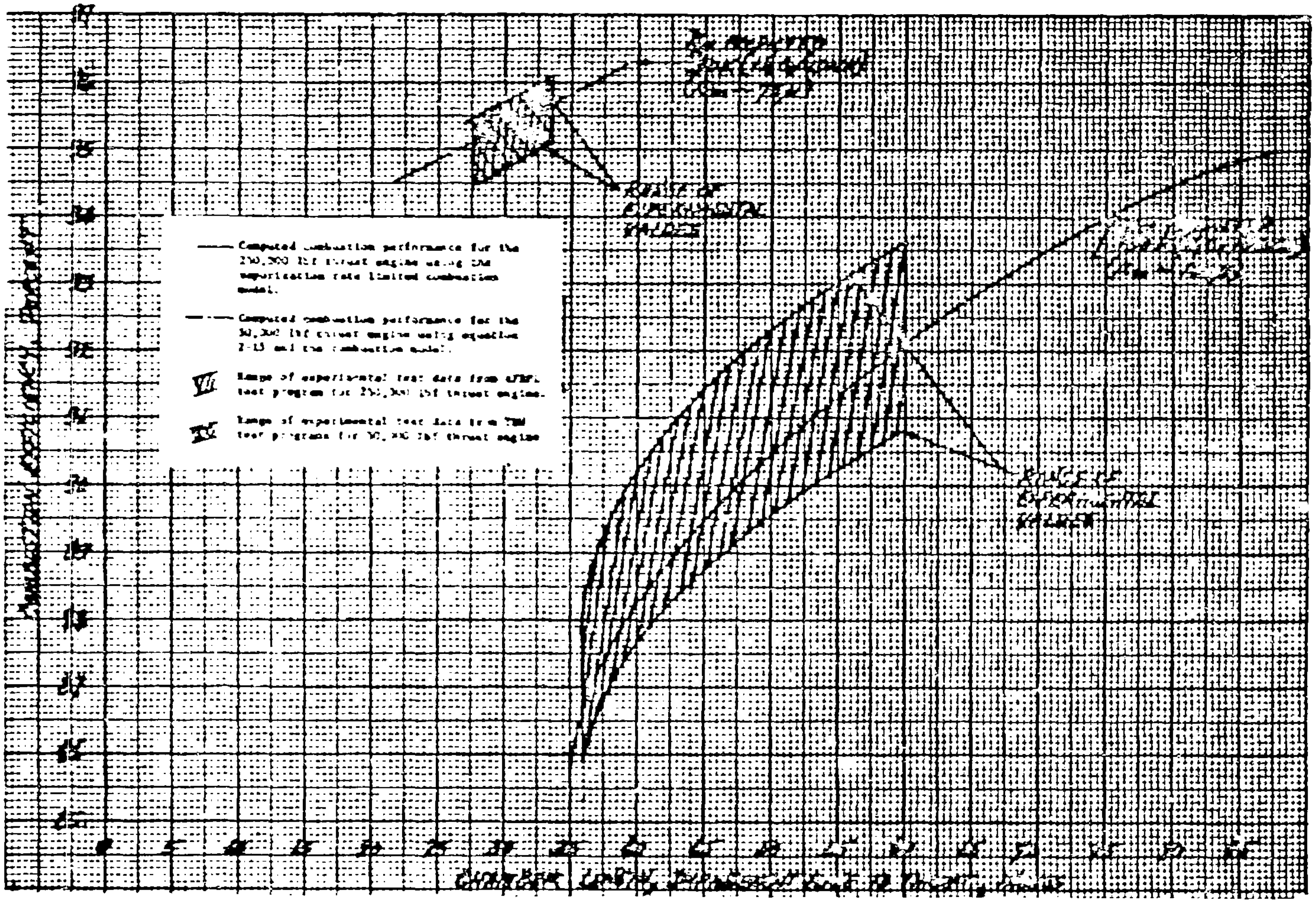

Figure 2-3. Correlation of Performance With Length (U)

(C) The initial fuel and oxidizer injection pressure drop levels specified were 35 psia and 140 psi, respectively, which corresponds to 25 psi and 105 psi for the LMDE injector. This pressure ratio selection would predict maximum performance at a mixture ratio of 1.60, or the normal operating mixture ratio for the LMDE.

(C The combustion chamber employed in the Facility Checkout Phase of Task I was sized on the basis of 300 psia at a throat diameter of 27.0 inches. The contraction ratio was $(39.0/27.0)^2$ or 2.09 which corresponds to the criteria given in 2.1.3.2. The original chamber length was 36.5 inches from the impingement plane to the throat which does not meet the L/D criteria. The original 250,000 lbf thrust TCA was fired only at 50,000 lbf and 60 psia at the TRW Systems Capistrano Test Site. Due to facility limitations the nozzle extension was limited to an expansion ratio of 2.0 at 20° divergence half-angle and the overall chamber length (impingement plane to throat) was limited to the 36.5 inches which is considerably shorter than predicted by the scaling criteria.

2.2 250,000 LB_F THRUST STATIC TEST ENGINE DESIGN

(U) The design of the 250,000 lb_f thrust static test engine is shown in Figure 2-4. This unit is comprised of two major assemblies - the centrally located, coaxial injector and the uncooled thrust chamber. The design is based on achieving the parameters shown in Table 2-1. Test durations are limited to 1.5 to 2.0 seconds which is sufficient time to establish the two primary objectives of the program; these objectives are the measurement of engine performance and the verification of injector stability.

(U) The design criteria, including propellant flows, calculated pressure drops, and predicted stress levels used in the development injector and thrust chamber design have been detailed in Appendix D. A summary of the stress analysis is presented in Table 2-2 for the injector and thrust chamber regions indicated in Figure 2-5. The stress analysis was based on a steady-state pressure of 600 psi in the injector and chamber with the engine at ambient temperature. The chamber will withstand 300 psi with a factor of safety of approximately 4 in all regions except at the weld connecting the long welding neck flange to the dome (Figure 2-5) where the factor of safety is 2.0.

(U) The thrust chamber was fabricated from United States Steel T-1 steel alloy in all areas except the long welding neck flange, which was ASTM A-181 carbon steel. The T-1 steel alloy was selected for use in the chamber because of its relatively high strength (approximately 100,000 psi yield strength) and low cost. The dome and plate sections of the chamber are 0.5 inches thick, except in the throat region, which has a minimum thickness of 0.8 inches. The allowable run duration at full thrust conditions is approximately 2.0 seconds to limit chamber throat erosion.

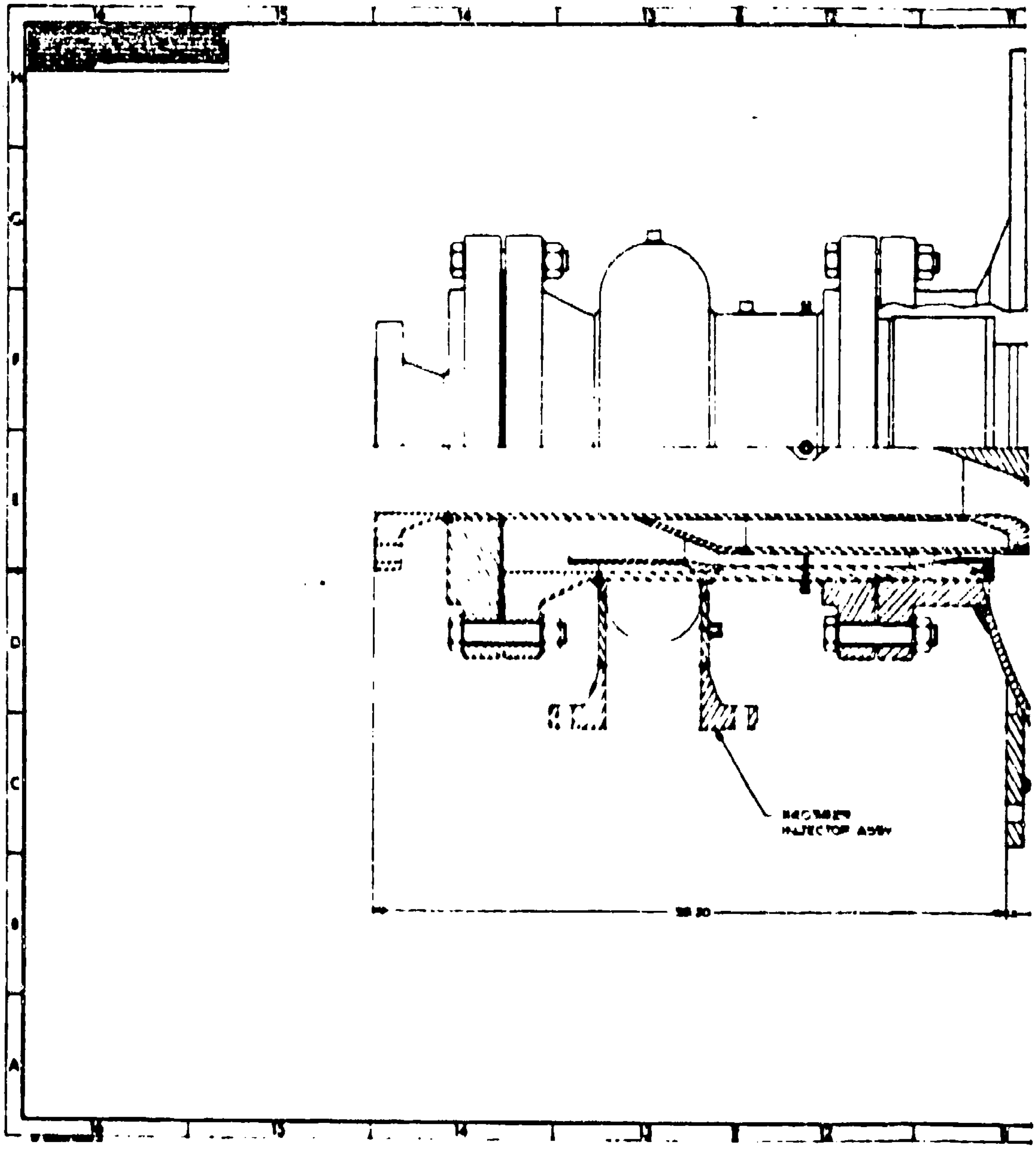
16
15
14
13
12
H
G
F
E
D
C
B
A
INJECTOR ASSY

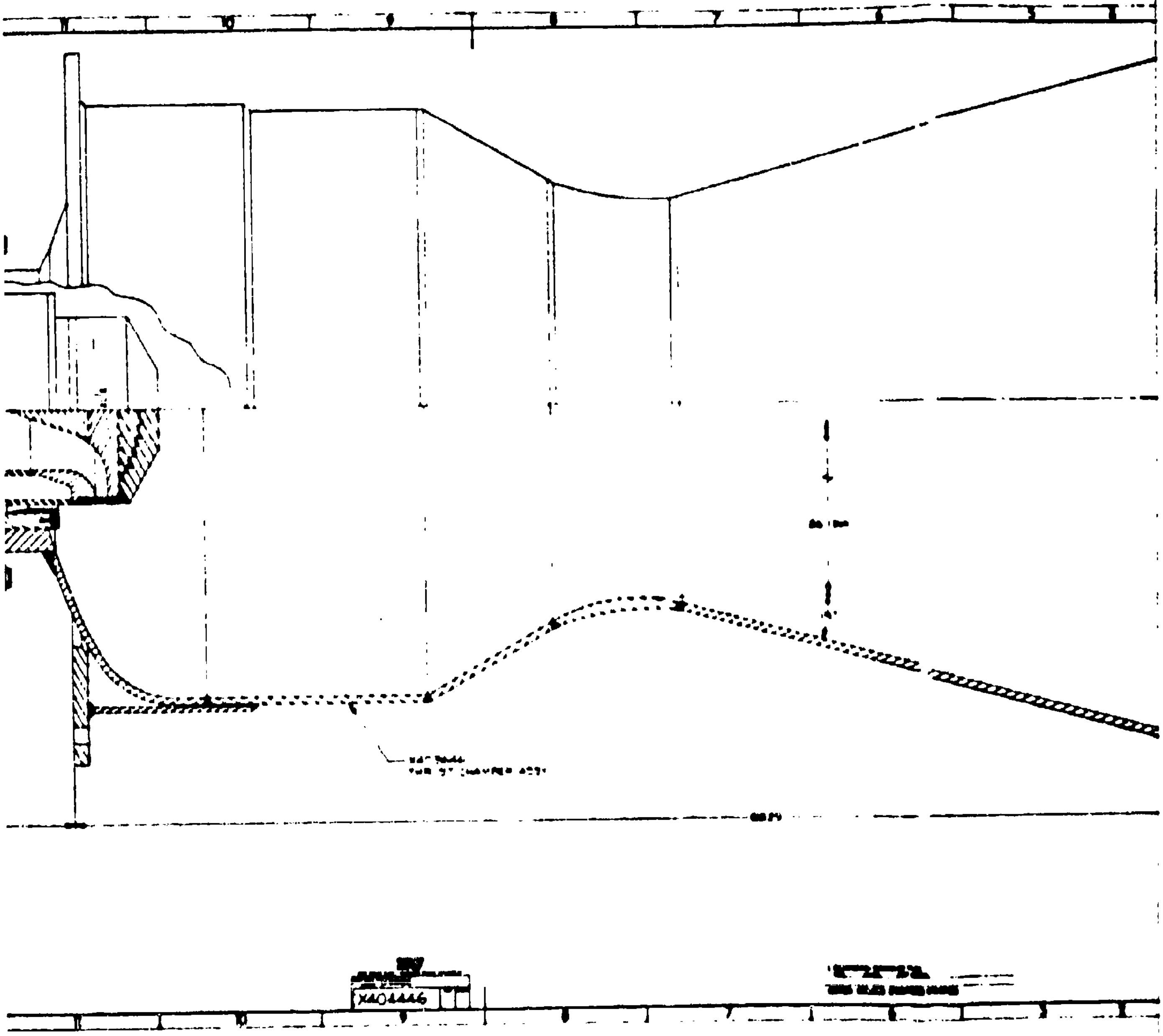

2

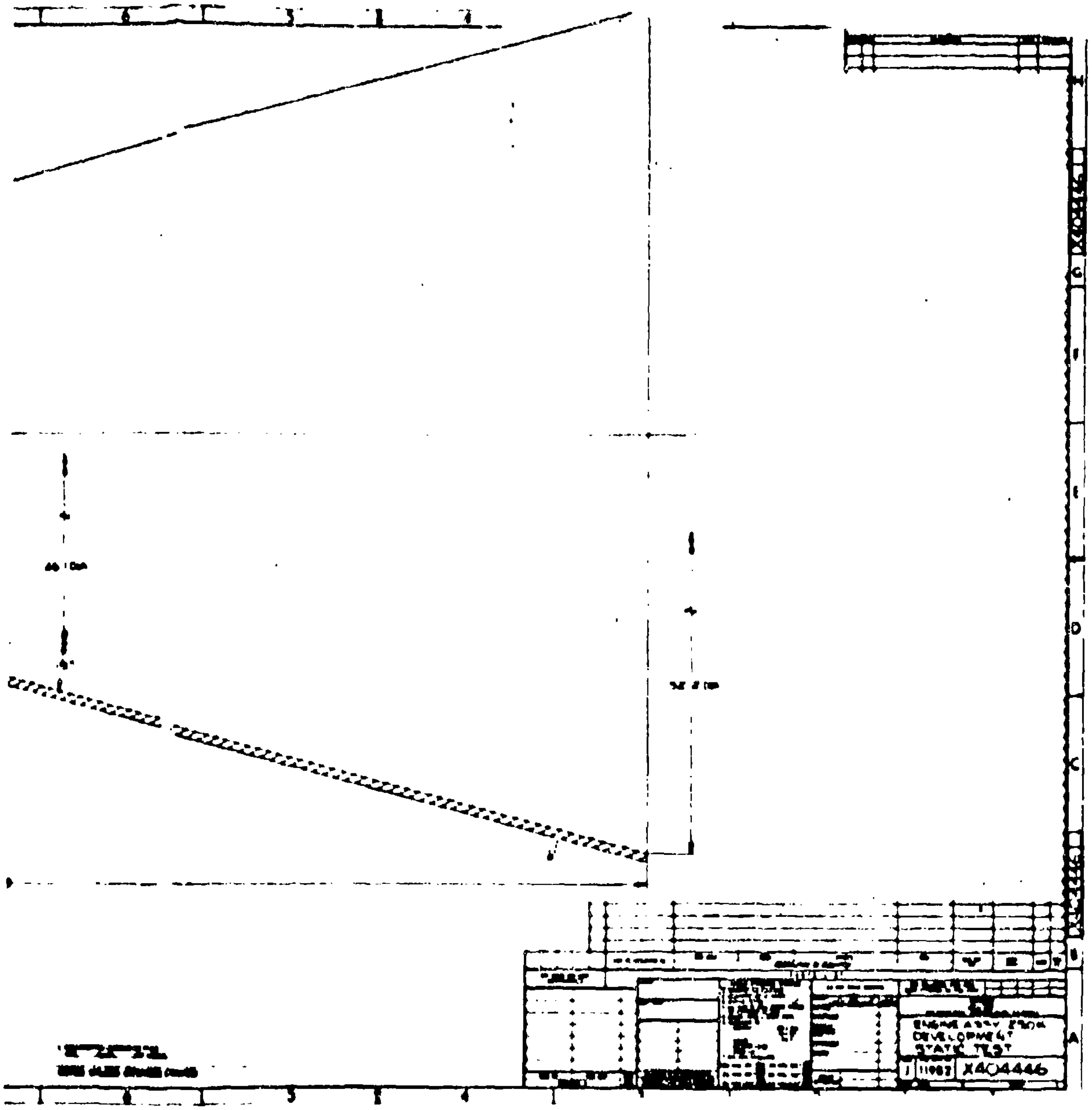
ENGINE ASSY ENGR
DEVELOPMENT
STATIC TEST
J
11982
X404446
H
G
F
E
D
C
B
A
6
5
4
3
2
1

(U) Figure 2-4. X404446 250,000 lbf Thrust Development Engine Assembly (U)

(C) Table 2-1. Static Test Engine Design Parameters (U)

F (vac), lb_f	-	250,000
P, psia	-	300
ϵ_e, A_e/A_t	-	4.0
ϵ_c, A_c/A_t	-	2.1
O/F,	-	2.60 (Nominal)
I_{sp} (vac), lb_f-sec/lb_m	-	283.3 (Theoretical Shifting Equil. @ O/F = 2.60)
η_{Isp}	-	0.90
C*, ft/sec	-	5596 (Theoretical Shifting Equil. @ O/F = 2.60)
η_{C*}	-	0.9375

Table 2-2. Static Test Engine Stress Analysis (U)

Section	Description	Material	Allowable Stress		Max. Calculated Stress Psi	Margin of Safety
			Ultimate Psi	Yield Psi		
1	Chamber Head Nozzle	A-181-II Steel	70,000	36,000	Rev. 1 15,500	3.50
2	Chamber Head	T-1 Steel	135,000	100,000	Rev. 1 67,400	1.00
3	Chamber	T-1 Steel	135,000	100,000	26,700	4.05
4	Chamber-Cone	T-1 Steel	135,000	100,000	27,400	3.93
5	Throat	T-1 Steel	135,000	100,000	14,000	8.65
6	Support Structure	T-1 Steel	135,000	100,000	-135,000	0*
7	Support Structure	T-1 Steel	135,000	100,000	-98,700	0.37*
8	Pintle Tip	A-212-B Steel	70,000	42,000	-25,300	1.76
9-14	ASME 300 psi Code Construction	A-181-II Flanges A-106-B Pipes				1.0
15	Pintle Shell	A-106-B	60,000	36,000	-30,000	1.0

*Due to thermal loads on chamber

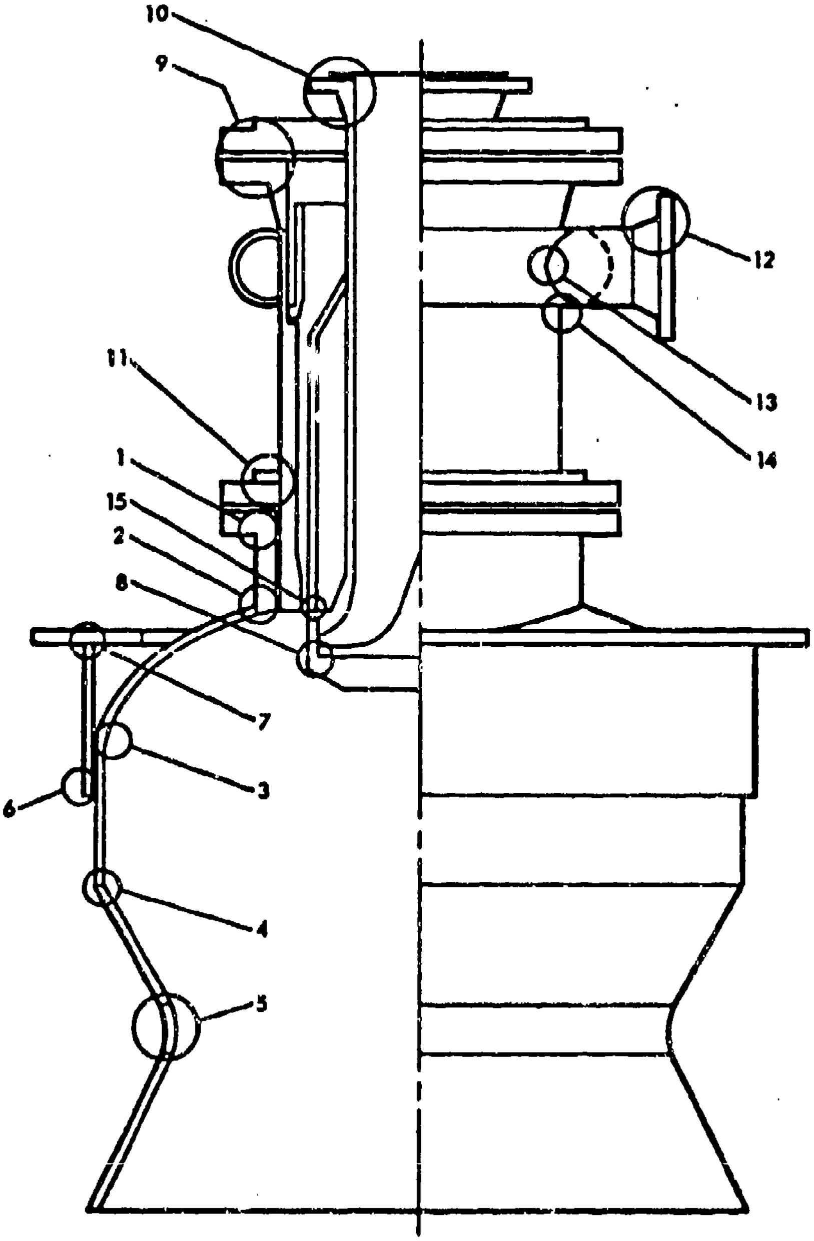
10
9
12
11
13
1
14
15
2
8
7
3
6
4
5

Figure 2-5. 250,000 lbf Thrust Test Engine - Stress Analysis Regions (U)

(U) The thrust mount consists of a skirt, welded to the cylindrical chamber section, which is welded to a ring containing the mounting hole bolt circle. This thrust mount configuration distributes the load uniformly. This type of thrust mount is also lower in cost than a bracket mount.

2.2.1 Engine Operation

(U) Combustion is initiated by opening an 8 inch facility oxidizer valve (propellant valves are not supplied with the TCA) so as to provide a positive oxidizer lead. Oxidizer enters the injector through an 8 inch diameter, 300 lb ASA, welding neck flange located on the injector centerline and flows through the oxidizer tube. The oxidizer flow is turned 90° by the contoured pintle tip and is injected radially through multiple orifices in the oxidizer orifice ring.

(U) Fuel enters the injector through a 6 inch diameter, 300 lb ASA, welding neck flange where it flows into a manifold fabricated from four 6 inch diameter, 90° elbows of schedule 80 pipe. The fuel flows through eight, 3 inch diameter, distribution orifices equally spaced around the outer fuel jacket into an internal plenum. Fuel is injected into the combustion chamber as a hollow cylindrical sheet; the fuel sheet impinges with the radial oxidizer streams approximately 2.5 inches from the fuel orifice. Since the propellants are hypergolic, combustion takes place upon contact of the fuel with the oxidizer.

(U) After 1.5 to 2.0 seconds of operation both facility propellant valves are closed and combustion ceases. The injector manifolds were then purged with gaseous nitrogen and the engine was ready for the next test firing.

2.3 COMPONENT DESIGN - DEVELOPMENT INJECTOR

(U) The design of the development injector assembly (X403829-1) is shown as Figure 2-6. (Figure 2-7 shows the injector during final assembly.) Oxidizer enters the injector through an 8 inch diameter, 300 lb ASA, welding neck flange located on the injector centerline and flows through the oxidizer tube X403829-6. The oxidizer flow is turned 90° by the contoured pintle tip, X403830-1 and is injected radially through both primary and secondary orifices. The pintle tip assembly (X404408), consisting of the pintle tip (X403830-1), oxidizer orifice ring, and ablative protection for the pintle tip was attached to the injector center body by means of a buttress thread. The pintle tip assembly was pinned to the center body to prevent rotation. Figure 2-8 is a photograph of the injector centerbody showing the buttress threads and machined fuel metering surface.

(U) Fuel enters the injector through a single 6 inch diameter, 300 lb ASA, welding neck flange where it flows into a manifold fabricated from four, 6 inch diameter, 90° elbows of schedule 80 pipe. Fuel flows through eight, 3 inch diameter distribution orifices equally spaced around the outer fuel jacket into an internal plenum created by the fuel jacket and the fuel sleeve. Fuel flows from this plenum into the annular opening created by

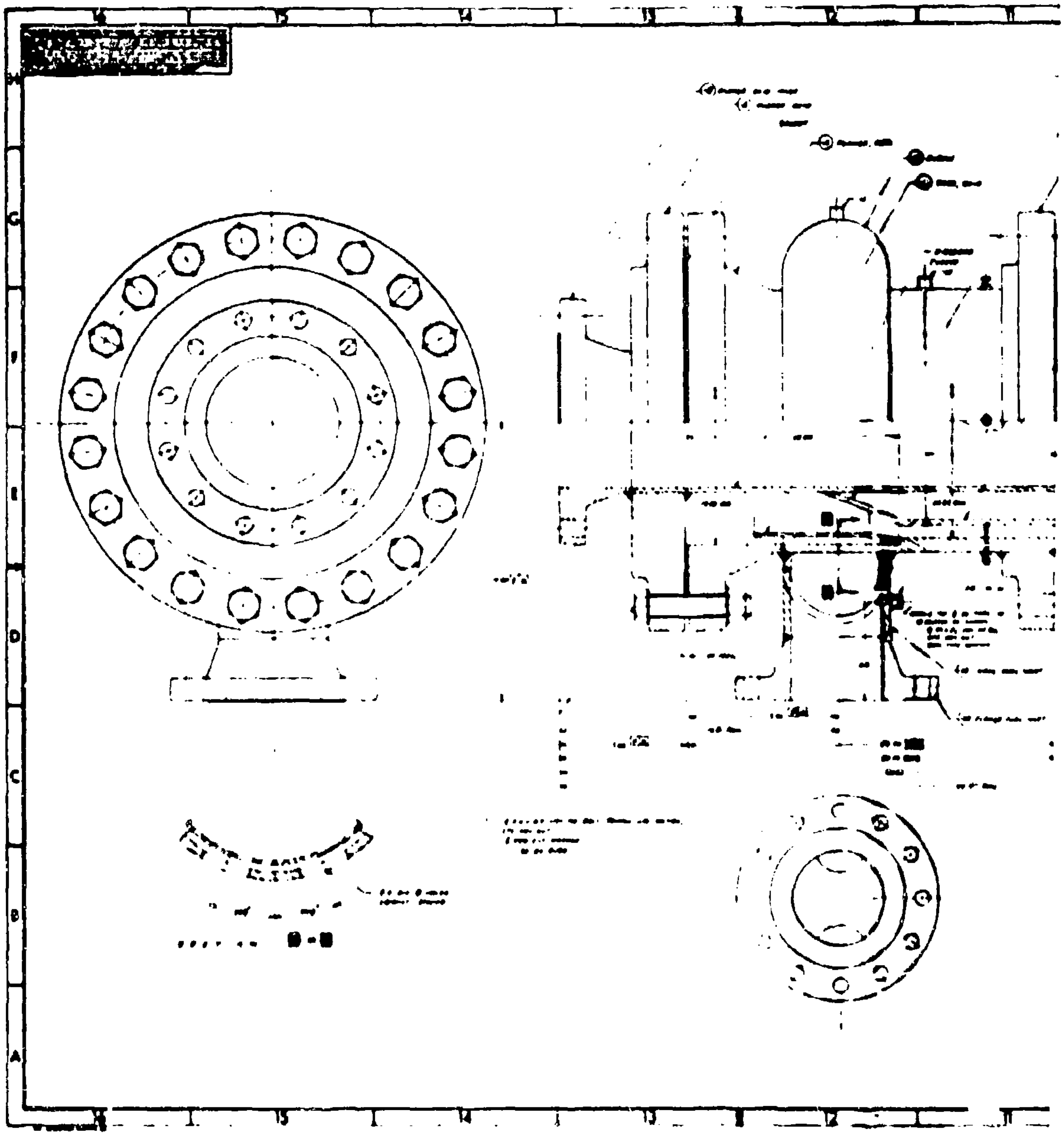
16
15
14
13
12
11
H
G
F
E
D
C
B
A

1

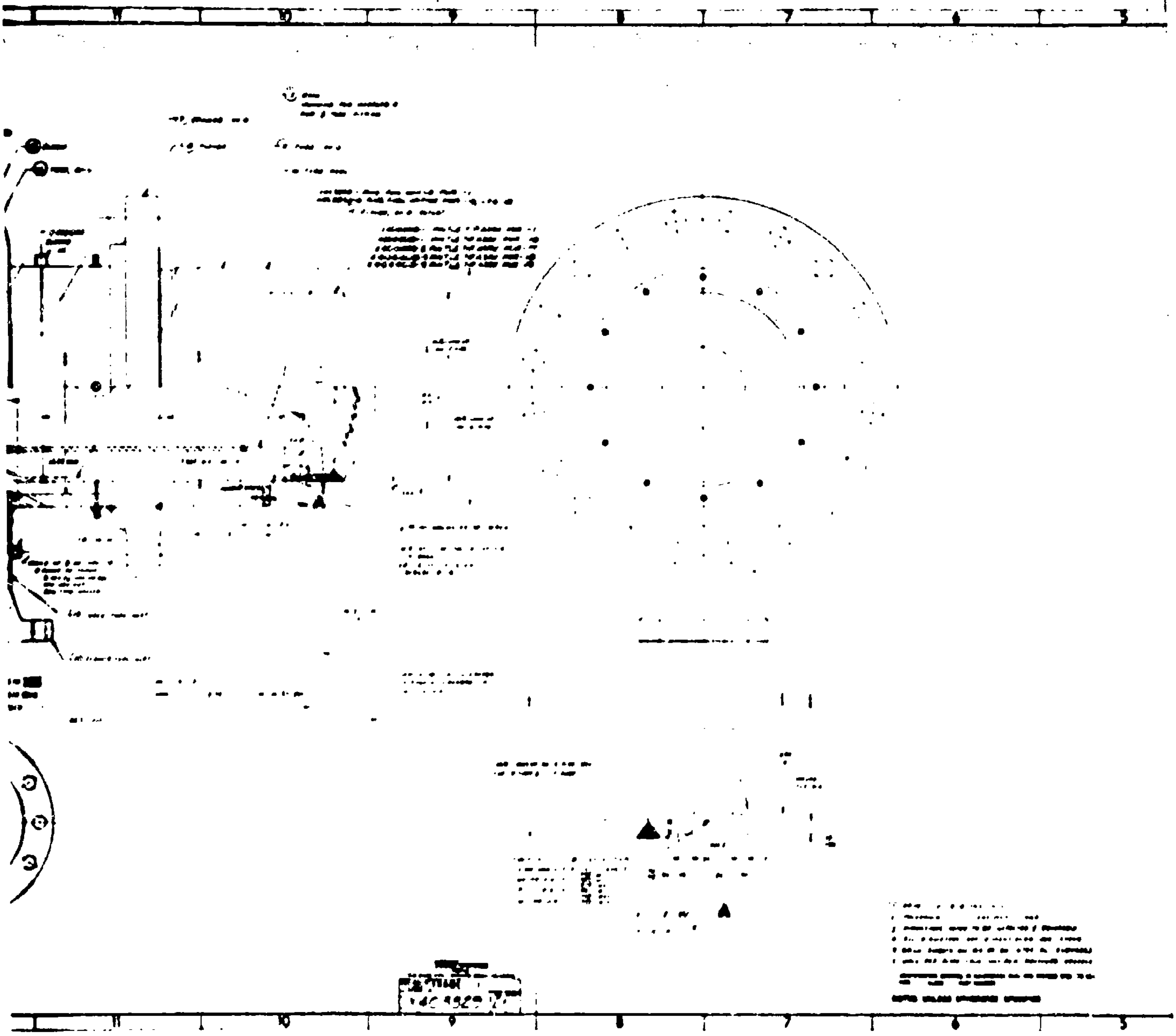
11
10
9
8
7
6
5
A
A
14C 8529

2

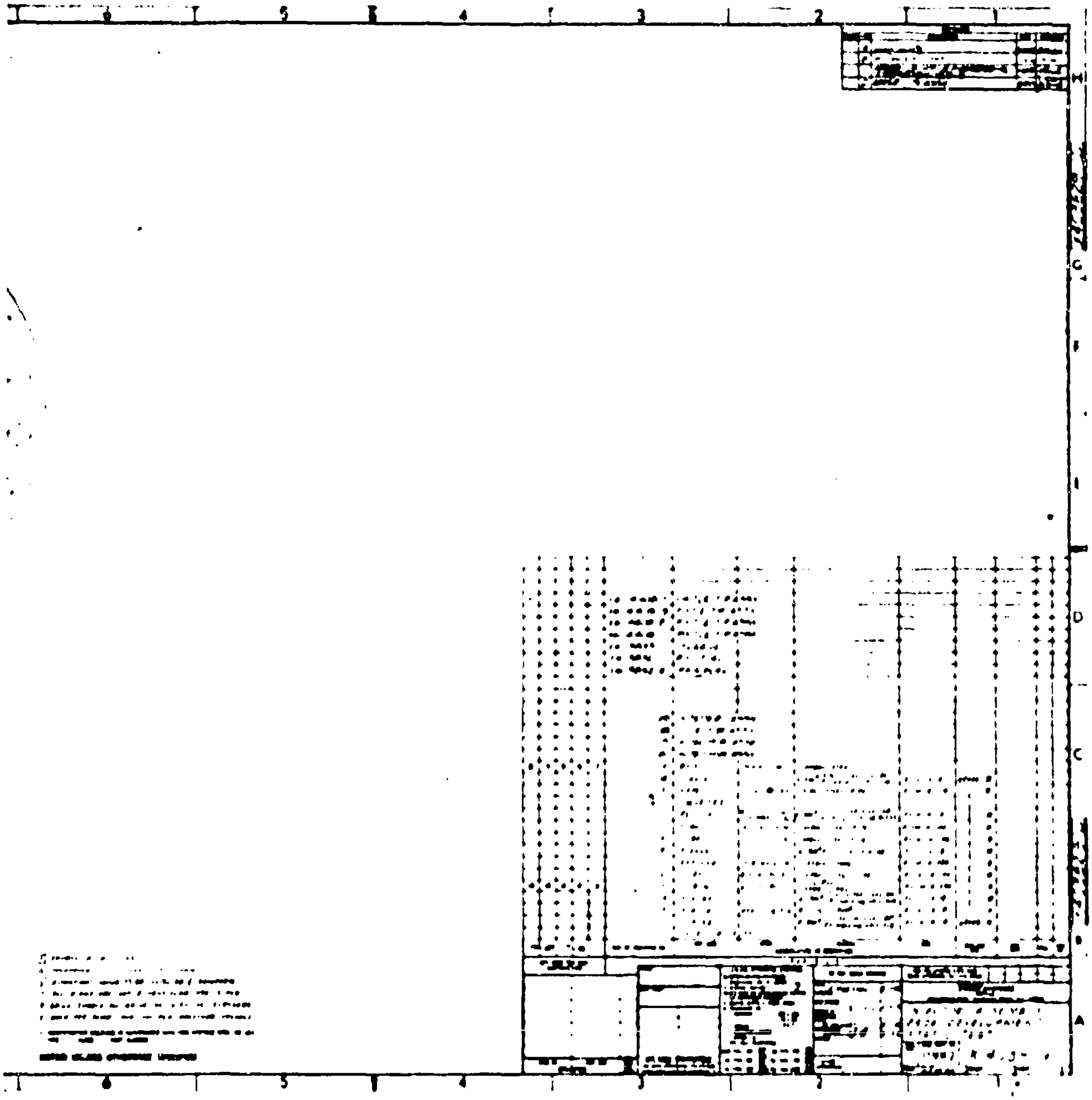
1
2
3
4
5
6
A
B
C
D
G
H

Figure 2-6. X403829 250,000 lb_f Thrust Development Injector Assembly (U)

Figure 2-7. 250,000 lb$_f$ Thrust Development Injector Assembly (U)

Figure 2-8. 250,000 lb$_f$ Thrust Development Injector Centerbody (U)

(U) the fuel jacket (Figure 2-9) and the injector centerbody. Fuel is injected into the combustion chamber as a hollow cylindrical sheet through the annular orifice created by the machined surface on the injector centerbody and the fuel metering orifice.

(U) The development injector design allowed rapid change of both fuel and oxidizer orifices without removing the injector from the test stand. Oxidizer orifices of 36 and 48 injection elements were evaluated during the injector development program. Table 2-3 gives a brief description of both the fuel and oxidizer orifices and the test series and firings on which they were used.

(U) The design criteria used for sizing the flow passages of the development injector is given as Appendix D.

2.3.1 Fuel Orifice

(U) Four fuel orifices (X403832) were fabricated during the course of the development program. The initial fuel orifice (X403832-3) was machined to provide a nominal annular fuel opening of 0.250 inch, ± .010 inch, when assembled into the X403829-1 development injector assembly. The clean-up diameter of the X403829-9 outer oxidizer tube was 12.733 inch while the I.D. of the initial fuel orifice ring (X403832-3) was 13.225 inch. The

(U) Table 2-3. Description of Fuel and Oxidizer Orifice Rings Used in Task I Injector Development (U)

Oxidizer Ring No.	Description	Areas	Test Series	Test Firings
01	36 elements 50% blockage	12.17 in^2 (pri) 1.44 in^2 (sec)	1, 2	11-17
01A	36 elements 60% blockage	13.16 in^2 (pri) 1.44 in^2 (sec)	3	18-23
01B	36 elements 60% blockage relocated secondary orifice	13.16 in^2 (pri) 1.74 in^2 (sec)	5	30-34, 37-39, 43,46
			8	101-102
02	48 elements 67% blockage	12.44 in^2 (pri) 1.36 in^2 (sec)	4	24-29 40-42
03	36 elements 67% blockage	12.68 in^2 (pri) 1.235 in^2 (sec)	6	35-36
05	36 elements 62% blockage flow straightener ring relocated secondary orifice	13.45 in^2 (pri) 1.45 in^2 (sec)	7	44-45
06	48 elements 60% blockage	12.341 in^2 (pri) 0.633 in^2 (sec)	9	108-110

Fuel Ring No.	Description	Areas	Test Series	Test Firings
F1	Annular orifice Fuel gap 0.246 in.	10.05 in^2	1	11-15
F2	Annular orifice Fuel gap 0.201 in.	8.05 in^2	2-7 8,9	16-46 101-102

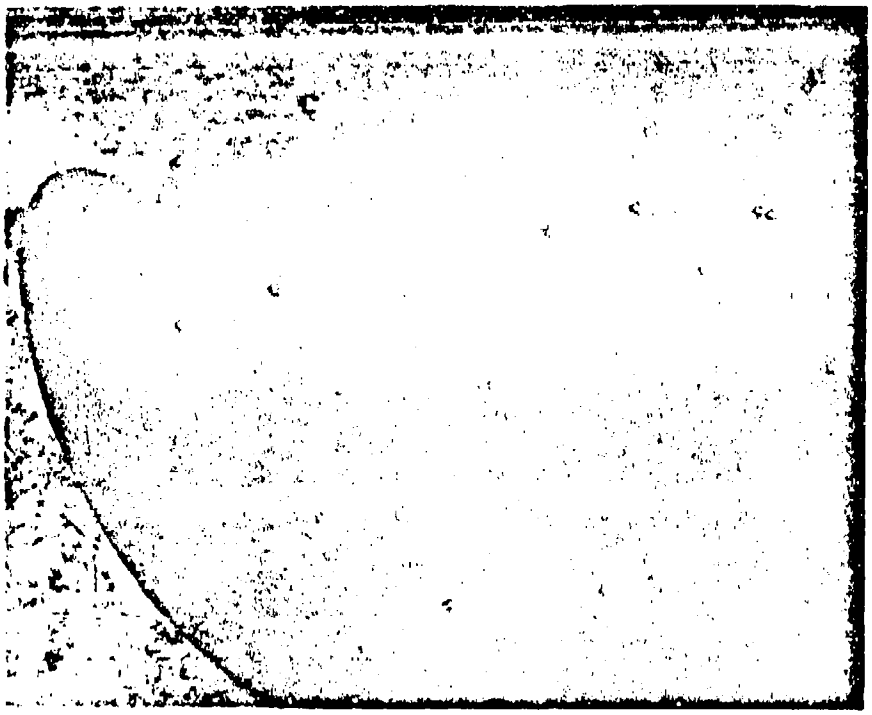

Figure 2-9. 250,000 lb_f Thrust Injector Fuel Jacket Assembly (U)

annular opening as measured prior to delivery of the development injector was 0.246, ± .001 inch. This resulted in a fuel injection area approximately 3 percent less than the design flow area. The X403832-3 fuel orifice ring was used on test firings 11-15, only.

(U) The second fuel orifice ring was machined to provide a nominal 0.200 inch annular opening. The X403832-4 fuel orifice ring I.D. was machined to a nominal 13.120 inch which resulted in an annular fuel opening of 0.201 inches at 7 of 8 places around the circumference of the opening. The eighth measurement indicated an opening of 0.197 inches. The X403832-4 fuel orifice ring was used on test firings 16-46, inclusive.

(U) Two additional fuel orifice rings (X403832-5) were fabricated and delivered to the AFRPL. These fuel orifice rings were finish machined with the exception of the I.D. which was left at the stock diameter of 12.876 inches.

2.3.2 Pintle Tip Assembly

(U) The pintle tip assemblies (X404408) were built up from the oxidizer orifice ring, X403830-1 pintle tip, and ablative material as required to form the configuration shown in Figure 2-10. Six pintle assemblies, consisting of five separate oxidizer orifice rings, were designed. In addition, the orifice ring employed in the X404408-1 assembly was modified on two

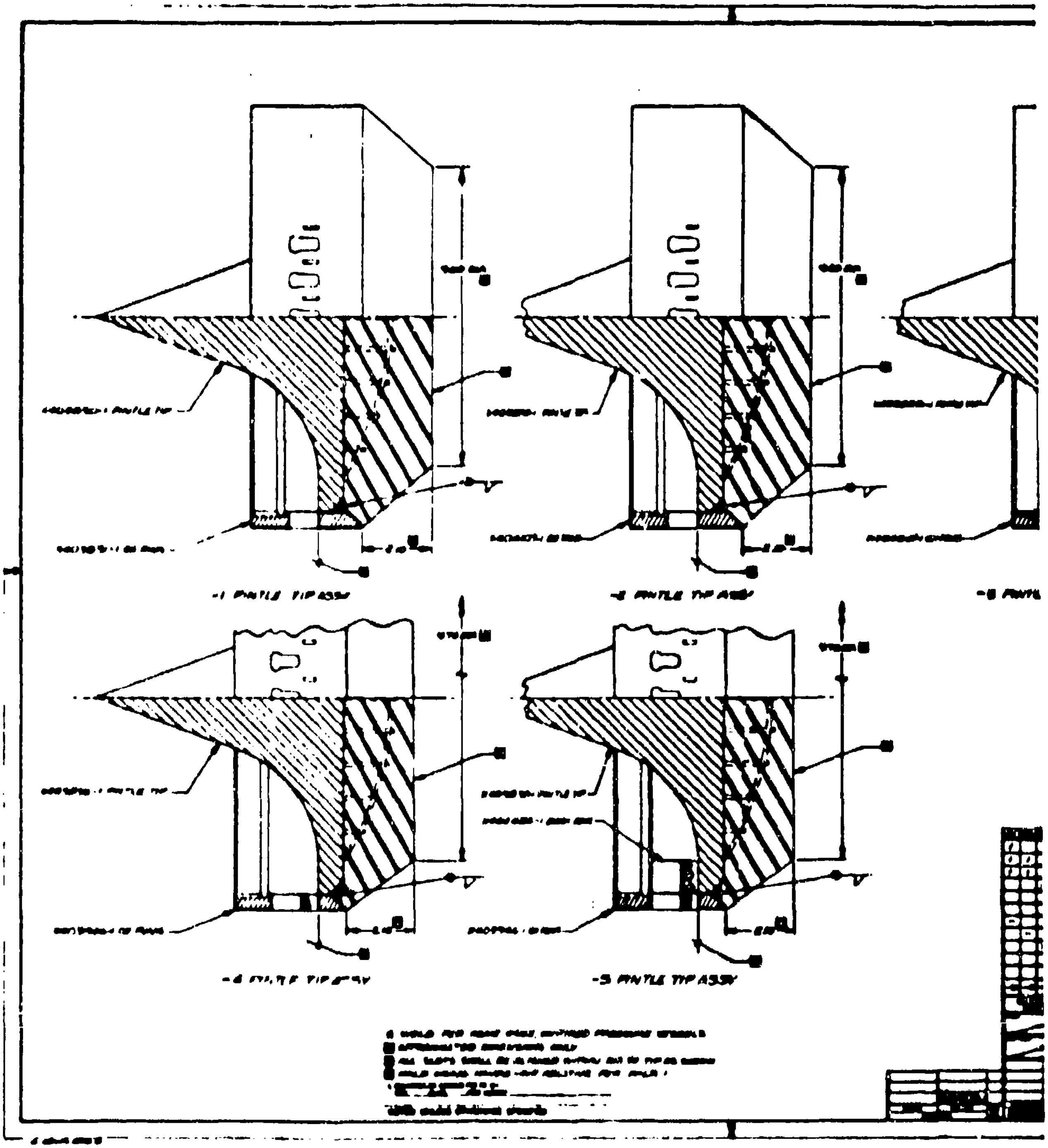
-1 PINTLE TIP ASSY
-2 PINTLE TIP ASSY
-3 PINTLE
-4 PINTLE TIP ASSY
-5 PINTLE TIP ASSY

Figure

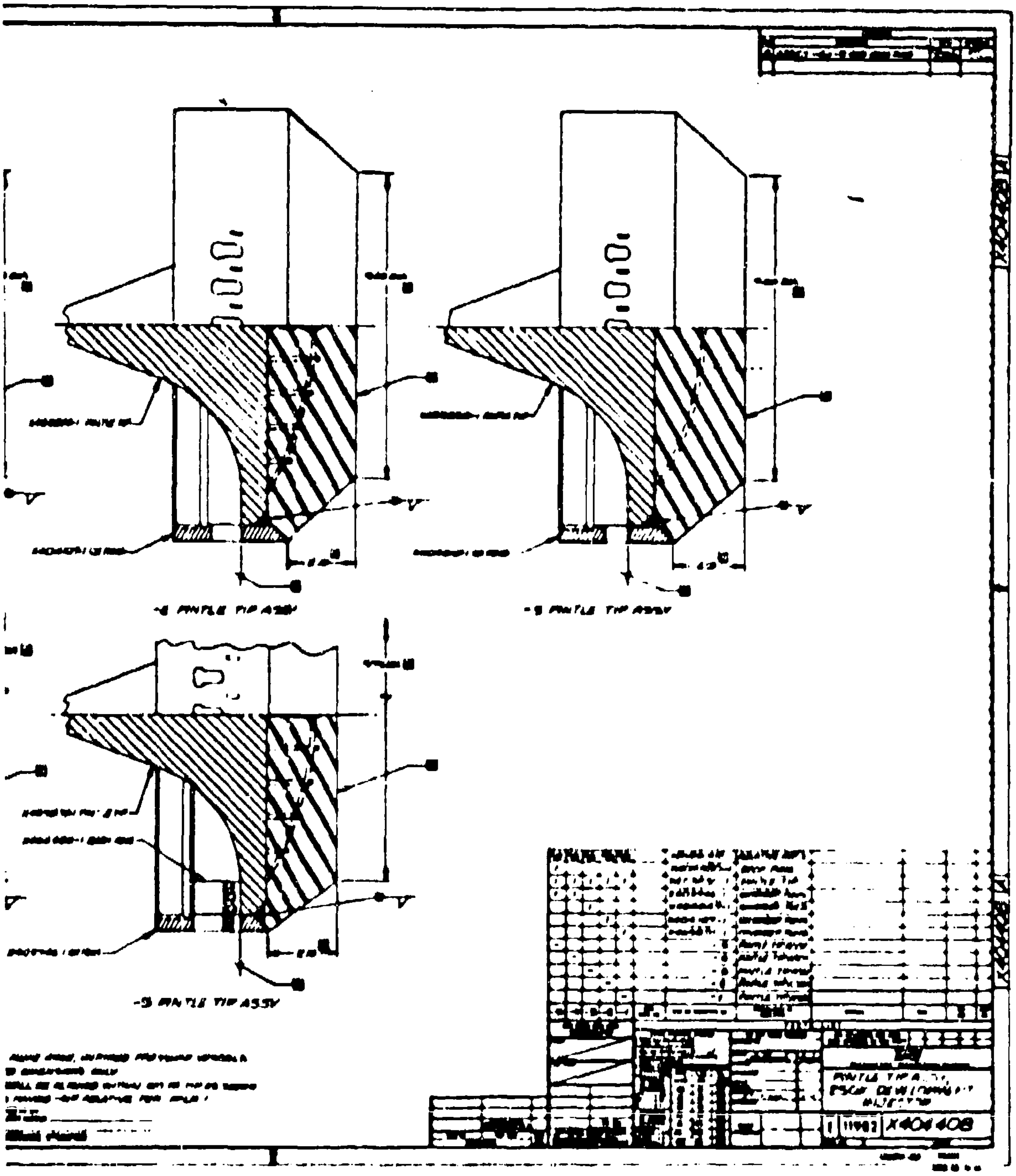
-6 PINTLE TIP ASSY
-5 PINTLE TIP ASSY
-3 PINTLE TIP ASSY
PINTLE TIP ASSY
X404408

Figure 2-10 250,000 lb_f Thrust Injector Pintle Tip Assemblies (U)

2

Figure 2-11 Initial Oxidizer and Fuel Orifice Rings (U)

(U) occasions. The oxidizer orifice ring configurations are described in the following sections. The initial oxidizer orifices were machined into the blank ring using conventional milling machine equipment. The additional three orifice configurations were machined into the blank rings by an electrical discharge machining (EDM) process. EDM produced more uniform, higher quality orifices at a reduced cost when compared with conventional milling of the orifices.

(U) Following delivery of the oxidizer orifice rings by the fabricator the X403831-1 pintle tip was welded to the orifice ring and the ablative protection was applied to the pintle tip. Haveg 41-F cement was used for all five pintle tip assemblies. Haveg 41-F cement is an asbestos-phenolic mixture which requires an acid catalyst to cause the mixture to set.

(U) Figure 2-11 is a closeup photograph of the initial pintle tip assembly (X404408-1) and fuel orifice ring (X403832-3) as assembled into the injector development assembly (X403829-1).

2.3.2.1 Oxidizer Orifice No. 1

(U) The initial replaceable oxidizer orifice ring which was fabricated for the development injector (X403829-1) was a 36 element configuration 01 (X403831-1, "A" change) as shown in Figure 2-12 This configuration was selected because it is nearly identical to oxidizer orifice configuration employed on the original TRW 250,000 lb_f thrust injector (X403666) which was used in the facility checkout firings (Tests 1-10) at the High Thrust Test Facility (1-56).

(U) The characteristics of the two oxidizer orifice configurations are shown in Figures 2-13a/2-13b and are tabulated in Table 2-4. As noted in Table 2-4 only one major change was made to the X403831-1 (01) oxidizer orifice ring when compared with the oxidizer orifice ring used in the original TRW 250,000 lb_f thrust injector. The only significant change made in the initial development injector oxidizer orifice ring was in the wall thickness of the orifice ring. The wall thickness was increased from 0.25 inch to approximately 0.50 inch to accommodate the American Standard Buttress thread which was used to make the orifice rings replaceable.

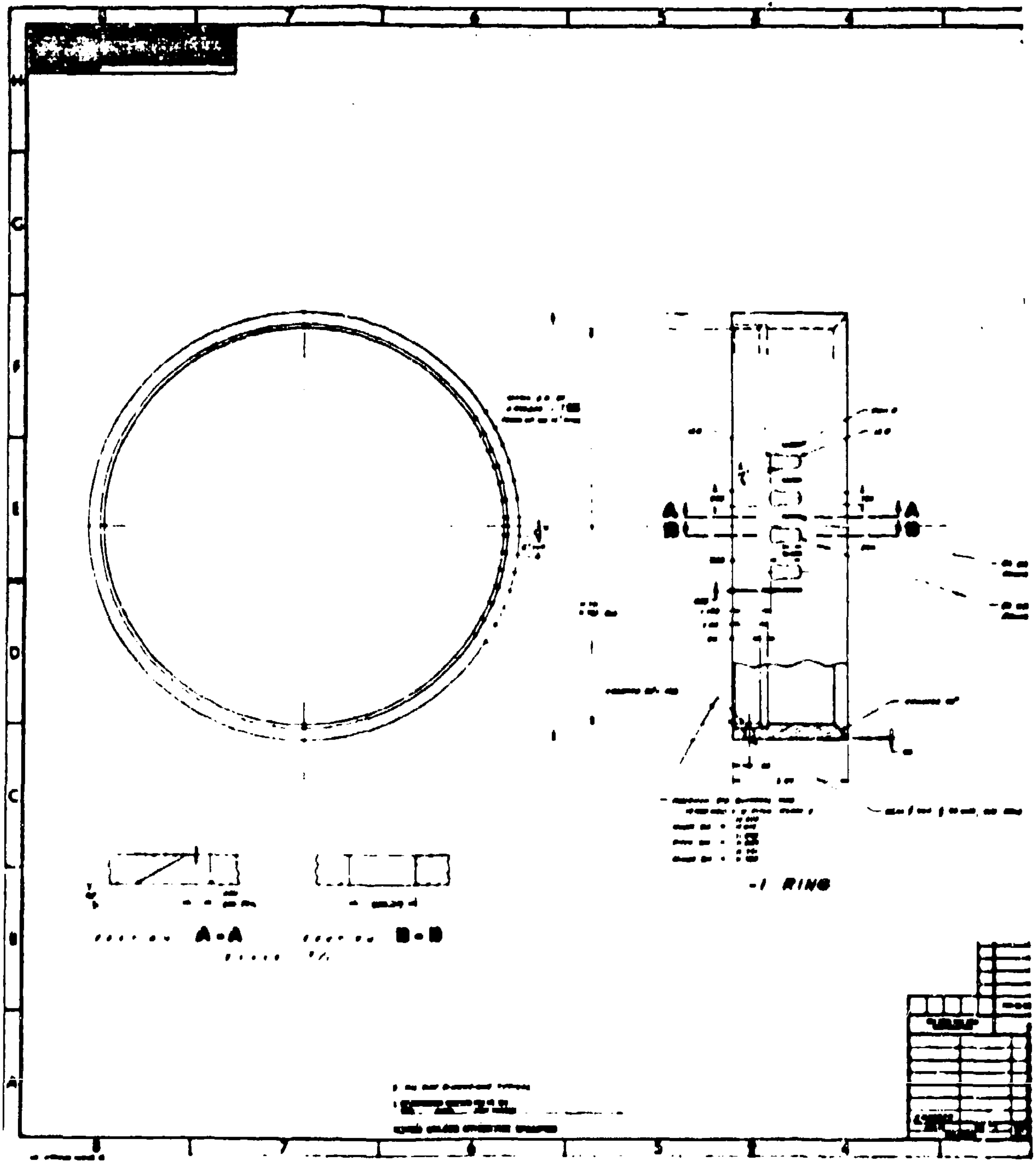
A
B
A
B
-1 RING
A-A
B-B

Fig

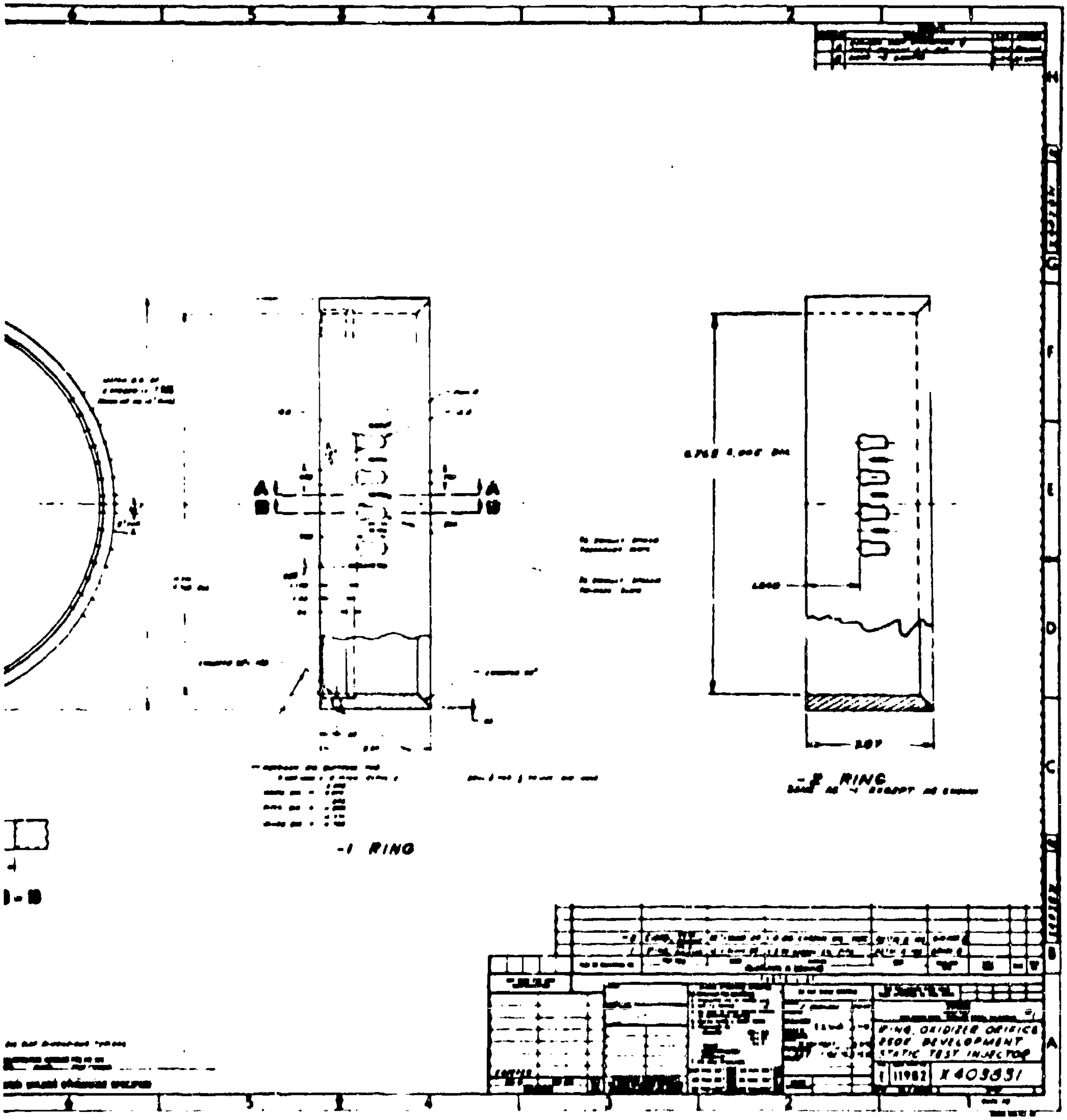
A
B
A
B
-1 RING
-2 RING
SAME AS -1 EXCEPT AS SHOWN
RING, OXIDIZER ORIFICE
250K DEVELOPMENT
STATIC TEST INJECTOR
11982
X403831

Figure 2-12 X403831 Ring, Oxidizer Orifice 250,000 lb_f Development Static Test Injector (U)

2

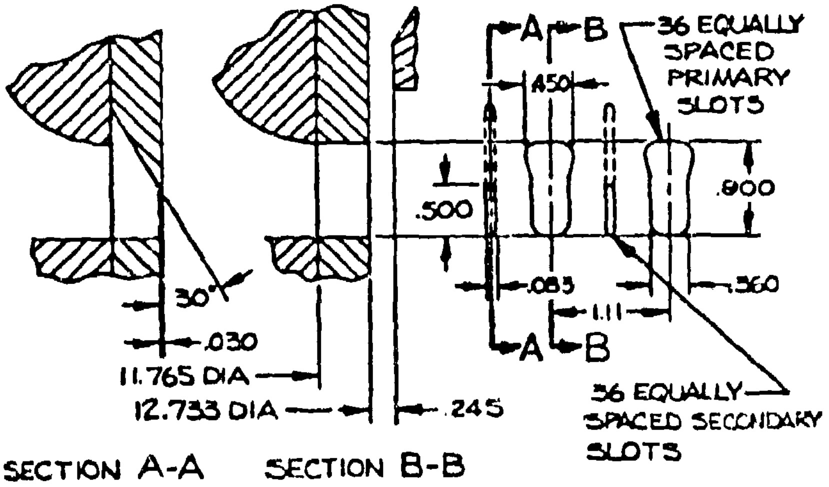
A
B
36 EQUALLY SPACED PRIMARY SLOTS
.450
.500
.900
.085
.360
1.11
A
B
30°
.030
11.765 DIA
12.733 DIA
.245
36 EQUALLY SPACED SECONDARY SLOTS
SECTION A-A
SECTION B-B

Figure 2-13a. Development Injector (01) Oxidizer Orifice Ring (U)

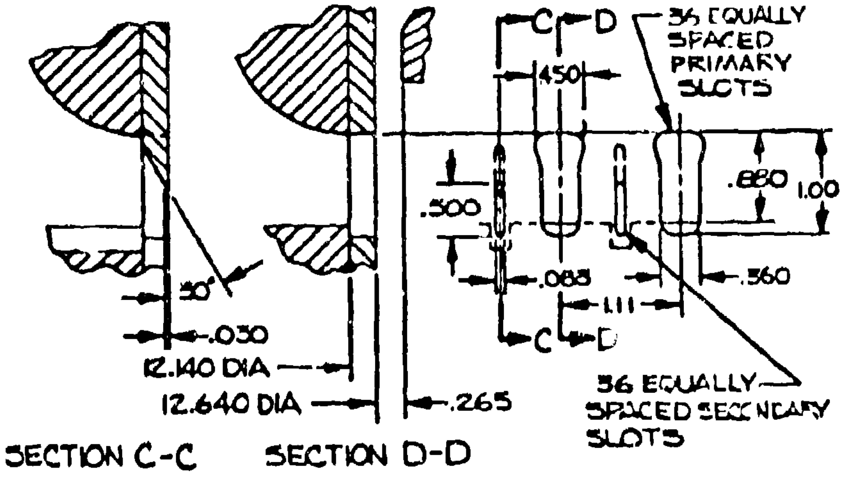
C
D
36 EQUALLY SPACED PRIMARY SLOTS
.450
.500
.880
1.00
.085
.360
1.11
C
D
30°
.030
12.140 DIA
12.640 DIA
.265
36 EQUALLY SPACED SECONDARY SLOTS
SECTION C-C
SECTION D-D

Figure 2-13b. Checkout Injector Oxidizer Orifice Ring (U)

Table 2-4 Initial Oxidizer Orifice Ring Characteristics (U)

	Checkout	01
Injection Area, A_{ot}, in^2	13.29	13.61
Primary Orifice, A_{op}, in^2	11.85	12.17
Secondary Orifice, A_{os}, in^2	1.44	1.44
Unit Width, UW, in.	1.10	1.11
Primary Orifice, W_p, in.	0.450	0.450
Secondary Orifice, W_s, in.	0.083	0.083
$UW-W_p$, in.	0.65	0.66
Space Factor, $W_p + W_s/UW \times 100\%$	48.5	48.1
Percent W_p, $W_p/UW \times 100\%$	40.9	40.5
Percent sec. flow, $A_{os}/A_{ot} \times 100\%$	10.82	10.58
Fuel Sheet Thickness, t_{fsh}, in.	0.265	0.245
$t_{fsh}/UW-W_p$	0.408	0.372
Secondary Orifice Setback, in.	0.500	0.400

(U) The orifices (36 primary plus 36 secondary) in the initial oxidizer orifice ring were machined into the blank ring using conventional milling operations. The measurement of the 72 individual orifices in the oxidizer orifice ring were made using "go/no go" gages. The measurements were then checked with venier calipers to ascertain the actual dimensions of all orifices. The measurement record is shown as Table 2-5. A total of seven out-of-tolerance measurements (out of 180 measurements) were observed. An estimate of the injection area change based on the actual measurements indicates an injection area one (1.0) percent greater than the design injection area (13.4 in^2).

(U) The predicted oxidizer injection ΔP for this initial configuration is shown in Figure 2-14 as a function of the volumetric flow rate. Actual test data for test firings 11-17 is also shown for comparative purposes. The oxidizer orifice ring was water-flowed at AFRPL. Two data points were taken; these are shown on the dashed line in Figure 2-14.

2.3.2.1.1 Modification A to Oxidizer Orifice No. 1

(U) The initial test firings with the X404408-1 Pintle Tip Assembly (X403831-1 "A" change, orifice ring) indicated excessive penetration. On 16 December 1968 a meeting was held at AFRPL to review the test results from test firings 11-17 and to investigate various means for modifying the

(U) Table 2-5. Measurement of X403831-1 Oxidizer Orifice Ring (U)

Orifice Number	a	b	c	d	Orifice Number	a	b	c	d
1	.893	.355	.500	.445	19	.900	.356	.499	.450
2	.897	.355	.500	.444	20	.901	.363	.499	.460
3	.915	.355	.500	.447	21	.900	.375	.509	.468
4	.905	.355	.500	.454 Fuel Inlet	22	.902	.363	.500	.459
5	.903	.357	.500	.453	23	.901	.357	.499	.462
6	.897	.363	.500	.455	24	.900	.357	.500	.459
7	.898	.357	.501	.448	25	.899	.353	.500	.455
8	.900	.360	.500	.454	26	.900	.356	.480	.452
9	.900	.359	.495	.451	27	.900	.355	.480	.459
10	.899	.361	.500	.455	28	.902	.355	.480	.464
11	.900	.359	.502	.459	29	.895	.363	.502	.450
12	.900	.353	.498	.463	30	.898	.362	.480	.450
13	.898	.360	.502	.456	31	.899	.363	.488	.451
14	.900	.356	.498	.455	32	.898	.363	.491	.453
15	.902	.355	.505	.455	33	.895	.363	.494	.450
16	.895	.353	.495	.450	34	.894	.361	.500	.448
17	.895	.356	.495	.452	35	.902	.358	.500	.447
18	.898	.360	.501	.451	36	.900	.357	.531	.448

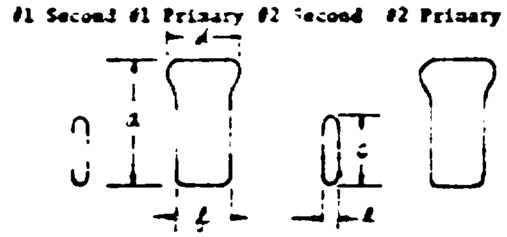

NOTE: Orifices are numbered clockwise looking toward oxidizer inlet.

"e" dimension passed "go/no-go" inspection gages on all orifices.

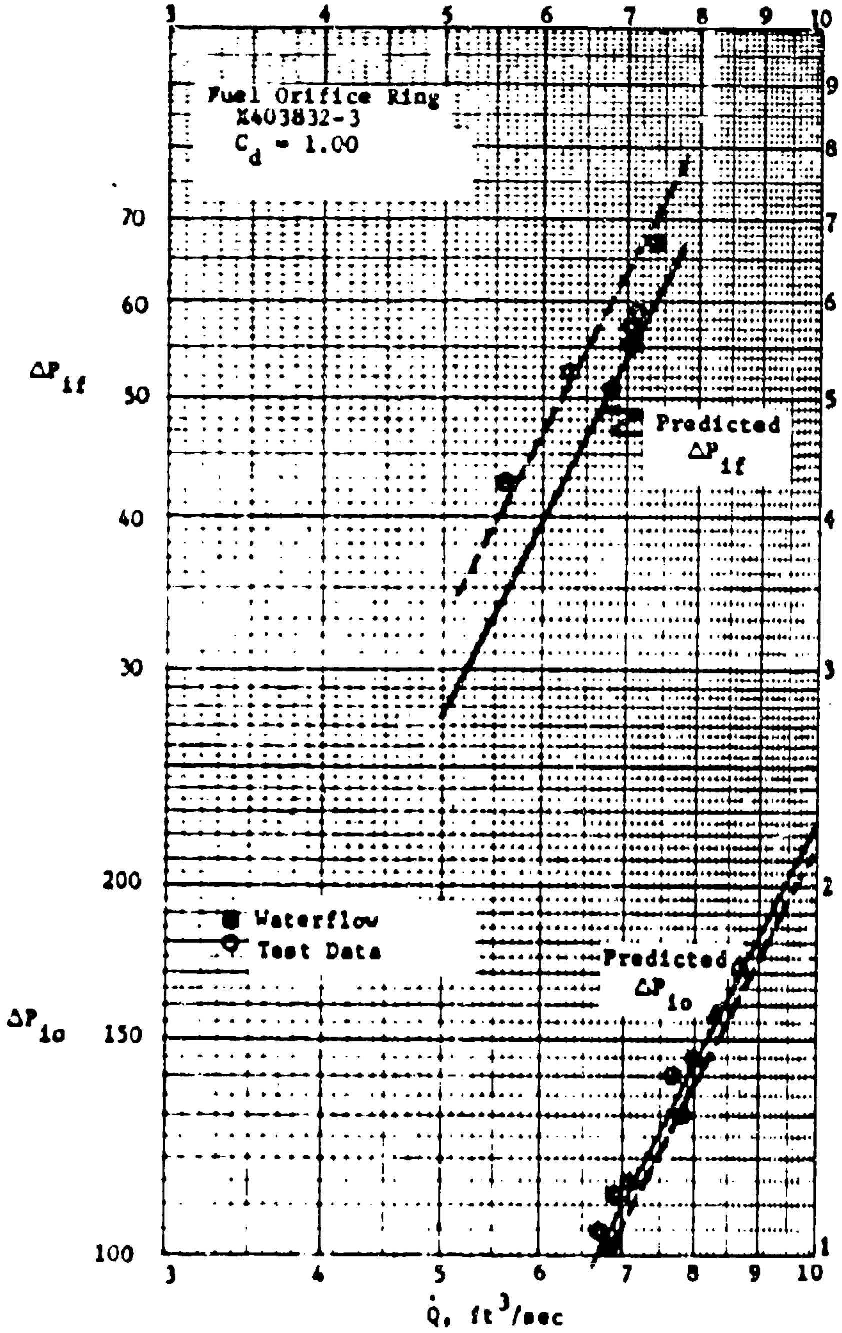

Figure 2-14. Predicted Injection Pressure Losses (O1/F1)(U)

(U) oxidizer orifice ring to increase the space factor $[(W_p + W_s)/UW \times 100\%]$ It was decided to rework only the primary orifices by increasing the W_p to 0.584 (from 0.450 inch) inch by using a 5/16 inch end mill as shown in Figure 2-15. This increased the total injection area to 14.60 in^2, an increase of 7.2 percent. The percentage of secondary flow decreased to 9.85 percent. This change decreased the $\Delta Po/\Delta Pf$ ratio, at the design conditions, from 2.15 to 1.85.

(U) The predicted oxidizer injection ΔP for this configuration, with the predicted fuel injection ΔP for the X403832-4 fuel orifice ring is shown in Figure 2-16 as a function of volumetric flow rate. Actual test data for test firings 18-23 is shown as the solid points on Figure 2-16.

2.3.2.1.2 Modification B to Oxidizer Orifice No. 1

(U) After test firing 23 the X404408-1 Pintle Tip Assembly (modified X403831-1 "A" change, orifice ring) was returned to TRW for rework of the secondary oxidizer orifices. The "B" modification to the X403831-1 oxidizer orifice ring consisted of lengthening the secondary orifices by 0.100 inches as shown in Figure 2-17. This modification increased the total injection area to 14.90 sq. inches, an increase of 2.0 percent. The percentage of secondary flow increased from 9.85 percent to 11.65 percent. This change permitted investigation of (1) the percentage of secondary flow (Item 2, page 2-2) and (2) location of secondary oxidizer orifices (Item 5, page 2-2).

2.3.2.2 Oxidizer Orifice No. 2

(U) One of the major injector parameters to be investigated in the injector development program was the number of oxidizer elements. A 48 element oxidizer orifice ring (48 primary plus 48 secondary orifices) was designed (TRW X404107) and fabricated. This design is shown as Figure 2-18. Based on data from test firings 11-17 only, the space factor $(W_p + W_s/UW \times 100\%)$ was increased to 67.2 percent, as compared to 48.5 percent for the original replaceable oxidizer orifice ring. Pertinent characteristics of the number 2 oxidizer orifice configuration are tabulated as Table 2-6. The characteristics of the X403831-1 oxidizer orifice ring are shown for comparison.

(U) The orifices (48 primary plus 48 secondary) in the X404107-1 "A" change oxidizer orifice ring were machined into the blank ring using electrical discharge machining. Two EDM passes were used on each orifice. On the primary orifices a roughing pass was first made; the electrode was then dressed off and a final pass made through the orifice. The finish pass electrode was then used as the roughing electrode for the next orifice. The secondary orifices were machined using EDM as described in Section 2.3.2.1.2. The individual orifices were measured using vernier calipers. The uniformity of the 96 individual orifices is apparent in the tabulation of the engineering measurements shown in Table 2-7. The indicated oxidizer injection area is less than one-half percent greater than the design injection area.

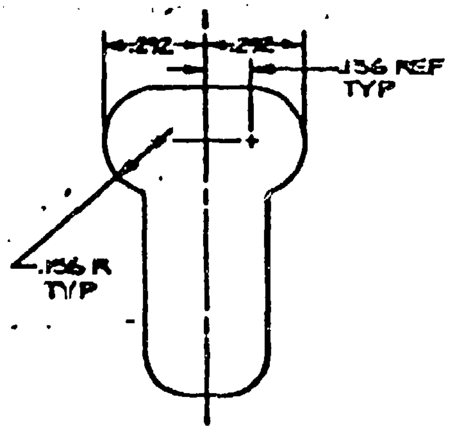
.292
.292
.156 REF
TYP
.156 R
TYP

Figure 2-15. Modification "A" to X403831-1 (U)

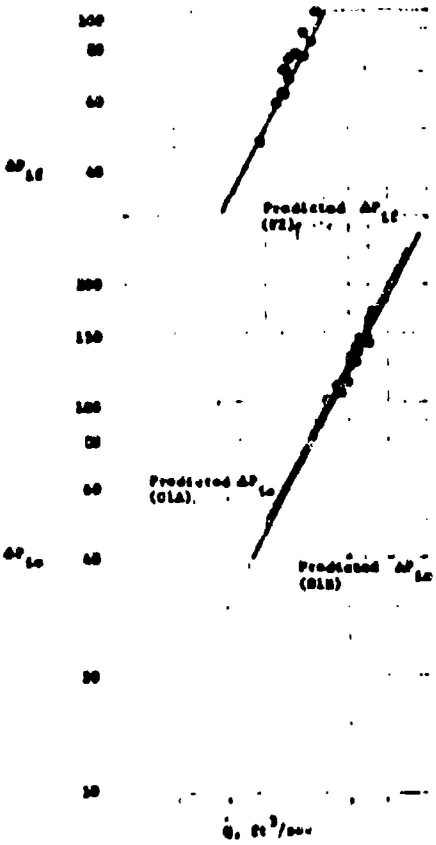

Figure 2-16. Predicted Injection Pressure Losses (01A/F2 - 01B/F2) (U)

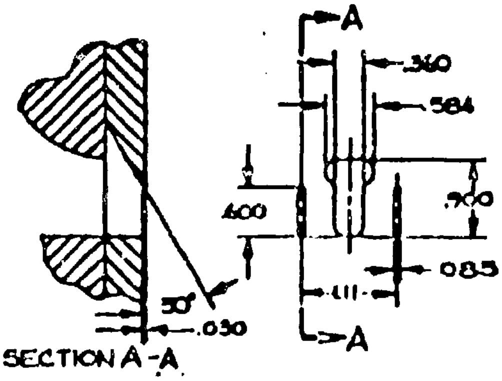
A
.360
.584
.400
.900
.085
.111
A
30°
.030
SECTION A-A

Figure 2-17. Modification "B" to X403831-1 (U)

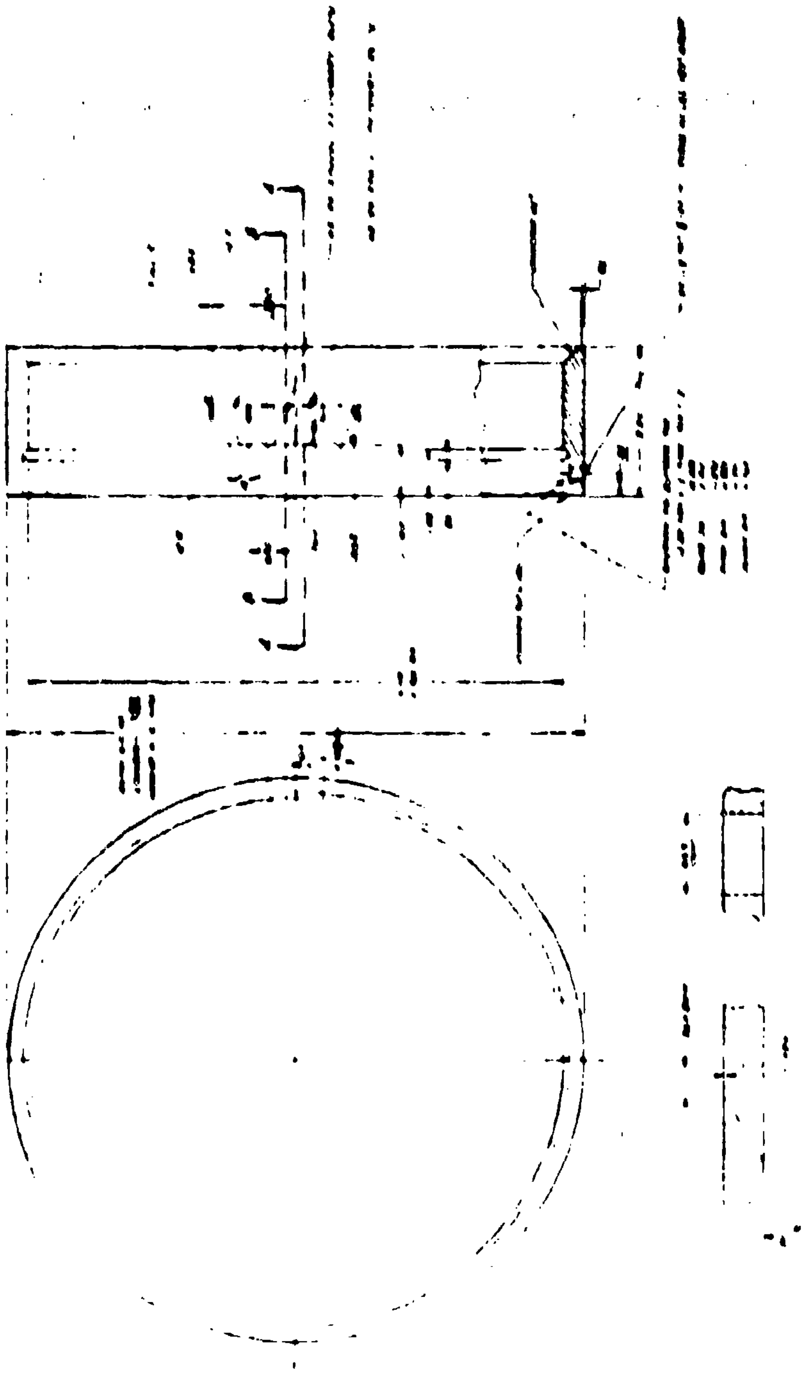

Figure 2-18. Oxidizer Orifice Ring (O2) (U)

Table 2-6. Characteristics of Oxidizer Orifice Ring 2 (U)

	01	02
Injection Area, A_{ot}, in^2	13.61	13.80
Primary Orifice, A_{op}, in^2	12.17	12.44
Secondary Orifice, A_{os}, in^2	1.44	1.36
Unit Width, UW, in.	1.11	0.830
Primary Orifice, W_p, in.	0.450	0.475
Secondary Orifice, W_s, in.	0.083	0.083
UW-W_p, in.	0.66	0.355
Space Factor, (W_p + W_s/UW x 100%)	48.1	67.2
Percent W_p, (W_p/UW x 100%)	40.5	57.2
Percent Sec. Flow, A_{os}/A_{ot} x 100%	10.58	9.85
Fuel Sheet Thickness, t_{fsh}, in.	0.245	0.201
t_{fsh}/UW-W_p	0.372	0.565
Secondary Orifice Setback, in.	0.400	0.305

(U) The predicted oxidizer injection ΔP for this configuration is shown in Figure 2-19 as a function of the volumetric flow rate. This ring was assembled into the X404408-2 Pintle Tip Assembly, Figure 2-20, and fired in conjunction with the X403832-4 fuel orifice ring on test firings 24-29 and 40-42. Actual injection pressure losses recorded during these firings are shown on Figure 2-19 for comparative purposes.

2.3.2.3 Oxidizer Orifice No. 3

(U) The third oxidizer orifice configuration fabricated and tested was the X404047-1 "A" change shown as Figure 2-21. This configuration is a 36 element configuration (36 primary plus 36 secondary orifices) with the same space factor (W_p + W_s/UW x 100%) as the No. 2 oxidizer orifice configuration to allow a direct comparison with the test results obtained with the 48 element configuration (X404107-1). Pertinent characteristics of the number 3 oxidizer orifice configuration are tabulated as Table 2-8.

(U) The orifices (36 primary plus 36 secondary) were machined into the blank ring using electrical discharge machining using procedures identical to those described in Section 2.3.2.2. Figure 2-22 is a photograph of the finished part prior to assembly into the X404408-3 Pintle Tip Assembly. The individual orifices were measured using vernier calipers. A tabulation of engineering measurements for the individual orifices is shown in Table 2-8. The indicated oxidizer injection area is approximately one-half percent less than the design injection area.

(U) Table 2-7. XA04107 "A" Oxidizer Orifice Ring Measurements (U)

Orifice Number	A	B	B-1	C	D
1	0.667	0.382	0.476	0.083	0.360
2	0.667	0.381	0.476	0.083	0.358
3	0.668	0.382	0.476	0.083	0.356
4	0.667	0.382	0.473	0.084	0.357
5	0.667	0.382	0.476	0.084	0.360
6	0.668	0.381	0.475	0.084	0.362
7	0.667	0.381	0.476	0.085	0.362
8	0.668	0.383	0.475	0.084	0.361
9	0.668	0.381	0.475	0.084	0.362
10	0.668	0.382	0.475	0.081	0.361
11	0.668	0.382	0.475	0.081	0.363
12	0.668	0.383	0.475	0.081	0.362
13	0.668	0.381	0.475	0.085	0.363
14	0.668	0.383	0.476	0.084	0.358
15	0.670	0.381	0.475	0.085	0.356
16	0.668	0.381	0.475	0.085	0.357
17	0.668	0.382	0.476	0.086	0.358
18	0.666	0.383	0.476	0.081	0.358
19	0.668	0.383	0.476	0.084	0.358
20	0.666	0.383	0.475	0.084	0.357
21	0.668	0.383	0.475	0.084	0.362
22	0.666	0.384	0.475	0.085	0.358
23	0.666	0.383	0.475	0.086	0.358
24	0.666	0.384	0.477	[illegible]	0.362
25	0.668	0.384	0.478	0.086	0.362
26	0.667	0.384	0.476	0.084	0.362
27	0.668	0.384	0.477	0.083	0.360
28	0.668	0.383	0.477	0.083	0.360
29	0.667	0.384	0.476	0.082	0.360
30	0.667	0.383	0.475	0.083	0.359
31	0.668	0.384	0.475	0.083	0.360
32	0.668	0.384	0.476	0.083	0.357
33	0.668	0.385	0.476	0.083	0.358
34	0.668	0.383	0.476	0.084	0.358
35	0.668	0.385	0.476	0.083	0.358
36	0.668	0.385	0.477	0.083	0.360
37	0.668	0.383	0.476	0.083	0.359
38	0.668	0.384	0.477	0.083	0.361
39	0.668	0.384	0.476	0.083	0.361
40	0.667	0.384	0.476	0.083	0.360
41	0.668	0.384	0.476	0.083	0.360
42	0.668	0.383	0.476	0.083	0.360
43	0.668	0.383	0.475	0.083	0.361
44	0.668	0.383	0.475	0.083	0.361
45	0.667	0.383	0.475	0.083	0.361
46	0.667	0.382	0.476	0.083	0.360
47	0.667	0.382	0.476	0.083	0.360
48	0.668	0.382	0.475	0.083	0.360

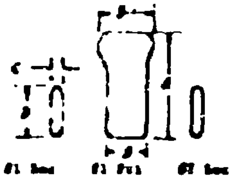

Required dimensions

"A" - .663 ± .010
"B" - .380 ± .010
"B1" - .475 ± .010
"C" - .081 ± .010
"D" - .360 ± .010

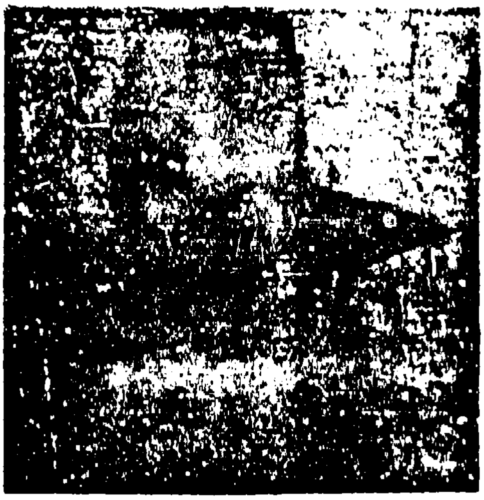

Figure 2-21. X404408-2 Pintle Tip Assembly (Photo 77009-69 (U)

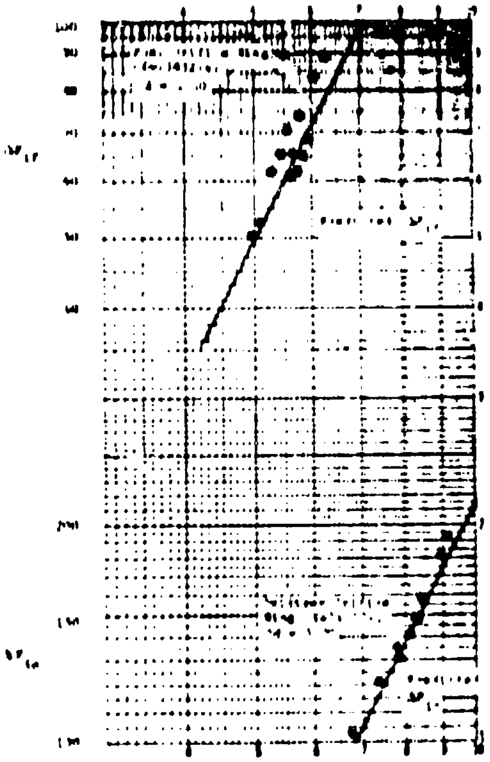

Figure 2-19. Predicted Injection Pressure Losses (O2/F2) (U)

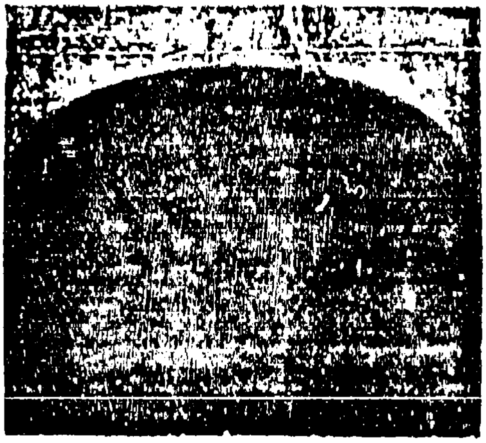

Figure 2-22 X404047-1 Oxidizer Orifice Ring (O2)(Photo 77116-69) (U)

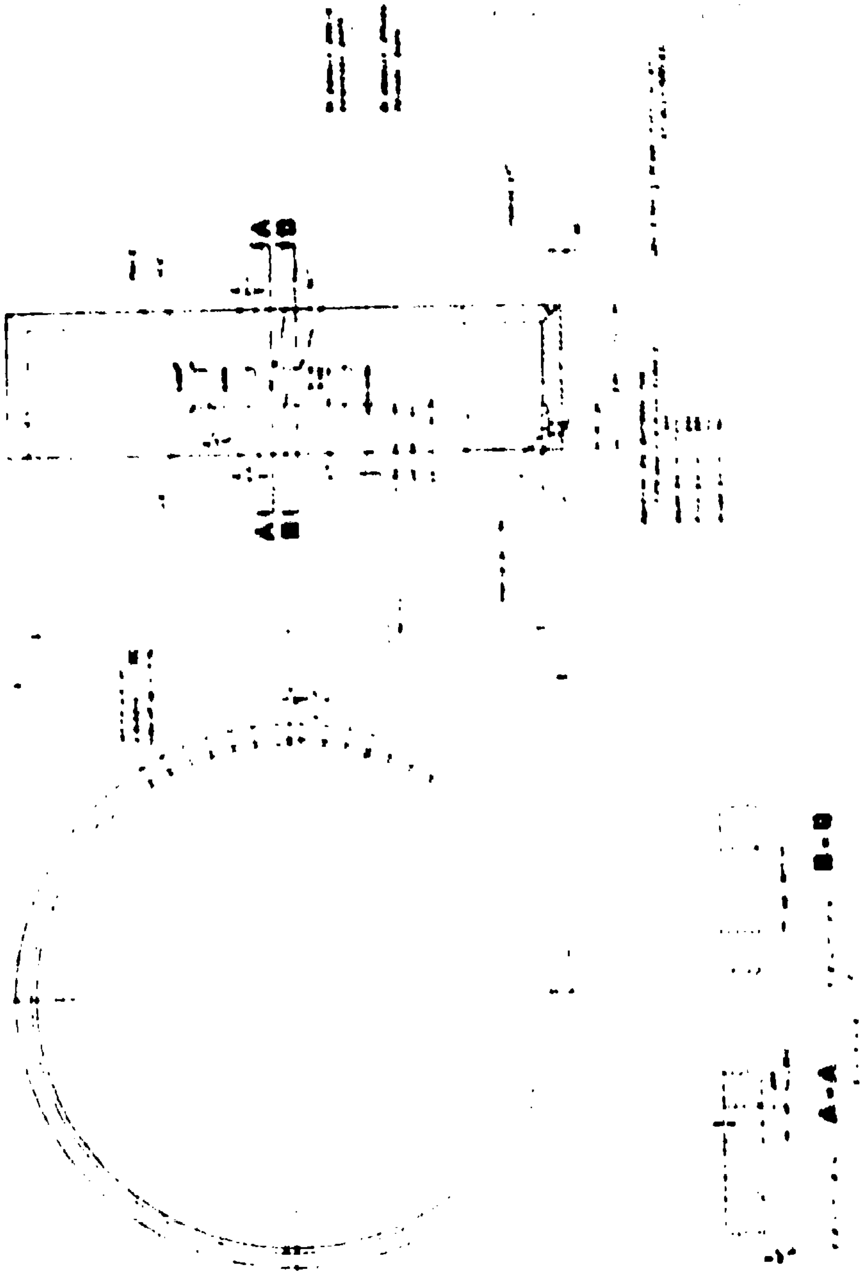

Figure 2-21. 7404047 Oxidizer Orifice Ring (O3)

Table 2-8. Characteristics of Oxidizer Orifice Rings 3 and 4 (U)

	03	04
Injection Area, A_{ot}, in^2	13.915	14.90
Primary Orifice, A_{op}, in^2	12.68	13.45
Secondary Orifice, A_{os}, in^2	1.235	1.45
Unit Width, UW, in.	1.112	1.112
Primary Orifice, W_p, in.	0.635	0.590
Secondary Orifice, W_s, in.	0.0965	0.106
UW-W_p, in.	0.477	0.522
Space Factor, ($W_p + W_s$/UW x 100%)	66.0	62.6
Percent W_p, (W_p/UW x 100%)	57.1	54.1
Percent Sec. Flow, A_{os}/A_{ot} x 100%	8.86	9.75
Fuel Sheet Thickness t_{fsh}, in.	0.201	0.201
t_{fsh}/UW-W_p	0.422	0.385
Secondary Orifice Setback, in.	0.300	1.000

(U) The predicted oxidizer injection ΔP for the configuration is shown in Figure 2-23 as a function of the volumetric flow rate. This ring was assembled into the X404408-3 pintle tip assembly and fired in conjunction with the X403832-4 fuel orifice ring on test firings 35 and 36. Actual injection pressure losses recorded during these firings are shown on Figure 2-23 for comparative purposes.

2.3.2.4 Oxidizer Orifice No. 4

(U) The fourth oxidizer configuration fabricated (but not tested) was the X403946-1 "A" change shown as Figure 2-24. This configuration is a 36 element configuration (36 primary plus 36 secondary orifices) with essentially the same orifice shapes, space factor ($W_p + W_s$/UW x 100%) and total injection area as the "B" modification of the X403831-1 oxidizer orifice ring. The major change in this configuration is in the setback of the secondary orifice. The setback was increased to 1.00 inch from the 0.30 inch setback used on the X403831-1, "B" modification, orifice ring. Pertinent characteristics of the number 4 oxidizer orifice configuration are tabulated as Table 2-8.

(U) The orifices were machined into the blank ring using electrical discharge machining procedures which have been described previously. A tabulation of engineering measurements for the individual orifices is shown as

(U) Table 2-9 X404047 "A" Oxidizer Orifice Ring Measurements (U)

Orifice Number	A	B	B-1	C	D	Orifice Number	A	B	B-1	C	D
1	0.663	0.499	0.634	0.100	0.364	19	0.662	0.501	0.636	0.098	0.365
2	0.664	0.499	0.632	0.099	0.366	20	0.663	0.501	0.634	0.099	0.365
3	0.663	0.499	0.632	0.099	0.365	21	0.663	0.501	0.636	0.098	0.366
4	0.663	0.499	0.632	0.099	0.366	22	0.663	0.501	0.636	0.098	0.366
5	0.663	0.499	0.633	0.099	0.365	23	0.662	0.501	0.636	0.098	0.366
6	0.663	0.500	0.633	0.099	0.365	24	0.663	0.500	0.635	0.098	0.365
7	0.663	0.498	0.633	0.098	0.365	25	0.663	0.501	0.635	0.098	0.365
8	0.663	0.498*	0.633	0.098	0.364	26	0.664	0.500	0.635	0.098	0.364
9	0.663	0.501	0.637	0.100	0.365	27	0.663	0.501	0.635	0.097	0.365
10	0.662	0.502	0.636	0.099	0.366	28	0.663	0.500	0.636	0.098	0.363
11	0.663	0.502	0.634	0.098	0.366	29	0.664	0.502	0.637	0.098	0.365
12	0.662	0.502	0.636	0.098	0.366	30	0.664	0.502	0.636	0.098	0.366
13	0.662	0.501	0.634	0.099	0.367	31	0.664	0.502	0.536	0.098	0.366
14	0.661	0.502	0.635	0.099	0.366	32	0.664	0.501	0.635	0.097	0.366
15	0.662	0.501	0.635	0.099	0.366	33	0.664	0.500	0.635	0.098	0.366
16	0.663	0.501	0.636	0.099	0.365	34	0.663	0.500	0.634	0.098	0.366
17	0.663	0.501	0.636	0.098	0.365	35	0.663	0.499	0.634	0.099	0.367
18	0.663	0.501	0.636	0.098	0.365	36	0.663	0.499	0.635	0.099	0.366

Requirements:
"A" = 0.665 ± 0.010
"B" = 0.300 ± 0.010
"B-1" = 0.635 ± 0.010
"C" = 0.100 ± 0.010
"D" = 0.365 ± 0.010

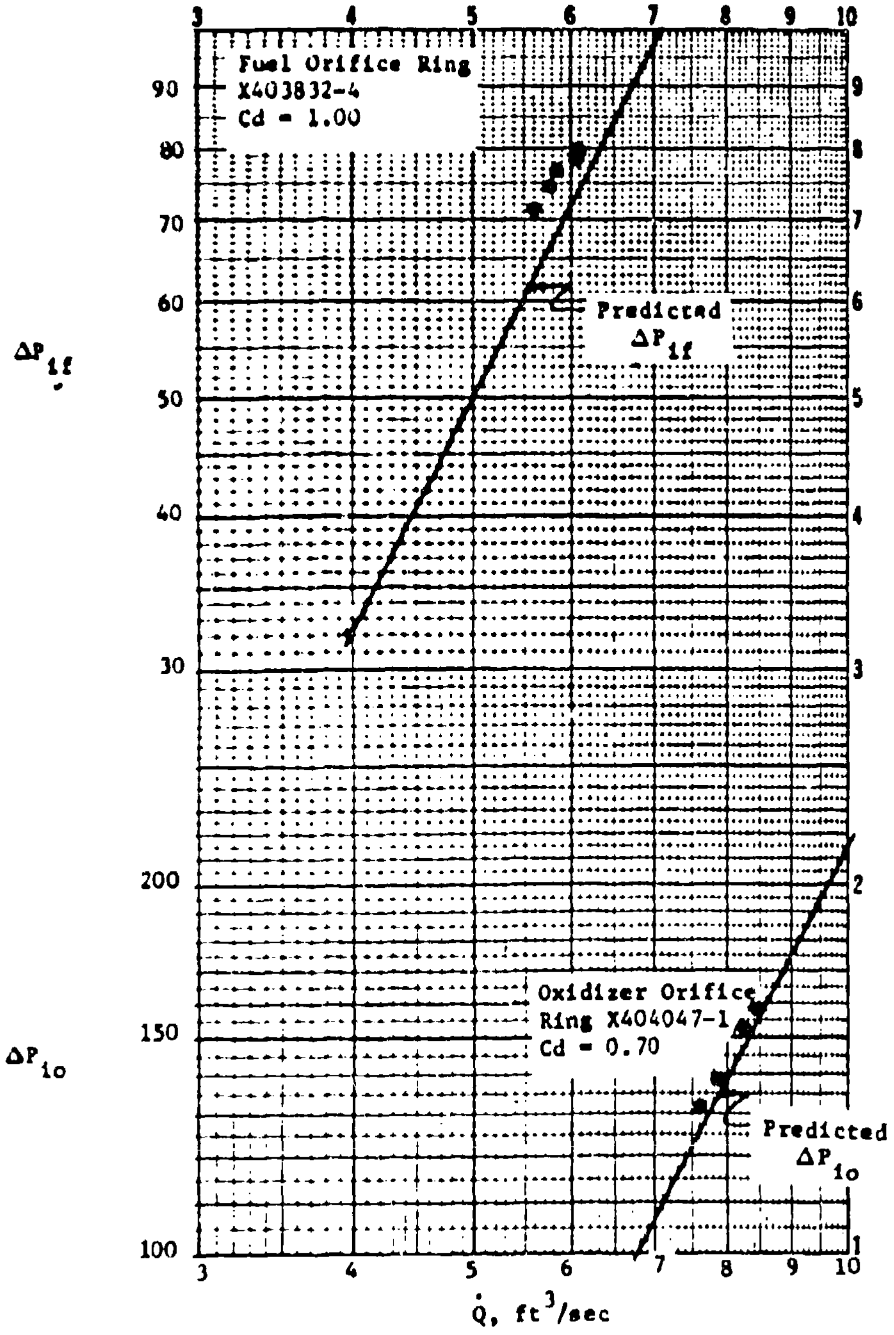

(U) Figure 2-23. Predicted Injection Pressure Loss (U)

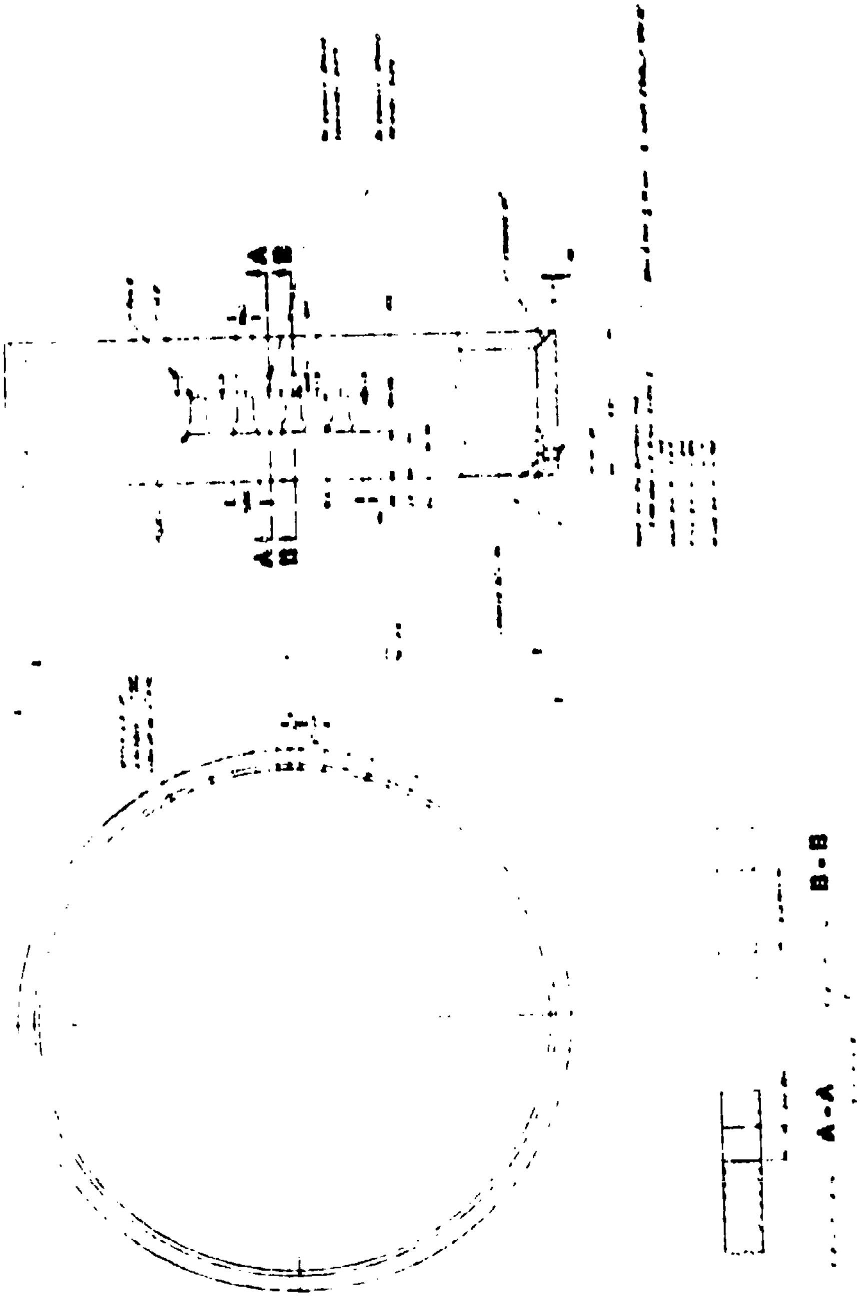

Figure 2-24. X403946 Oxidizer Orifice Ring No. 4 (U.

Table 2-10. The indicated oxidizer injection area is nearly identical to the injection area of the X403831-1, "B" modification, orifice ring. The predicted oxidizer injection ΔP for this configuration is shown in Figure 2-25 as a function of the volumetric flow rate.

(U) This ring was assembled into the X404408-4 Pintle Tip Assembly as shown in Figure 2-26. This pintle tip assembly was not fired during the injector development program.

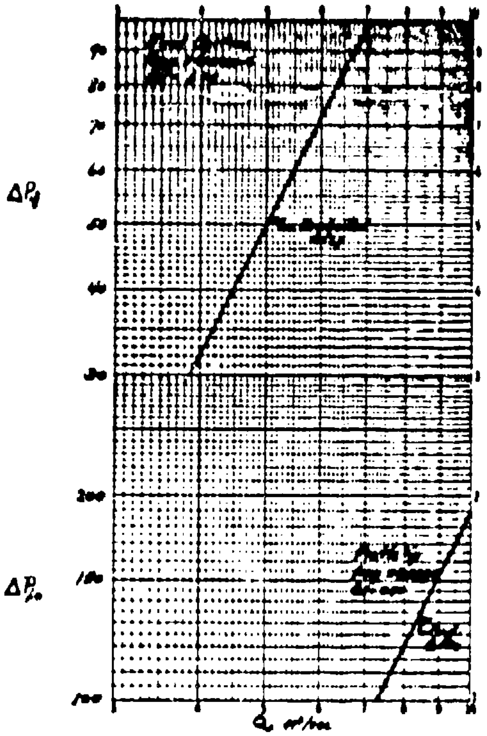

Figure 2-25. Predicted Injection Pressure Loss (U)

Figure 2-26. X404408-4 Pintle Tip Assembly (U)

2.3.2.5 Oxidizer Orifice No. 5

(U) The oxidizer orifice ring described in Section 2.3.2.4 was designed to operate with a back orifice ring (X404480-1) assembled into the X404408-5 Pintle Tip Assembly. Figure 2-27 is a photograph of the back ring, X404480-1 installed inside of the X403946-1, oxidizer orifice ring. The purpose of the back ring was to increase the L/D of both primary and secondary orifices by providing a flow channel for the oxidizer prior to injection.

(U) The component parts for the X404408-5 Pintle Tip Assembly, i.e., the X404408-4 Pintle Tip Assembly and the X404480-1 Oxidizer Back Ring, were delivered to the AFRPL and the final assembly was made at the AFRPL. Tack welds were used to retain the back ring in its proper orientation. This configuration was tested on test firing 44 and 45.

(U) Table 2-10. X403946 "A" Oxidizer Orifice Ring Measurements

Orifice Number	A	B	B-1	C	D	Orifice Number	A	B	B-1	C	D
1	0.912	0.362	0.590	0.103	0.402	19	0.908	0.365	0.587	0.107	0.404
2	0.909	0.363	0.590	0.105	0.403	20	0.908	0.365	0.590	0.107	0.403
3	0.910	0.365	0.590	0.105	0.404	21	0.906	0.367	0.590	0.105	0.405
4	0.908	0.364	0.589	0.105	0.403	22	0.906	0.367	0.590	0.105	0.405
5	0.905	0.364	0.590	0.105	0.403	23	0.908	0.366	0.590	0.105	0.405
6	0.905	0.365	0.590	0.105	0.405	24	0.906	0.368	0.590	0.105	0.405
7	0.905	0.365	0.590	0.103	0.403	25	0.906	0.368	0.590	0.105	0.403
8	0.906	0.365	0.590	0.102	0.402	26	0.907	0.367	0.590	0.103	0.405
9	0.907	0.365	0.590	0.104	0.400	27	0.906	0.367	0.590	0.108	0.403
10	0.905	0.365	0.590	0.105	0.405	28	0.906	0.366	0.590	0.109	0.403
11	0.905	0.365	0.590	0.105	0.404	29	0.906	0.367	0.590	0.103	0.405
12	0.905	0.365	0.590	0.110	0.405	30	0.905	0.367	0.590	0.106	0.405
13	0.905	0.365	0.590	0.105	0.402	31	0.905	0.366	0.590	0.105	0.402
14	0.905	0.365	0.590	0.108	0.404	32	0.905	0.366	0.590	0.106	0.403
15	0.905	0.365	0.590	0.105	0.402	33	0.905	0.365	0.590	0.110	0.402
16	0.906	0.365	0.590	0.105	0.404	34	0.905	0.366	0.590	0.105	0.405
17	0.907	0.365	0.590	0.105	0.404	35	0.906	0.366	0.590	0.105	0.405
18	0.907	0.367	0.590	0.105	0.403	36	0.907	0.366	0.590	0.105	0.404

Requirements:

"A" - 0.900 ± .010
"B" - 0.360 ± .010
"B-1" - 0.584 ± .010
"C" - 0.100 ± .010
"D" - 0.400 ± .010

Figure 2-27. X404408-5 Pintle Tip Assembly Showing X404480-1 Back Oxidizer Ring (U)

2.3.2.6 Oxidizer Orifice No. 6

(U) The sixth oxidizer configuration fabricated was the X404108-1 shown in Figure 2-28. This configuration is a 48 element configuration (48 primary plus 48 secondary orifices) with essentially the same orifice shape factor ($W_p + W_s/LW \times 100\%$) as the "B" modification to the X403831-1 oxidizer orifice ring. The percentage of secondary flow was reduced from a nominal 10.0 percent to 4.8 percent of the total flow. Pertinent characteristics of the number 6 oxidizer orifice configuration are tabulated in Table 2-11.

(U) The orifices were machined into the blank ring using electrical discharge machining procedures which have been described previously. A tabulation of engineering measurements for the individual orifice is shown as Table 2-12. This orifice ring configuration was utilized on test firings 108, 109 and 110.

2.4 COMPONENT DESIGN - DEMONSTRATION INJECTOR

(U) The design of the demonstration injector assembly (X404056-1) is shown as Figure 2-28. Figure 2-29 shows the injector during final assembly prior to shipment from L. W. LeFort Co., Anaheim, California to AFRPL. The injector assembly is nearly identical to the development injector assembly (X403829-1) described in Section 2.3. The major change in the demonstration injector design from the development injector is the incorporation of the oxidizer orifice ring into the centerbody assembly by welding rather than by means of a buttress thread.

(U) Oxidizer enters the injector through an 8-inch diameter, 300 lb ASA, welding neck flange located on the injector centerline and flows through the X404056-9, oxidizer tube. The oxidizer flow is turned 90° by the contoured pintle tip, X403030-1 and is injected radially through both primary

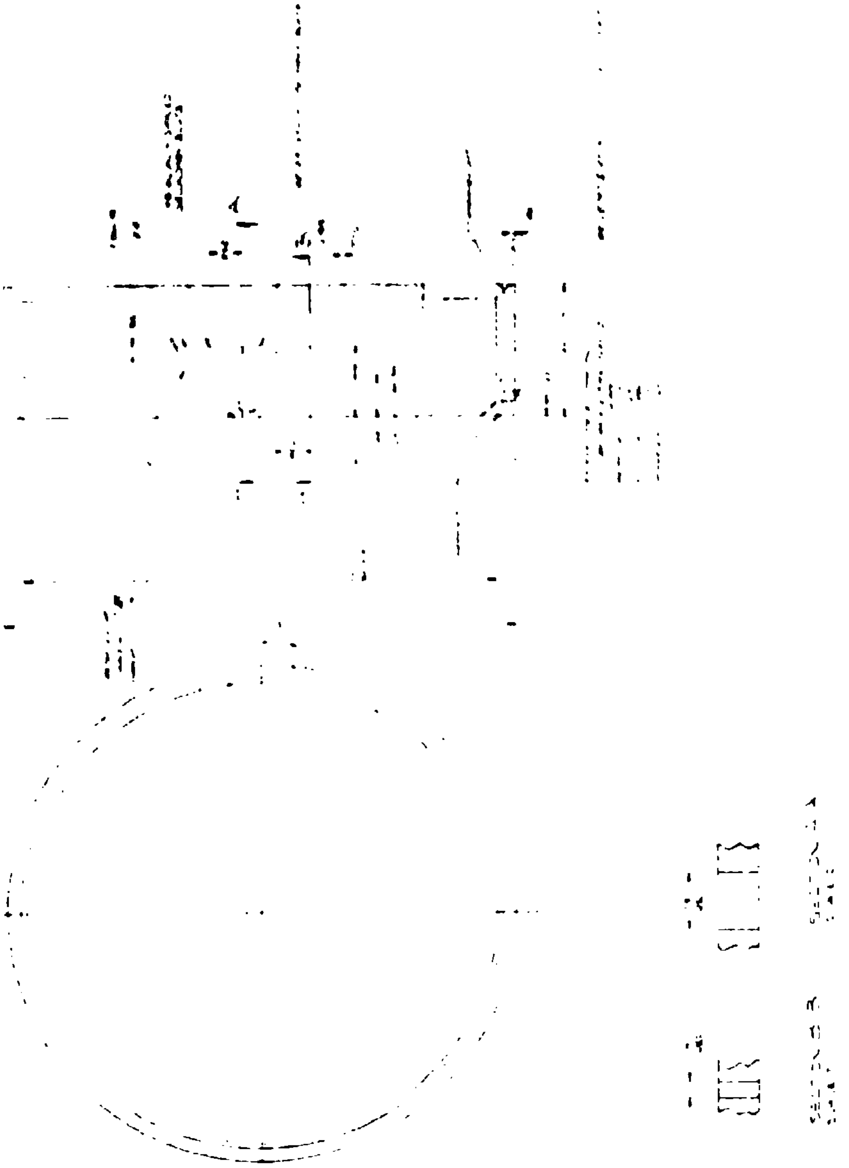

Figure 2-28. X404108-1 Oxidizer Orifice Ring (06) (U)

Table 2-11. Characteristics of Oxidizer Orifice Rings 4 and 6 (U)

	04	06
Injection Area, A_{ot}, in^2	14.90	12.97
Primary Orifice, A_{op}, in^2	13.45	12.34
Secondary Orifice, A_{os}, in^2	1.45	0.63
Unit Width, UW, in.	1.112	0.834
Primary Orifice, W_p, in.	0.590	0.419
Secondary Orifice, W_s, in.	0.106	0.080
UW-W_p, in.	0.522	0.415
Space Factor, (W_p + W_s/UW x 100%)	62.6	60.0
Percent W_p, (W_p/UW x 100%)	54.1	50.3
Percent Sec. Flow, A_{os}/A_{ot} x 100%	9.75	4.80
Fuel Sheet Thickness, t_{fsh}, in.	0.201	0.201
t_{fsh}/UW-W_p	0.385	0.497
Secondary Orifice Setback, in.	1.00	0.545

and secondary orifices. The oxidizer orifice ring employed in the demonstration injector was based on test results obtained in the injector development phase of the program. The orifice ring contains 36 elements (primary orifice plus secondary orifice) and is described in Section 2.4.1.1. The pintle tip is protected with ablative material (HAVEG 41F) cement. HAVEG 41-F cement is an asbestos-phenolic mixture which uses an acid catalyst to cause the mixture to set.

(U) The fuel enters the injector through a single 6 inch diameter, 300 lb ASA, welding neck flange where it flows into a manifold fabricated from four 6 inch diameter, 90° elbows of schedule 80 pipe. The fuel flows through eight, 3 inch diameter, distribution orifices equally spaced around the outer fuel jacket (X404056-10) into an internal plenum created by the fuel jacket and fuel sleeve (X403833-1). Fuel flows from this plenum into the annular opening created by the fuel jacket and injector centerbody. Fuel is injected into the combustion chamber as a hollow cylindrical sheet through the 0.200 inch annular opening created by the machine surface on the injector centerbody and the fuel metering orifice (X403832-1).

(U) Table 2-12. X404108 Oxidizer Orifice Ring Measurements (06)

Orifice Number	A	B	B-1	C	D		Orifice Number	A	B	B-1	C	D
1	0.728	0.353	0.413	0.080	0.183		25	0.730	0.352	0.417	0.079	0.180
2	0.728	0.354	0.419	0.080	0.183		26	0.730	Damaged	0.415	0.078	0.181
3	0.728	0.354	0.418	0.079	0.182		27	0.730	0.352	0.418	0.078	0.183
4	0.728	0.351	0.414	0.080	0.183		28	0.730	0.351	0.420	0.083	0.185
5	0.724	0.354	0.419	0.079	0.181		29	0.728	0.353	0.419	0.082	0.182
6	0.729	0.351	0.419	0.079	0.182		30	0.726	0.349	0.420	0.083	0.184
7	0.731	0.352	0.414	0.080	0.180		31	0.727	0.350	0.417	0.083	0.184
8	0.730	0.351	0.419	0.078	0.182		32	0.720	0.349	0.420	0.083	0.185
9	0.739	0.355	0.423	0.082	0.183	**Requirements**	33	0.728	0.351	0.420	0.082	0.183
10	0.733	0.364	0.430	0.079	0.183	"A" - 0.730 ± 0.010	34	0.726	0.350	0.420	0.083	0.183
11	0.729	0.352	0.419	0.079	0.184	"B" - 0.350 ± 0.010	35	0.732	0.353	0.420	0.080	0.183
12	0.729	0.352	0.419	0.079	0.183	"B1"- 0.420 ± 0.010	36	0.730	0.353	0.420	0.081	0.185
13	0.730	0.352	0.418	0.082	0.183	"C" - 0.083 ± 0.010	37	0.730	0.352	0.420	0.080	0.183
14	0.729	0.352	0.419	0.080	0.182	"D" - 0.185 ± 0.010	38	0.733	0.350	0.419	0.079	0.183
15	0.728	0.352	0.418	0.080	0.183		39	0.730	0.351	0.418	0.079	0.182
16	0.727	0.352	0.419	0.081	0.181		40	0.729	0.352	0.419	0.080	0.182
17	0.728	0.352	0.419	0.080	0.182		41	0.729	0.352	0.420	0.080	0.182
18	0.730	0.352	0.419	0.083	0.184		42	0.729	0.352	0.419	0.081	0.182
19	0.728	0.332	0.419	0.081	0.182		43	0.731	0.352	0.415	0.081	0.182
20	0.730	0.354	0.421	0.080	0.182		44	0.732	0.352	0.416	0.079	0.181
21	0.730	0.354	0.422	0.080	0.182		45	0.729	0.352	0.421	0.079	0.181
22	0.730	0.346	0.419	0.080	0.180		46	0.730	0.354	0.422	0.081	0.181
23	0.730	0.354	0.421	0.080	0.181		47	0.728	0.354	0.421	0.081	0.184
24	0.729	0.350	0.419	0.079	0.182		48	0.727	0.354	0.422	0.080	0.182

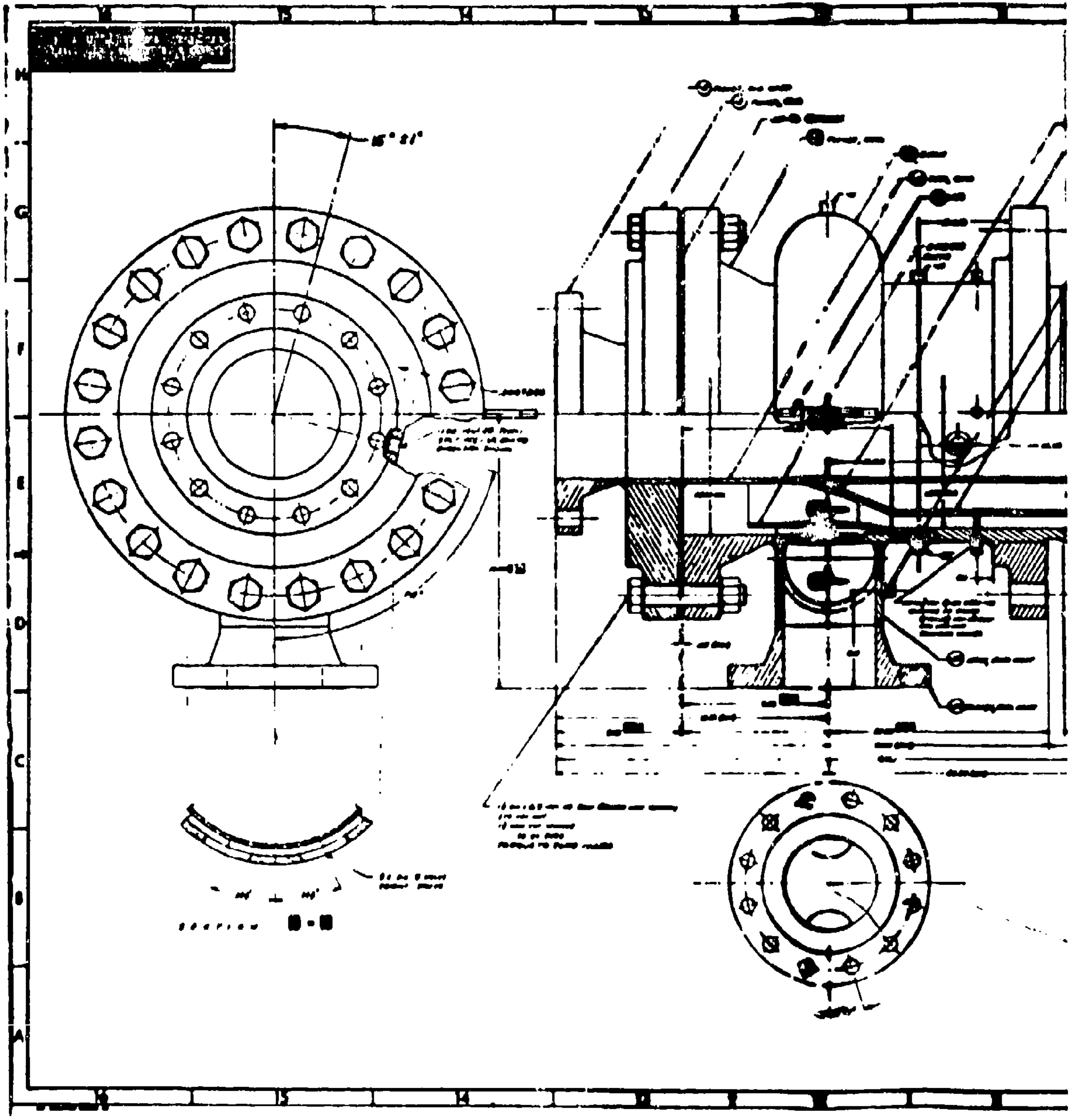
15° 21'
SECTION B-B
H
G
F
E
D
C
B
A

1

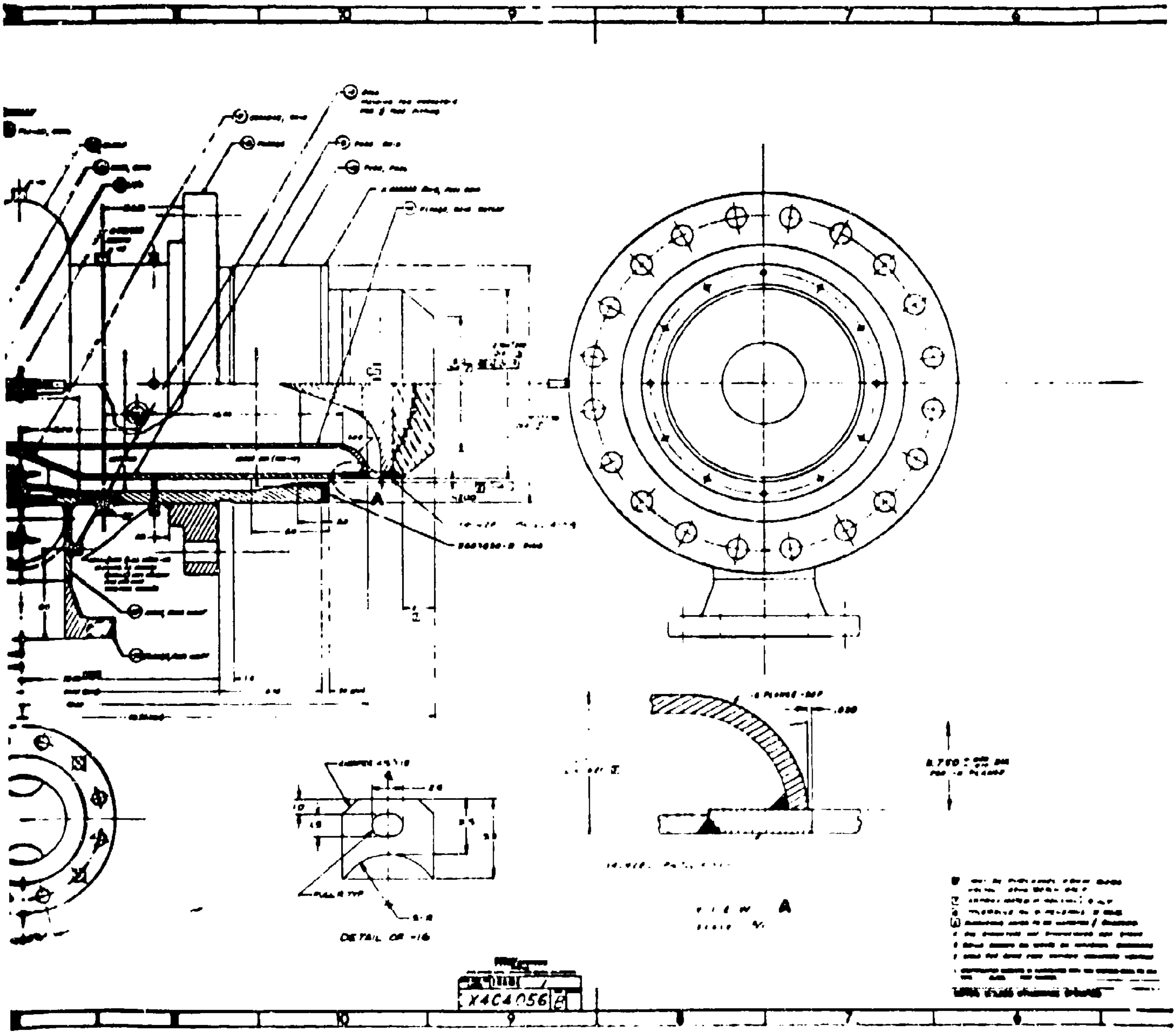
10
9
8
7
6
A
.030
DETAIL OF -16
VIEW A
X4C4056 B

2

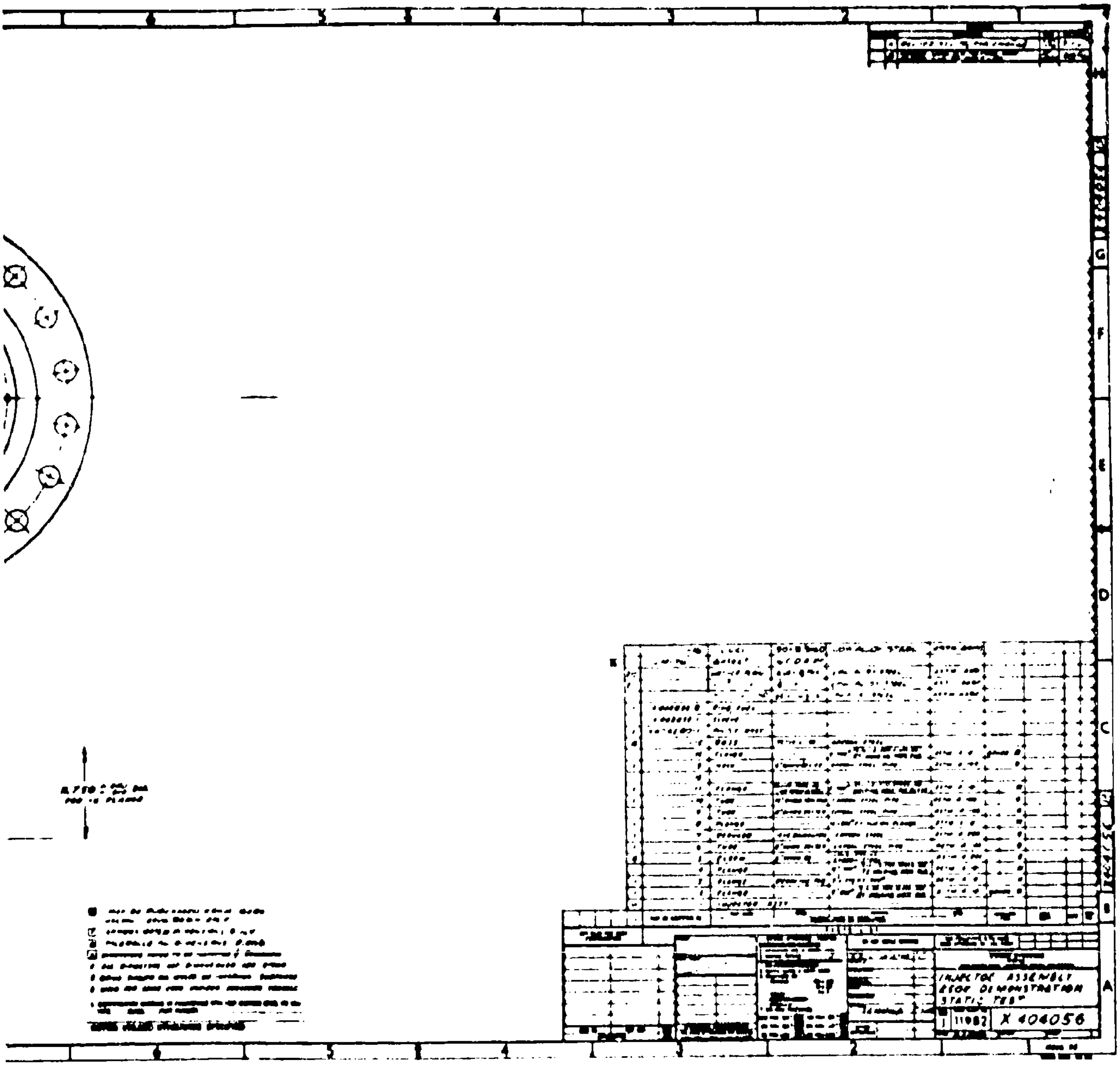
6
5
4
3
2
1
G
F
E
D
C
B
A
INJECTOR ASSEMBLY
DEMONSTRATION
STATIC TEST
11982
X 404056

Figure 2-29. X404056 250,000 lb_f Thrust Demonstration Injector Assembly

3

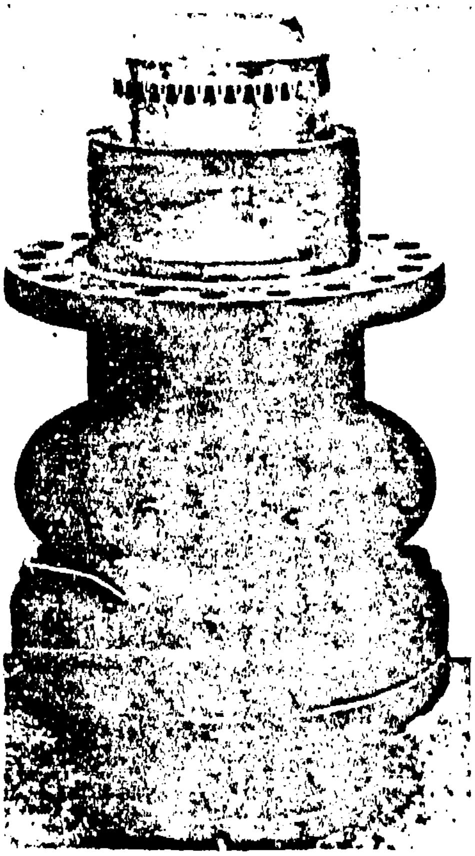

Figure 2-30. Demonstration Injector During Final Assembly (U)

2.4.1 Pintle Tip Assembly

(U) The pintle tip assemblies (X404280-1) are built up from the oxidizer orifice ring (X404693-1), the X403830-1 pintle tip and ablative material as required to form the configuration shown in Figure 2-31. The orifices in the oxidizer orifice rings were machined into the blank rings by an electrical discharge machining (EDM) process. EDM produced more uniform, higher quality orifices at a reduced cost when compared with conventional milling of the orifices.

(U) Following delivery of the oxidizer orifice ring (from the EDM fabricator) the X403830-1 pintle tip was welded to the orifice ring and then welded to the injector centerbody. The ablative protection was then applied to the pintle tip. The LeFort Co. applied the HAVEG-41F cement to the tip. HAVEG-41F cement was used for all pintle tip assemblies. The cement is an asbestos-phenolic mixture which requires an acid catalyst to cause the mixture to set.

2.4.1.1 Ring, Oxidizer Orifice

(U) The oxidizer orifice rings fabricated for the demonstration injectors were made to TRW drawing X404693-1 as shown in Figure 2-32. This configuration was selected on the basis of test results obtained in the injector development test program. The X404693-1 configuration (36 primary orifices plus 36 secondary orifices) is based primarily on the 01A configuration (Section 2.3.2.1.1) tested during firings 18-23.

(U) The pertinent design characteristics of the X404693-1 oxidizer orifice configuration are tabulated as Table 2-13. The design characteristics of the 01A oxidizer orifice ring are shown for comparative purposes. Two major changes are evident; the total oxidizer injection area has been increased to 15.97 sq. inches, while the percentage of secondary flow has been decreased to 9.1 percent of the total flow area. This change resulted in an oxidizer injection ΔP of 100 psi at the design operating point. Operation at this ΔP had been demonstrated in the injector development phase of the program.

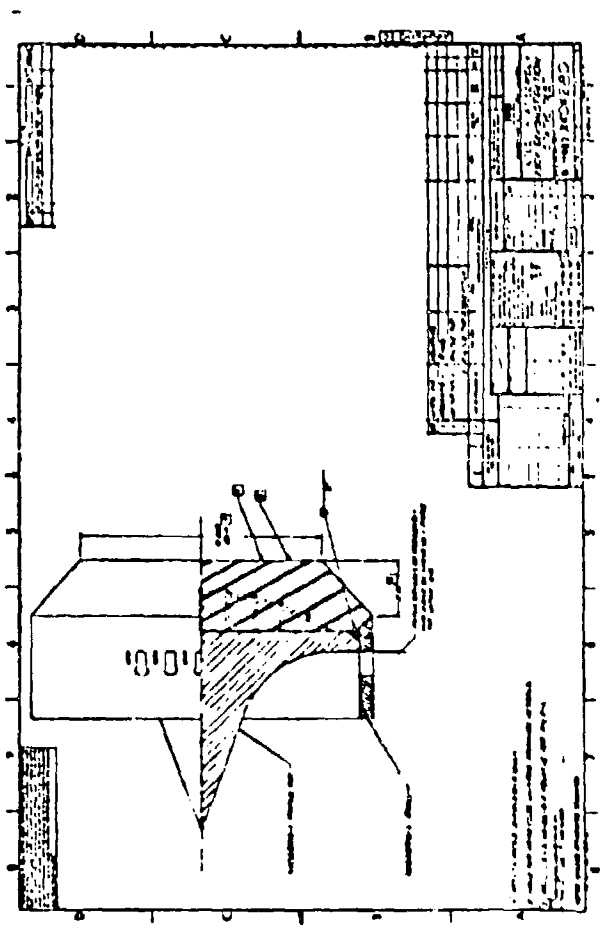

Figure 2-31. X404280-1 Pintle Tip Assembly (U)

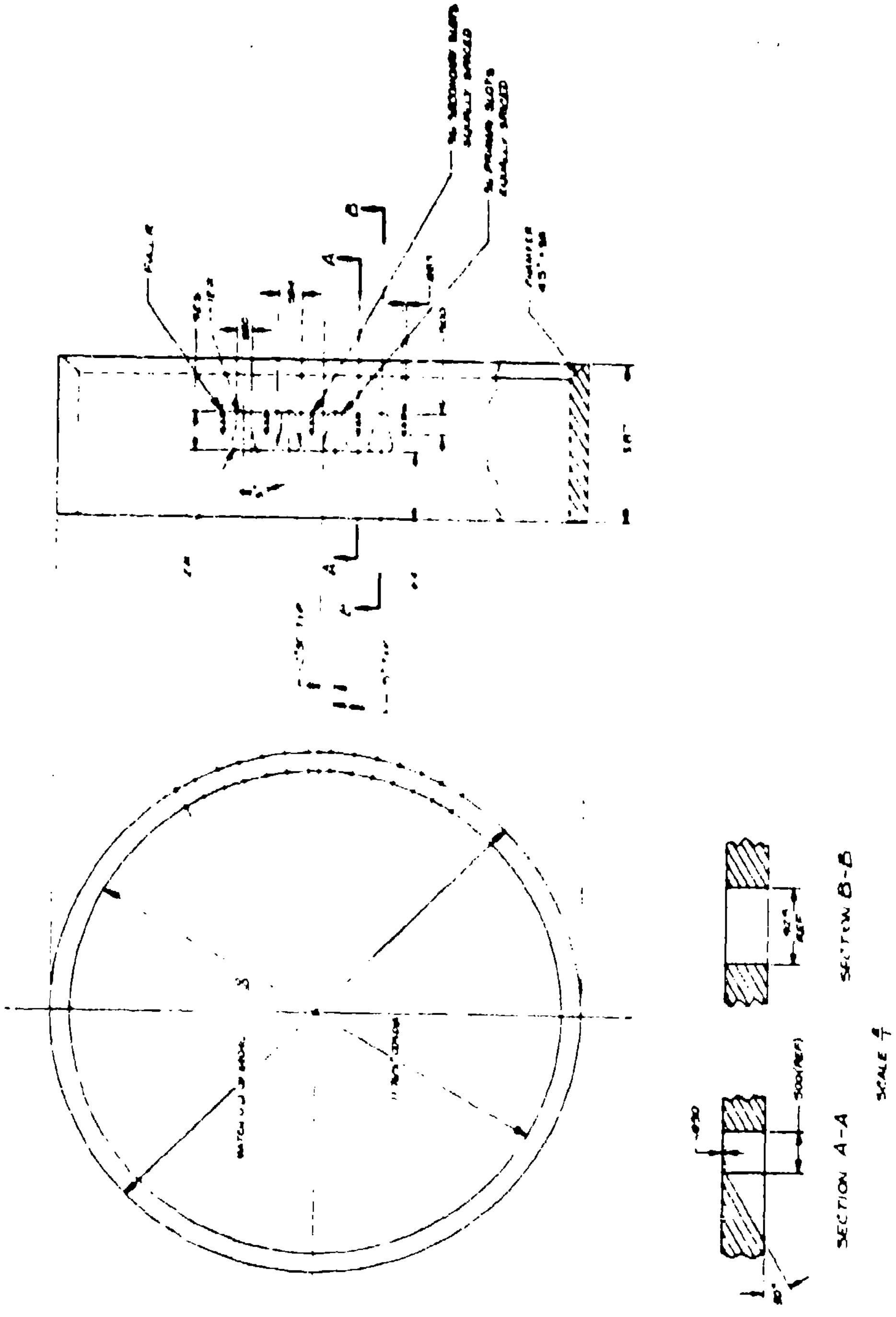
A
B
A
B
CHAMFER 45°
SECTION A-A
SECTION B-B
SCALE 4/1
.500(REF)

Figure 2-32. X404693-1 Oxidizer Orifice Ring (U)

Table 2-13. Characteristics of X404693-1 Oxidizer Orifice Ring (U)

	X404693-1	X403831-1 ("A" change)
Injection Area, A_{ot}, in^2	15.97	14.60
Primary Orifice, A_{op}, in^2	14.53	13.16
Secondary Orifice, A_{os}, in^2	1.44	1.44
Unit Width, UW, in.	1.10	1.11
Primary Orifice, W_p, in.	0.584	0.584
Secondary Orifice, W_s, in.	0.083	0.083
$(UW-W_p)$, in.	0.516	0.526
Space Factor, $(W_p + W_s)/UW \times 100\%$	60.6	60.1
Percent W_p, $W_p/UW \times 100\%$	53.1	52.6
Percent Sec. Flow, $A_{os}/A_{ot} \times 100\%$	9.1	9.85
Fuel Sheet Thickness, t_{fsh}, in.	0.200	0.200
$t_{fsh}/(UW-W_p)$	0.390	0.388
Secondary Orifice Setback, in.	0.425	0.400

(U) The orifices (36 primary plus 36 secondary) in the oxidizer orifice rings were machined into blank rings using an electrical discharge machining (EDM) process. Two passes of the EDM tool were used on each orifice. On the primary orifices a roughing pass was first made; the electrode was then dressed off and a finish pass made through the orifice. The finish pass electrode was then used as the roughing electrode for the next orifice. The secondary orifices were machined using the EDM process also. In the first pass the 0.083 by 0.500 slot was machined normal to the workpiece surface. In the second pass the 30° angled feed slot was machined from the inside of the ring leaving the 0.030 inch metering flat.

(U) The individual orifices of each of the three demonstration injector oxidizer orifice rings were measured using vernier calipers. The uniformity of the 72 individual orifices is apparent in the tabulation of the engineering measurements shown in Tables 2-14, 2-15, and 2-16 for the three orifice rings. The area of the primary orifices for the three rings varies from 0 to 1 percent greater than the design area. The secondary oxidizer flow areas vary from 9.1 percent to 9.4 percent of the total flow area. This results in an oxidizer injection area which is greater than the design injection area by 0.3 percent for the S/N 002 ring, and by 1.5 percent for the S/N 001 and S/N 003 rings. This area change results in a predicted oxidizer injection ΔP of approximately 97 psi as compared with the design value of 100 psi.

(U) Table 2-14. X404693-1 Ring, Oxidizer Orifice
S/N 001 (U)

Orifice Number	A	B	B-1	C	D	Orifice Number	A	B	B-1	C	D
1	0.926	0.390	0.586	0.085	0.505	19	0.927	0.384	0.587	0.086	0.502
2	0.927	0.391	0.586	0.085	0.504	20	0.927	0.384	0.587	0.085	0.502
3	0.927	0.383	0.584	0.085	0.505	21	0.926	0.384	0.588	0.085	0.503
4	0.927	0.386	0.588	0.085	0.505	22	0.927	0.383	0.588	0.090	0.505
5	0.925	0.384	0.584	0.085	0.505	23	0.927	0.384	0.588	0.093	0.504
6	0.927	0.395	0.586	0.085	0.504	24	0.925	0.390	0.587	0.093	0.504
7	0.927	0.385	0.585	0.086	0.503	25	0.925	0.389	0.588	0.091	0.502
8	0.925	0.385	0.585	0.086	0.502	26	0.926	0.390	0.588	0.092	0.502
9	0.927	0.385	0.587	0.086	0.504	27	0.925	0.380	0.587	0.090	0.503
10	0.927	0.385	0.583	0.086	0.505	28	0.925	0.390	0.591	0.087	0.504
11	0.927	0.384	0.586	0.087	0.504	29	0.925	0.383	0.586	0.087	0.502
12	0.928	0.385	0.586	0.086	0.504	30	0.925	0.387	0.586	0.087	0.502
13	0.928	0.384	0.585	0.087	0.505	31	0.925	0.385	0.590	0.088	0.506
14	0.928	0.385	0.587	0.087	0.503	32	0.926	0.383	0.589	0.085	0.505
15	0.927	0.395	0.586	0.087	0.505	33	0.927	0.389	0.586	0.086	0.504
16	0.927	0.384	0.586	0.087	0.502	34	0.927	0.385	0.586	0.086	0.503
17	0.926	0.383	0.586	0.088	0.504	35	0.926	0.384	0.584	0.086	0.503
18	0.927	0.383	0.587	0.087	0.503	36	0.925	0.385	0.587	0.087	0.502

Requirements:

"A" - 0.925 ± 0.010
"B" - 0.380 ± 0.010
"B-1" - 0.584 ± 0.010
"C" - 0.083 ± 0.010
"D" - 0.500 ± 0.010

(U) Table 2-15. X404693-1 Ring, Oxidizer Orifice
S/N 002 (U)

Orifice Number	A	B	B-1	C	D	Orifice Number	A	B	B-1	C	D
1	0.923	0.382	0.583	0.083	0.501	19	0.922	0.382	0.584	0.086	0.501
2	0.923	0.382	0.584	0.082	0.501	20	0.922	0.382	0.384	0.085	0.501
3	0.923	0.384	0.585	0.082	0.501	21	0.923	0.382	0.584	0.085	0.501
4	0.923	0.383	0.585	0.082	0.502	22	0.926	0.382	0.584	0.084	0.501
5	0.922	0.383	0.585	0.082	0.502	23	0.923	0.383	0.584	0.084	0.502
6	0.924	0.384	0.584	0.082	0.501	24	0.924	0.382	0.583	0.083	0.501
7	0.922	0.385	0.584	0.085	0.501	25	0.922	0.380	0.584	0.083	0.501
8	0.921	0.382	0.583	0.085	0.501	26	0.923	0.381	0.583	0.083	0.500
9	0.922	0.383	0.583	0.085	0.502	27	0.922	0.382	0.584	0.083	0.502
10	0.922	0.382	0.583	0.085	0.501	28	0.922	0.381	0.584	0.082	0.502
11	0.922	0.382	0.583	0.085	0.501	29	0.923	0.381	0.584	0.083	0.501
12	0.922	0.383	0.584	0.085	0.502	30	0.923	0.381	0.584	0.083	0.501
13	0.921	0.382	0.583	0.085	0.500	31	0.923	0.381	0.584	0.084	0.501
14	0.921	0.382	0.583	0.086	0.502	32	0.923	0.381	0.584	0.083	0.502
15	0.922	0.381	0.583	0.086	0.501	33	0.922	0.382	0.585	0.083	0.502
16	0.922	0.382	0.583	0.088	0.501	34	0.923	0.381	0.584	0.084	0.501
17	0.922	0.382	0.584	0.086	0.502	35	0.923	0.383	0.583	0.084	0.500
18	0.923	0.381	0.583	0.087	0.502	36	0.923	0.382	0.584	0.084	0.500

Requirements:

"A" - 0.925 ± 0.010
"B" - 0.380 ± 0.010
"B-1" - 0.584 ± 0.010
"C" - 0.083 ± 0.010
"D" - 0.500 ± 0.010

(U) Table 2-16. X404693-1 Ring, Oxidizer Orifice
S/N 003 (U)

Orifice Number	A	B	B-1	C	D	Orifice Number	A	B	B-1	C	D
1	0.927	0.385	0.583	0.091	0.505	19	0.926	0.392	0.586	0.086	0.502
2	0.925	[illegible]	0.586	0.088	0.505	20	0.926	0.391	0.587	0.085	0.499
3	0.926	0.384	0.587	0.087	0.504	21	0.925	0.382	0.587	0.085	0.504
4	0.925	0.384	0.584	0.087	0.504	22	0.927	0.384	0.587	0.085	0.500
5	0.925	0.384	0.586	0.087	0.501	23	0.927	0.385	0.587	0.091	0.502
6	0.925	0.385	0.585	0.089	0.500	24	0.926	0.385	0.587	0.091	0.503
7	0.926	0.385	0.586	0.087	0.500	25	0.925	0.384	0.586	0.091	0.503
8	0.926	0.385	0.585	0.086	0.500	26	0.926	0.384	0.587	0.092	0.503
9	0.926	0.384	0.586	0.086	0.500	27	0.926	0.384	0.587	0.093	0.504
10	0.926	0.385	0.586	0.085	0.500	28	0.927	0.384	0.588	0.090	0.503
11	0.925	0.385	0.586	0.086	0.501	29	0.927	0.384	0.588	0.085	0.500
12	0.926	0.388	0.588	0.087	0.505	20	0.927	0.384	0.588	0.086	0.505
13	0.926	0.386	0.589	0.087	0.503	31	0.927	0.384	0.588	0.086	0.504
14	0.927	0.384	0.587	0.086	0.504	32	0.927	0.385	0.590	0.085	0.503
15	0.927	0.393	0.591	0.086	0.502	33	0.927	0.384	0.588	0.090	0.591
16	0.927	0.393	0.590	0.086	0.502	34	0.927	0.384	0.588	0.089	0.505
17	0.926	0.392	0.586	0.085	0.502	35	0.926	0.384	0.588	0.091	0.505
18	0.925	0.396	0.587	0.085	0.502	36	0.926	0.384	0.587	0.091	0.505

Requirements:

"A" - 0.925 ± 0.010
"B" - 0.380 ± 0.010
"B-1" - 0.584 ± 0.010
"C" - 0.083 ± 0.010
"D" - 0.500 ± 0.010

2.5 COMPONENT DESIGN - THRUST CHAMBER

(C) The design point conditions were used to size the thrust chamber for a nozzle stagnation pressure, P_o, of 300 psia. The chamber design is shown on drawing X403646-1 (Figure 2-33) and Figure 2-34 is a photograph of the second chamber prior to shipment to the AFRPL. The throat diameter, D_t, is calculated as follows:

$$A_t = \frac{\eta_C \times C^*_{theo} \dot{W}_T}{P_o \, g_o} = \pi/4 \, D_t^2$$

or

$$D_t = \left[\frac{4\eta_C \times C^*_{theo} \dot{W}_T}{\pi \, P_o \, g_o} \right]^{1/2}$$

For a combustion efficiency of 94 percent the required throat diameter is

$$D_t = \left[\frac{4 \times 0.94 \times 5596 \times 980}{\times 300 \times 32.17} \right]^{1/2} = 26.10 \text{ in.}$$

The pertinent internal geometry characteristics of the chamber design are:

Throat Diameter, D_t	- 26.1 inch
Chamber Diameter, D_c	- 39.0 inch
Nozzle Exit Diameter, D_c	- 52.2 inch
Length of Chamber	- 36.5 inch
Nozzle Length	- 50.25 inch
Overall Length	- 96.5 inch
Contraction Ratio, ϵ_c	- 2.22
Expansion Ratio, ϵ_n	- 4.00
Chamber Length/D_c	- 0.94
Nozzle Half Angle	- 15°
L*	- 70 inches

2.5.1 Combustion Chamber

(U) The combustion chamber material was USS T-1 steel in all areas except the long weld neck flange (X403646-9) which is ASTM A-181, Grade II, carbon steel. The head (X403646-8) is a 2:1 ASME Code elliptical head of T-1 steel, 39.0 inch I.D. by 0.5 in. wall thickness supplied by the Universal Head Co. Joliet, Illinois, The plate sections of the chamber and the nozzles are 0.50 inches thick. In the throat region the minimum thickness is 0.8 inches. The throat section (X403646-3) was fabricated from 2.0 inch thick T-1 steel plate. The internal contour was machined with a tracer lathe. The allowable run duration at the full thrust condition is approximately 2 seconds to limit inside surface wall temperatures to approximately 1700°F. The results of the thermal analysis are presented in Appendix B.

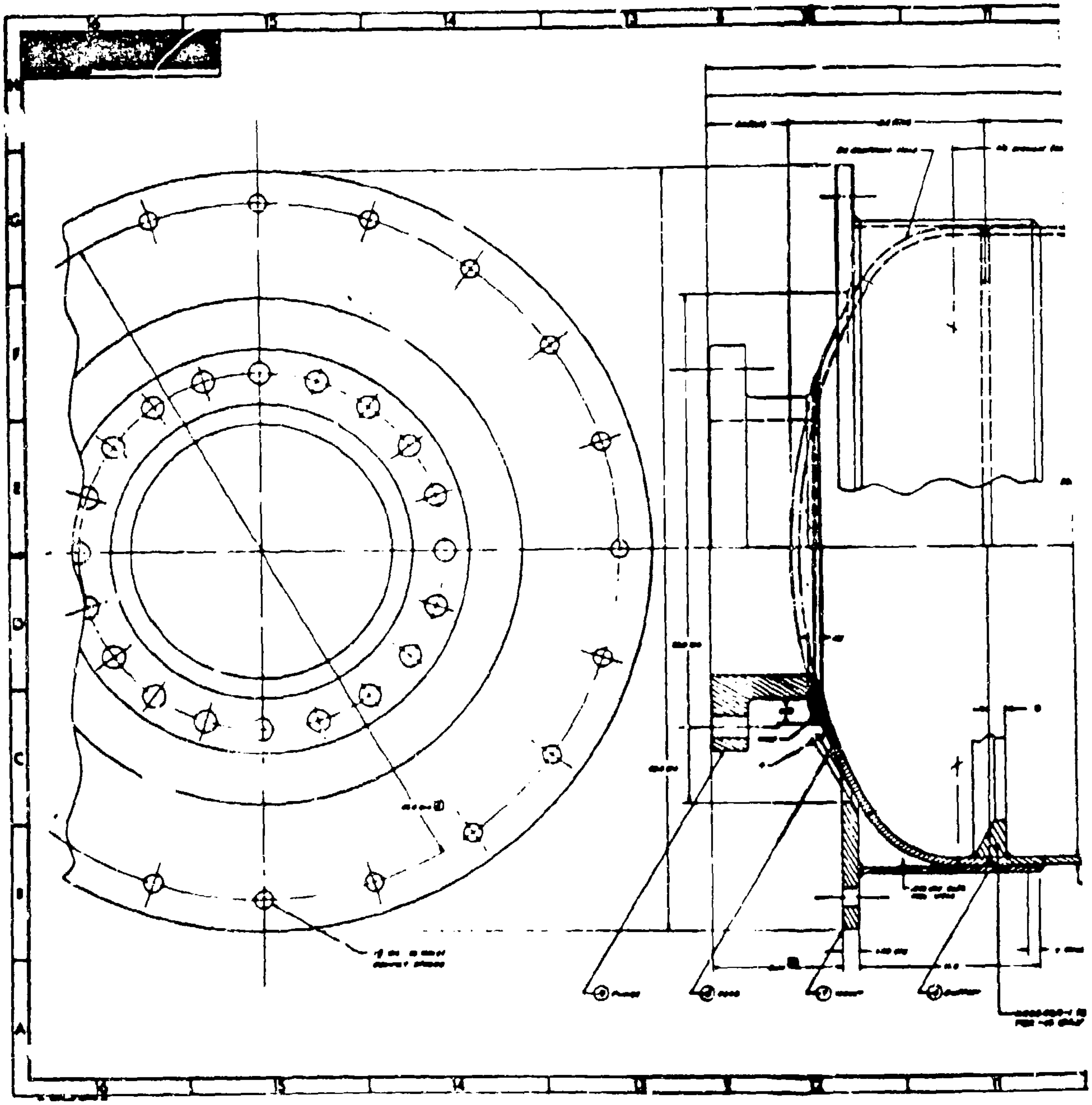

1

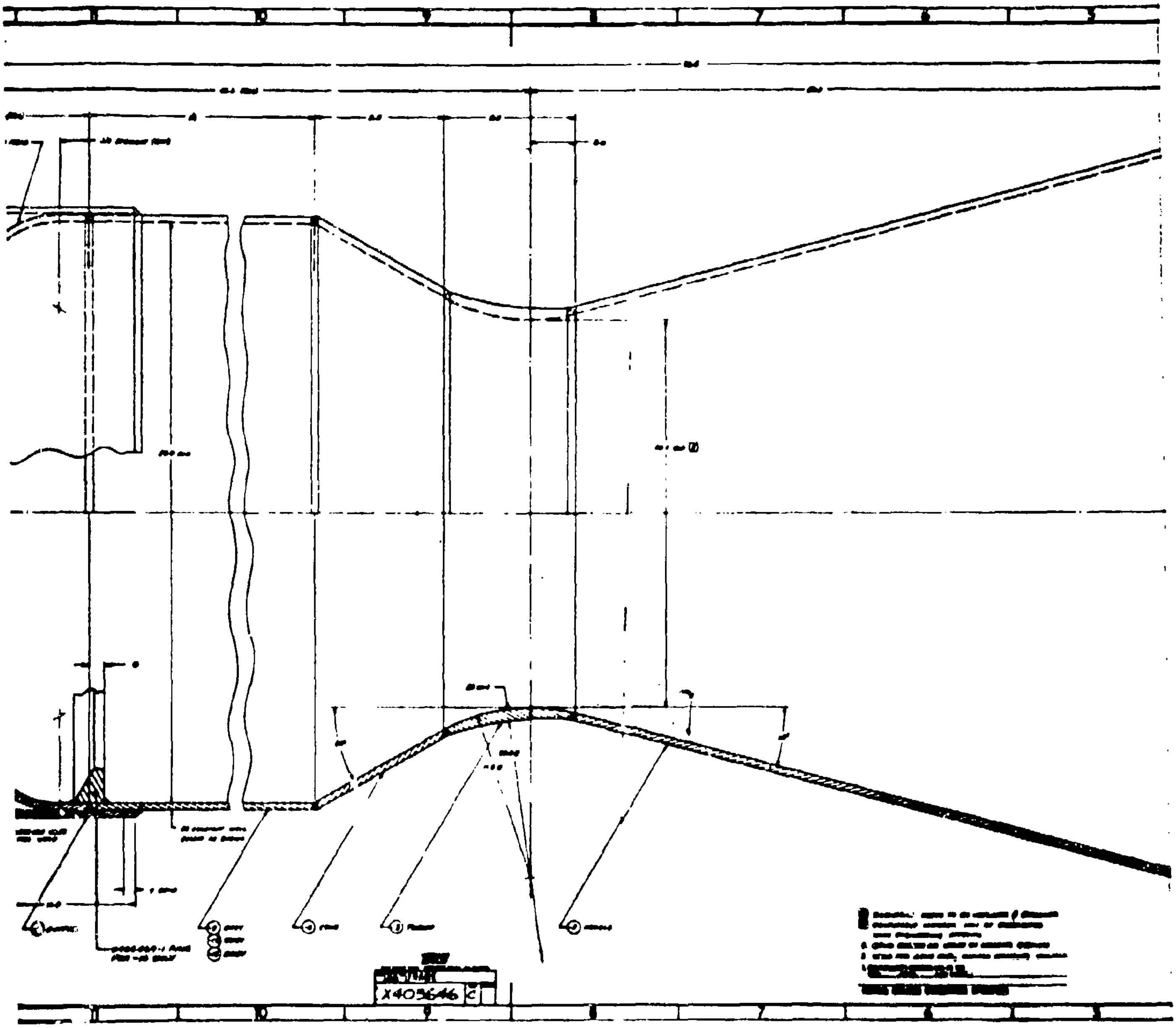
X405646
C
11
10
9
8
7
6
5

2

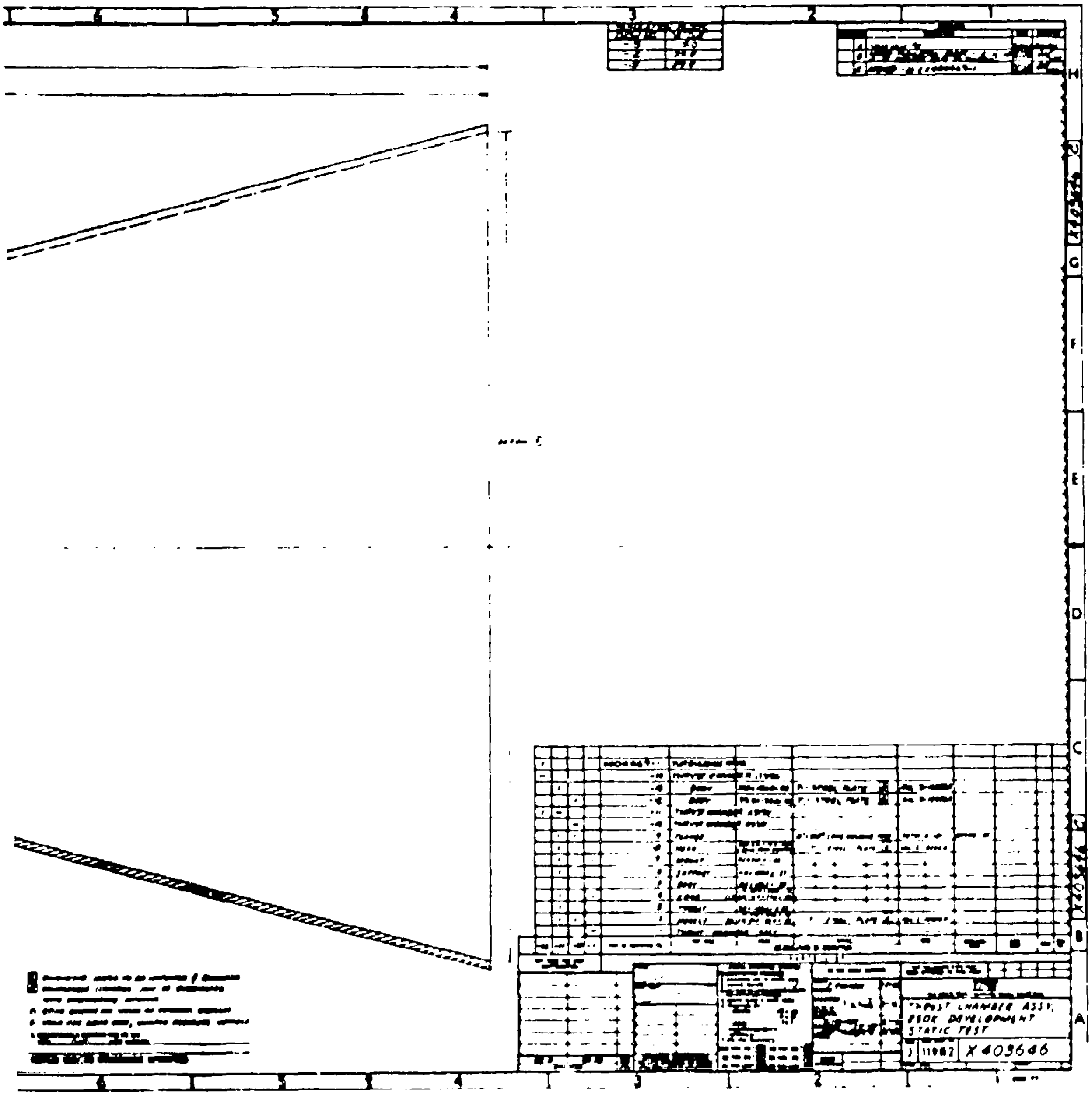
THRUST CHAMBER ASSY,
250K DEVELOPMENT
STATIC TEST
11982
X403646
H
G
F
E
D
C
B
A
6
5
4
3
2
1

Figure 2-33. X403646 250,000 lb$_f$ Thrust Development Chamber Assembly (U)

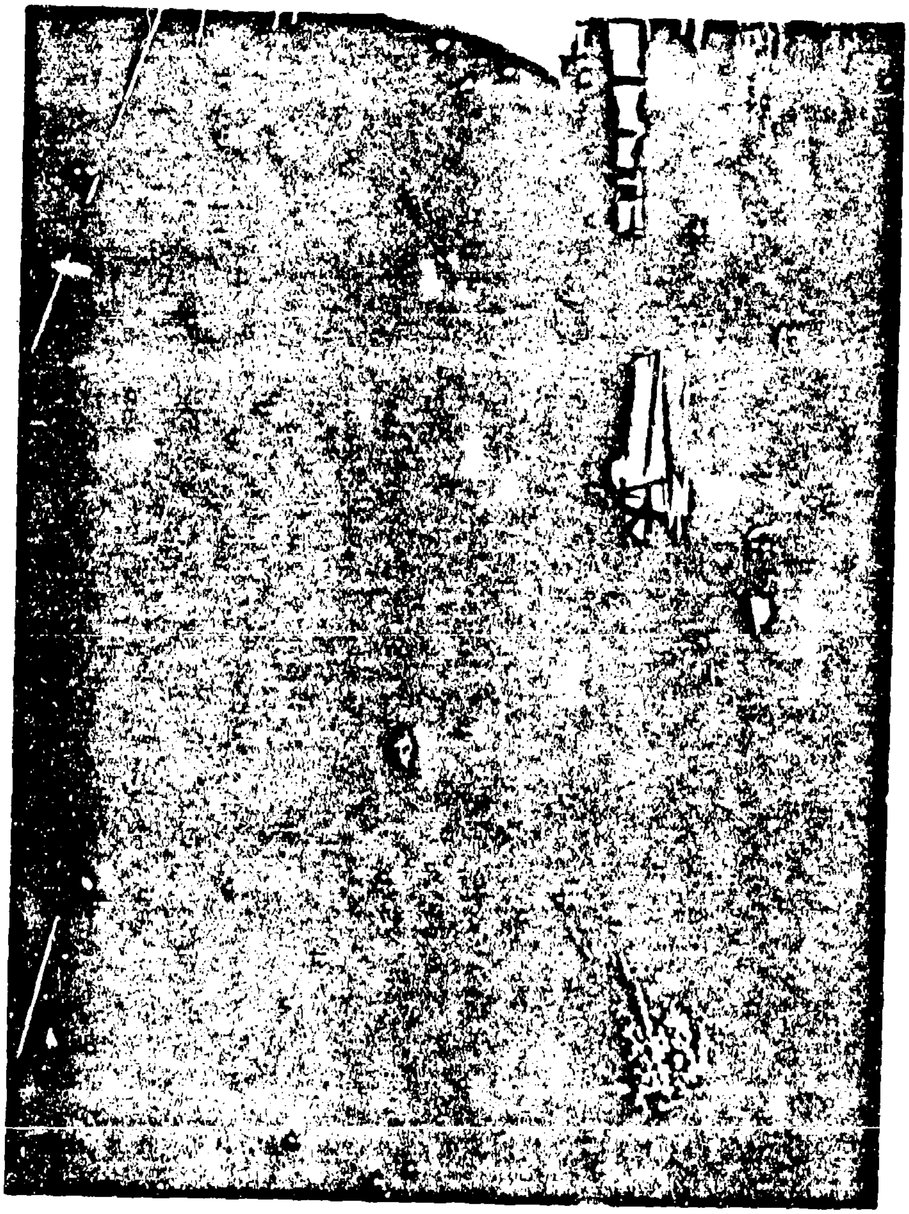

Figure 2-34. X403646-1 Thrust Chamber Assembly (Grano Steel) (U)

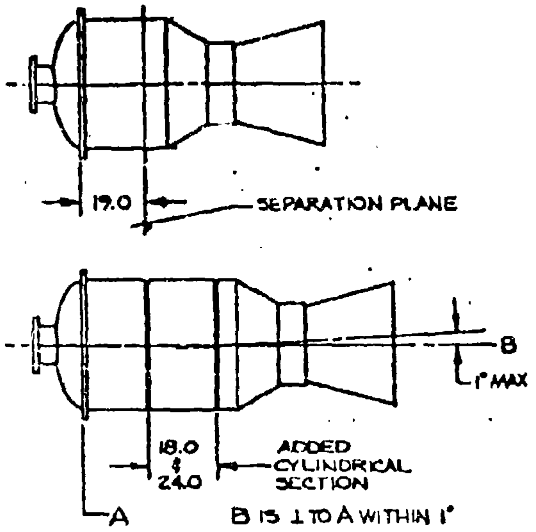

Figure 2-35. Modification 1 and 2 to X403646-1 (U)

2.5.1.1 Combustion Chamber - Modification 1

(U) The initial combustion chamber delivered to the AFRPL was modified after the initial 22 test firings. In order to determine the effect of chamber length on performance a 24 inch long cylindrical section was added to the baseline X403646 chamber as shown in Figure 2-35. The cylindrical section was rolled from 1/2 inch T-1 steel plate, welded, chamfered and delivered to the AFRPL for welding into the development thrust chamber. This combustion chamber was employed on test firings 35-46, 101, 102 and 108-110. A 12 inch longer chamber (modification of the facility checkout chamber) was employed on test firings 33 and 34. The modification of this chamber is described in Appendix A, Section 1.2.2.1.

(U) This chamber was also used in the checkout of the S/N 001 and S/N 002 demonstration injectors (X404056-1) during test firings 72-77 and 98-100.

2.5.1.1.1 Combustion Chamber - Modification 1A

(U) After test firing 77 a turbulence ring (X404469-1) was welded into the lengthened development combustion chamber assembly. This chamber configuration (X403646-14) was used on test firings 90-93.

2.5.1.2 Combustion Chamber - Modification 2

(U) The second of the two original heat-sink combustion chambers delivered to the AFRPL was modified in much the same manner as the initial development combustion chamber. An 18 inch long cylindrical section was rolled from T-1 steel plate, welded, chamfered, and delivered to the AFRPL for welding into the X403646 thrust chamber at a point 19 inches downstream of the thrust plate. This chamber was not used in any test firings as a heat-sink thrust chamber.

(U) The S/N 002 chamber was lined with a low-cost gypsum-phenolic insulation at AFRPL by personnel of the Insulation Systems Inc. This lined combustion chamber was test fired on 4 June 1969 (Test Firing 78) for approximately 10 seconds to check injector durability and material performance.

2.5.2 Thrust Mount

(U) The thrust mount consisted of a 3/8 in. thick support ring (X403646-6) fabricated from T-1 steel plate 11.0 inch wide by 135.0 inch long. The support ring was welded to the cylindrical chamber section downstream of the weld which connected the semi-elliptical head (X403668-8) to the cylindrical chamber body (X403668-5). Shims were used to space the -6 support ring so that a minimum 0.040 in. clearance was maintained between the support ring and main chamber section. The thrust mount ring (X403668-7) was fabricated from 1.00 inch thick USS T-1 steel plate which was welded to the support skirt. The mounting hole pattern was 20, 1-1/8 inch diameter holes, on a 44.0 inch diameter bolt circle.

2.5.3 Instrumentation Ports

(U) Instrumentation and pulse gun bosses were added to the basic thrust chamber assembly (X403646-1) as shown on TRW drawings X404053-1 and X404097-1. Three tangential pulse gun bosses and two radial pulse gun bosses were added to the combustion chamber as shown in Figure 2-36. These bosses were located in the same plane approximately 6.0 inches below the impingement plane. Four bomb bosses were installed on the thrust chamber assembly as shown in Figure 2-36. Two of the bomb bosses were installed in the elliptical head; the other two were added in the combustion chamber section.

(U) Four Photocon pressure transducer ports (1.00 - 14NF-28-2B thread) were tapped in the basic pressure shell. Three ports were in the same plane as the pulse gun bosses; the fourth port was located just upstream of the convergent section, in line with the 180° port at the pulse-gun plane. Four 1/4-18 NPT standard pressure ports were also installed in the basic pressure shell for making static pressure measurements.

(U) In addition to the pressure taps a total of 50 thermocouple ports (1/4-18 NPT) were installed at 6 planar locations as shown on TRW drawing X404097 (Figure 2-37). Not all of the thermocouple ports were used on all test firings.

2.6 ACQUISITION COSTS

2.6.1 Development Hardware

2.6.1.1 Development Injector

(U) One complete development injector assembly (X403829-1), three additional pintle tip assemblies, three fuel orifice rings (X403832) and one blank oxidizer orifice ring (X403831) were fabricated and delivered to the AFRPL. The orifices in the initial oxidizer orifice ring were machined into the blank rings using conventional milling processes. The orifices in the oxidizer orifice rings used in the Pintle Tip Assemblies (X404408) were machined into blank rings using an electrical discharge machining (EDM) process.

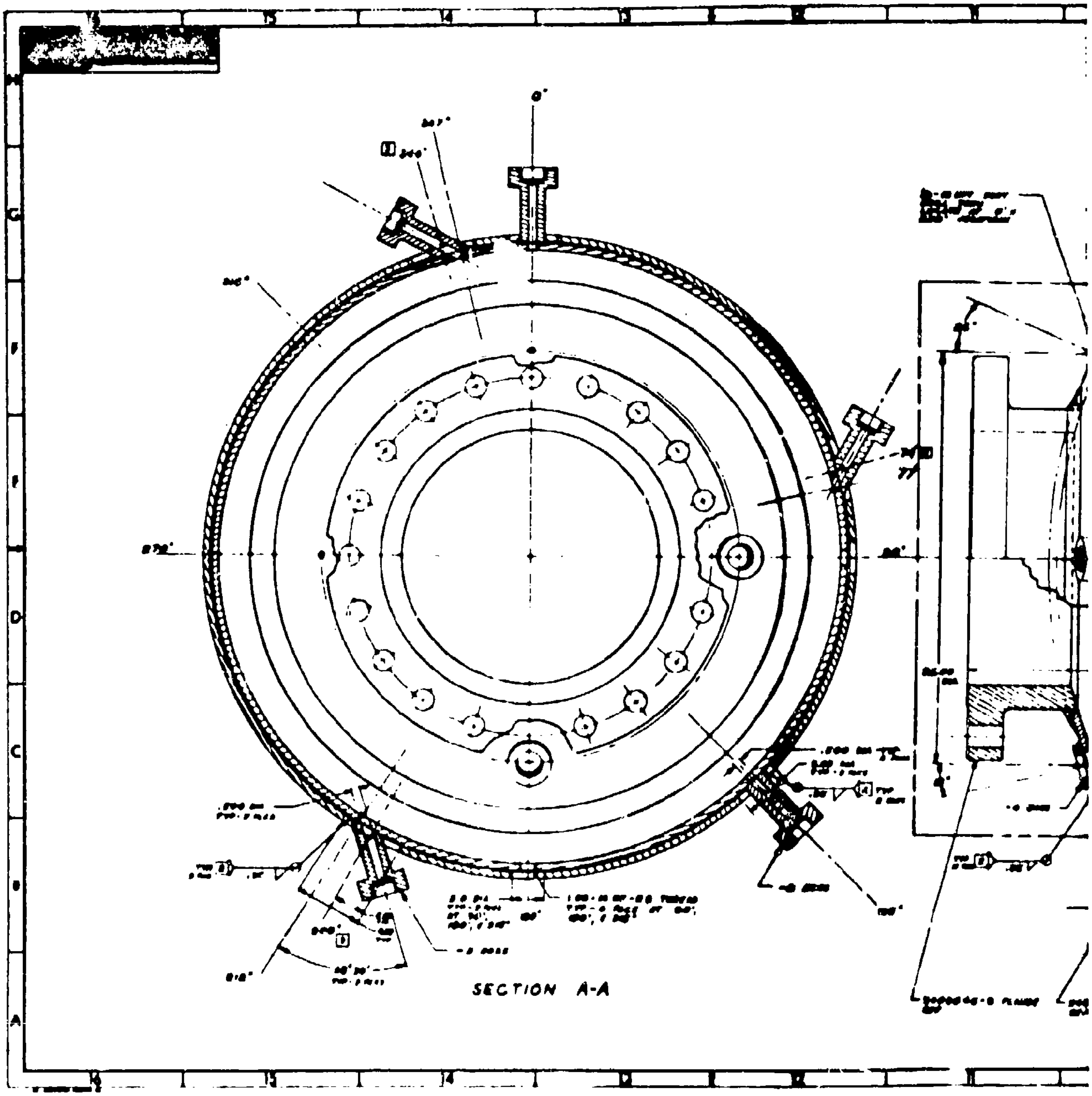
0°
SECTION A-A
15
14
H
G
F
E
D
C
B
A

1

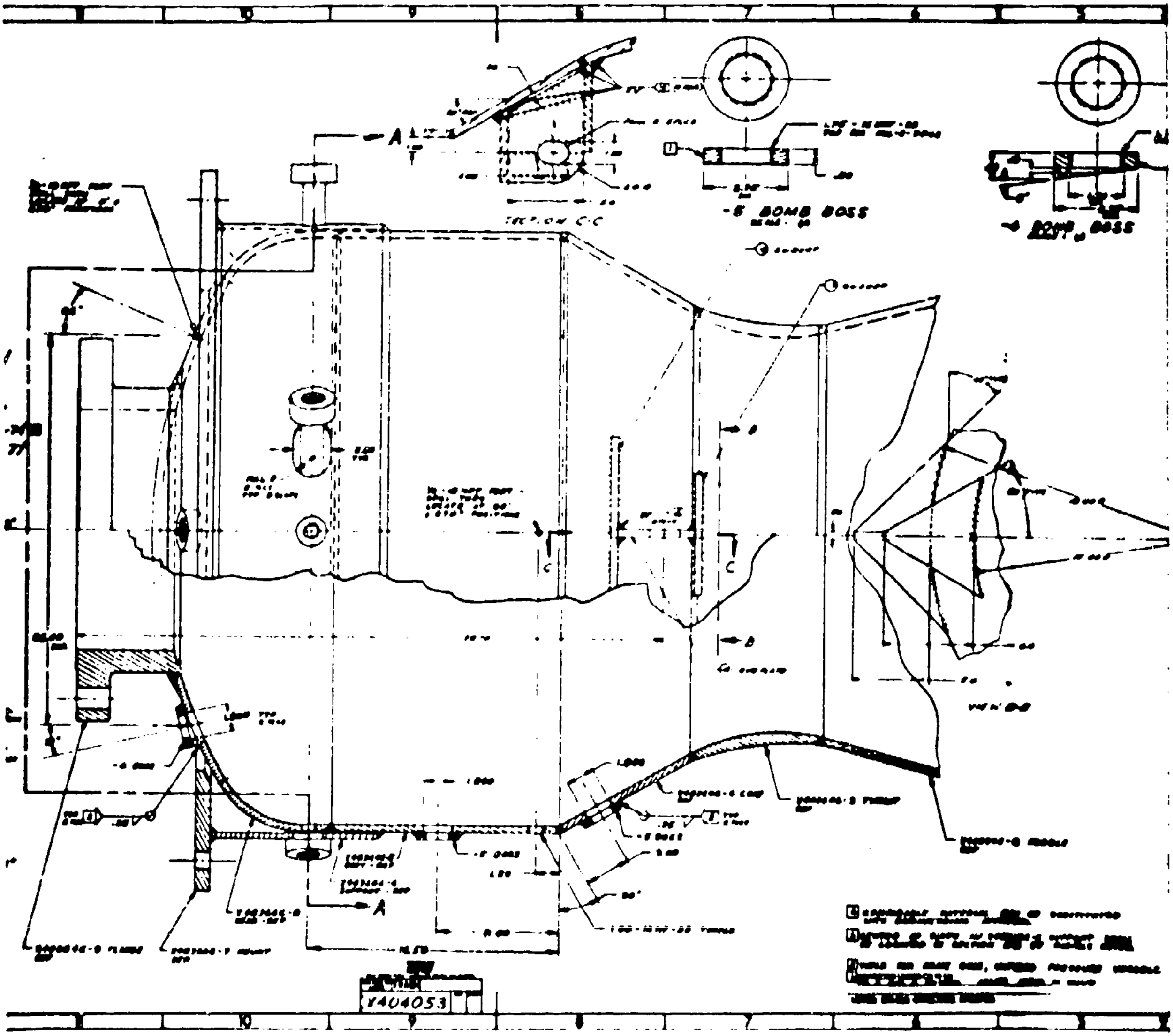
SECTION C-C
-5 BOMB BOSS
-4 BOMB BOSS
A
A
B
B
C
C
16.50
8.00
Y404053

2

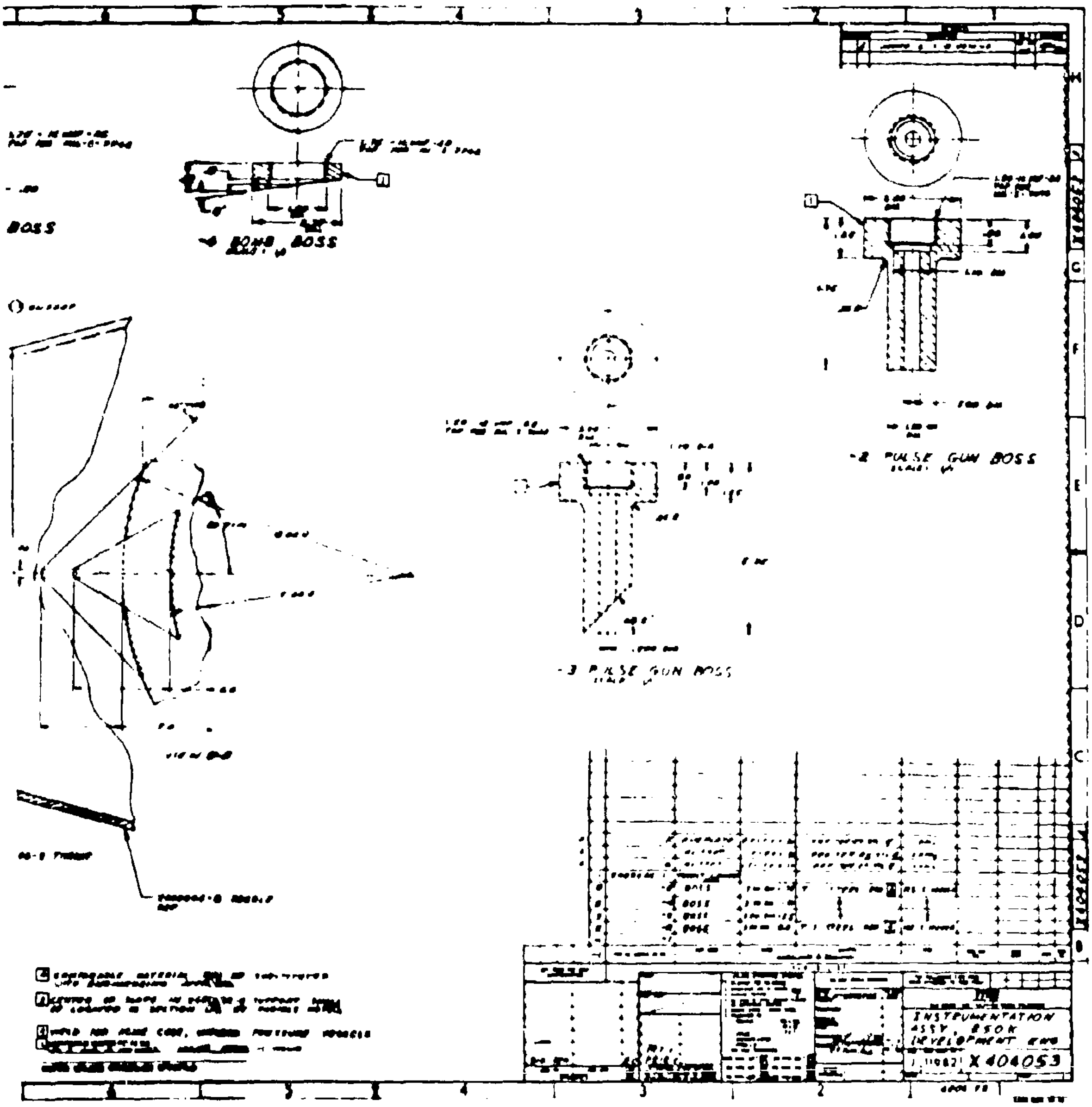
-4 BOMB BOSS
BOSS
-2 PULSE GUN BOSS
-3 PULSE GUN BOSS
VIEW
INSTRUMENTATION ASSY 250K DEVELOPMENT ENG
X404053

Figure 2-36. X404053 Instrumentation Assembly, 250,000 lbf Development Engine (U)

3

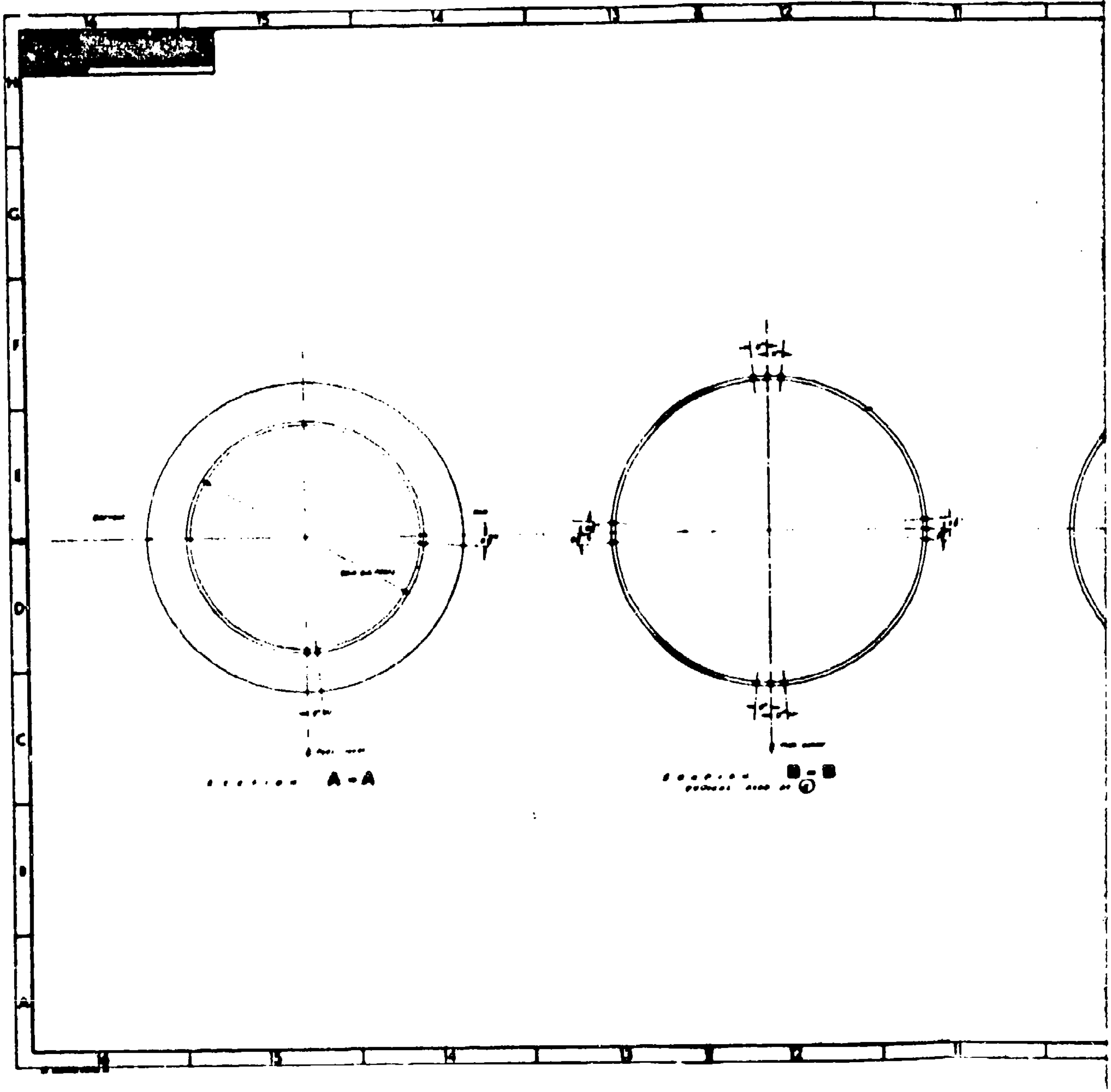

A - A
B - B

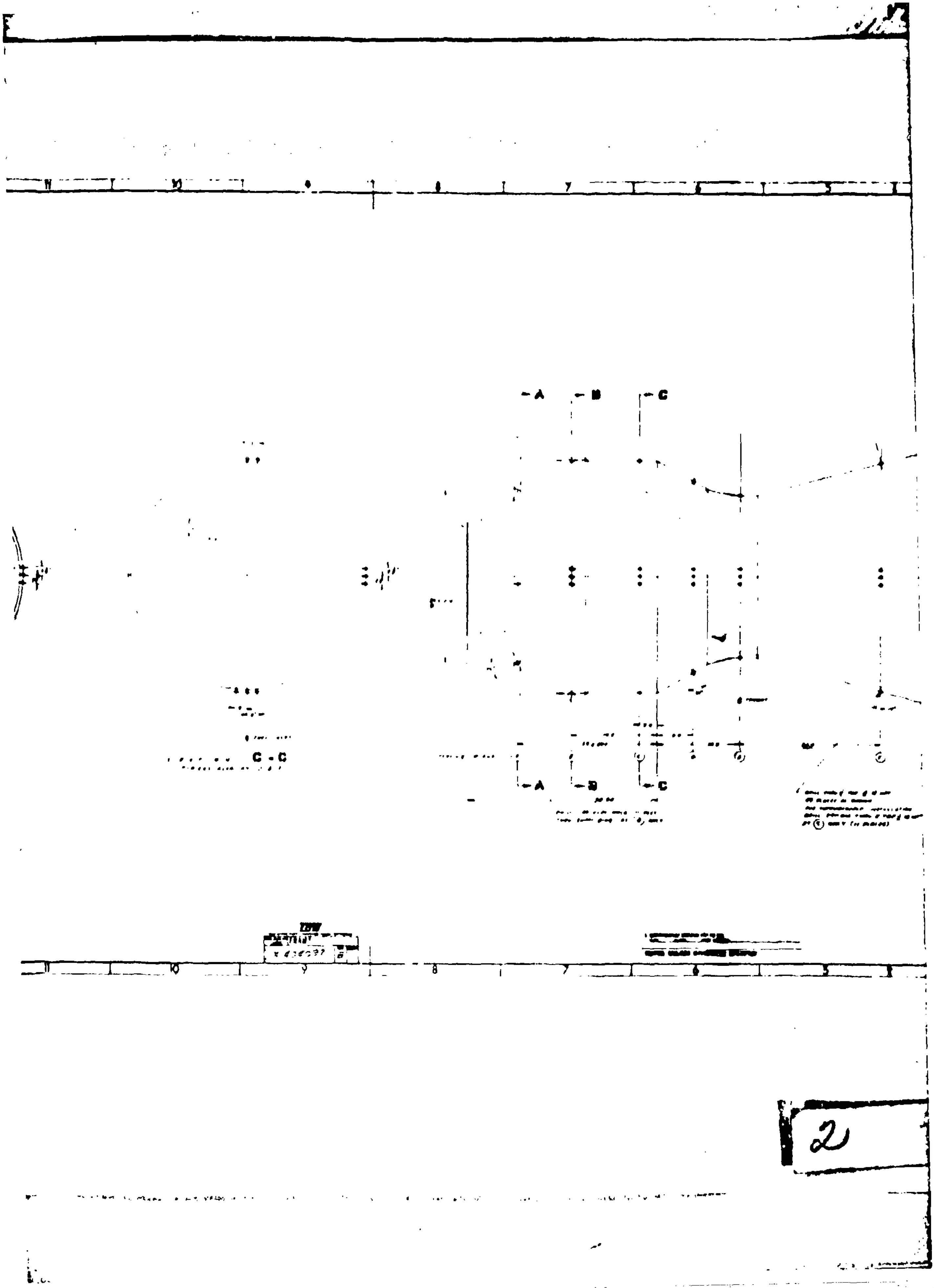
11
10
9
8
7
6
5
A
B
C
C - C
A
B
C
TRW

2

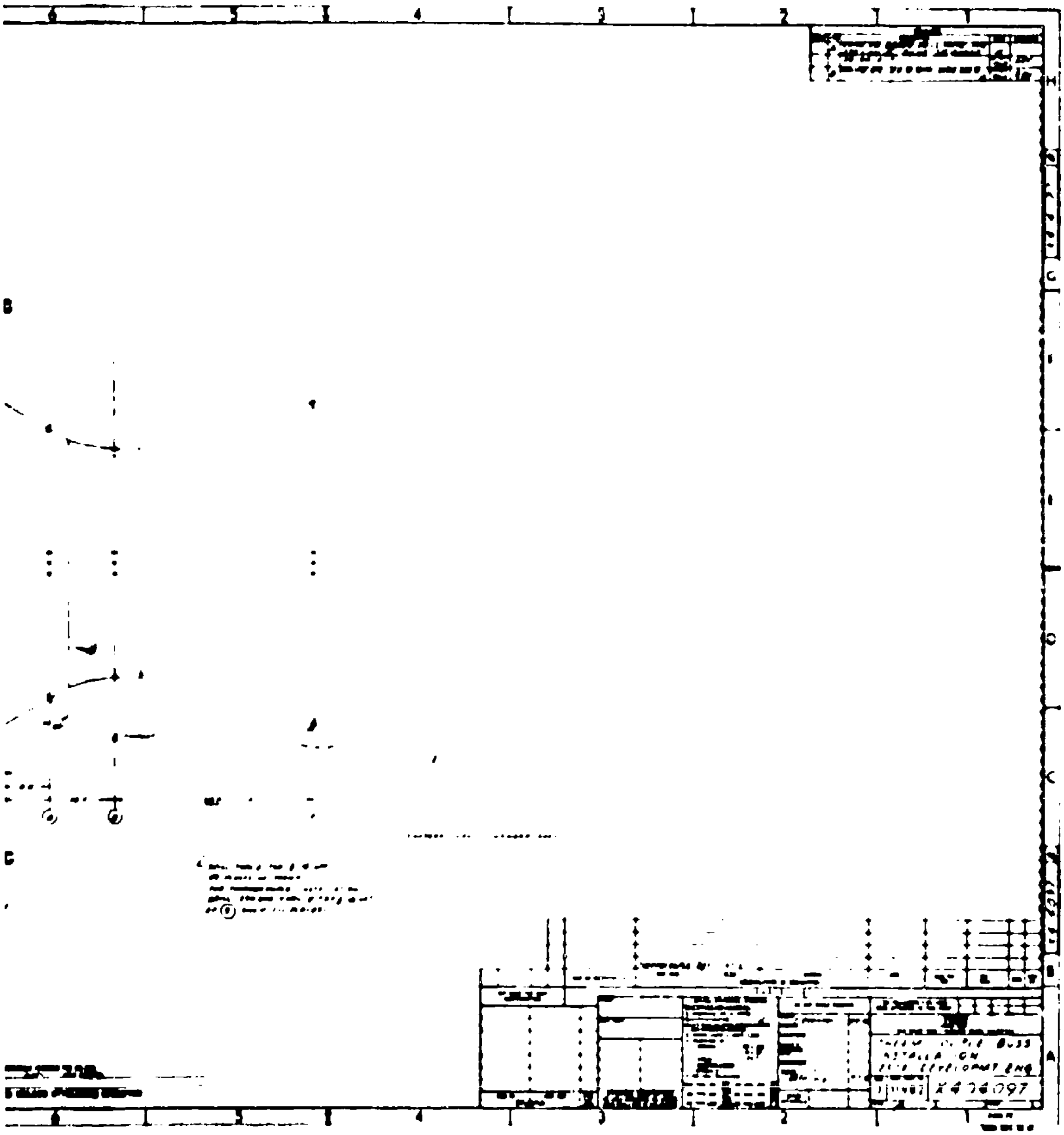

Figure 2-37. X404097 Thermocouple Locations, Development Chamber (U)

3

(U) Acquisition costs for the development injector hardware are tabulated as Table 2-17. The costs include TRW Systems material handling and G&A charges but do not include fee. The major cost component of the development injector assembly is the Pintle Tip Assembly (X404408) which consists of the oxidizer orifice ring, pintle tip and ablative insulation. The oxidizer orifice ring is the most costly of the three components of the Pintle Tip Assembly.

2.6.1.2 Combustion Chambers

(U) Two heat-sink combustion chambers were fabricated for use with the development injectors. The basic combustion chambers were fabricated to TRW drawing X403646. Pulse-gun and bomb bosses were installed per TRW drawing X404053. The 50 thermocouple bosses were located as shown on TRW drawing X404097.

(U) The two chambers were fabricated by different fabricators; Capital Westward, Inc., Paramount, Calif. fabricated the S/N 001 chamber which was used in all development firings, except firing number 78. The Grano Steel Co., Los Angeles, Calif. fabricated the S/N 002 chamber which was used for firing number 78, only. The total cost of the two chambers (with instrumentation and thermocouple bosses) and including nuts, bolts and gaskets for the injector mating flange is shown in Table 2-17. As was the case for the injector these acquisition costs include TRW Systems material handling and G&A charges, but do not include fee.

Table 2-17. Development Hardware Acquisition Costs (U)

Injector Assembly	
X403829-1	$6350
Pintle Tip Assembly	
X404408-2	$1775
X404408-3	1595
X404408-5	1830
Fuel Orifice Ring	
X403832-3	$ 278
X403832-4	278
X403832-5	278
Oxidizer Orifice Ring	
X403831-1 (Blank)	$ 910
Combustion Chamber (*)	
X403646-1 (2)	$14,000

NOTE (*): Includes instrumentation ports, thermocouple bosses, nuts, bolts, and gaskets

PRECEDING PAGE BLANK - NOT FILMED

2.6.2 Demonstration Injectors

(U) Three demonstration injector assemblies (X404056-1) were fabricated and delivered to the AFRPL. The injector assemblies were all fabricated to the same drawing. Neither the fuel or oxidizer orifices are replaceable. The orifices in the oxidizer orifice rings used in the Pintle Tip Assemblies (X404280) were machined into the blank rings using an electrical discharge machining (EDM) process. Fabrication techniques were nearly identical to that employed on the development injector assembly (X403829-1).

(U) Requests for quotations were submitted to ten fabricators. Responses to the RFQ were received from six of the ten fabricators. The successful bidder was the L. W. LeFort Co., Anaheim, Calif. The LeFort Co. did all of the fabrication with exception of the oxidizer orifice ring. The Brackell Co., Culver City, Calif. machined the orifices into the ring using an EDM process. The LeFort Co. also fabricated the ablative pintle tip using Haveg 41F cement.

(U) The unit costs for quantities of 1, 3 and 10 injector assemblies are given in Table 2-18. As in the case of the development hardware the acquisition costs include TRW Systems material handling and G&A charges but do not include fee. The unit costs quoted by the six fabricators for three assemblies varied by $^{+25}_{-60}$ percent of the median value. In all cases the quoted costs indicated a 95 percent shop learning curve.

Table 2-18. Demonstration Hardware Acquisition Costs (U)

Injector Assembly		
X404056-1		
Quantities	1	[illegible]
	3	$4200
	10	$3790

SECTION 3.

TEST RESULTS

3.1 SUMMARY

(U) The results of the Task I test effort are summarized in this section. Detailed discussions of each test series are given in the following sections, together with data reduction procedures and a tabulation of test hardware. The Task I test effort was essentially divided into three phases as follows:

Phase I	Facility Checkout
Phase II	Injector Development
Phase III	Demonstration Injector Checkout

All of the testing was of short duration in a heat-sink thrust chamber with one exception. That exception was firing 78 which was of approximately 10 seconds duration in a low-cost gypsum-phenolic lined heat-sink combustion chamber.

3.1.1 Facility Checkout Firings

(U) A total of ten facility checkout firings were made during the month of October 1968 using the TRW 250,000 lbf Thrust Injector Assembly (X403666) and Thrust Chamber Assembly (X403668). The combustion chamber has a 63-inch L*, 0.87 length to diameter ratio, and a 2.1 contraction ratio. The initial test firing in the series was a short duration Ignition Transient Test and no data for that firing was furnished TRW Systems by the AFRPL. Some minor operating difficulties with the oxidizer feed system were observed during the test series. The welds holding the fuel distribution weir in place were found broken after the test series. This allowed the weir to become cocked and was assessed to be the probable cause of propellant maldistribution observed in the movies of the test firings.

(U) The computed specific impulse efficiency η_{Isp} for test firings 2-10, except 3, is shown in Figure 3-1 as a function of mixture ratio. The Isp is based on the theoretical specific impulse for an $\epsilon = 2.0$ at the computed nozzle stagnation pressure and a 13.2 psia ambient pressure. The η_{Isp} are approximately 6 percent lower than efficiencies which would be realized in a conventional 4:1 nozzle with a 15° half-angle. The 6 percent loss is due to the very low η_{CF} measured in the 2:1 nozzle with 20° half angle.

(U) The computed combustion efficiency (η_{C*}) is shown in Figure 3-2 as a function of mixture ratio. The peak efficiency is strongly dependent on the operating mixture ratio and indicated excessive penetration of the fuel sheet. This results in a fuel rich core and oxidizer rich mantle with a drop-off in performance as mixture ratio is increased.

(U) Similar behavior was experienced with the initial development orifice ring (01), and led to an increase in the percentage open of the primary orifice.

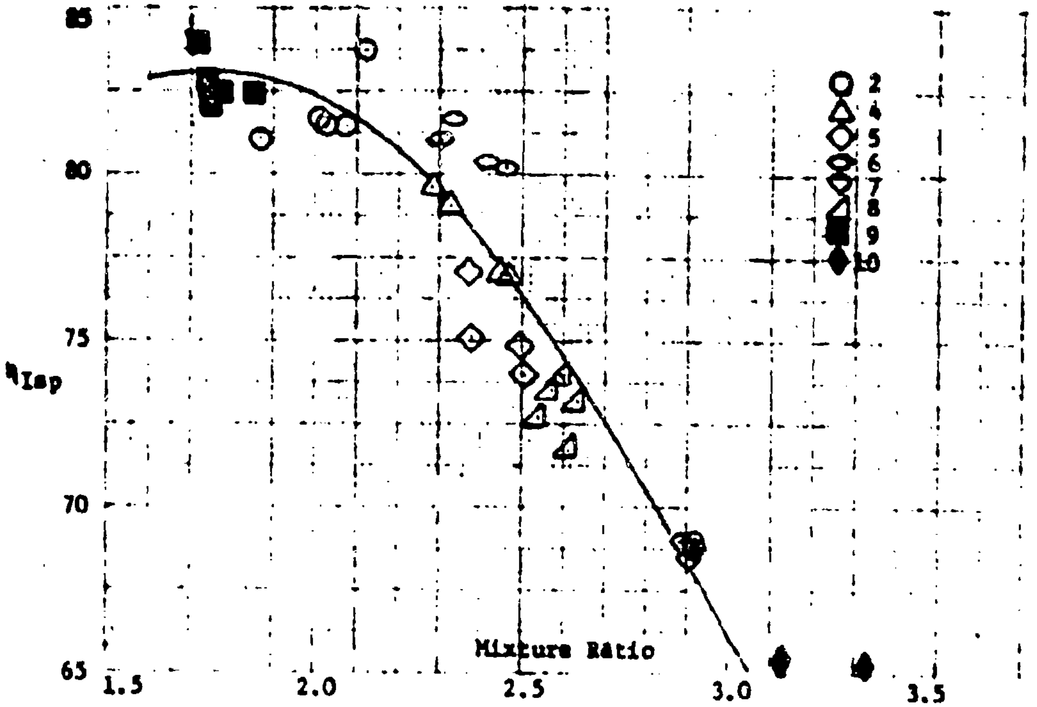

(C) Figure 3-1. Specific Impulse Efficiency - Test Firings 2-10 (U)

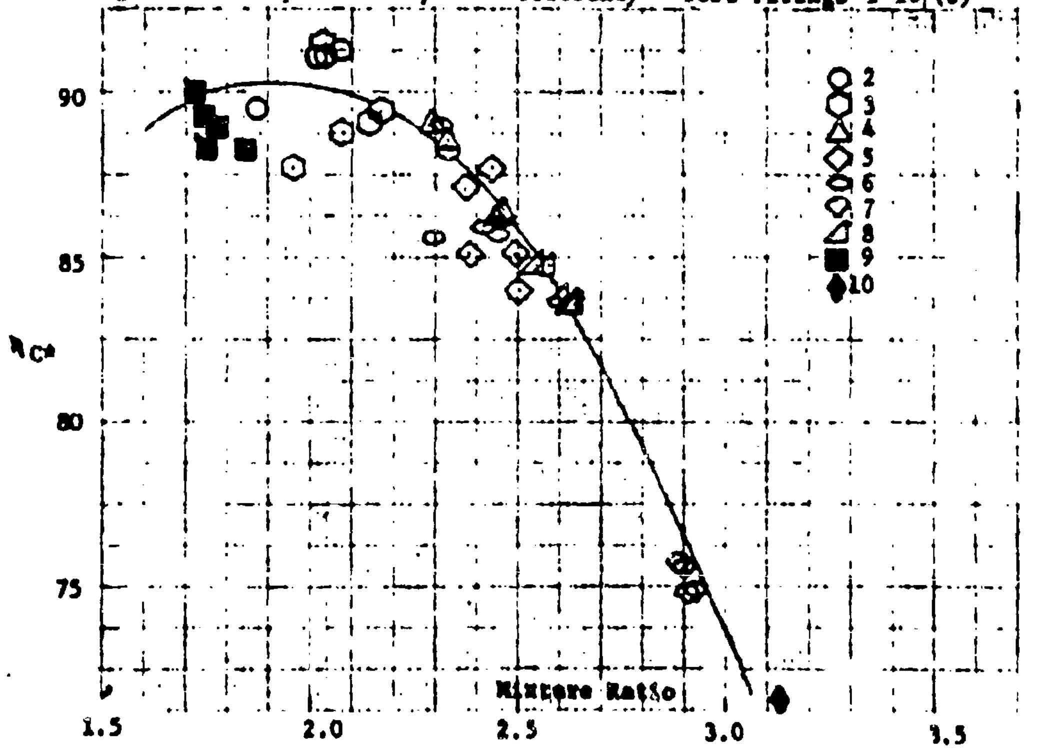

(C) Figure 3-2. Combustion Efficiency - Test Firings 2-10 (U)

3.1.2 Development Injector Firings

(U) A total of forty-one test firings were made with the development hardware to obtain performance, heat transfer, and stability data. Eight injector configurations (fuel-oxidizer orifice configurations) were tested in three different heat-sink chamber configurations (L* of 70, 88 and 120 inches). The initial injector configuration tested (O1/F1) failed to produce test results which duplicated the results obtained with the facility checkout injector. The lowered performance was attributed to excessive oxidizer penetration of the fuel sheet resulting in a fuel rich core and oxidizer rich mantle. The oxidizer orifice ring was reworked to the O1A configuration which provided additional blockage. In addition the fuel injection area was reduced (to increase fuel injection velocity) with the F2 fuel orifice ring. Both 36 and 48 element oxidizer orifice rings were tested during the three month development phase. The O1B/F2 (36 element) and O2/F2 (48 element) injector configurations produced nearly identical performance at the design mixture ratio. Three chamber lengths were investigated with the O1B/F2 injector configuration.

(U) The thrust vs nozzle stagnation pressure graph for firings 11-32 and 35-46 indicated a constant thrust coefficient C_f for all mixture ratios and nozzle stagnation pressures between 200 psia and 300 psia. Test firings 33 and 34 employed a chamber with a 4:1 expansion ratio and 20° half-angle and resulted in a somewhat lower η_{CF}. Figure 3-3 shows the thrust as a function of nozzle stagnation pressure.

(U) The specific impulse efficiency of the O1A/F2 (36 element), O1B/F2 (36 element), and O2/F2 (48 element) injector configurations is shown in Figure 3-4 as a function of mixture ratio. These tests were conducted in a baseline heat-sink combustion chamber with an L* of 70 inches, L_c of 36 inches, and a length to diameter ratio of 0.87. The data for firings 18-21 and 30-32 are shown as one group representing the 36 element oxidizer orifice configuration. Figure 3-5 shows the combustion efficiency for the same three injector configurations. Again the data for firings 18-21 and 30-32 are shown as one group.

(C) The maximum performance was achieved with the thirty-six element oxidizer orifice configuration operating at nearly 60% open area. This performance, both in η_{Isp} and η_{C*} was at the low end of the mixture ratio operating regime. At the design mixture ratio the maximum performance was achieved with the 36 element oxidizer orifice configuration.

(U) In addition to investigating various injection parameters to determine the effect on performance the chamber length was varied for another series of tests. The O1B/F2 injector configuration was used for this test series. Figure 3-6 shows the specific impulse efficiency, η_{Isp}, for three mixture ratios at three discrete chamber lengths. The performance for the 2.4 and 2.6 mixture ratios are essentially constant for chamber lengths 12 inches or longer than the baseline chamber length. This is due to the flattening of combustion efficiency curve, η_{C*}, as shown in Figure 3-7. The increased chamber length results in a greater performance increase at the extremes of the mixture ratio operating regime.

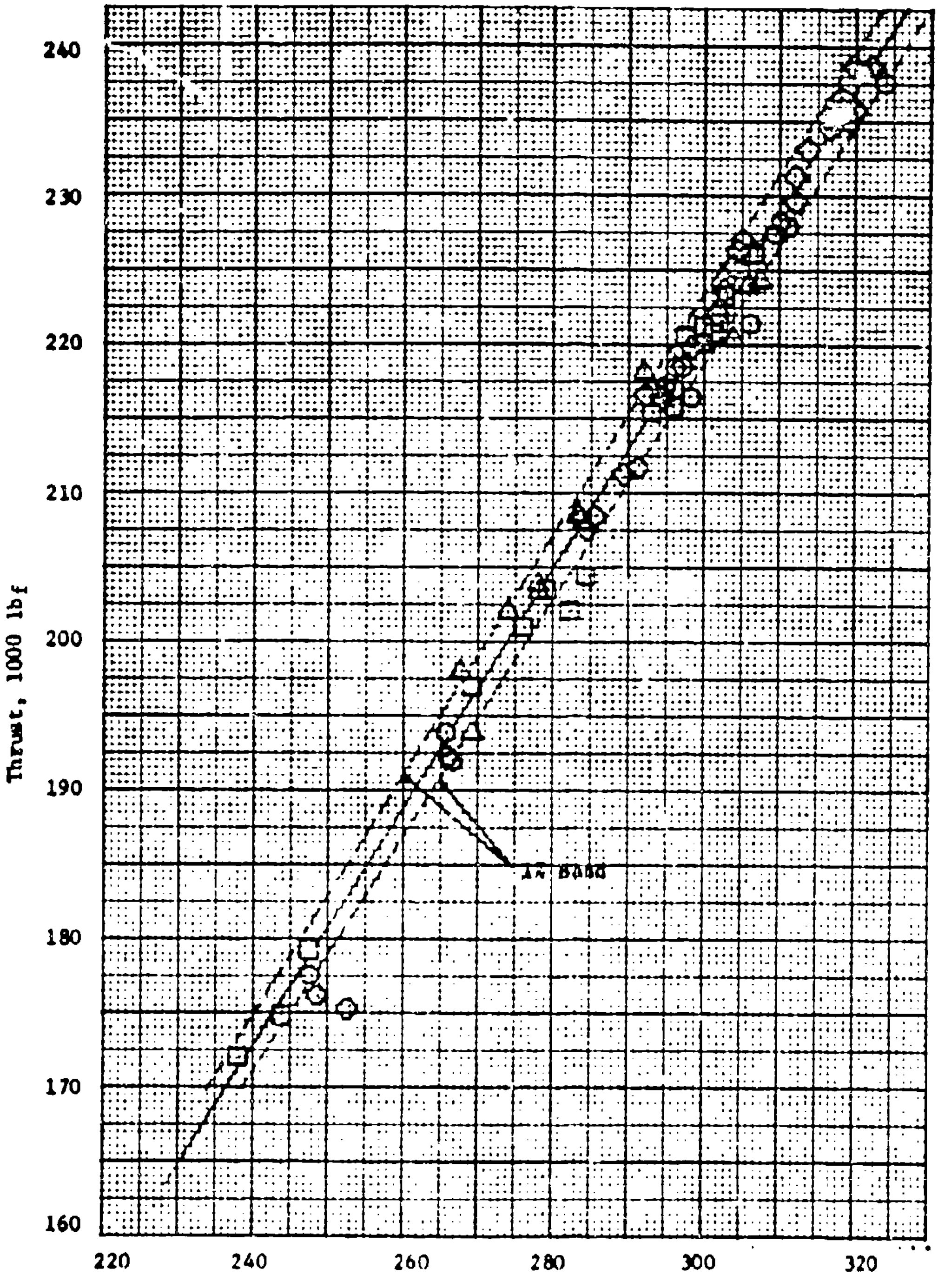

(C) Figure 3-3. Measured Thrust - Development Injector Firings (U)

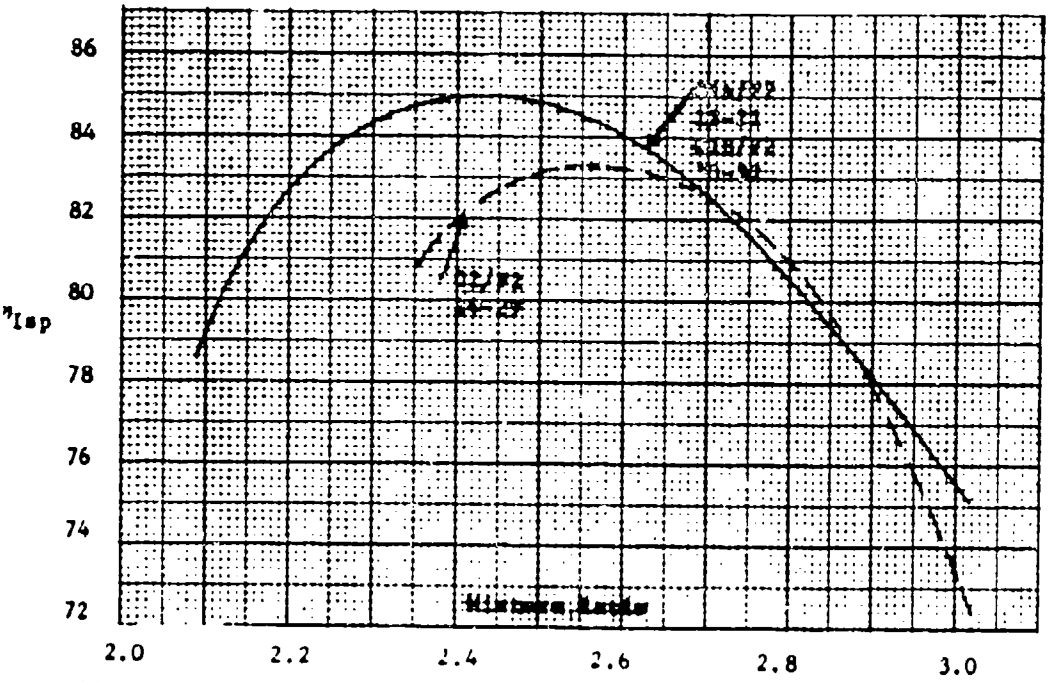

(C) Figure 3-4. Specific Impulse Efficiency - Baseline Chamber (U)

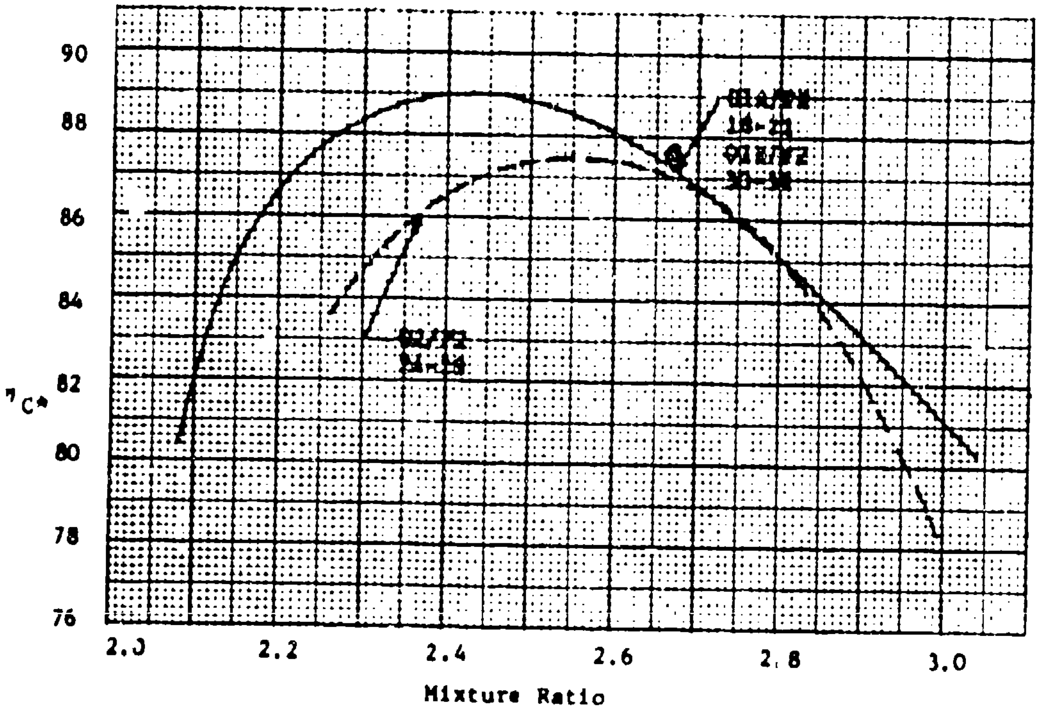

(C) Figure 3-5. Combustion Efficiency - Baseline Chamber (U)

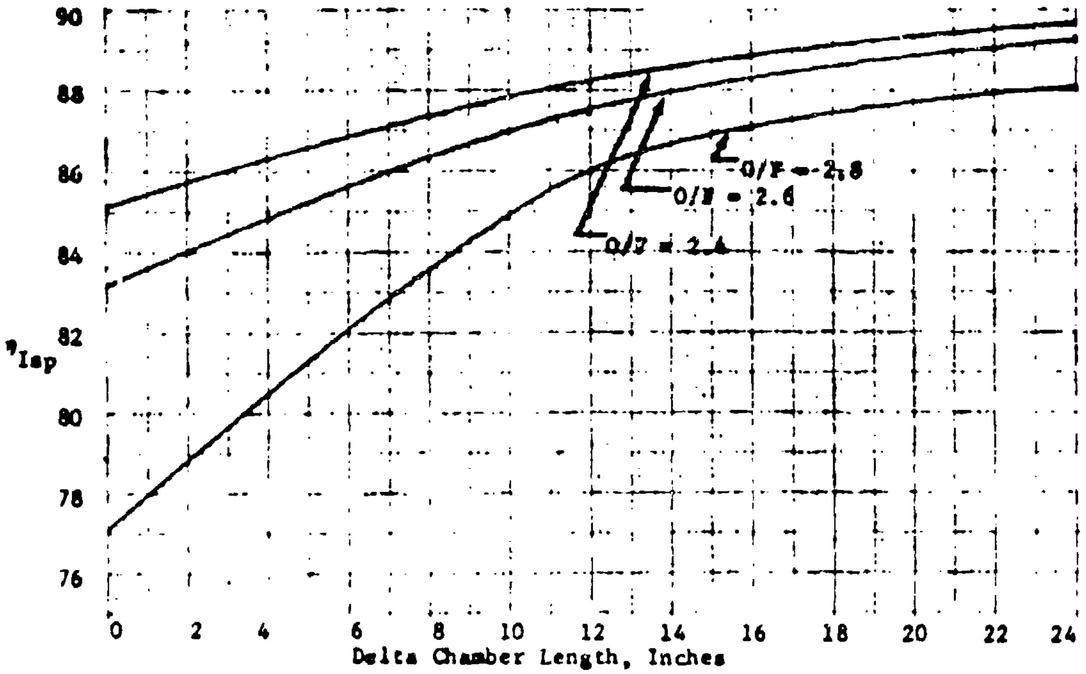

(C) Figure 3-6. Effect of Chamber Length on Specific Impulse Efficiency (U)

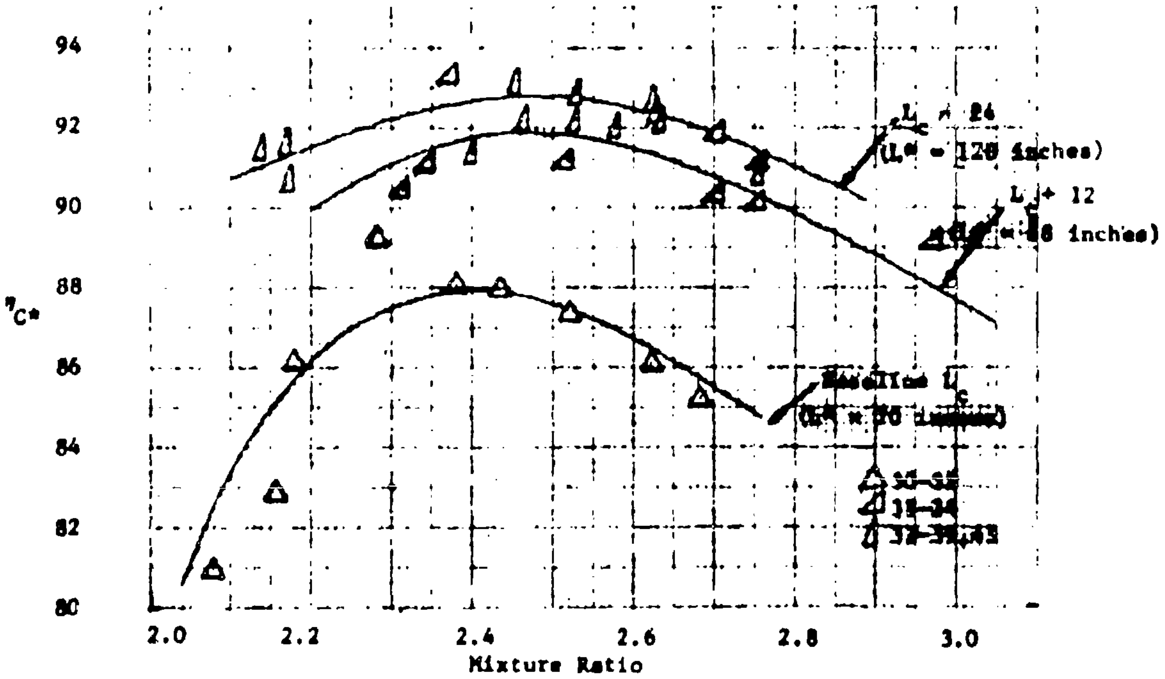

(C) Figure 3-7. Effect of Chamber Length on Combustion Efficiency (U)

3.1.3 Demonstration Injector Firings

(C) A total of fourteen firings were made using two of the three identical demonstration injectors which were fabricated (see Section 2.4). Eleven firings were made with the initial demonstration injector delivered to the AFRPL (S/N 001) while only three firings were made using the S/N 002 injector. The initial six firings of the S/N 001 injector were made in the 60-inch long (L^* = 120 inches) heat-sink combustion chamber; the seventh firing was of approximately 10 seconds duration in the 54-inch long (L^* = 108 inches) heat-sink combustion chamber which had been lined with a low-cost gypsum-phenolic insulation. The final four firings of the S/N 001 demonstration injector were made using the 60-inch long chamber with turbulence ring (X403646-14). During the initial three checkout firings of the S/N 001 demonstration injector high amplitude oscillations at a 5000 cps frequency were experienced in the oxidizer feed system. The three checkout firings of the S/N 002 demonstration injector were made using the 60-inch long heat-sink combustion chamber (without turbulence ring).

(U) Thrust measurements for test firings 72-77 and 90-93 with the S/N 001 injector indicate a constant thrust coefficient C_f, for all mixture ratios and nozzle stagnation pressures between 200 psia and 300 psia. For test firings 98-100 with the S/N 002 injector there is an unexplained loss of 4 percent in C_f as indicated in Figure 3-8

(U) Figure 3-9 shows the calculated specific impulse efficiency for the S/N 001 demonstration injector checkout firings at a nominal 300 psia (72-75), S/N 001 injector firings in the heat-sink chamber with turbulence ring (90-93) and the S/N 002 demonstration injector checkout firings (98-100). The data from the S/N 001 injector firings in the 60-inch heat-sink combustion chamber with turbulence ring indicate an approximate one (1) percent increase in specific impulse efficiency over that obtained on firings 72-75 although the data from firings 72-75 is so widely scattered that a valid comparison is not possible.

(C) The specific impulse efficiency calculated for the S/N 002 demonstration injector (test firings 98-100) indicate a performance level approximately two percent lower than the η_{Isp} measured during firings 72-75 with the S/N 001 demonstration injector. Figure 3-10 shows that the lower specific impulse efficiency is not due to a loss in combustion efficiency since the combustion performance of the S/N 002 demonstration injector is at least equal to or greater than that measured with the S/N 001 demonstration injector. Since the thrust coefficient efficiency is roughly four (4) percent lower than measured during test firings 72-75 the loss in specific impulse efficiency is apparently due to erroneous thrust measurements or chamber pressure measurements or a combination thereof.

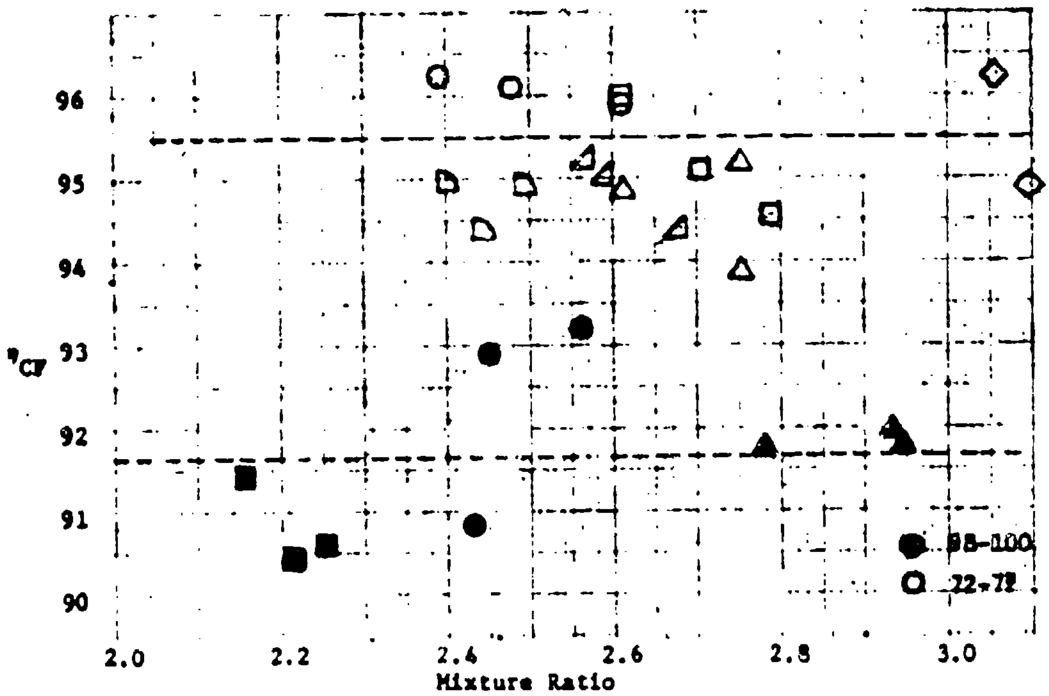

(C) Figure 3-8. Nozzle Efficiency - Demonstration Injector Firings (U)

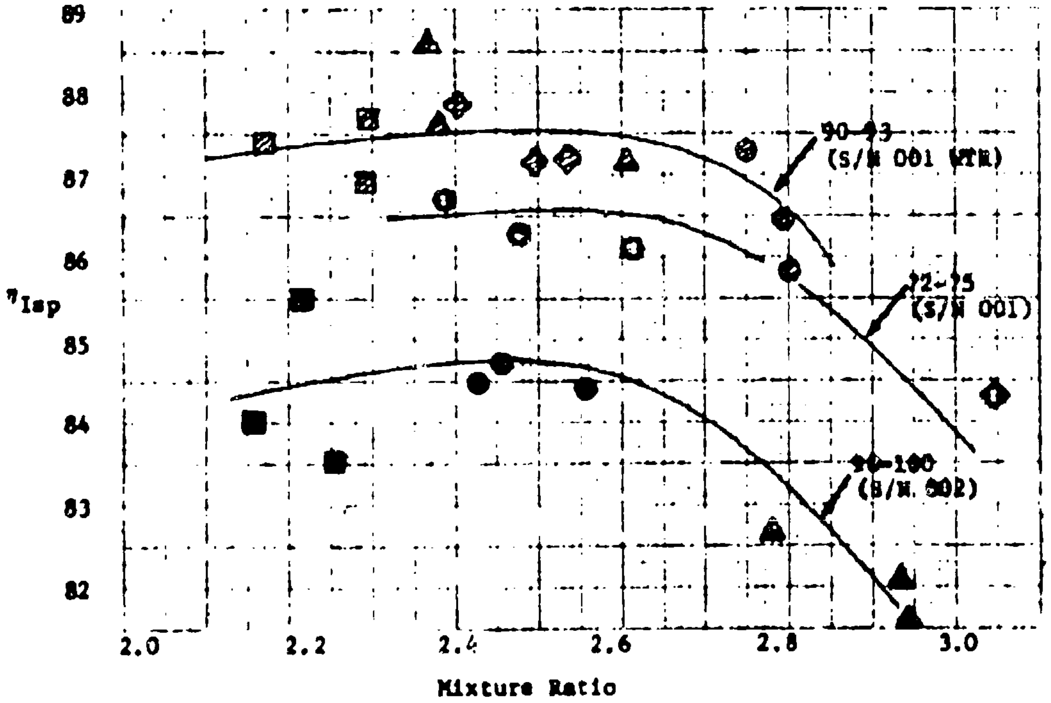

(C) Figure 3-9. Specific Impulse Efficiency - Demonstration Injector (U)

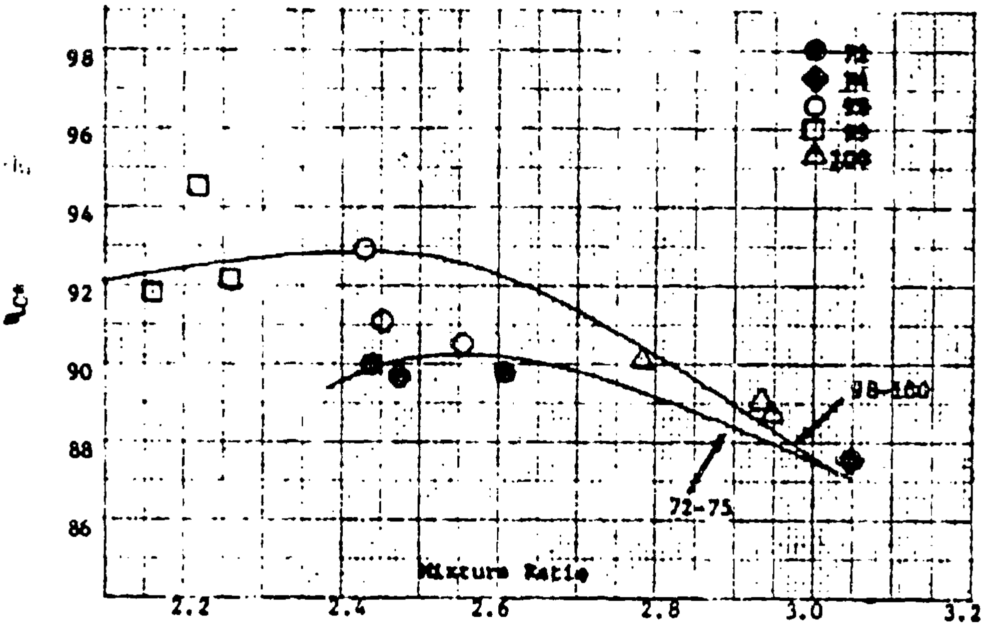

(C) Figure 3-10 Combustion Efficiency - Demonstration Injector Firings (U)

3.2 DATA REDUCTION PROCEDURES

(U) The test results presented herein are derived from computer printout data furnished TRW by the AFRPL. The AFRPL furnished TRW reduced performance data for test firings 2 through 17 and general performance data for test firings 18 through 46, 72-78, 90-93, 98-102, and 108-110. TRW Systems reduced the latter 48 firings; standard data reduction procedures were employed throughout.

(U) The theoretical I_{sp} and C* data for the pressure range of 200 psia 300 psia and mixture ratio of 1.80 to 3.20 (O/F) were curve-fit and used in equation form to compute the theoretical I_{sp} and C*. In general, the nozzle stagnation pressure used to compute the theoretical I_{sp} and C* was based on correcting the injector and chamber pressure measurements for the pressure loss between nozzle throat and injector. This correction assumed isentropic flow in the nozzle and a specific heat ratio γ, of 1.235. Detailed data reduction procedures used in arriving at the test results are given in Appendix C.

3.3 TEST HARDWARE

(U) The test hardware, including injector configuration, used in the 65 test firings is tabulated as Table 3-1. The initial 10 test firings employed the TRW 250,000 lbf thrust engine which was test fired in 1967 at a reduced chamber pressure of 60 psia and approximately 50,000 lbf thrust.

(U) Table 3-1. Test Hardware Configurations (U)

TEST FIRINGS HARDWARE	1-10	11-15	16-17	18-23	24-29	30-32	33-34	35-36	37-38,43,46	40-42	44-45	72-77	78	90-93	94-100	101-102	108-118
INJECTOR ASSEMBLY																	
XA03666	X																
XA03829-1		X															
XA03829-16			X	X		X	X		X							X	
XA03829-17					X					X							
XA03829-18								X									
XA03829-19											X						
XA04036-1 (S/N 1)												X	X	X			
(S/N 2)															X		
(S/N 3)																	
XA03829-20																	X
PINTLE TIP ASSEMBLY																	
XA04408-1		X	X	X		X	X		X							X	
XA04408-2					X					X							
XA04408-3								X									
XA04408-5											X						
XA04280-1												X	X	X	X		
XA04408-6																	X
OXIDIZER ORIFICE RING																	
XA03831-1		X	X														
XA03831-1A				X													
XA03831-1B						X	X		X							X	
XA04107-1					X					X							
XA04047-1								X									
XA03846-1											X						
XA04693-1												X	X	X	X		
XA04100-1																	X
FUEL ORIFICE RING																	
XA03832-3		X															
XA03832-4			X	X	X	X	X	X	X	X	X					X	X
THRUST CHAMBER ASS'Y																	
XA03648-1	X																
XA03648-1A							X										
XA03646-1		X	X	X	X	X											
XA03646-11								X	X	X	X	X			X	X	X
XA03646-10 (Mod)													X				
XA03646-14														X			

(U) The test hardware was modified to allow operation at rated conditions. These modifications are described in Appendix A. The development injector assembly (X403829) was used in test firings 11 through 46. Various injection orifice configurations were tested. The X403646 development thrust chamber assembly was employed in test firings 11 through 46 except for 33 and 34 which used a modified X403668 thrust chamber.

(U) The demonstration injector assembly (X404056) was used in test firings 72-78, 90-93 and 98-100. The X403646-11 development thrust chamber was used in test firings 72-77 and 98-100. The X403646-10 (insulated with a low-cost gypsum-phenolic insulation) was used for the 10 second test firing (number 78). The X403646-14, modified to include the turbulence ring was used on test firings 90-93.

(U) The last two test series conducted in Task I (101-102 and 108-110) were made using the development injector assembly (X403829), and the X403646-11 development thrust chamber assembly

3.4 DETAILED TEST RESULTS

3.4.1 Facility Checkout Firings

3.4.1.1 Performance Data

(U) Test results obtained in the initial facility checkout firings (2-10) are discussed in the following paragraphs. Ten firings were made with the X403666/X403668 Injector/Thrust Chamber combination ($L^* = 63$ inches). Test firing 1 was a very short duration start transient test and no data for this firing was furnished to TRW Systems.

(U) Figure 3-11 shows the measured thrust as a function of nozzle stagnation pressure. The nozzle stagnation pressure is the average of the two head-end pressure transducers (PC-1 and PC-2), corrected for an $\epsilon_C = 2.10$ and a $\gamma = 1.235$, for test firings 2 through 8. For test firings 9 and 10 the nozzle stagnation pressure is computed from PC-1, only. Thrust data for test firing 3 is not available. The data for test firing 8 falls outside of the normal band of data. This is due to an unusually high PC-2 measurement which results in a P_o average higher than normal. Information required to ascertain the cause of the high PC-2 measurement is not available. This high PC-2 for test firing 8 also results in a lowered C_f and η_{CF} shown in subsequent sections. The computed specific impulse efficiency, η_{Isp}, is shown in Figure 3-12 as a function of mixture ratio.

(U) The computed combustion efficiency, η_{C*}, for this test series is shown in Figure 3-13 as a function of mixture ratio. The nozzle stagnation pressure in the C* equation is computed from the average of PC-1/PC-2 for firings 2 through 8, and from PC-1 only for test firings 9 and 10. The dashed curve on Figure 3-13 is for a combustion efficiency based on the nozzle stagnation pressure computed from the PC-3 (nozzle entrance pressure measurement. The PC-3 measurement was available for firings 9 and 10 only. The ratio of PC-1/PC-2 (average)/PC-3 for test firings 9-17 was 1.071 which results in a β term value (Appendix C) of 0.982. This value was used to recompute the combustion efficiency based on nozzle entrance pressure.

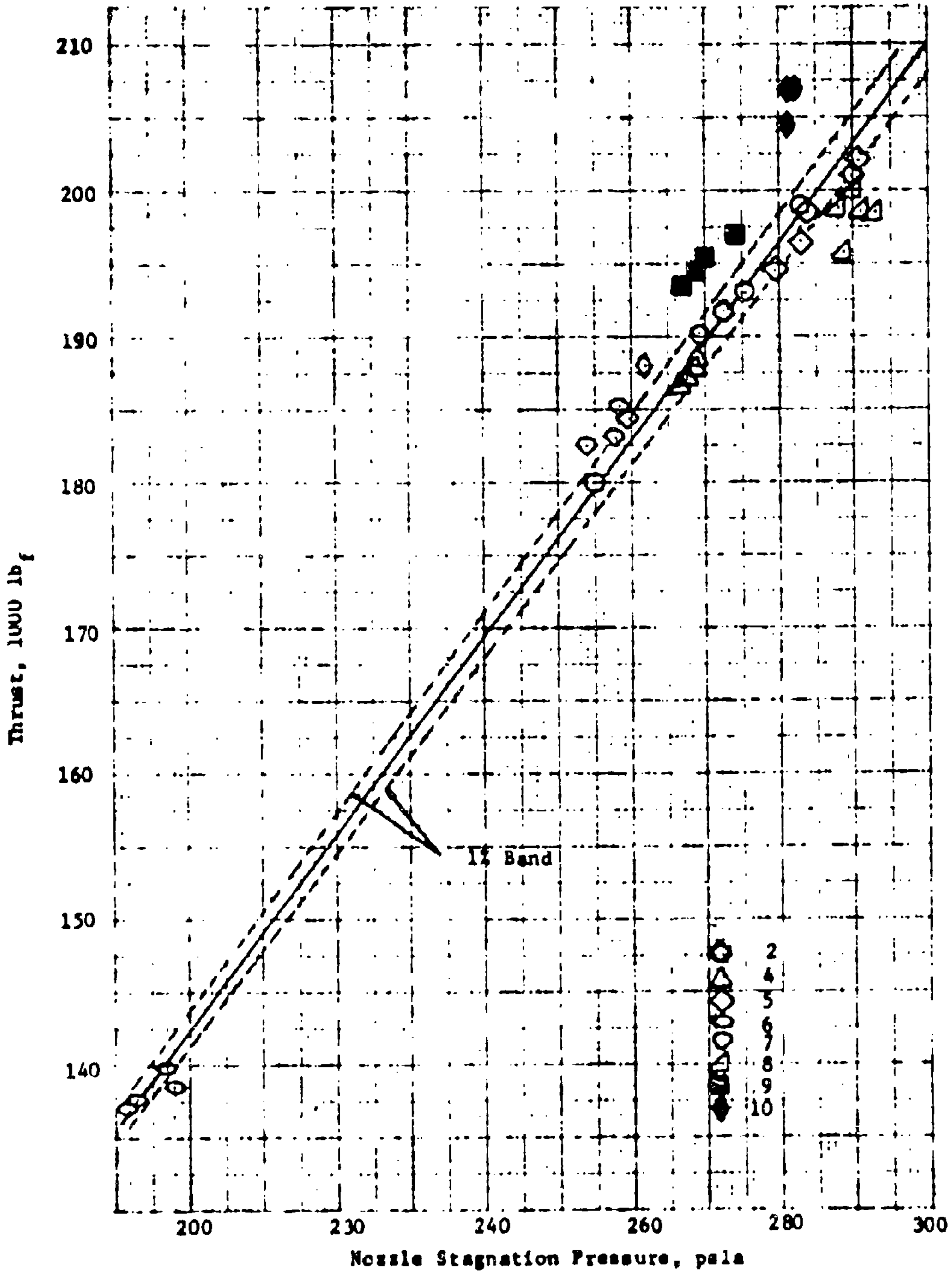

(C) Figure 3-11 Measured Thrust - Facility Checkout Firings (U)

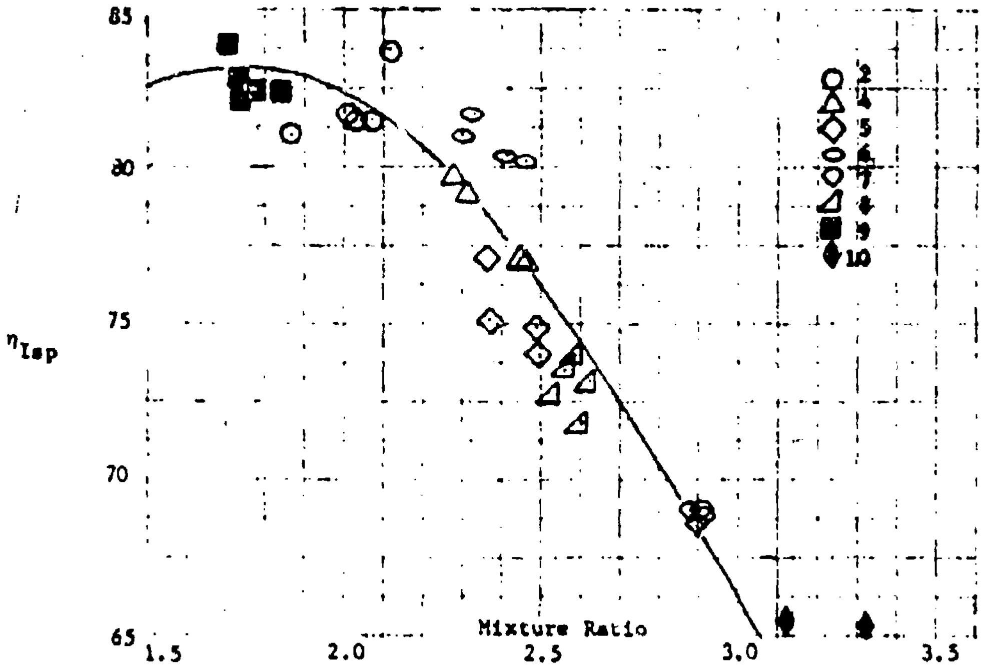

(C) Figure 3-12 Specific Impulse Efficiency - Facility Checkout Firings (U)

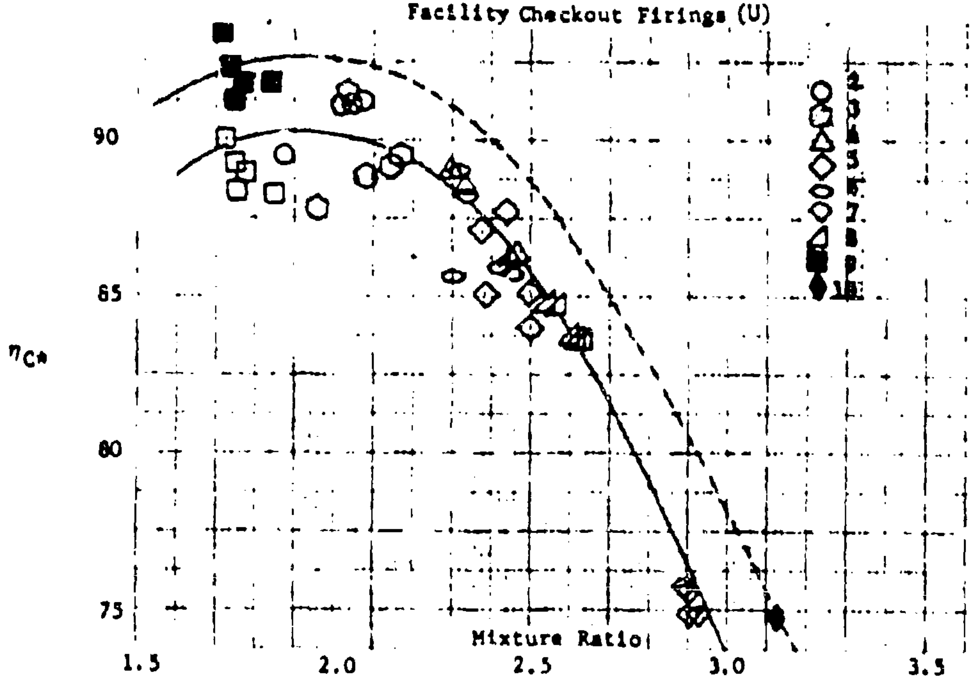

(C) Figure 3-13 Combustion Efficiency - Facility Checkout Firings (U)

(C) The computed nozzle efficiency, η_{CF}, for this test series is shown in Figures 3-14 and 3-15 as a function of mixture ratio and nozzle stagnation pressure respectively. The nozzle efficiency is based on a nozzle stagnation pressure computed from PC-1/PC-2 average for test firings 2-8 and from PC-1 for test firings 9 and 10. The mean nozzle efficiancy over the mixture ratio range of approximately 1.70 to 3.30 (O/F) is 0.903 with a range of $\pm$ 0.018 at a nominal nozzle stagnation pressure of 275 psia. No trend with mixture ratio is apparent. Theoretical calculations for mixture ratios of 0.5 to 10.0 (O/F) show less than 0.3 percent variation in the theoretical thrust coefficient. Figure 3-15 indicates higher nozzle efficiency at lower pressures (less under expansion as shown in Figure 3-15). The expected η_{CF} for the 2/1 expansion ratio, 20 degree half-angle conical nozzle was 0.955. The difference of approximately 5 percent between the computed η_{CF}, the theoretical η_{CF} is unexplained.

3.4.1.2 Injector Characteristics

(U) The fuel injection pressure loss (ΔP_{if}) varied considerably during the course of most test firings. The injector conductance, KIJCF, is plotted in Figure 3-16 as a function of time. The injector conductance is defined as

$$\text{KIJCF} = \frac{Q_f \sqrt{\rho_f}}{\sqrt{\Delta P_{if}}} \qquad (3\text{-}1)$$

and should be invariant for a fixed area injection orifice operating over a narrow range of volumetric flow rates. This behavior was unexplained until the test series was completed and the test hardware was returned to TRW Systems. Upon disassembly of the injector, the inner fuel shell (weir), P/N X403666-7, was observed to be cocked in the fuel jacket as shown in Figure 3-17. All welds holding the weir in place were broken. The time dependent KIJCF was probably due to this defective component. Examination of the high speed motion pictures taken of the test firings show a propellant maldistribution which is also attributed to this condition.

(U) The engine performance cannot be shown as a function of the scaling parameter $\left[(\Delta P_T)^{0.5}(\mu)^{0.4}\right]$ due to the invalid ΔP_{if} measurements. The injector conductance for the oxidizer side, KIJCO, is shown in Figure 3-18 as a function of the volumetric flow rate. The nominal discharge coefficient computed from the following equation:

$$C_d = \frac{1.495}{A_{io}} \left[\text{KIJCO}\right] \qquad (3\text{-}2)$$

is 0.730 which compares with the value of 0.74 predicted from water flow data Appendix A.

3.4.2 Development Injector Firings

3.4.2.1 Test Series 1 and 2 - Firings 11-17

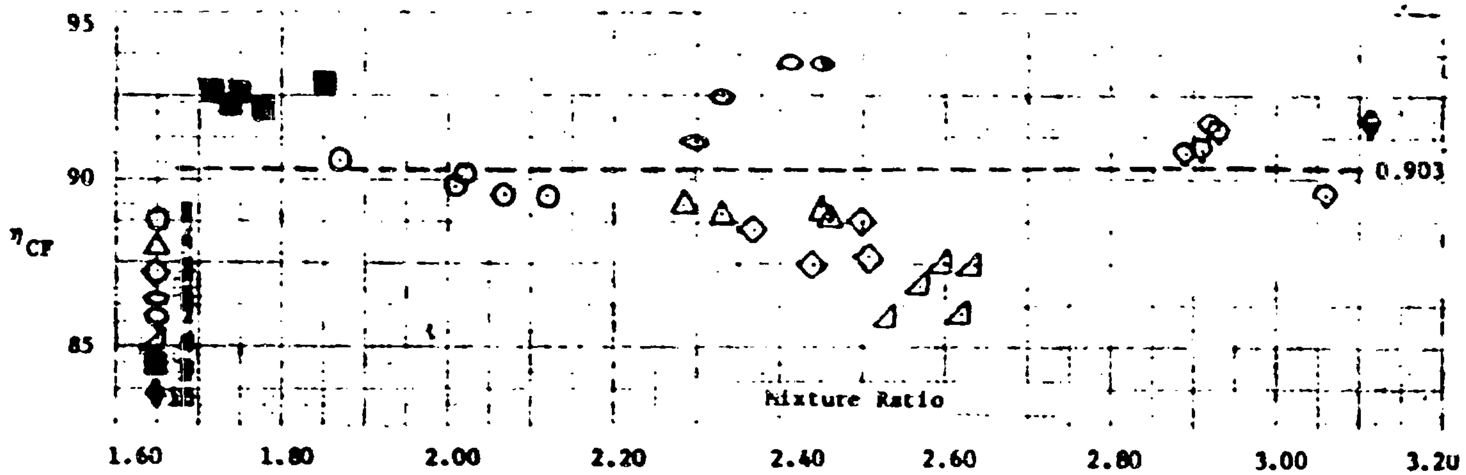

(C) Figure 3-14. Nozzle Efficiency - Function of Mixture Ratio (U)

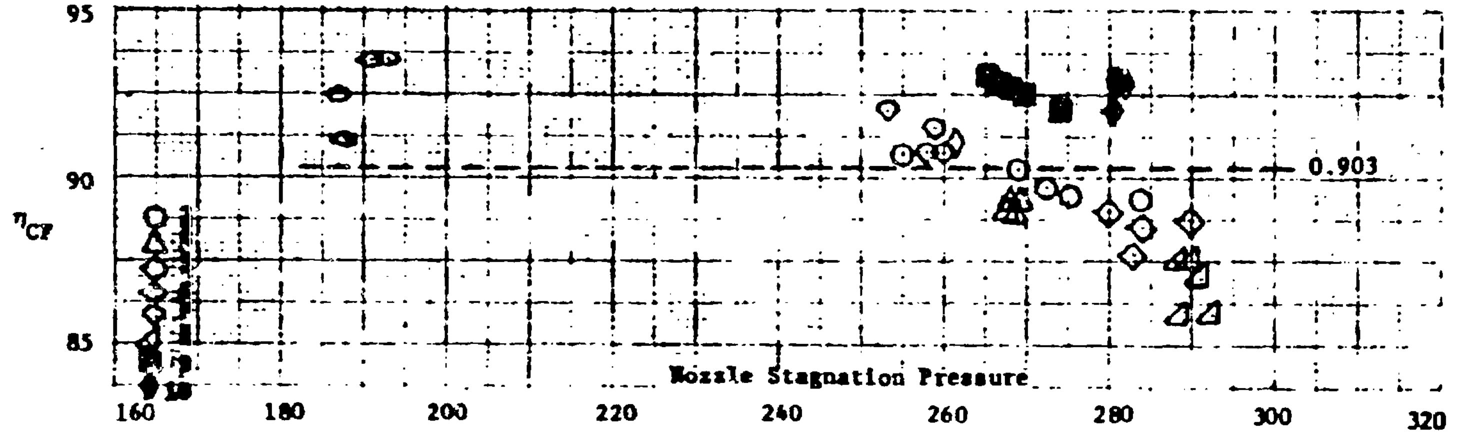

(C) Figure 3-15. Nozzle Efficiency - Function of Nozzle Stagnation Pressure (U)

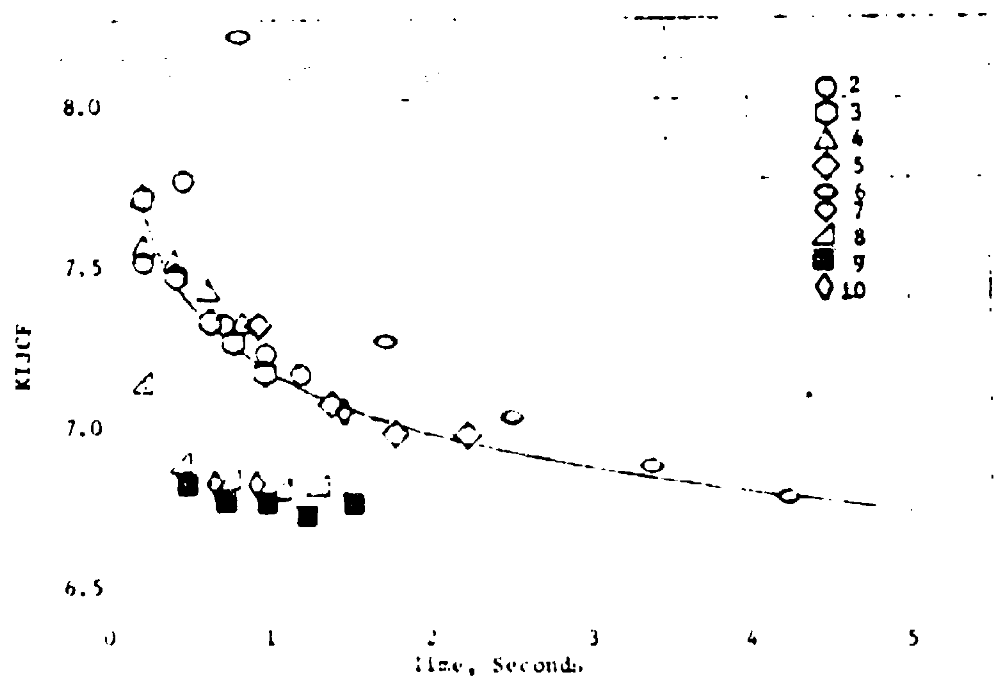

(U) Figure 3-16. Fuel Injector Conductance - Facility Checkout Firings (U)

(U) Figure 3-17. Facility Checkout Injector - Photo showing cocked weir (U)

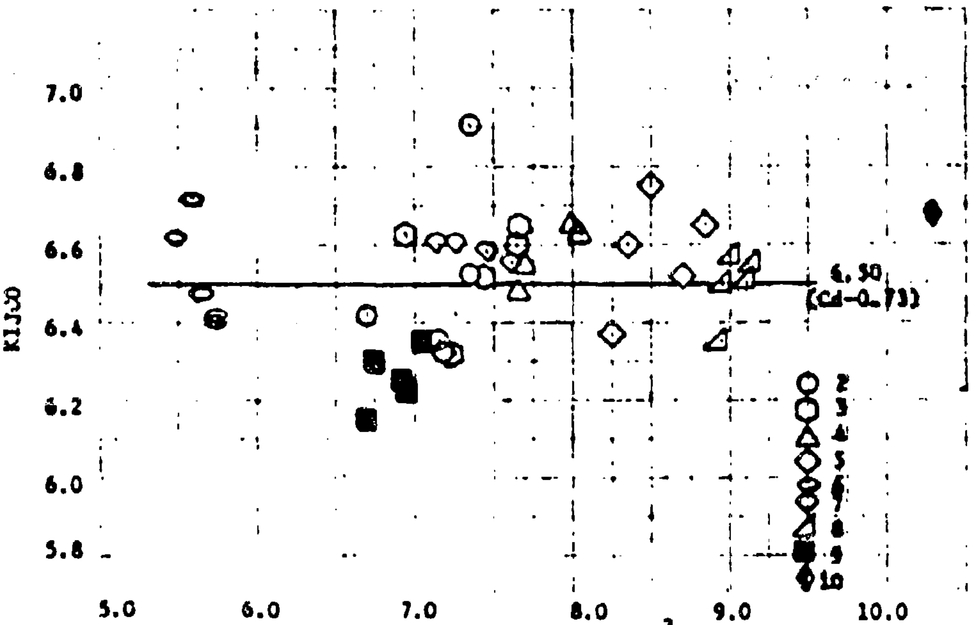

(U) Figure 3-18. Oxidizer Injector Conductance - Facility Checkout Firings (U)

3.4.2.1.1 Performance Data

(U) The fuel and oxidizer orifice configurations selected for the initial firings of the development injector assembly (X403829) were chosen so as to duplicate the features used in the facility checkout injector (X403666). The initial test results obtained with the X404408-1 Pintle Tip Assembly failed to duplicate the test results obtained with the facility checkout hardware. The failure to achieve the same performance is attributed to the minor design changes made in the oxidizer orifices as described in Section 2.3.2.1.

(U) Figure 3-19 shows the measured thrust as a function of nozzle stagnation pressure. The nozzle stagnation pressure is the average of two injector and pressure transducers (PC-1 and PC-2), corrected for an $\epsilon_C = 2.25$ and a $\gamma = 1.235$. The computed specific impulse efficiency, η_{Isp}, is shown in Figure 3-20 as a function of mixture ratio. The solid points and dashed line is for test firing 16 and 17 while the solid line is for test firings 11 through 15. Following test firing 15 the X403832-4 fuel orifice ring was substituted for the X403832-3 fuel orifice ring. This change was expected to move the performance peak to a higher mixture ratio. Insufficient data was taken to define the exact peak.

(U) The computed combustion efficiency η_{C^*}, for this test series is shown in Figure 3-21 as a function of mixture ratio. The average of PC-1 and PC-2 was used in computing the nozzle stagnation pressure used in the C* equation. Combustion efficiency for firings 16 and 17 are shown as solid points and the dashed line.

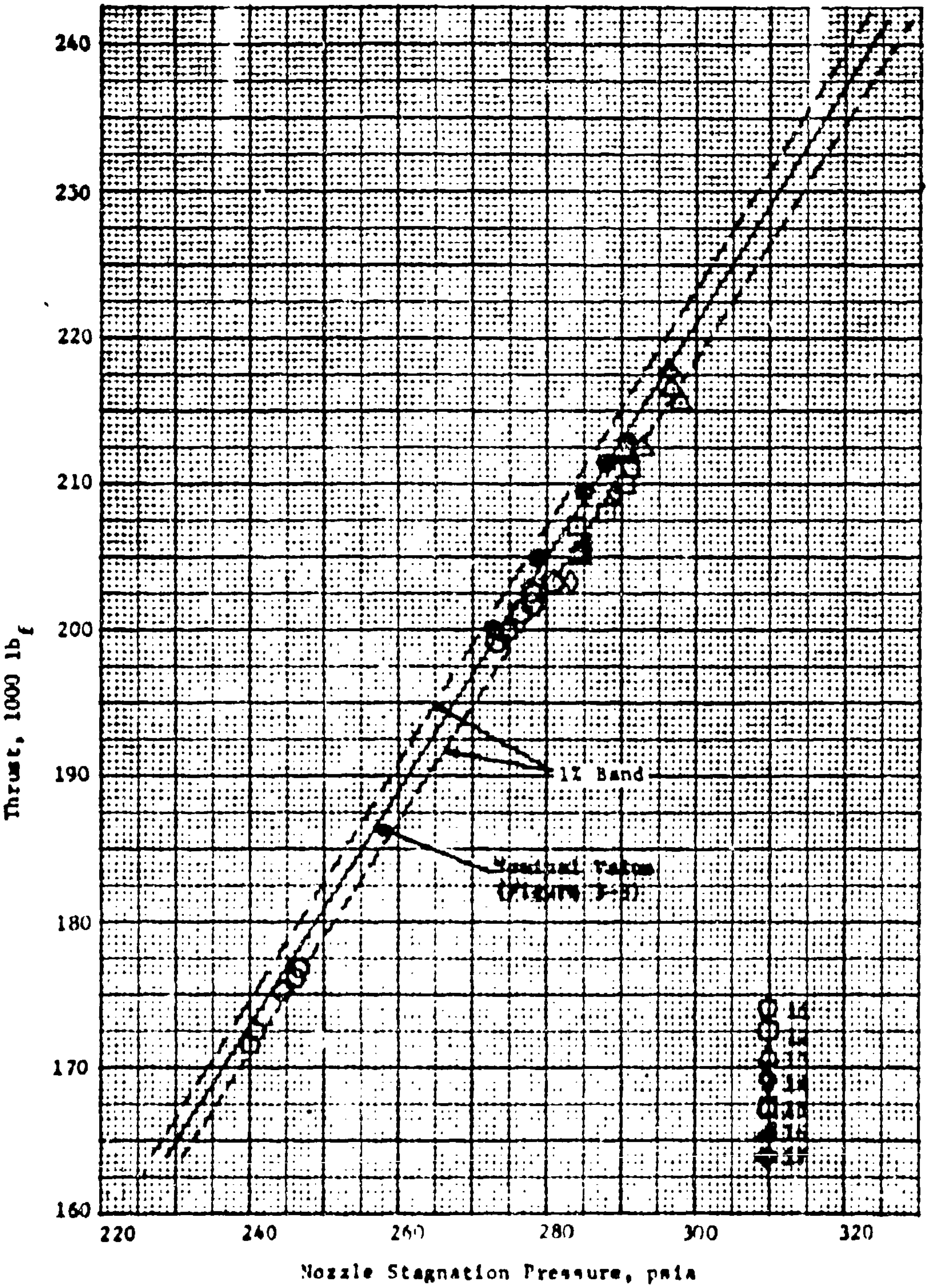

(C) Figure 3-19. Measured Thrust - Test Series 1 and 2 (U)

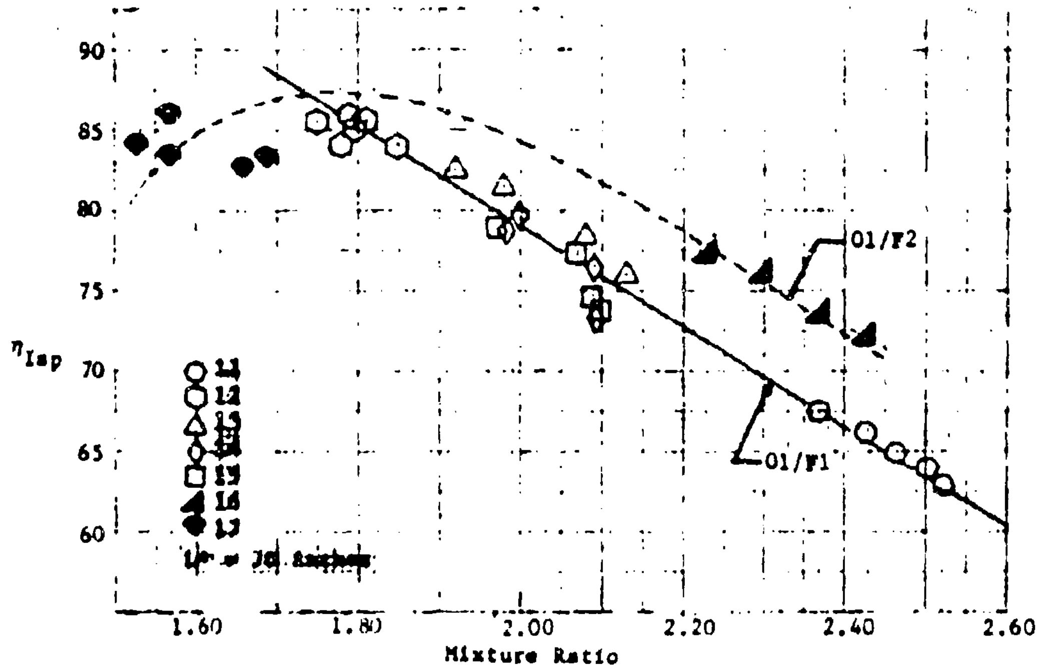

(C) Figure 3-20. Specific Impulse Efficiency - Test Series 1 and 2 (U)

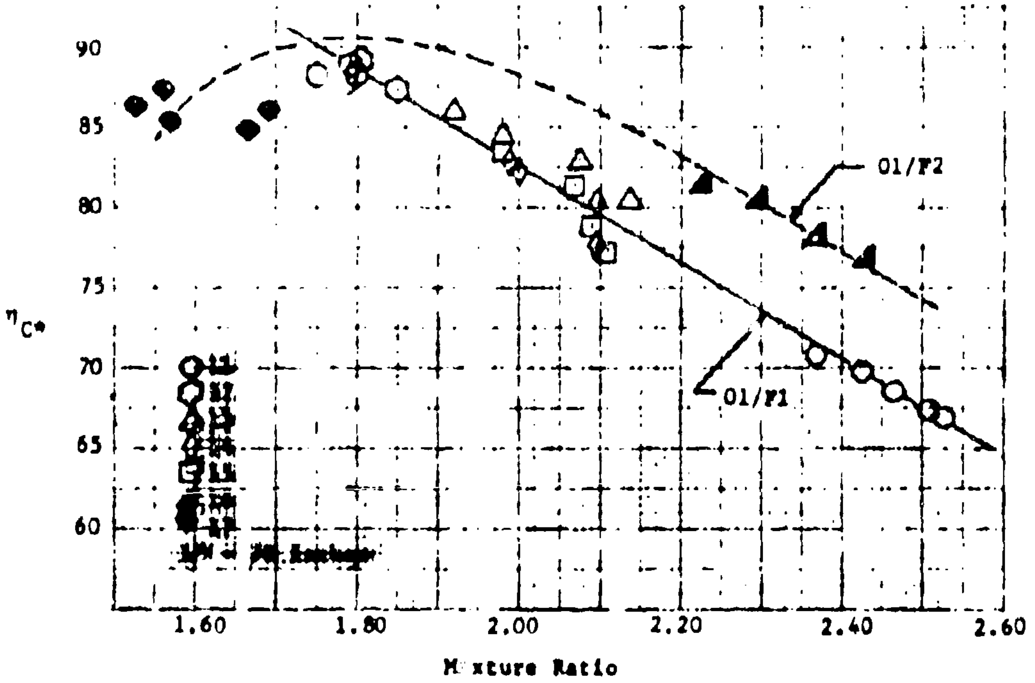

(C) Figure 3-21. Combustion Efficiency Test Series 1 and 2 (U)

(C) The computed nozzle efficiency, η_{CF}, for this test series is shown in Figures 3-22 and 3-23 as a function of mixture ratio and nozzle stagnation pressure. The nozzle efficiency is based on a nozzle stagnation pressure computed from PC-1/PC-2 average for this test series. The mean nozzle efficiency over the mixture ratio range of 1.50 to 2.60 (O/F) is 0.960 with a range of ± 0.020 at a nominal nozzle stagnation pressure of 285 psia. Figure 3-22 shows that the thrust coefficient efficiency is apparently a function of the mixture ratio (or performance level) which does not agree with the theoretical data (Appendix C, Section 2.2). The expected η_{cf} for the 4/1 expansion ratio, 15 degree half-angle, conical nozzle was 0.980. This value was only approached at the lowest mixture ratio. No trend with nozzle stagnation pressure is apparent.

3.4.2.1.2 Injector Characteristics

(U) The fuel injector conductance, KIJCF, for test firings 11-15 is shown in Figure 3-24 as a function of the volumetric flow rate. The KIJCF value for firings 12-15 indicate a nominal discharge coefficient of 0.99 which was expected. The fuel injector conductance for test firing 11 is approximately 10 percent lower than the average KIJCF for 12-15. Both the thrust/nozzle stagnation pressure correlation and the system losses between fuel tank and injector appear normal. It is concluded that the discrepancy is due to an abnormally high ΔP_{if} caused by an erroneous PIF measurement.

(U) The injector conductance for the oxidizer side of the injector, KIJCO, is shown in Figure 3-25 as a function of the volumetric flowrate. The nominal discharge coefficient computed from the conductance is 0.68 which is somewhat lower than the 0.725 value computed for the orifice configuration tested in firings 1-10. The differences in orifice design are apparently responsible for this change in discharge coefficient.

(U) The specific impulse efficiency for both injector configurations, X403829-1 and X403829-16 are shown in Figure 3-26 as a function of $(\Delta P_r)^{0.5} (\mu)^{0.4}$. Insufficient data was taken to establish the performance peaks.

3.4.2.2 Test Series 3 - Firings 18-23

3.4.2.2.1 Performance Data

(U) It was apparent that the oxidizer spray pattern produced by the X403831-1 orifice ring was considerably different than the spray pattern generated by the orifice configuration of the X403666 injector used in the facility checkout firings. The reduced discharge coefficient is evidence of this difference. The cause of the lowered performance was attributed to the excessive penetration of the fuel sheet; that is the spacing of the primary oxidizer orifices was insufficient to prevent the fuel from flowing axially by the oxidizer orifices and out the nozzle unreacted. Increasing the fuel momentum was only partially successful in preventing the fuel penetration. Therefore, the X403831-1 oxidizer orifice ring was modified at the AFRPL to increase the space factor ($W_p + W_s/UW \times 100\%$) to approximately 60 percent by widening the keyhole portion of each primary orifice to 0.584 inches.

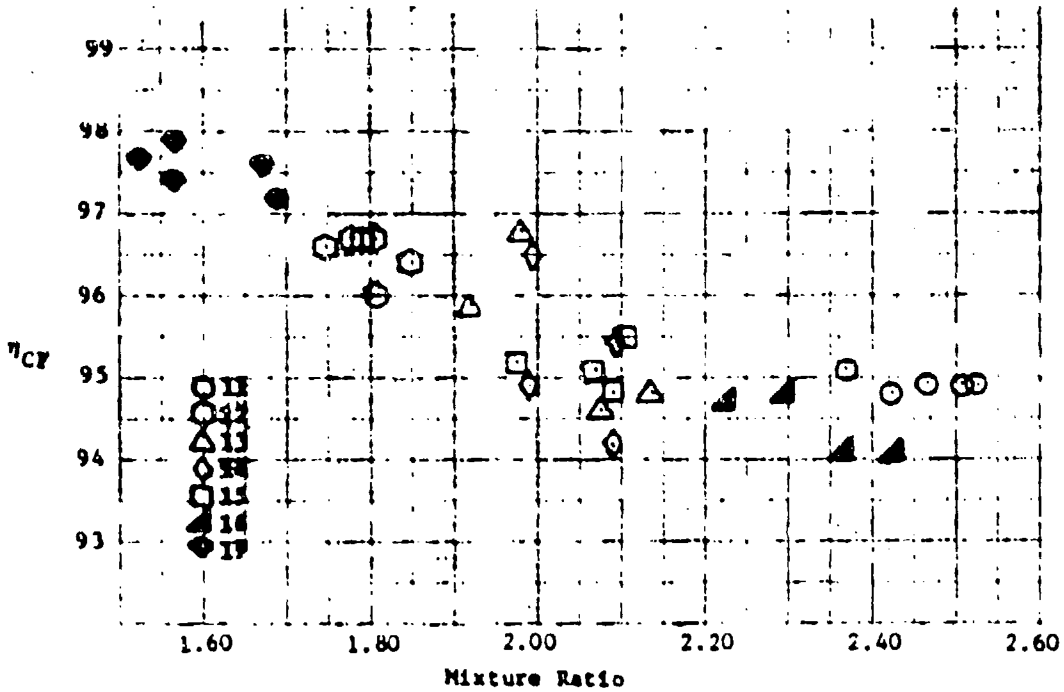

(C) Figure 3-22. Nozzle Efficiency, Test Series 1 and 2 - Function of Mixture Ratio (U)

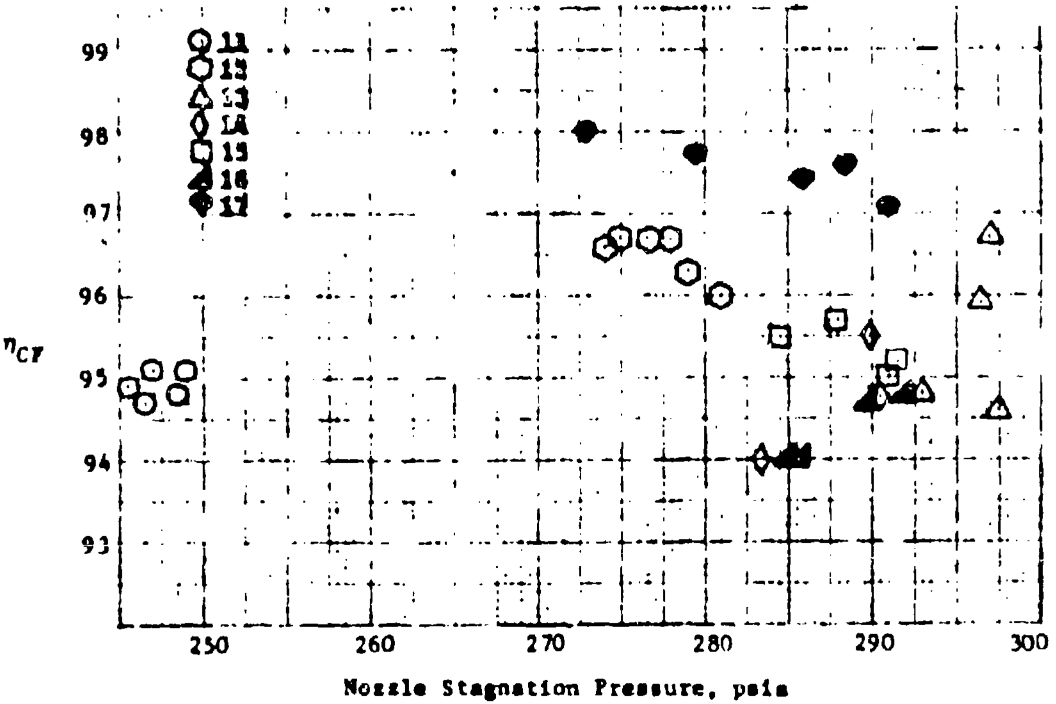

(C) Figure 3-23. Nozzle Efficiency, Test Series 1 and 2 - Function of Nozzle Stagnation Pressure (U)

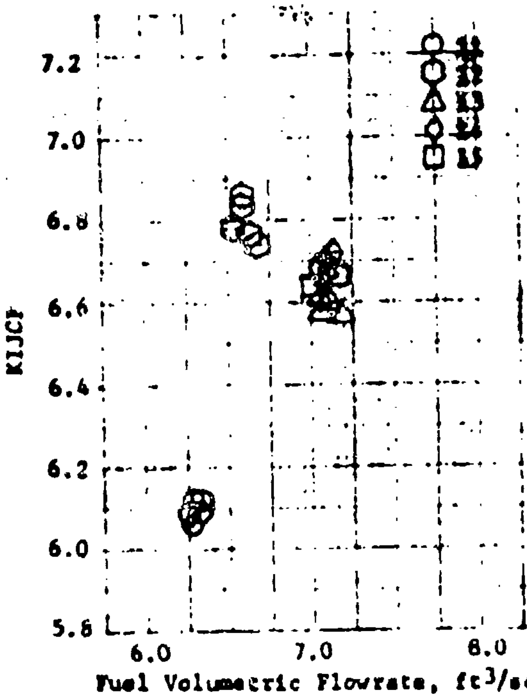

(U) Figure 3-24. Fuel Injector Conductance, Test Series 1 (U)

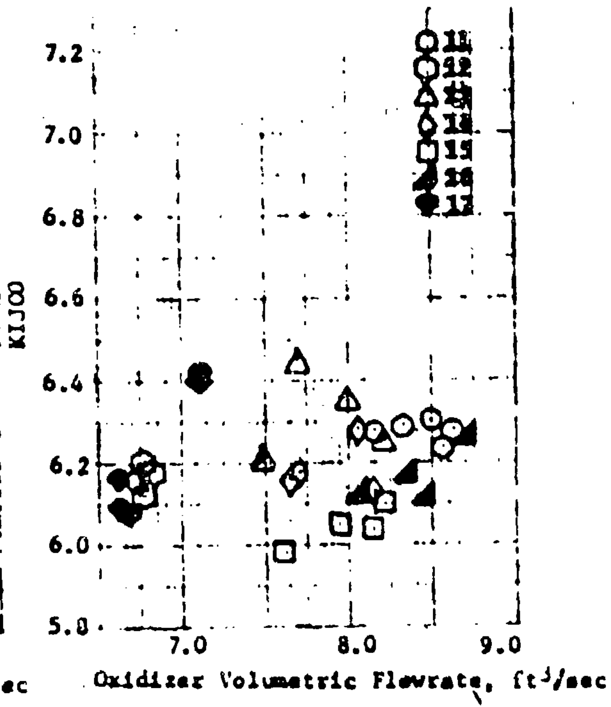

(U) Figure 3-25. Oxidizer Injector Conductance, Test Series 1 and 2 (U)

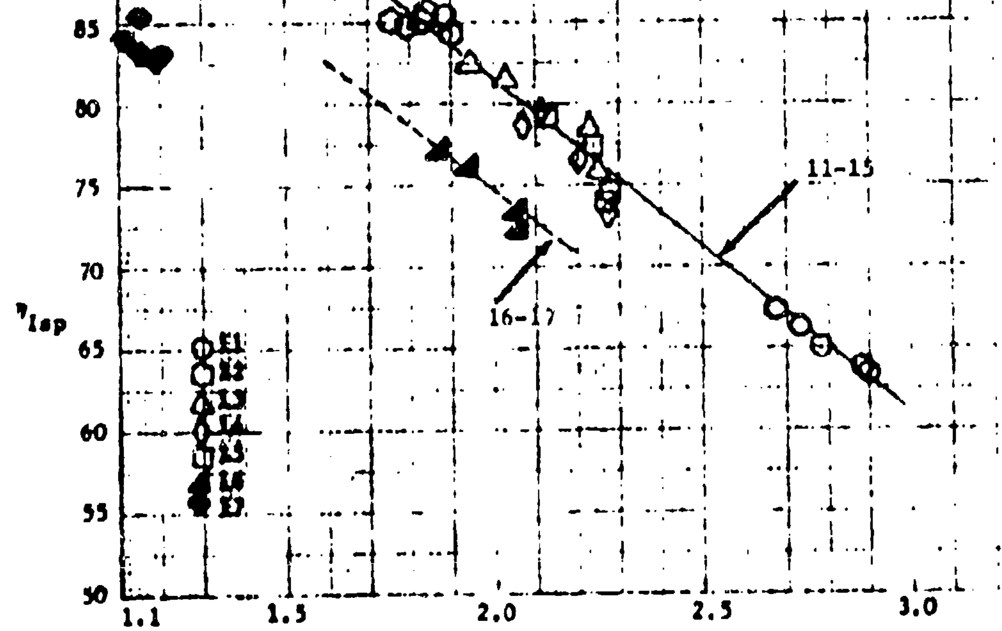

(C) Figure 3-26. Specific Impulse Efficiency - Function of $(\Delta P_f)^{0.5}(\mu)^{0.4}$ (U)

(U) Figure 3-27 shows the measured thrust as a function of nozzle stagnation pressure. As in prior test series the nozzle stagnation pressure is the average of the two injector end pressure transducers (PC-1 and PC-2) corrected for an $\epsilon_c = 2.25$ and $\gamma = 1.235$. The computed specific impulse efficiency, η_{Isp}, is shown in Figure 3-28 as a function of mixture ratio. The η_{Isp} for firings 11-15, shown as the dashed line, indicates that increasing the width of the primary orifice is particularly effective in increasing the absolute performance level.

(U) The computed combustion efficiency, η_{C*} for this test series is shown in Figure 3-29 as a function of mixture ratio. Test firings 18-21 were made at a nozzle stagnation pressure of approximately 300 psia. Test firing 22 was made at a nozzle stagnation pressure of approximately 260 psia while test firing 23 was made at a P_o of approximately 245 psia. Figure 3-29 shows the effect of lowered injection pressures on performance achieved at the same mixture ratio.

(C) The computed nozzle efficiency, η_{CF} for this test series is shown in Figure 3-30 as a function of mixture ratio. This figure shows an average η_{CF1} of 0.955 for test firings 18-46 inclusive, excepting 33 and 34 which used the modified X403668 chamber (20° half angle). This average is valid for both the original combustion chamber employed on firings 11-32 and the lengthened combustion chamber employed on test firings 35 through 46. The expected η_{CF} noted in Appendix C for this nozzle was 0.980. The difference of approximately 2.5 percent between the computed η_{CF} is unexplained.

3.4.2.2.2 Injector Characteristics

(U) The fuel injector conductance, KIJCF, for test firings 18-23 is shown in Figure 3-31 as a function of the volumetric flow rate. Data for test firings 16 and 17 which employed the same fuel orifice, is included for comparative purposes. The fuel side discharge coefficient, computed from the conductance is 0.940 as compared with the C_d value of 0.99 computed for firings 12-15 employing the X403832-3 fuel orifice.

(U) The conductance on the oxidizer side of the injector assembly is shown in Figure 3-32 as a function of the volumetric flow rate. The nominal discharge coefficient computed from the conductance is 0.70 which is lower than the 0.725 C_d computed for the orifice configuration tested in firings 1-10. The 0.70 C_d is a small improvement over that obtained with the unmodified configuration.

(C) The specific impulse efficiency for the X403829-16 (X403831-1 Mod. A Oxidizer orifice ring) is shown in Figure 3-33 as a function of the injector scaling parameter $\left[(\Delta P)^{0.5}(\mu)^{0.4}\right]$. The peak performance is achieved at a value of approximately 1.80.

3.4.2.3 Test Series 4 - Firings 24-29, 40-42

3.4.2.3.1 Performance Data

(U) One of the major injector parameters to be investigated in the injector development program was the number of oxidizer elements. A 48 element oxidizer orifice ring was fabricated and tested during firings 24 through

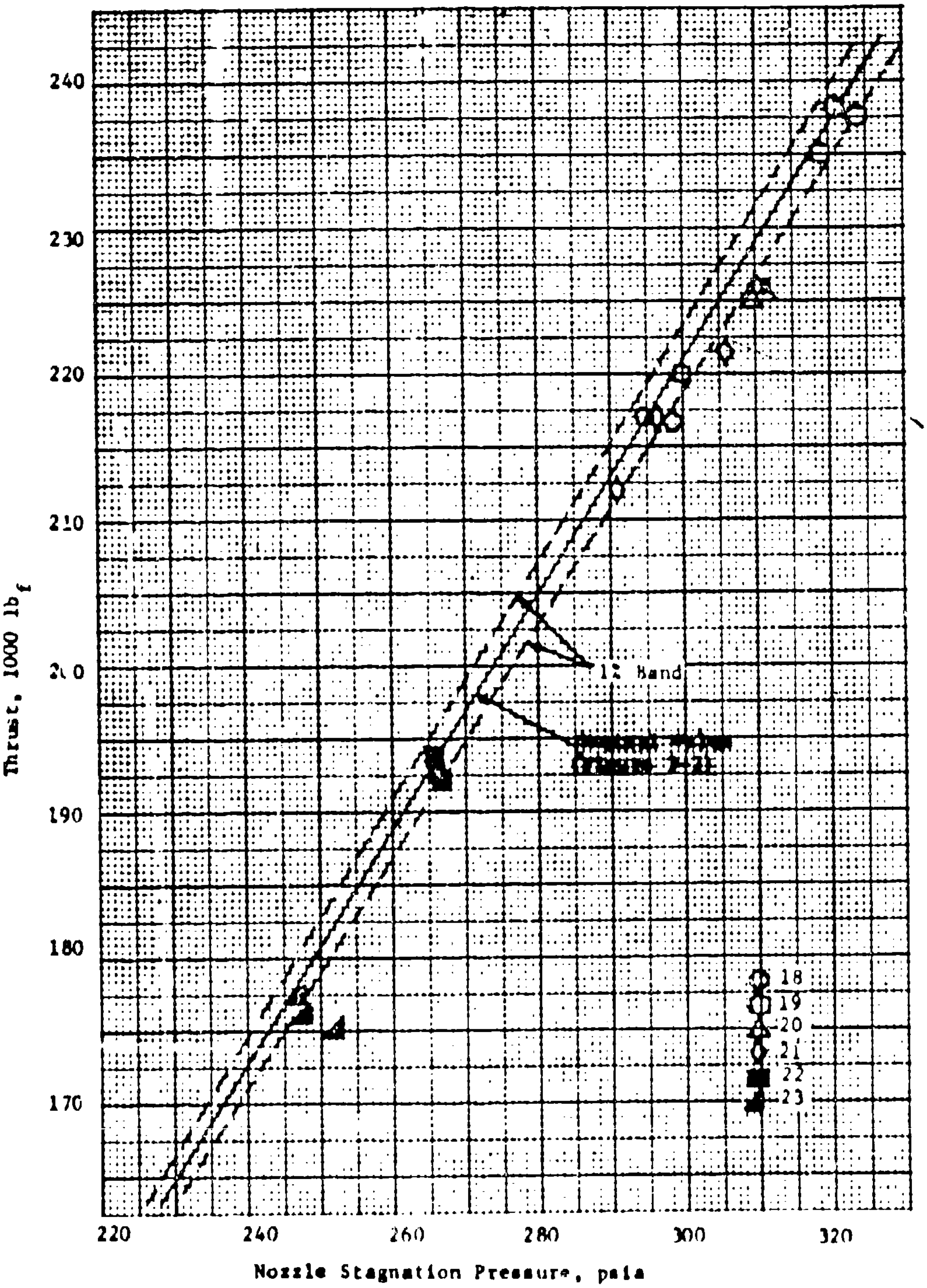

(C) Figure 3-27. Measured Thrust, Test Series 3 (U)

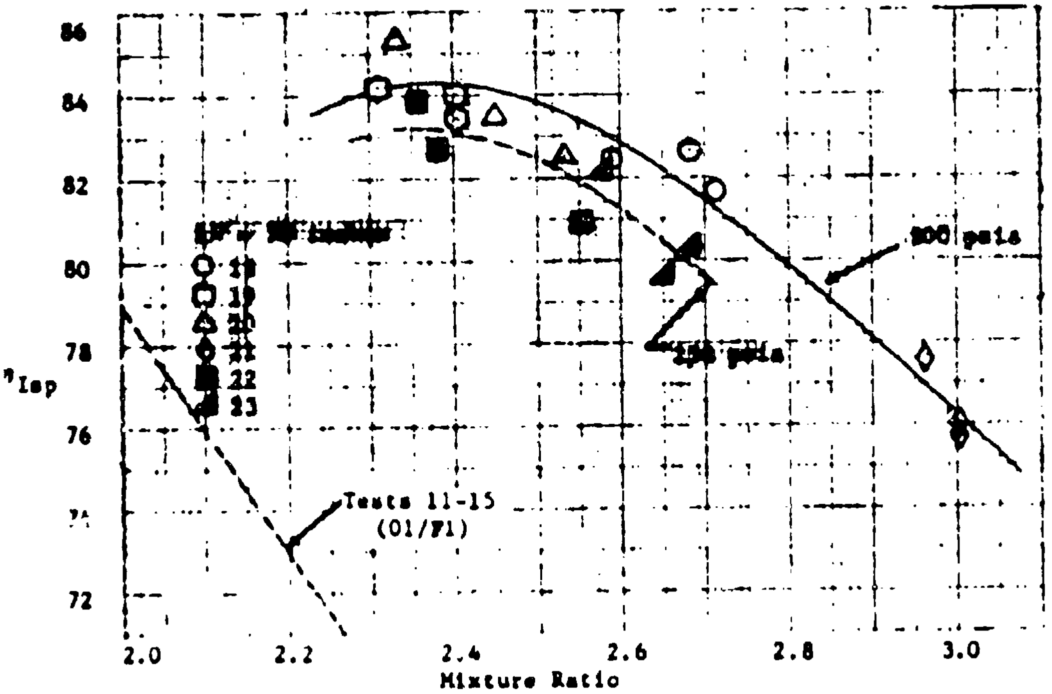

(C) Figure 3-28. Specific Impulse Efficiency - Test Series 3 (U)

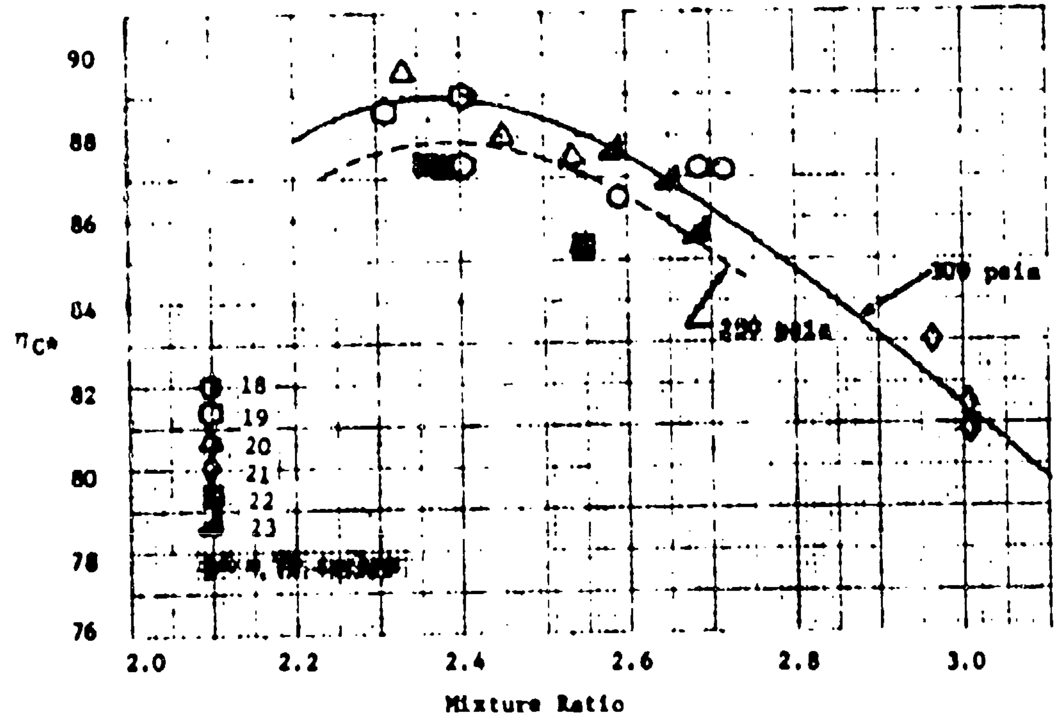

(C) Figure 3-29. Combustion Efficiency - Test Series 3 (U)

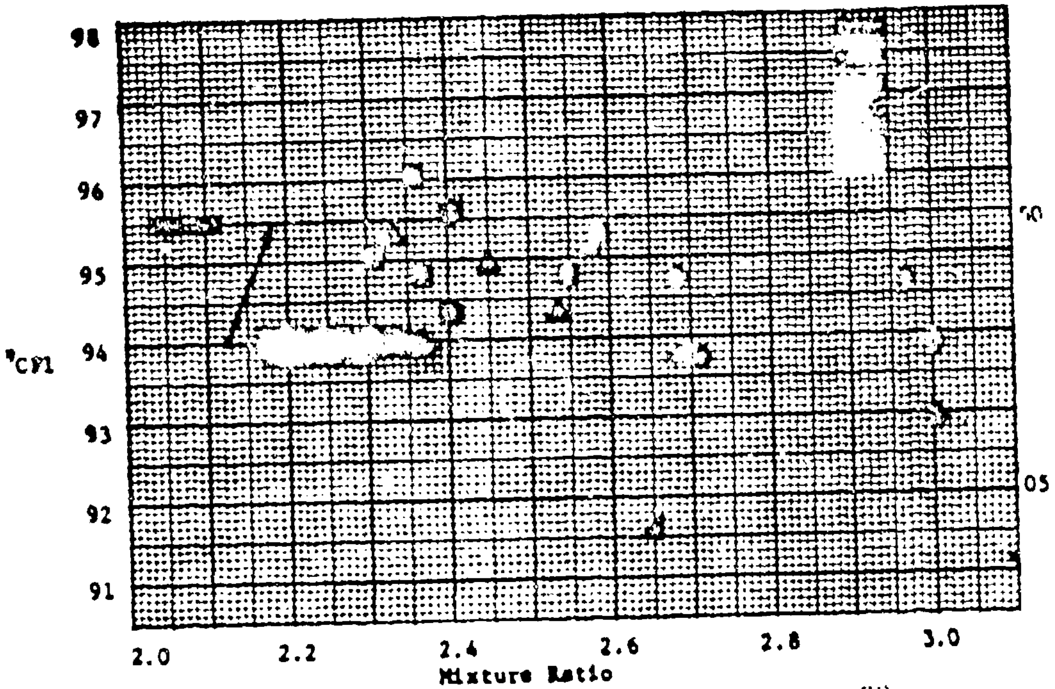

(C) Figure 3-30. Nozzle Efficiency - Test Series 3 (U)

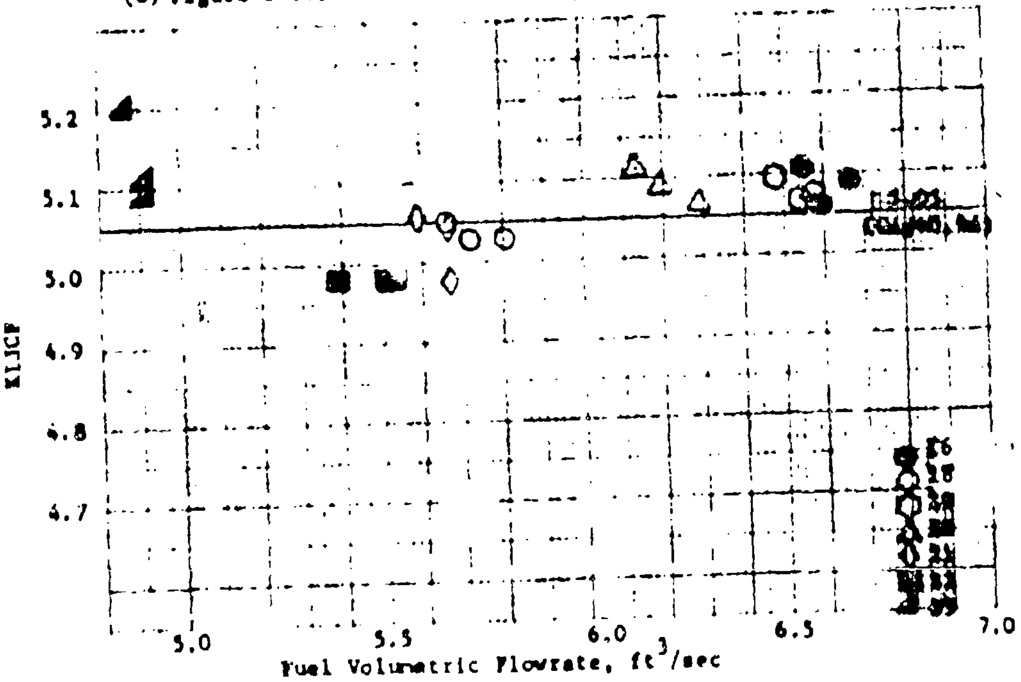

Figure 3-31. Fuel Injector Conductance - Test Series 3 (U)

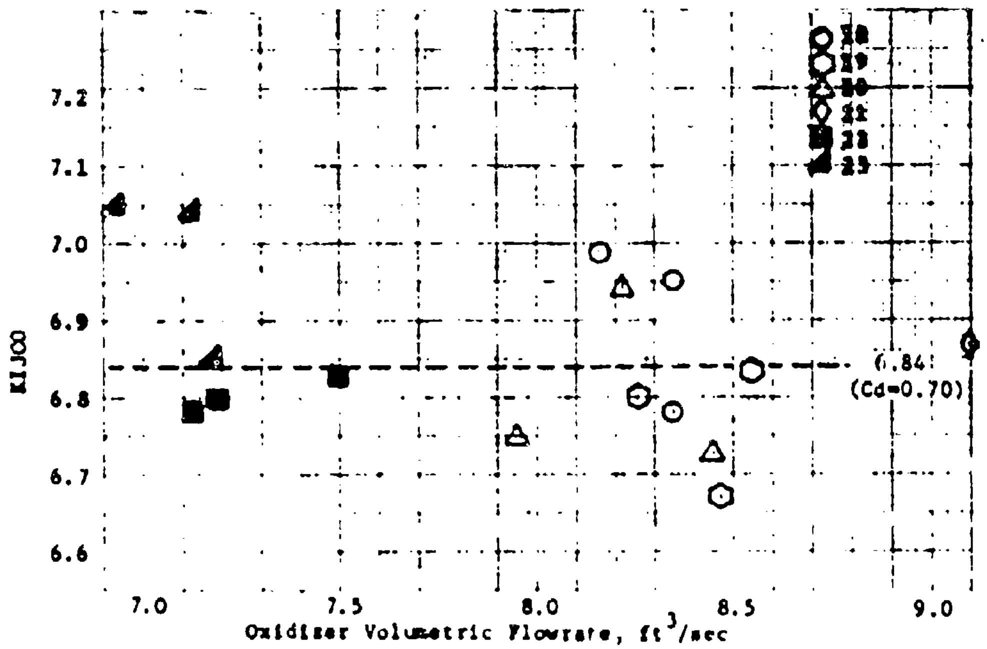

(U) Figure 3-32. Oxidizer Injector Conductance - Test Series 3 (U)

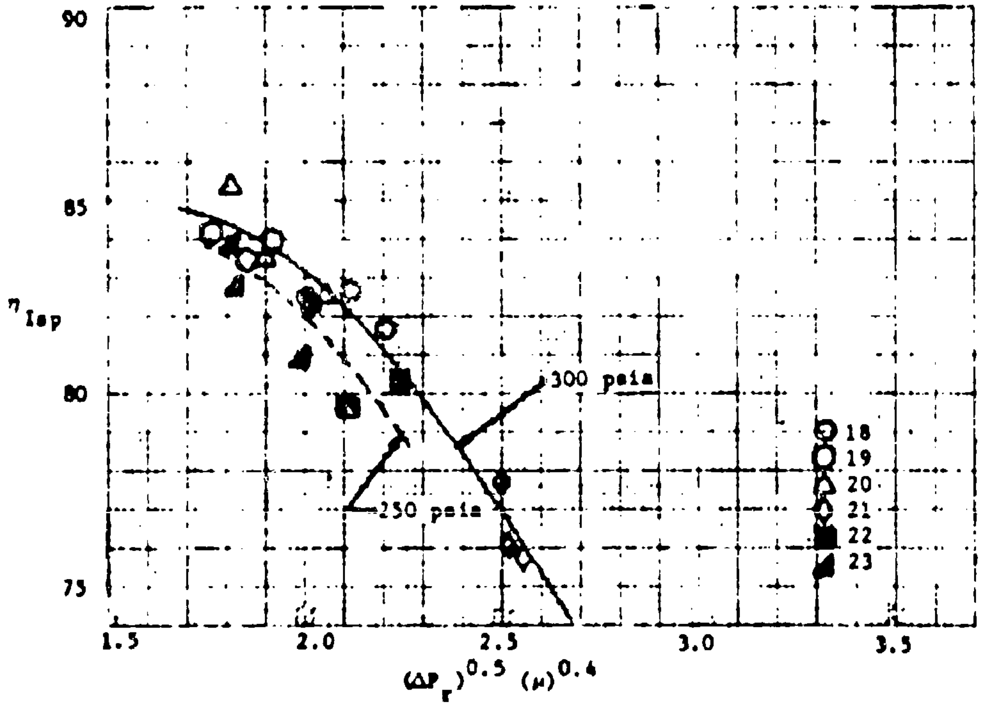

(C) Figure 3-33. Specific Impulse Efficiency - Function of $(\Delta P_r)^{0.5} (\mu)^{0.4}$ (U)

(U) 29 and later on in test firings 40-42 in the lengthened (+24in.) chamber. The orifice ring (X404107-1) was designed with a space factor of 67 percent in order that the effect of that parameter could be determined. The X404107-1 orifice ring was committed to fabrication prior to start of Test Series 3.

(U) Figure 3-34 shows the measured thrust for this configuration as a function of nozzle stagnation pressure. As in prior test series the nozzle stagnation pressure is the average of the two injector end pressure transducers (PC-1 and PC-2) corrected for an ϵ_C = 2.25 and a γ = 1.235. The computed specific impulse efficiency, η_{Isp} is shown in Figure 3-35 as a function of mixture ratio. In the baseline chamber configuration (L_C = 36.5 inches and L* = 70 inches) the maximum performance attained with the 48 element configuration (02/F2) is approximately 0.7 percent lower than the performance value obtained in Test Series 3 (18-23). However, the peak performance does occur near the design mixture ratio and is slightly higher at the design mixture ratio.

(C) The computed combustion efficiency, η_{C^*}, for this test series is shown in Figure 3-36 as a function of mixture ratio. Test firings 25-27 and 29 were made at a nominal nozzle stagnation pressure of 300 psia while test firings 24 and 28 were made at a reduced P_o of 275 and 245 psia, respectively. The effect of lowered injection pressures on performance is shown in Figure 3-36. The 24 inch increase in chamber length (L* = 120 inches) results in an approximate 3.5 percent increase in combustion efficiency for the 02/F2 injector configuration. This increase is reflected in the specific impulse efficiency as shown in Figure 3-35.

(C) The computed nozzle efficiency, η_{CF}, for this test series is shown in Figure 3-37 as a function of mixture ratio. Figure 3-37 shows an average η_{CF} of 0.955 for test firings 18-32. The η_{CF} for 24-29, 40-42 is in agreement with the data of the other test series. The nozzle efficiency for test firings 24-29, 40-42 from the nozzle entrance pressure (PC-3) corrected to nozzle stagnation pressure is shown in Figure 3-38. The η_{CF3} computed using PC-3 is .930 ± .015 for mixture ratio range of 2.25 to 3.05 (O/F) for test firings 24-29. The discrepancy in η_{CF} is due to the differences in P_o computed from either PC-1/PC-2 (average) or PC-3. The use of the theoretical correction from injector end to nozzle entrance results in a larger correction than is measured in any of the test firings.

3.4.2.3.2 Injector Characteristics

(U) The fuel injector conductance, KIJCF, for test firings 24-28 and 40-42 is shown in Figure 3-39 as a function of the volumetric flow rate. The fuel side conductance agrees with the conductance computed for test firings 16-23 resulting in a nominal C_{df} of 0.94. The unexplained shift in fuel side injector conductance which occurred between firings 28 and 30 is seen in the data for test firings 40-42.

(U) The conductance on the oxidizer side of the injector assembly is shown in Figure 3-40 as a function of the volumetric flow rate. The nominal discharge coefficient computed from the conductance is 0.70 which agrees with that obtained in test firings 18-23.

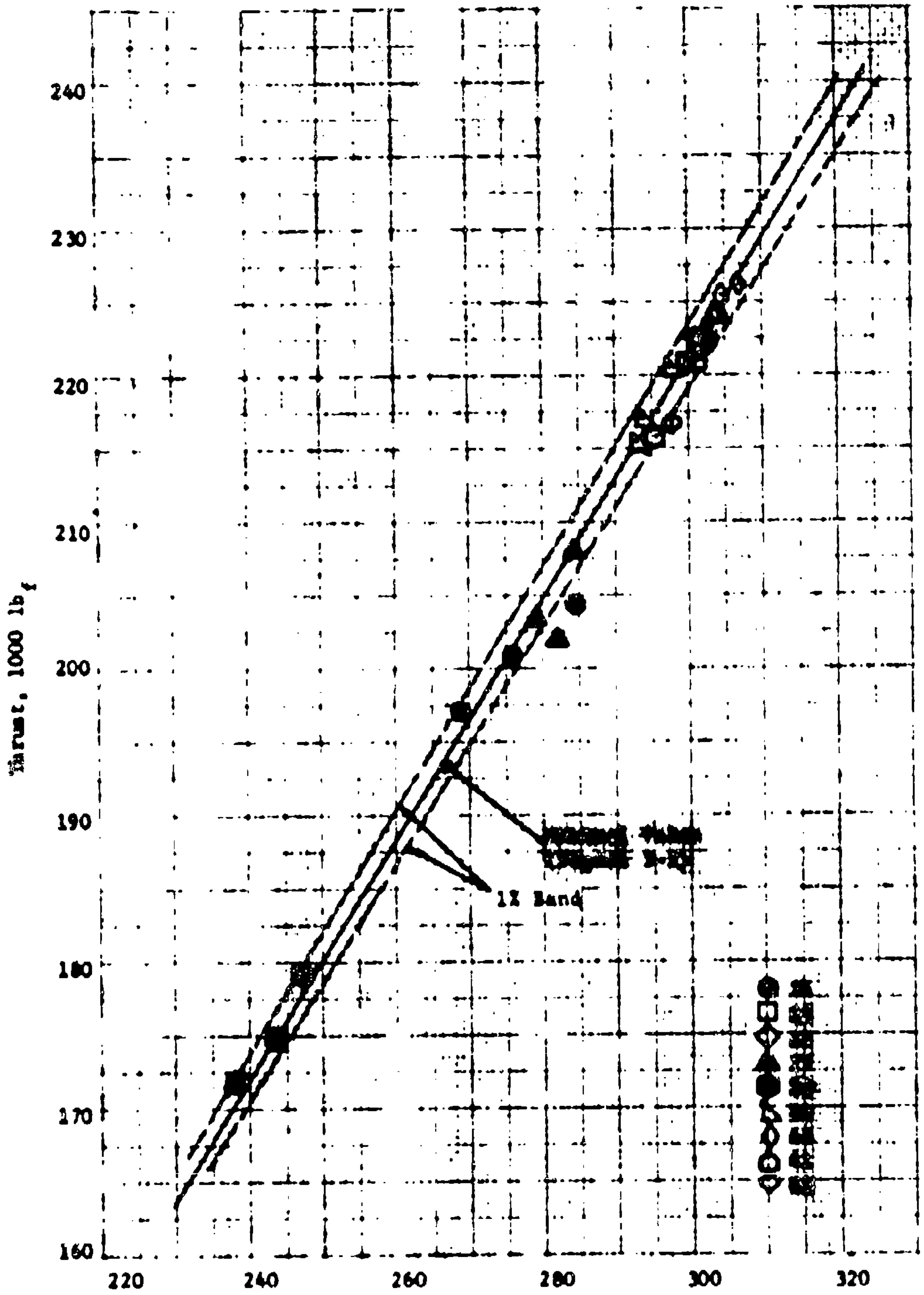

(C) Figure 3-34. Measured Thrust - Test Series 4 (U)

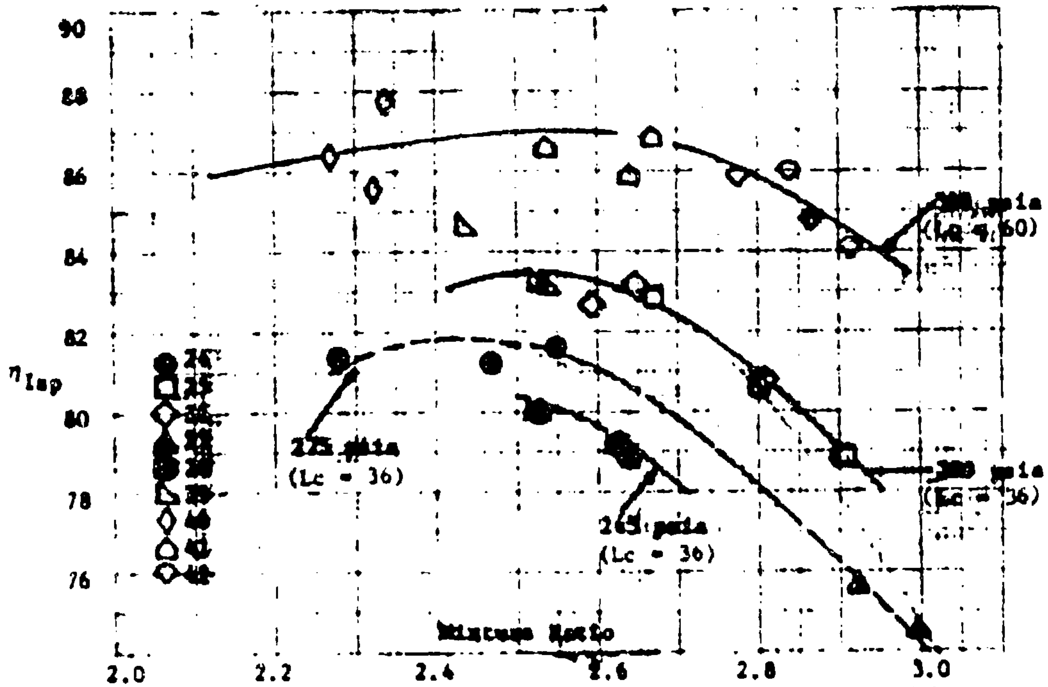

(C) Figure 3-35. Specific Impulse Efficiency - Test Series 4 (U)

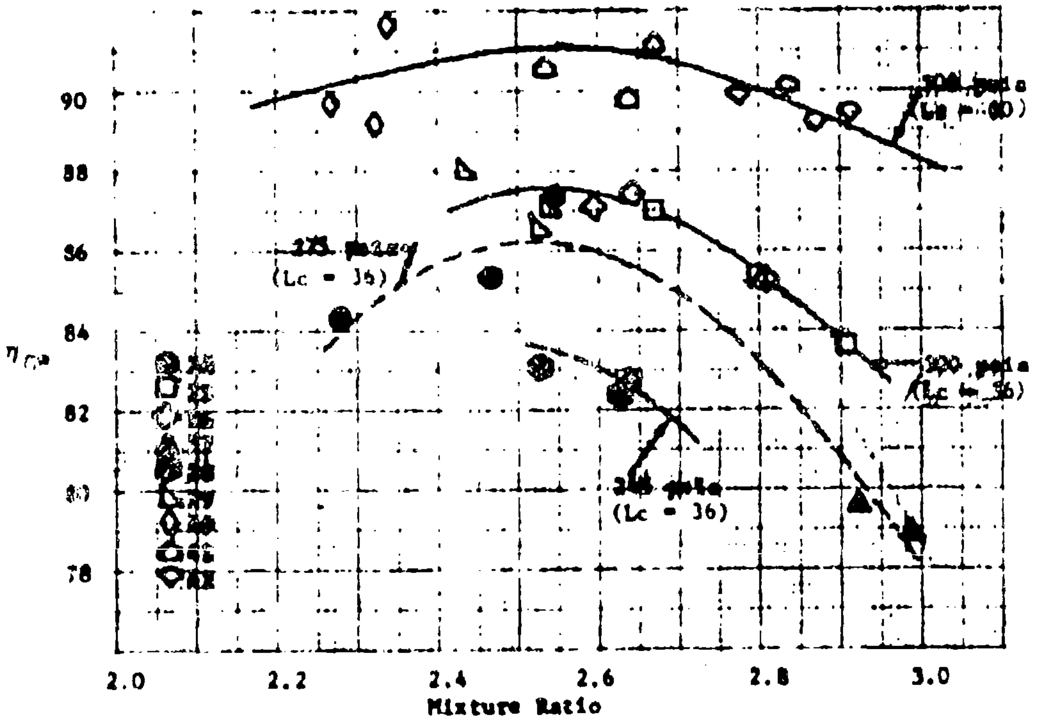

(C) Figure 3-36. Combustion Efficiency - Test Series 4 (U)

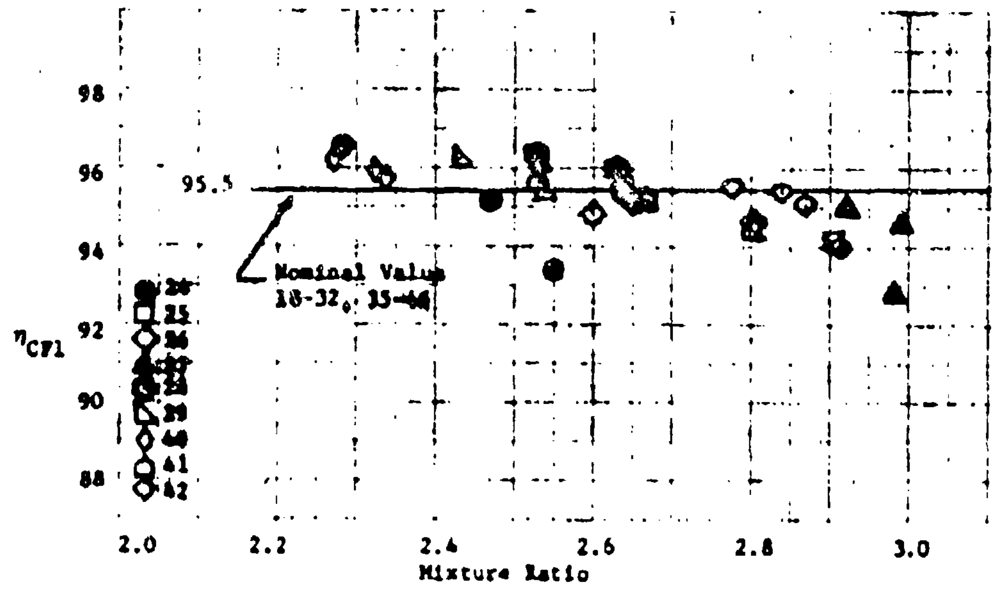

(C) Figure 3-37. Nozzle Efficiency - Test Series 4 (U)

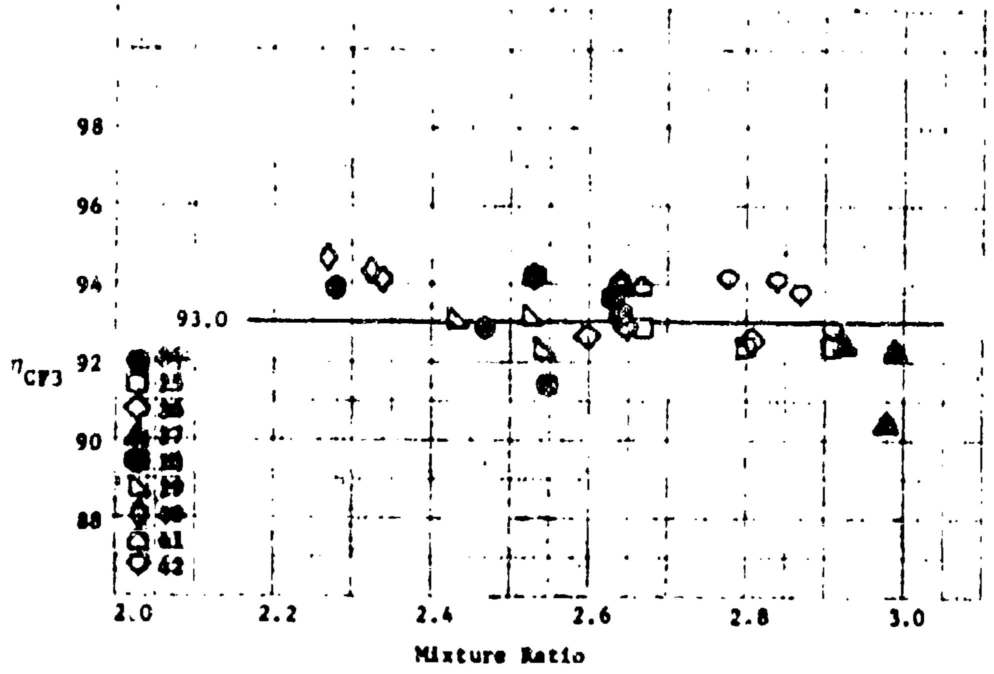

(C) Figure 3-38. Nozzle Efficiency - Test Series 4 (U)

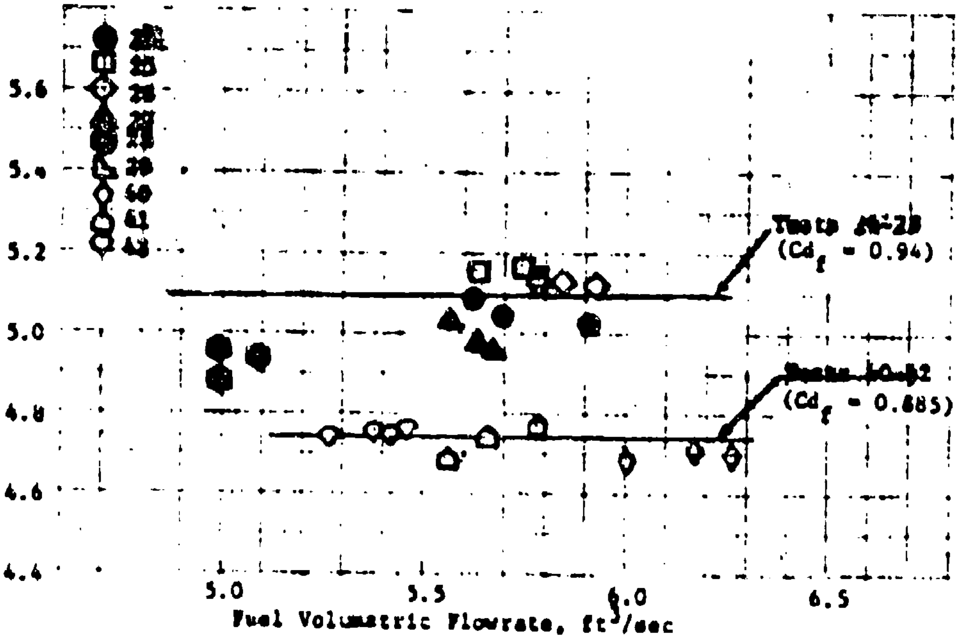

(U) Figure 3-39. Fuel Injector Conductance - Test Series 4 (U)

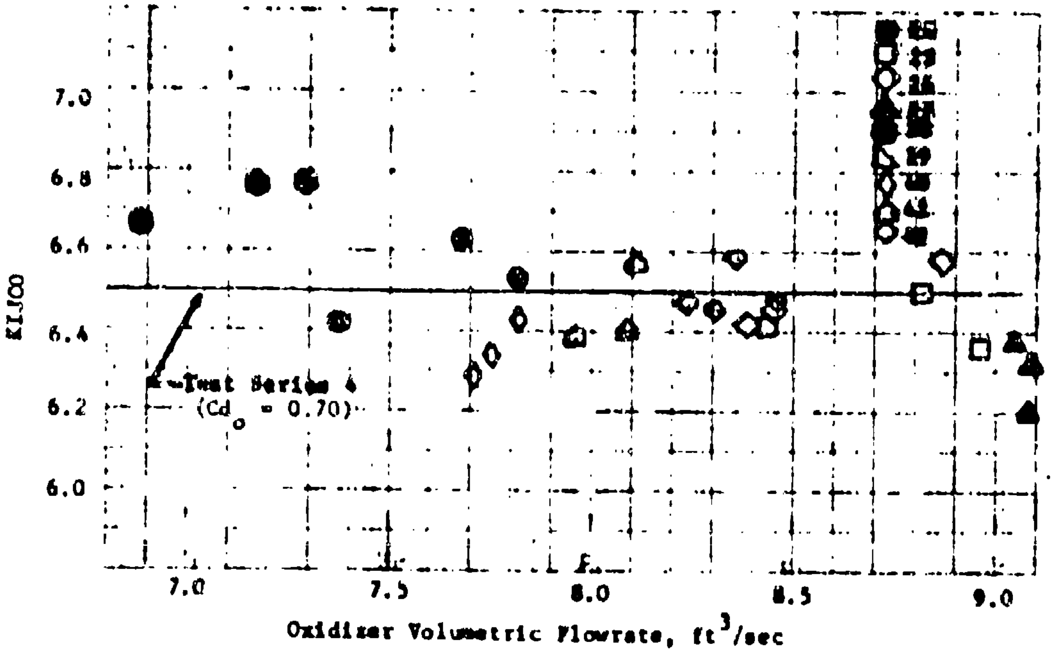

(U) Figure 3-40. Oxidizer Injector Conductance - Test Series 4 (U)

(C) The specific impulse efficiency for the X403829-17 injector assembly is shown in Figure 3-41 as a function of $(\Delta P_r)^{0.5} (\mu)^{0.4}$. The peak performance occurs at a nominal value of 2.0.

3.4.2.4 Test Series 5 - Firings 30-34, 37-39, 43, 46

3.4.2.4.1 Performance Data

(U) The X403831-1 oxidizer orifice ring employed in test series 3 was modified by increasing the length of the secondary orifice to 0.500 inch. This was accomplished using an electrical discharge machining process. Thus, the setback of the secondary orifice was decreased to 0.300 inch. This configuration (O1B) was used to determine the effect of chamber length on performance. Test firings 30-32 were made in the 70 inch L* baseline heat-sink thrust chamber (X403646-1) while test firings 33-34 were made in a 12 inch longer chamber (X403668-1) with an 88 inch L*. Test firings 37-39, 43 and 46 were made in a 24 inch long chamber (X403646-11) with a 120 inch L*.

(U) Figure 3-42 shows the measured thrust as a function of nozzle stagnation pressure. As in prior test series the nozzle stagnation pressure is the average of the two injector end pressure transducers (PC-1 and PC-2) corrected for an $\epsilon_c = 2.25$ and a $\gamma = 1.235$. The computed specific impulse efficiency, η_{Isp} is shown in Figure 3-43 as a function of mixture ratio for three chamber lengths. The increase in chamber length is particularly effective in increasing the absolute performance level.

(U) The computed combustion efficiency, η_{C*}, for test firings 30-32, as a function of mixture ratio is shown in Figure 3-44. Data for test series 3 is shown for comparative purposes. The data shows that increasing the length of the secondary orifice by 0.100 inch (O1B) does not result in any performance increase over the mixture ratio range of interest.

(C) Figure 3-45 shows the computed combustion efficiency, η_{C*}, for the three chamber lengths investigated in this test series. Over the mixture ratio range of 2.3 to 2.9 the combustion efficiency achieved in the 24 inch longer chamber is approximately 1.9 percent greater than that measured in the 12 inch longer chamber. Increasing the chamber length flattens out the performance curves at the extremes of the mixture ratio curve.

(U) Test firings 43 and 46 were also made with the O1B oxidizer orifice configuration to recheck the performance of the injector. All of the data for firing 43 fell on the previously established curve for firings 37-39. Test firing 46 was a stability rating test; data slice 46-1 indicates that the injector was performing as expected prior to detonation of the stability rating device. Data slices taken after the detonation shows a reduced performance level and abnormal injector behavior as discussed in the following section.

(C) The computed nozzle efficiency $\eta_{C\gamma}$ for test firings 30-32 of this test series is shown in Figure 3-46 as a function of mixture ratio. This figure shows that the $\eta_{C\gamma}$ for 30-32 falls on the same curve as that established for test firings 18-29. The $\eta_{C\gamma}$ for test firings 33-34 is 0.9205 or approximately 3.7 percent lower than the average $\eta_{C\gamma}$ measured for the other firings. The X403668-1 "A" chamber was employed in test firings

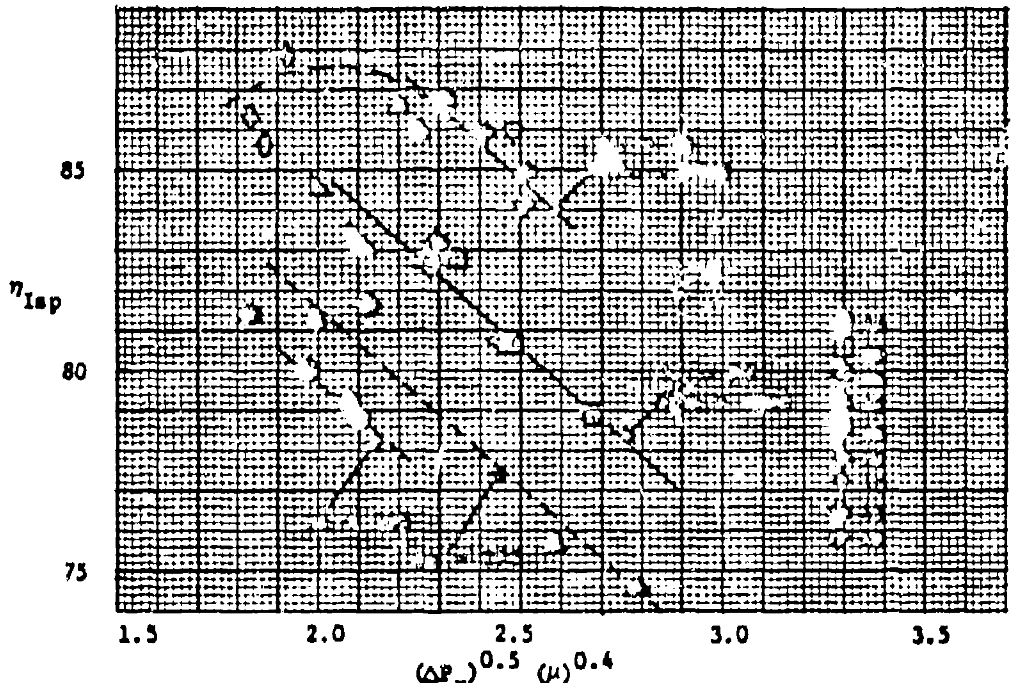

(C) Figure 3-41. Specific Impulse Efficiency, Test Series 4, Function of $(\Delta P_r)^{0.5}(\mu)^{0.4}$ (U)

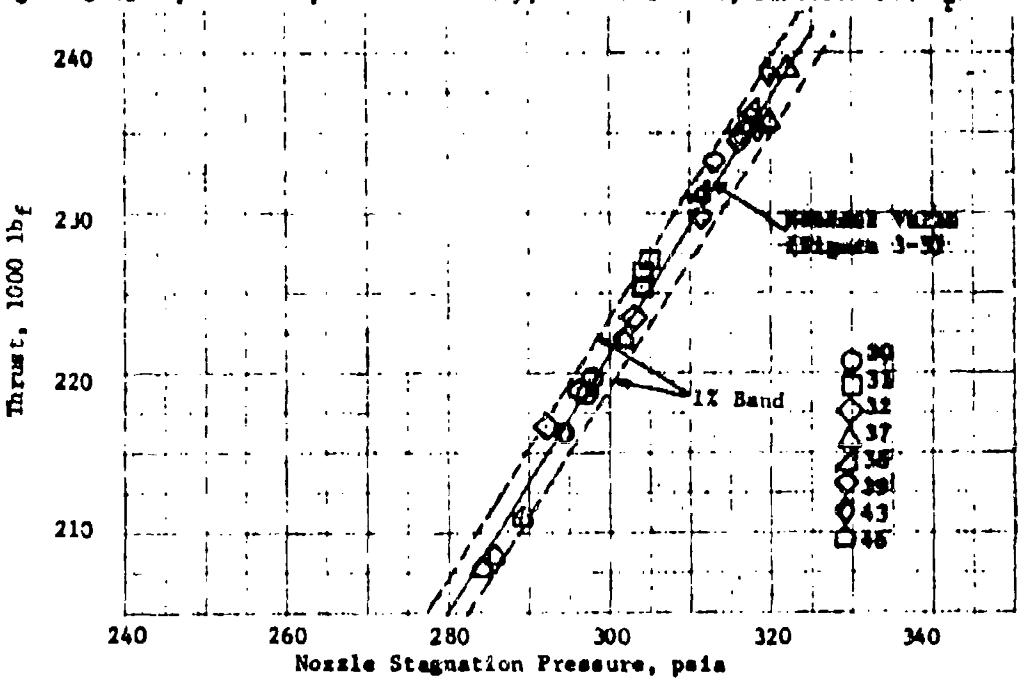

(C) Figure 3-42. Measured Thrust - Test Series 5 (U)

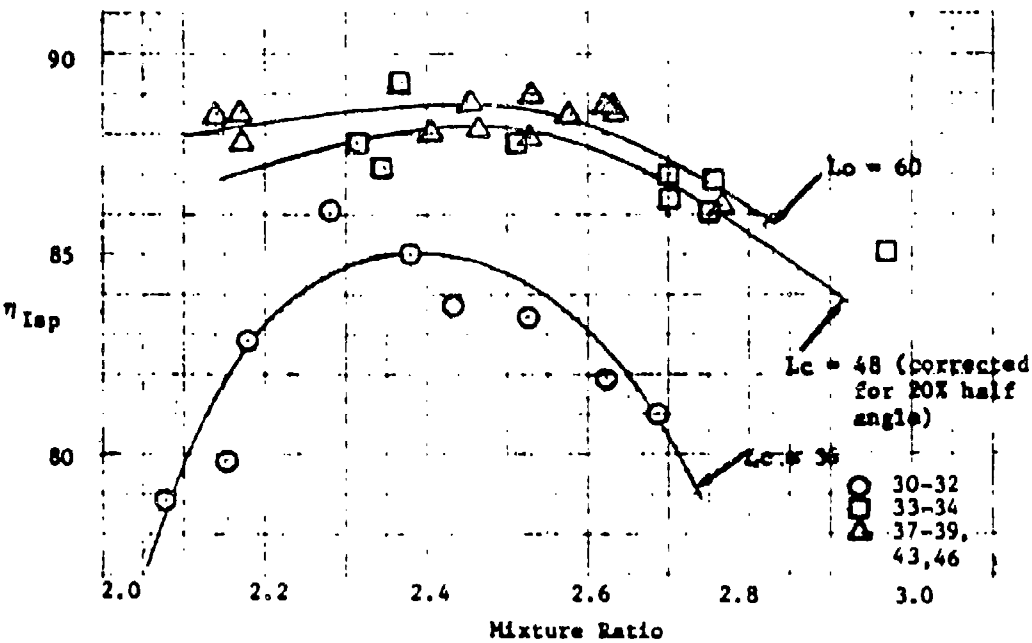

(C) Figure 3-43. Specific Impulse Efficiency, Test Series 5 (U)

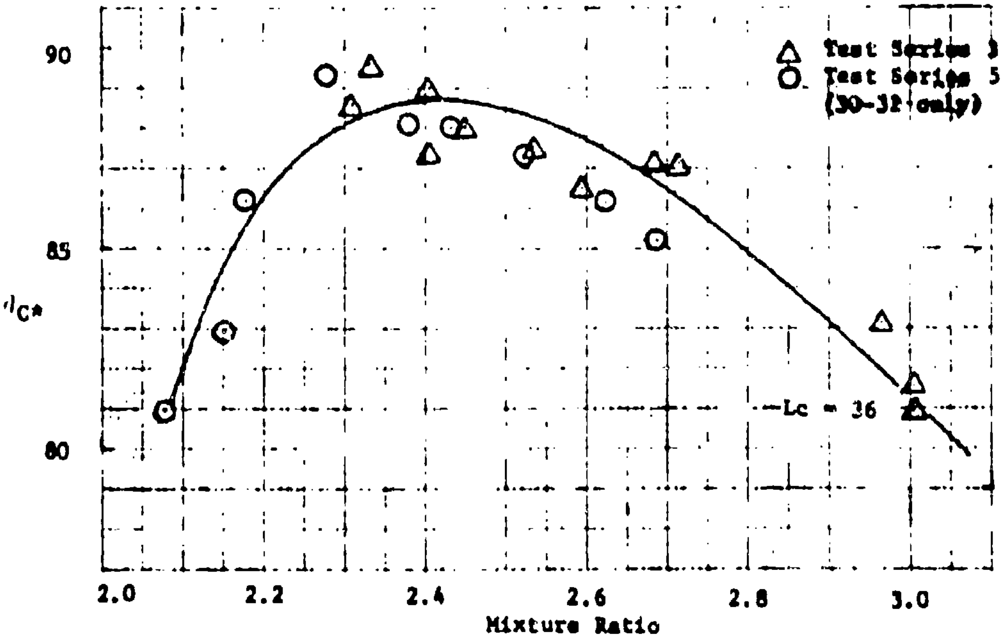

(C) Figure 3-44. Combustion Efficiency, Test Series 3/5 (U)

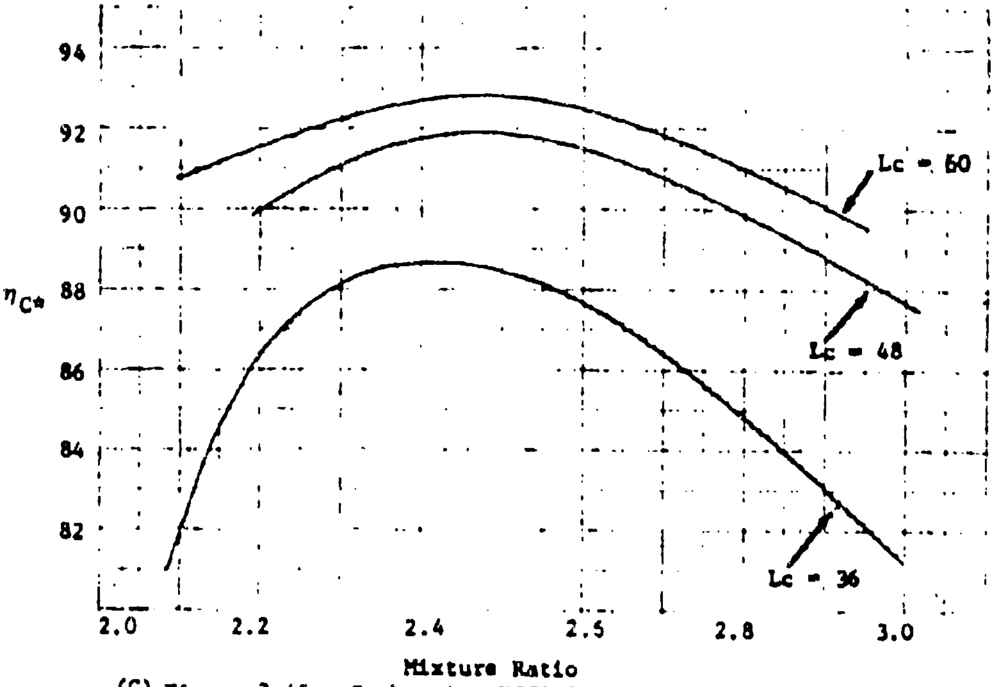

(C) Figure 3-45. Combustion Efficiency, Test Series 5 - Effect of Chamber Length (U)

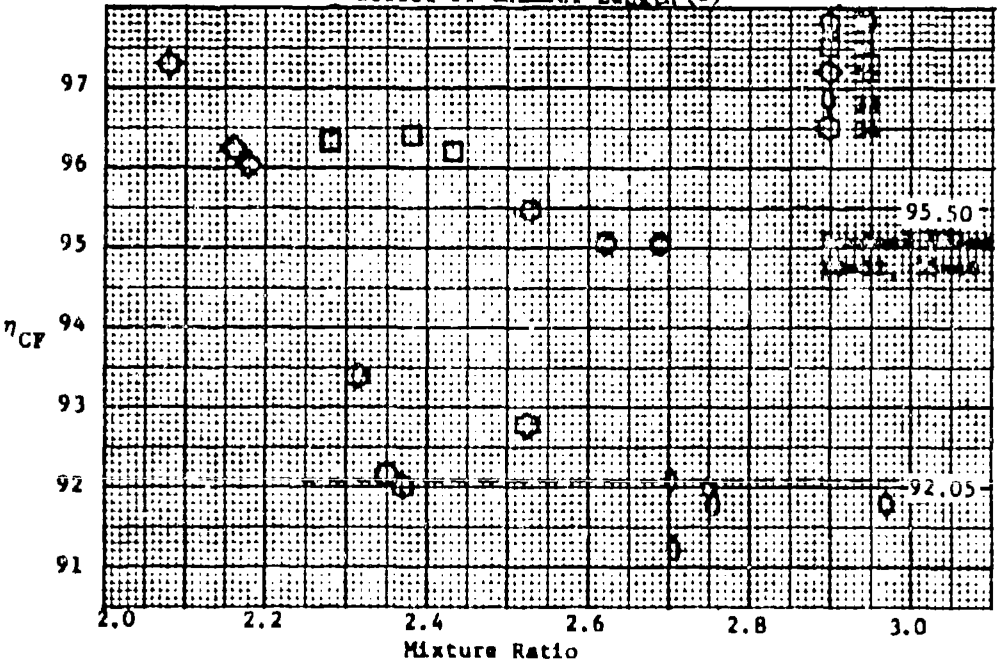

(C) Figure 3-46. Nozzle Efficiency, Test Series 5 - Effect of Nozzle Divergence Angle (U)

(U) 33-34. This chamber has a 4/1 expansion nozzle with a half-angle of 20 degrees as compared with the 15 degree expansion nozzle half angle on the baseline chamber. Figure 3-47 shows that the average η_{CF} for test firing 35-39 is 0.955. The data for test firings 43 and 46 also fall on the same curve as the data obtained in previous firings with this nozzle configuration.

(C) The nozzle efficiency (η_{CF3}) based on nozzle entrance pressure (PC-3) for firings 30-32, 37-39, 43 and 46 is shown in Figure 3-48. The average η_{CF3} of 93.50 agrees with the η_{CF3} Of 93.0 computed for the O2/F2 injector configuration (Test Series 4).

3.4.2.4.2 Injector Characteristics

(U) The fuel injector conductance, KIJCF, for test firings 30-34, 37-39, 43 and 46 is shown in Figure 3-49 as a function of the volumetric flow rate. The fuel side discharge coefficient computed from the average conductance is 0.885 as compared with the C_d value of 0.940 computed for the same fuel orifice ring in test firings 16-28. Some transducer changes were made between test firings 28 and 30 and the C_d value of 0.885 is believed incorrect due to the fuel injection pressure measurement.

(U) The conductance on the oxidizer side of the injector assembly is shown in Figure 3-50 as a function of the volumetric flow rate. The nominal discharge coefficient computed from the conductance is 0.714 which is essentially in agreement with the 0.700 C_d computed for the O-A oxidizer orifice configuration tested in firings 18-23. The 0.714 C_d represents a slight improvement over the 0.68 C_d measured for the unmodified configuration.

(C) The specific impulse efficiency for the X403829-16 (X403831-1 Mod. B oxidizer orifice ring) is shown in Figure 3-51 as a function of $(\Delta P_f)^{0.5}$ $(\mu)^{0.4}$. The measured ΔP_f for this series is corrected by the ratio of $(Cd_2/Cd_1)^2$ or $\left[\frac{.885}{.940}\right]^2 = 0.886$. The peak performance occurs at a nominal value of 1.90.

3.4.2.5 Test Series 6 - Firings 35-36

3.4.2.5.1 Performance Data

(U) The third oxidizer orifice configuration (O3) tested was the X404047-1 (36 element) ring. This ring had essentially the same space factor (W_p + W_s/UW x 100%) as the No. 2 oxidizer orifice configuration, with approximately the same injection area as the No. 1 and No. 2 oxidizer orifices. Only two test firings were made with this configuration. Both firings (35-36) were in the 24 inch longer chamber.

(U) Figure 3-52 shows the measured combustion efficiency, η_{C*}, for the two firings. The performance in the mixture ratio range of 2.3 - 2.4 is comparable to that obtained with the O1B/F2 injector configuration. At the higher mixture ratio (~2.7 O/F) performance was reduced drastically. This lowered performance is believed due to excessive penetration of the oxidizer streams at the high $\Delta P_o/\Delta P_f$ ratio.

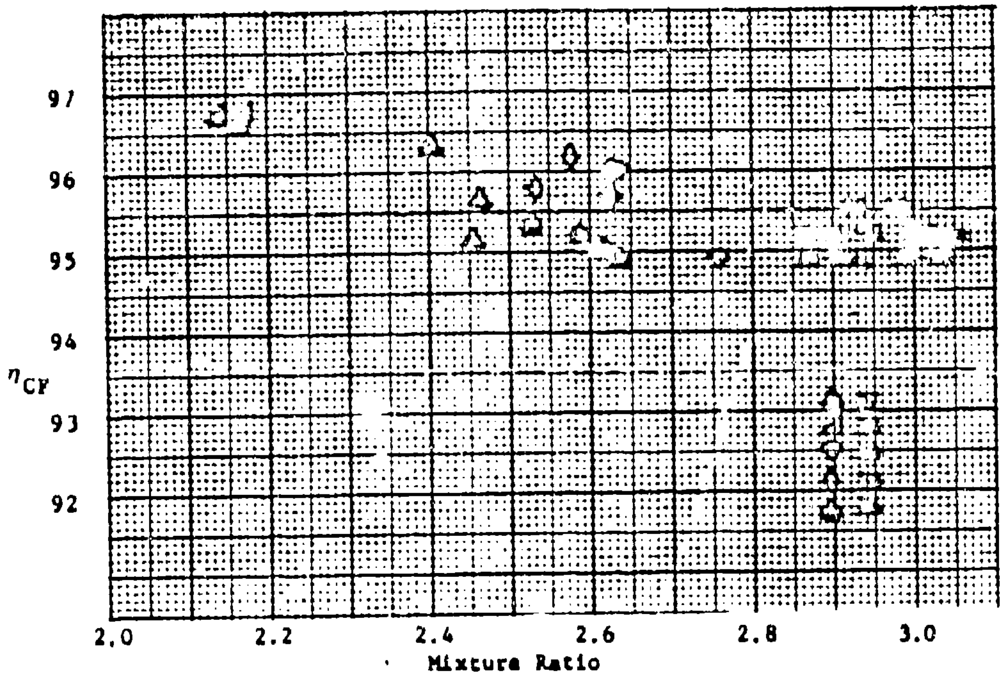

(C) Figure 3-47. Nozzle Efficiency, Test Series 5 - Effect of Chamber Length (U)

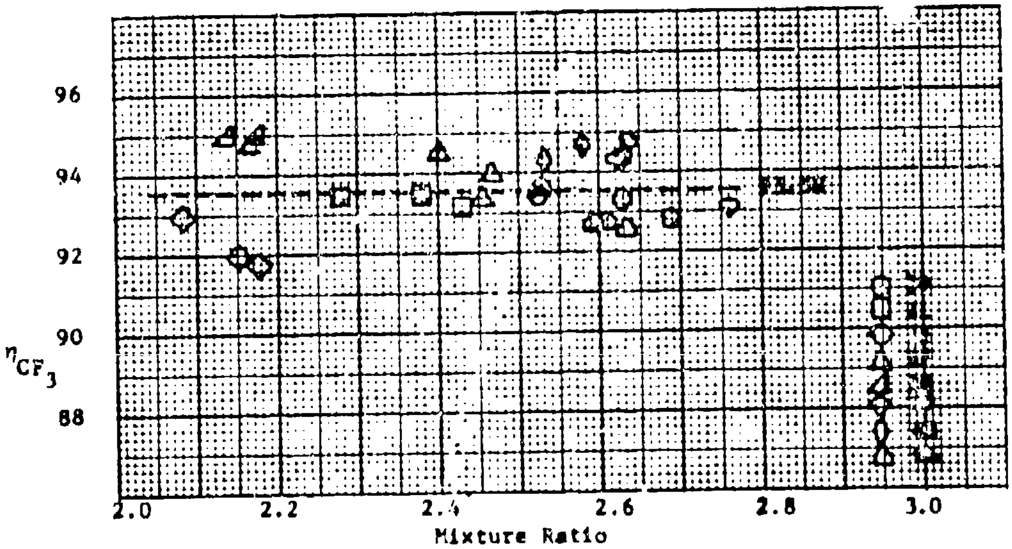

(C) Figure 3-48. Nozzle Efficiency, Test Series 5 - Effect of Chamber Length (U)

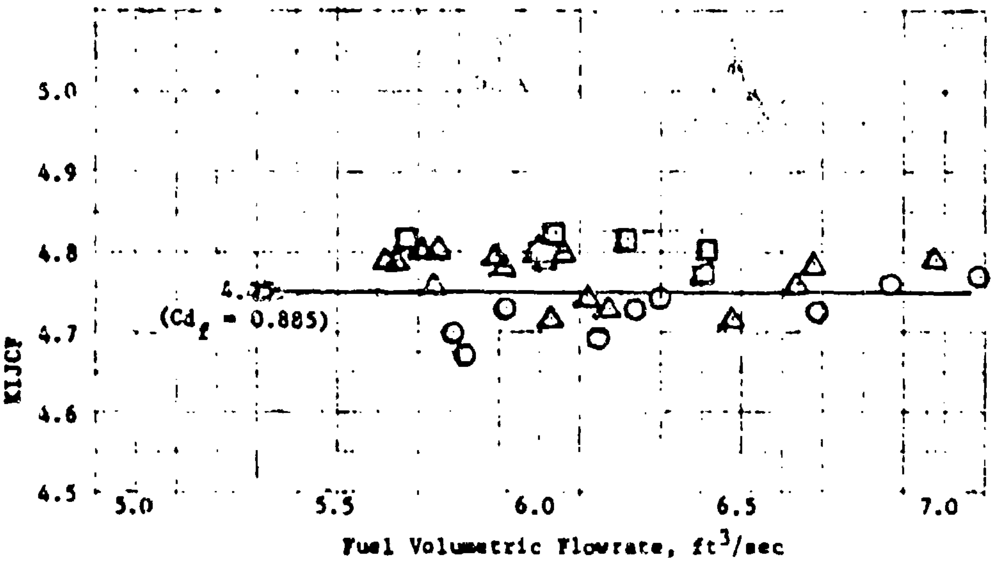

(U) Figure 3-49. Fuel Injector Conductance, Test Series 5 (U)

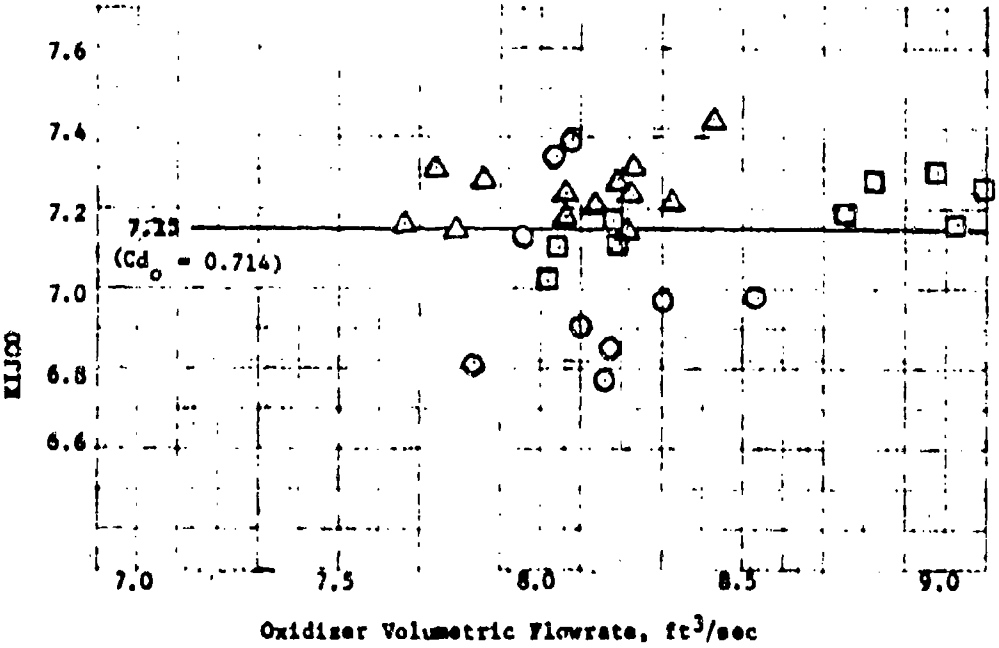

(U) Figure 3-50. Oxidizer Injector Conductance, Test Series 5 (U)

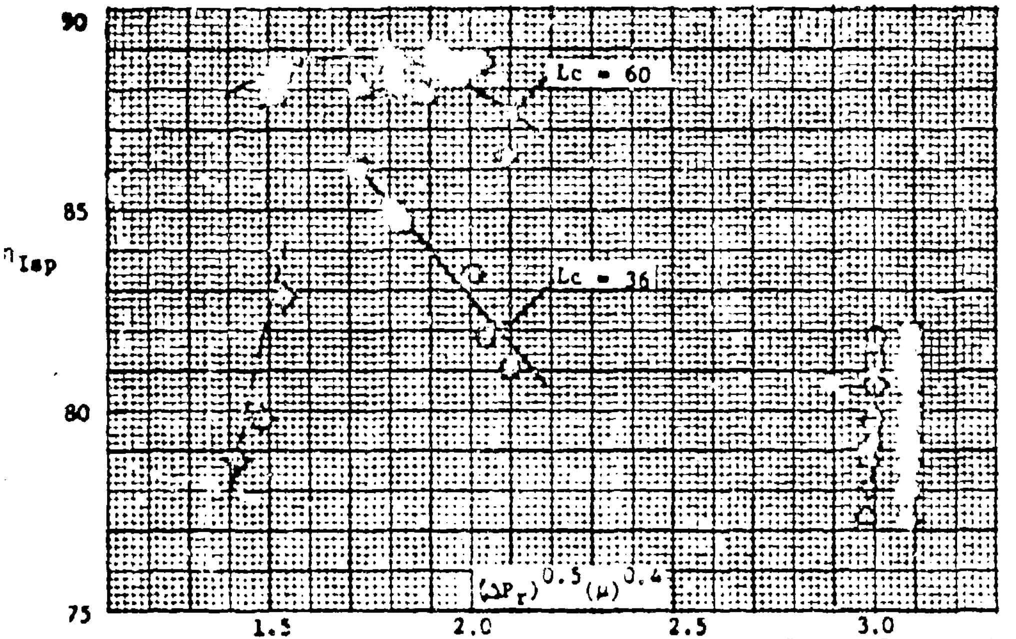

(C) Figure 3-51. Specific Impulse Efficiency, Test Series 5, Function of $(\Delta Pr)^{0.5}(\mu)^{0.4}$ (U)

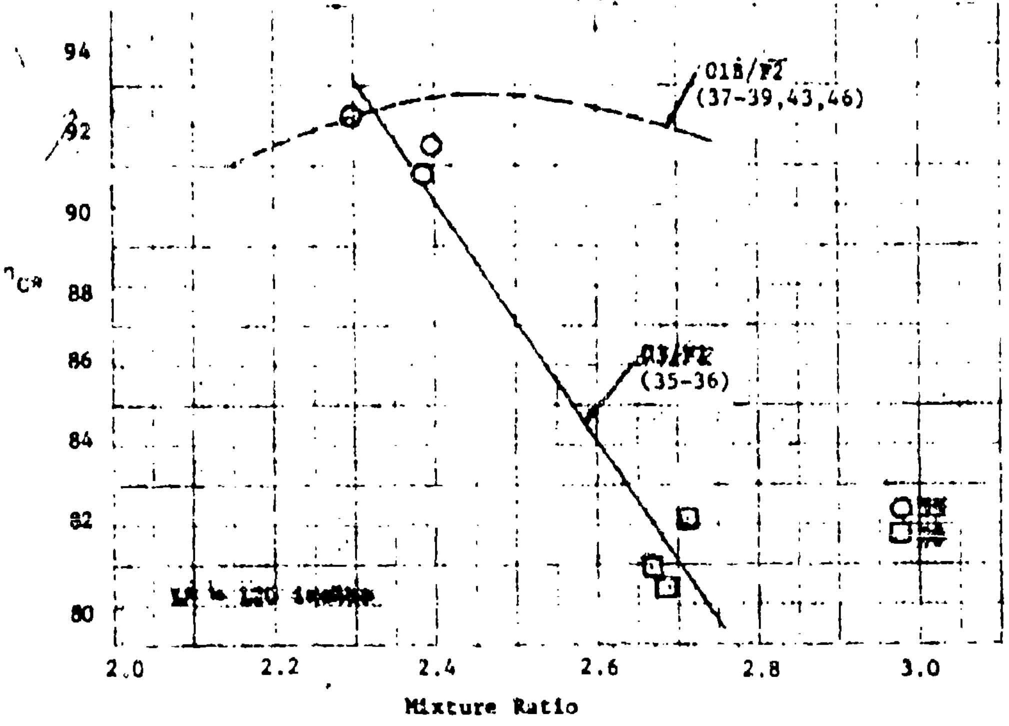

(C) Figure 3-52. Combustion Efficiency, Test Series 6 (U)

(C) The computed nozzle efficiency, η_{CF1}, for this series agrees with η_{CF1} computed for the prior test series as shown in Figure 3-53. The η_{CF3} for firings 35-36 is 0.935 which compares with the nominal value computed for firings 30-32, 37-39, 43 and 46.

3.4.2.5.2 Injector Characteristics

(U) The fuel injector conductance, KIJCF, for test firings 35 and 36 is shown in Figure 3-54 as a function of the volumetric flow rate. The data for firing 35 and 36 are in good agreement with that measured during firings 30-46. The low discharge coefficient for the fuel orifice is still indicated.

(U) The conductance on the oxidizer side of the injector assembly is shown in Figure 3-55 as a function of the volumetric flow rate. The nominal discharge coefficient computed from the conductance is 0.685 which corresponds to that measured for the X403831-1 orifice ring used in test firings 11-17.

(U) With the limited number of firings and the disagreement in fuel injection ΔP's for 35 and 36 the specific impulse efficiency was not computed as a function of injection pressure loss ratio $(\Delta P_r)^{0.5}(\mu)^{0.4}$.

3.4.2.6 Test Series 7 - Firings 44-45

3.4.2.6.1 Performance Data

(U) The fourth oxidizer orifice configuration (05) tested was the X403946-1, 36 element ring. This ring was desinged to operate with a back orifice ring (X404480-1) assembled into the X404408-5 Pintle Tip Assembly. The purpose of the back ring was to increase the L/D of both primary and secondary orifices by providing a flow channel for the oxidizer prior to injection. The orifice ring was characterized with essentially the same orifice shape, space factor and total injection areas as the "B" modification of the X403831-1 orifice ring. Only two test firings were made with this configuration. Both firings (44-45) were made with the 24 inch longer chamber.

(U The measured combustion efficiency for this configuration was much lower than anticipated, and is believed due to insufficient penetration of the fuel sheet into the oxidizer filaments at the injector operating conditions. This is evidenced by increasing performance as the mixture ratio is increased as shown in Figure 3-56. However, even this performance is less than measured with the 01B configuration.

(C) The computed nozzle efficiency, η_{CF1} for this series (Figure 3-57) agrees with the nozzle efficiency computed for test series 3, 4, 5 and 6, with a nominal efficiency of 0.935.

3.4.2.6.2 Injector Characteristics

(U) The fuel injector conductance, KIJCF, for test firing 45 indicates an orifice discharge coefficient (C_d) of 0.39 (see Figure 3-54). As in test series 5 and 6, this C_d is believed to be incorrect due to the fuel injection pressure measurement. The conductance on the oxidizer side of the injector assembly shows a wide variation with volumetric flow rate. The C_{do} variation is from 0.765 to 0.360 which would account for the reduced performance.

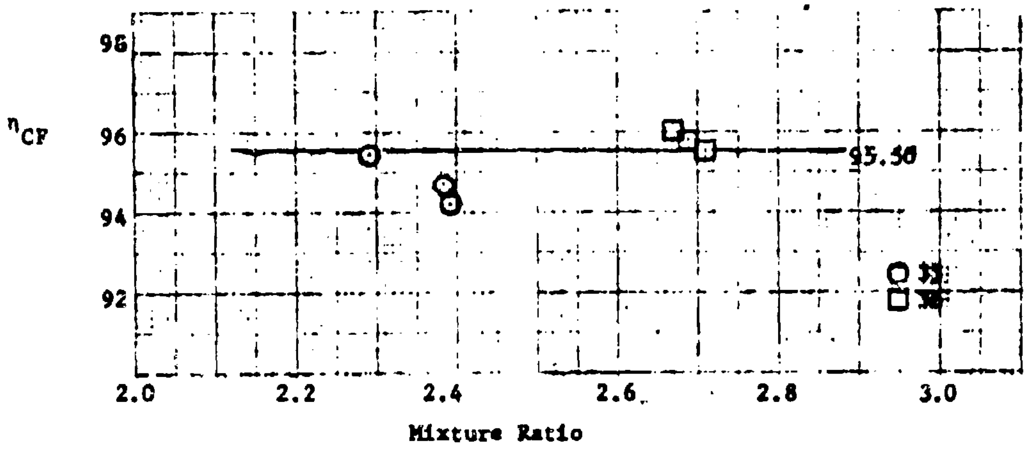

(C) Figure 3-53. Nozzle Efficiency, Test Series 6 (U)

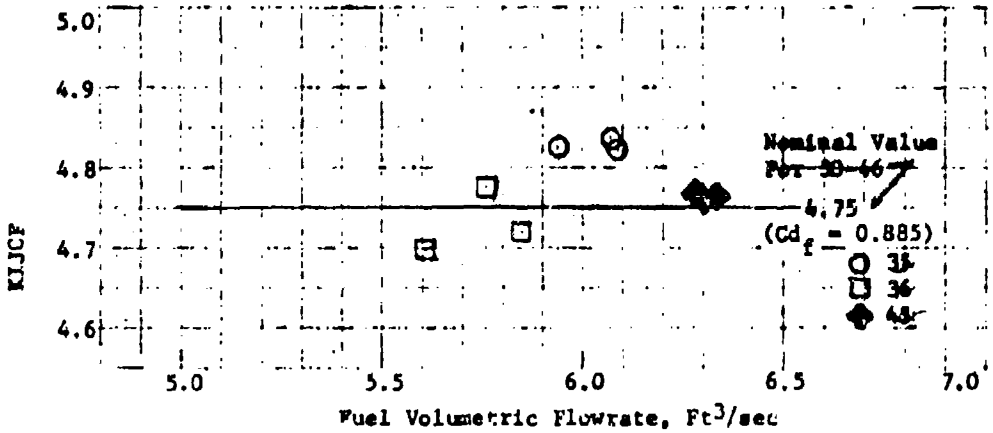

(U) Figure 3-54. Fuel Injector Conductance, Test Series 6 and 7 (U)

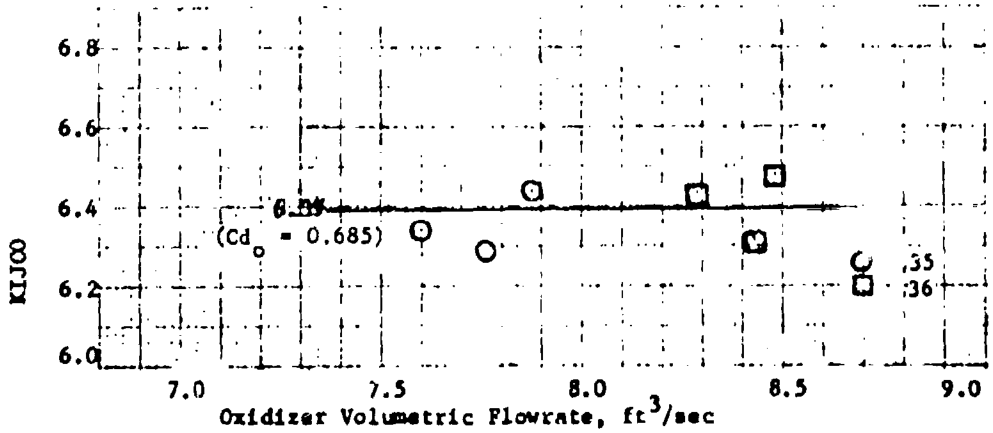

(U) Figure 3-55. Oxidizer Injector Conductance, Test Series 6 (U)

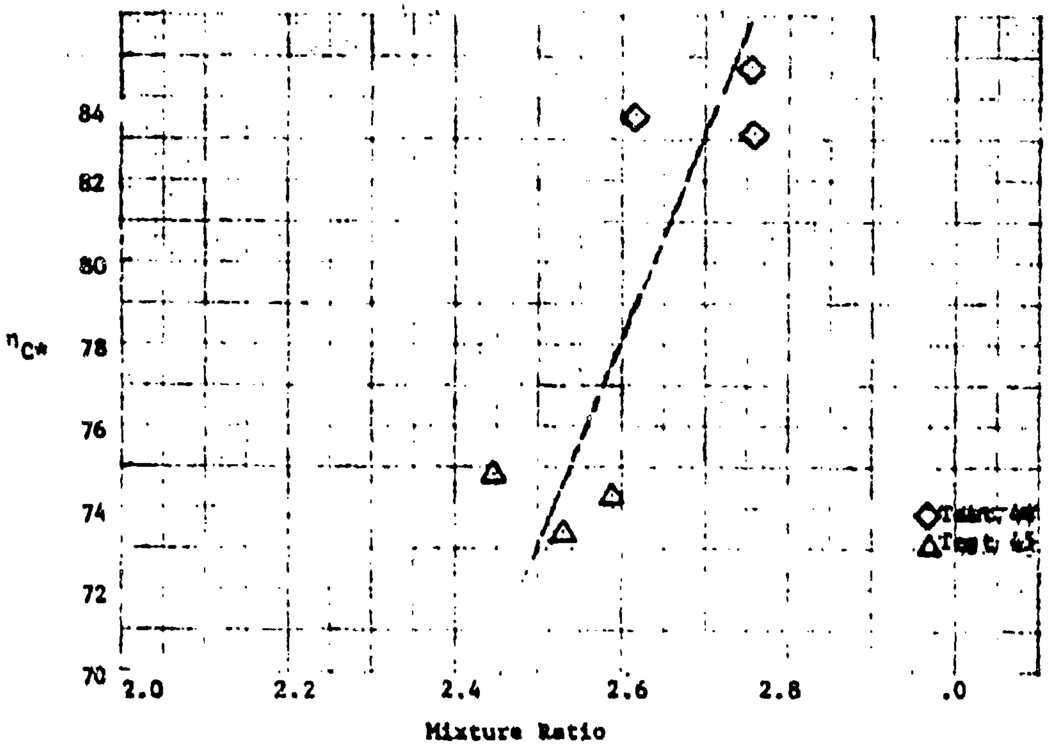

(C) Figure 3-56. Combustion Efficiency, Test Series 7 (U)

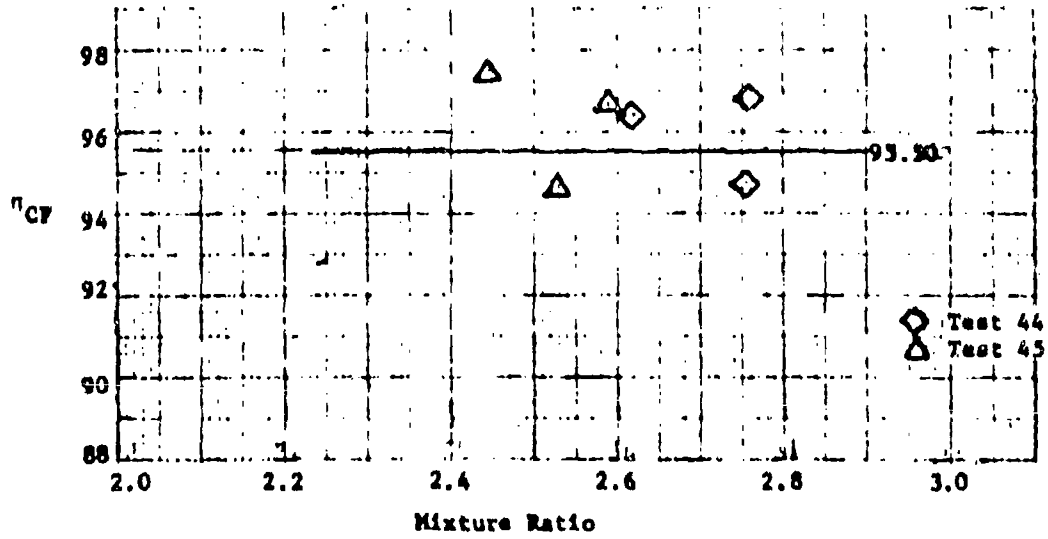

(C) Figure 3-57. Nozzle Efficiency, Test Series 7 (U)

3.4.2.7 Test Series 8 - Firings 101-102

3.4.2.7.1 Performance Data

(U) The majority of the development injector firings were made during the winter months (December, January and February) with propellants at a relatively low temperature (less than 55°F). To check the effect of propellant temperature on performance the 01B/F2 development injector configuration was reinstated in the 24 inch longer chamber and two test firings were made on 7 July 1969. Propellants were in the 80°F to 90°F temperature range. The 01B/F2 injector configuration was previously used in Test Series 5 (See Section 3.4.2.4).

(U) Figure 3-58 shows the measured thrust as a function of the nozzle stagnation pressure computed from the PC-1 measurement. The data for Test Series 5 is shown for comparison purposes. The computed specific impulse efficiency, η_{Isp}, is shown in Figure 3-59 as a function of mixture ratio. Again, the data for Test Series 5 is shown for comparison purposes. The computed nozzle efficiency shown in Figure 3-60 indicates a loss in efficiency of about 1 percent when compared with the nominal nozzle efficiency.

(U) The computed combustion efficiency, η_{C*}, for firings 101-102 is shown in Figure 3-61 as a function of mixture ratio. The data for Test Series 5 is shown also. Following test firings 101-102 the 01B/F2 development injector configuration was water-flowed at the TRW Systems Capistrano Test Site. Photographs taken of the water-flow show considerable leakage at the threaded joint between the oxidizer ring and centerbody. This leakage would cause a disruption of the normal fuel flow and is assessed to be the probable cause of the lowered performance measured on firings 101-102. Waterflow of the injector is discussed further in Section 3.4.4.

3.4.2.7.2 Injector Characteristics

(U) The fuel injector conductance, KIJCF, for test firings 101-102 is shown in Figure 3-62 as a function of the volumetric flowrate. The computed conductance is based on the assumption that the data tabulated as PIF-1 in the General Performance Data listing is in reality PIF-2. Using this assumption results in a reasonable system conductance (measured between PLF and PIF-2). The computed conductances for the two firings are both greater than that measured during firings 30-46 and approximately the same as measured during firings 16-28.

(U) The oxidizer injector conductance, KIJCO, is shown in Figure 3-63 as a function of the volumetric flow rate. Even though leakage was observed post-test the computed conductance is in agreement with the nominal value measured during test firings 30-46 with the 01B orifice configuration.

3.4.2.8 Test Series 9 - Firings 108-110

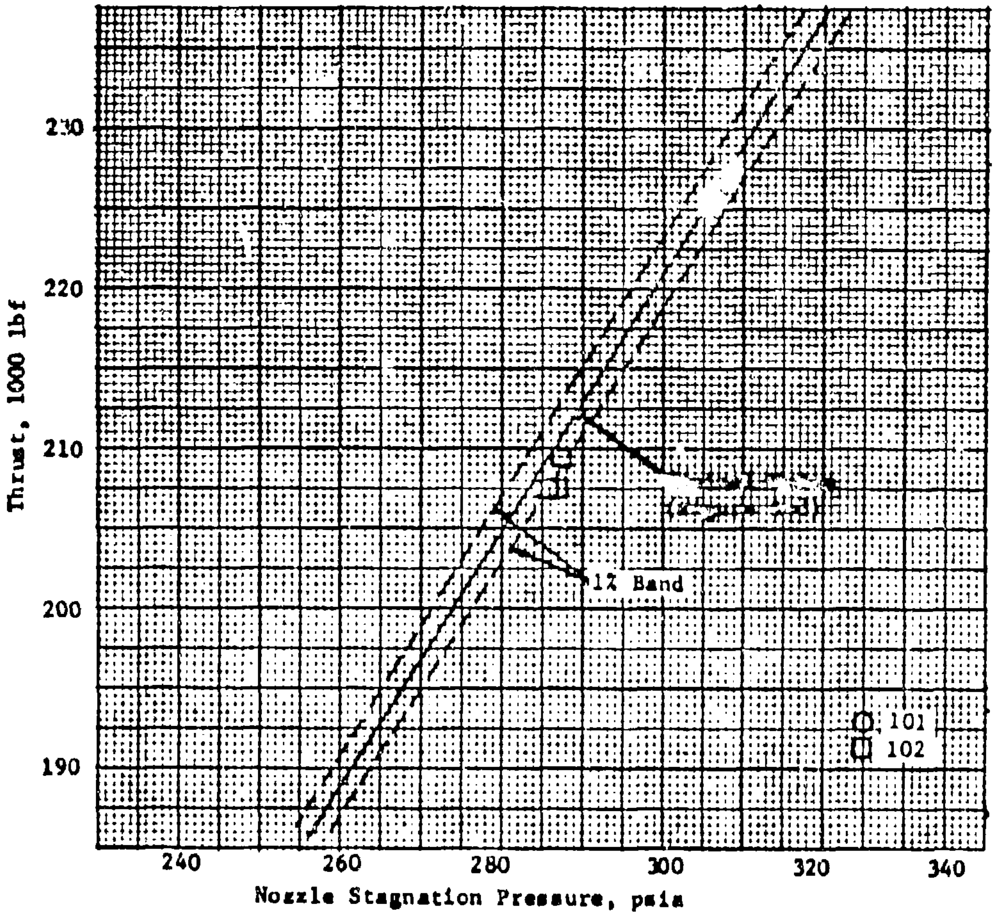

(C) Figure 3-58. Measured Thrust, Test Series 8 (U)

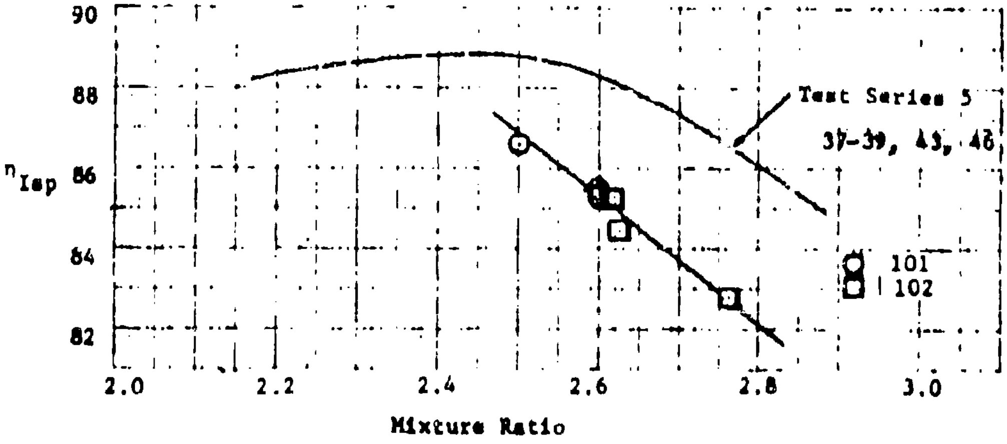

(C) Figure 3-59. Specific Impulse Efficiency, Test Series 8 (U)

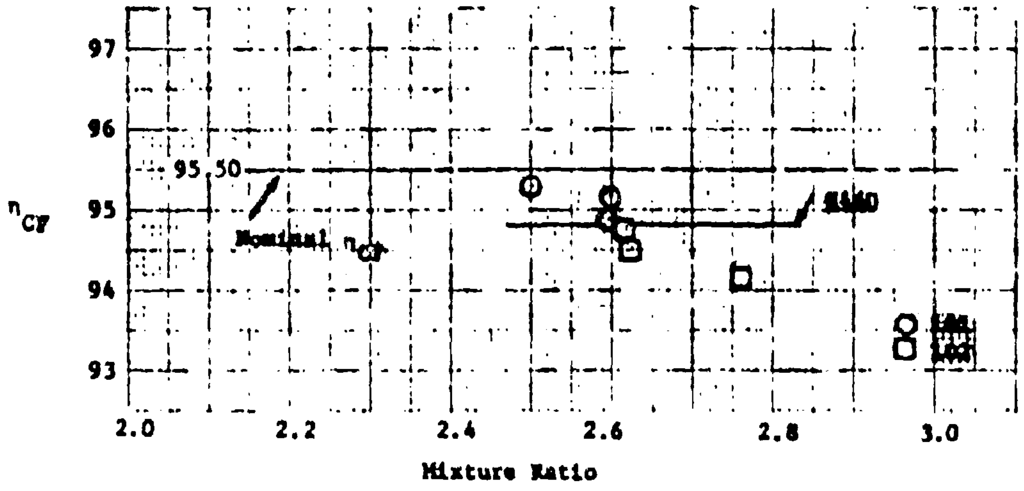

(C) Figure 3-60 Nozzle Efficiency, Test Series 8 (U)

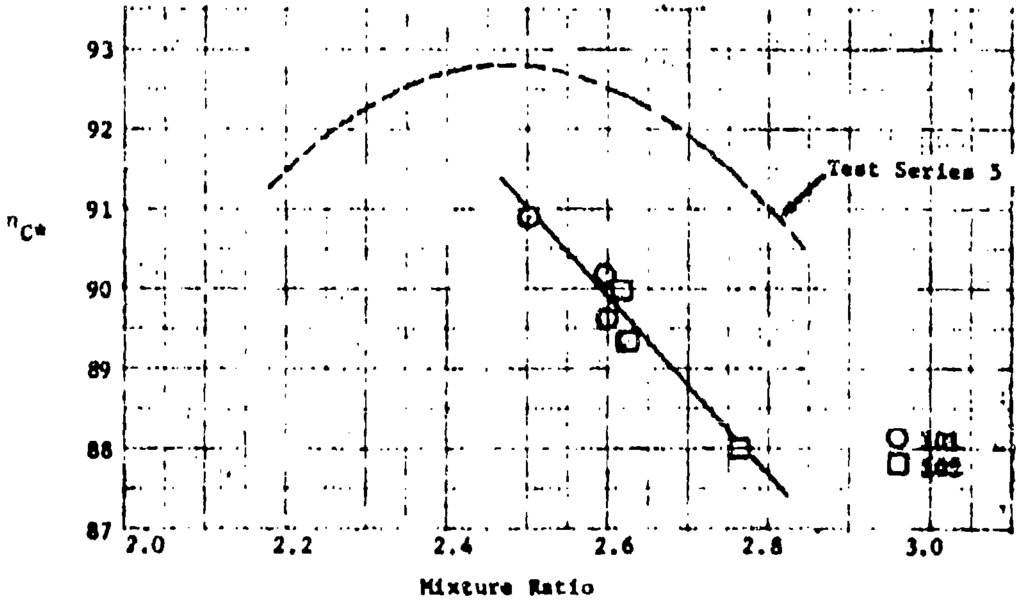

(C) Figure 3-61 Combustion Efficiency, Test Series 8 (U)

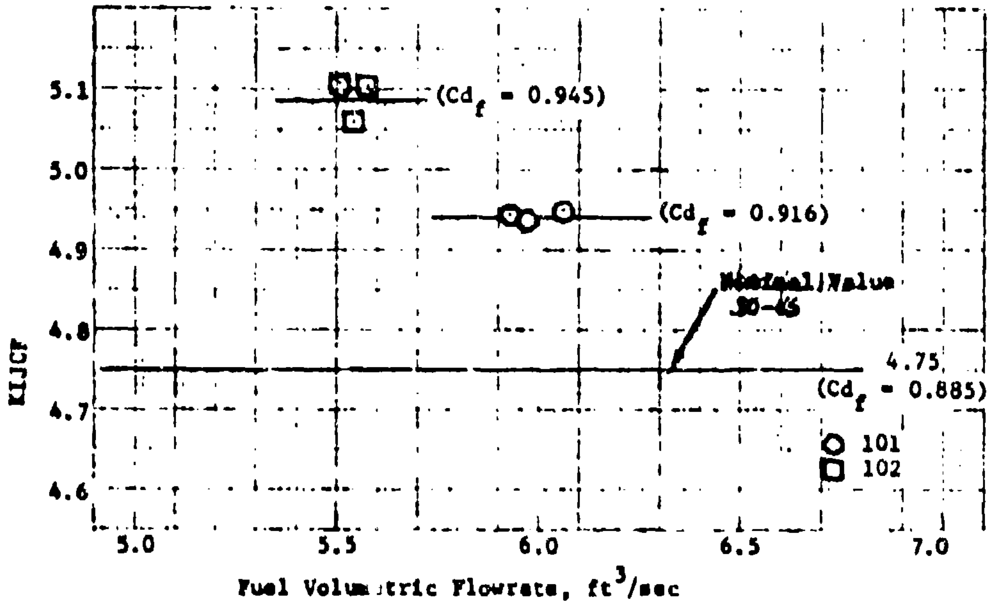

(U) Figure 3-62. Fuel Injector Conductance, Test Series 8 (U)

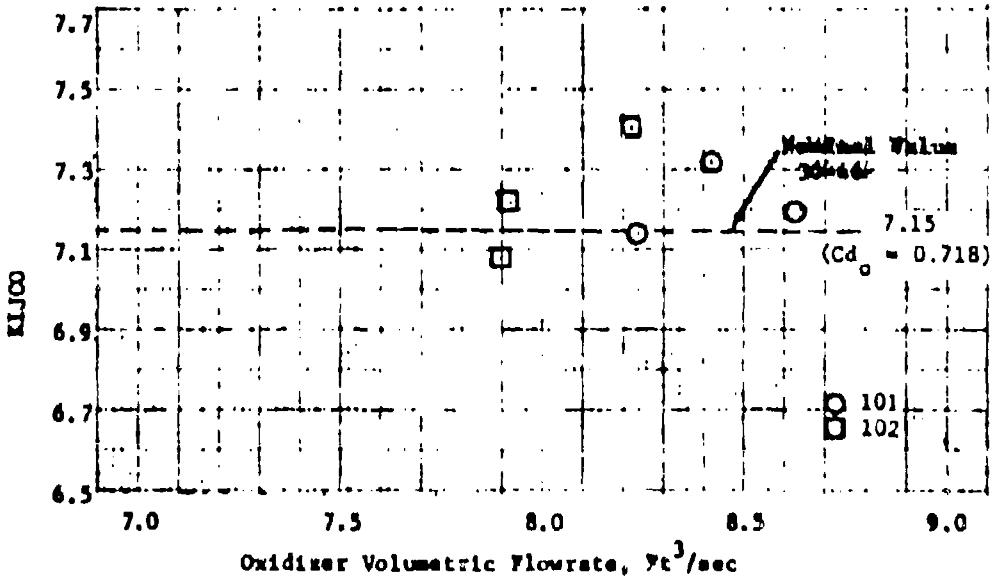

(U) Figure 3-63. Oxidizer Injector Conductance, Test Series 8 (U)

3.4.2.8.1 Performance Data

(U) Following the firing (107) of the configuration 1 ablative lined chamber in December of 1969 (See Volume II) a decision was made to check the performance of the development injector with the 06 oxidizer ring (X404108-1) and F2 fuel ring. This oxidizer ring had been fabricated and water-flowed, but not tested, during Task I and showed a more uniform spray pattern than was observed for the demonstration injectors. The $[W_p + W_s)/UW]$ factor for the 06 oxidizer ring was 0.60 while the percentage of secondary flow was reduced from a nominal 10.0 percent to 4.8 percent of the total flow. The number of oxidizer elements was increased to 48 primaries and 48 secondaries as in the 02 oxidizer ring (X404107-1).

(U) Three test firings of the 06/F2 injector configuration were made. Figure 3-64 shows the measured thrust as a function of the nozzle stagnation pressure. The data taken during this series shows excellent agreement with the earlier data (Figure 3-3). The computed specific impulse efficiency, η_{Isp} is shown in Figure 3-65 as a function of mixture ratio and the combustion efficiency is also shown in Figure 3-65. Figure 3-66 shows the specific impulse efficiency, η_{Isp} as a function of the injector correlating parameter. The dashed line is for the 02/F2 injector configuration used in test series 4. Insufficient data was taken to determine if both injectors would show performance peaks at the same value of the correlating parameter. It is apparent that this configuration requires a higher fuel injection velocity at the design mixture ratio than was possible with the F2 fuel ring.

3.4.2.8.2 Injector Characteristics

(U) The fuel and oxidizer injector conductances, KIJCF and KIJCO, for test firings 108-110 are shown in Figure 3-67 as a function of the volumetric flow rate. The fuel conductance of the F2 fuel orifice ring results in a discharge coefficient of 0.95 which is in agreement with the value computed for this ring during firings 16-28. However, the 0.95 discharge coefficient is higher than the value measured during firings 30-46 and 101-102.

(U) The average oxidizer injector conductance of 5.65 results in a discharge coefficient of 0.64 which is somewhat lower than the discharge coefficients measured for previous injector development orifice rings.

3.4.3 Demonstration Injector Firings

3.4.3.1 Checkout Firings - S/N 001 Injector

3.4.3.1.1 Performance Data

(U) The S/N 001 injector was the initial demonstration injector delivered to the AFRPL for test. The demonstration injector oxidizer orifice configuration was nearly identical in shape to the 01A oxidizer orifice configuration tested in Test Series 3. The major change in this configuration was an increase in area by approximately 10 percent in order to reduce the oxidizer injection ΔP by approximately 20 percent. Injector performance was expected to be nearly identical to that shown on Figure 3-43 for the 01B/F2 configuration.

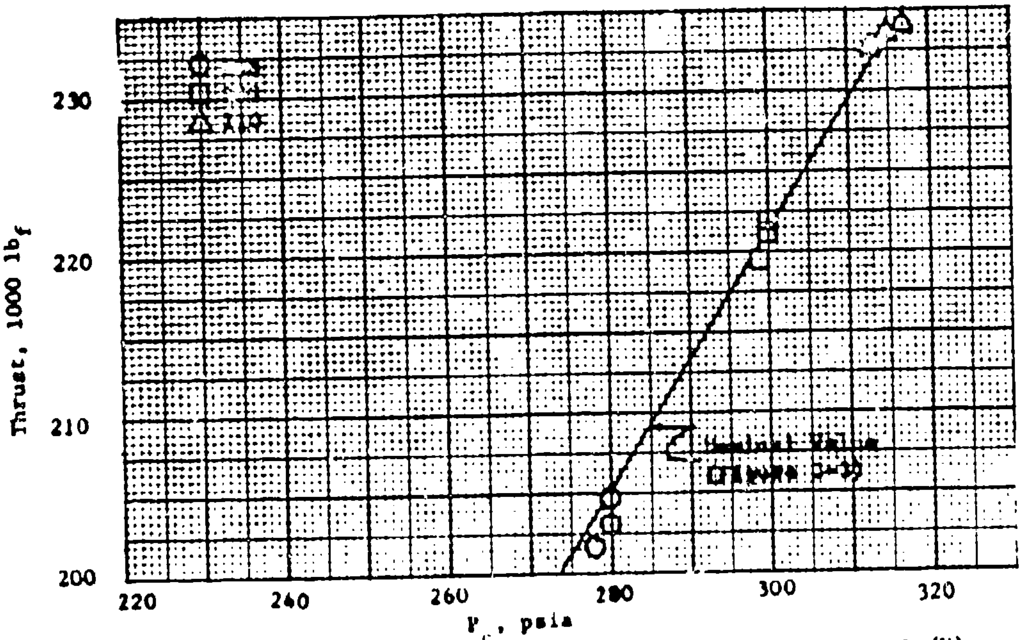

(C) Figure 3-64. Measured Thrust, Test Series 9 (U)

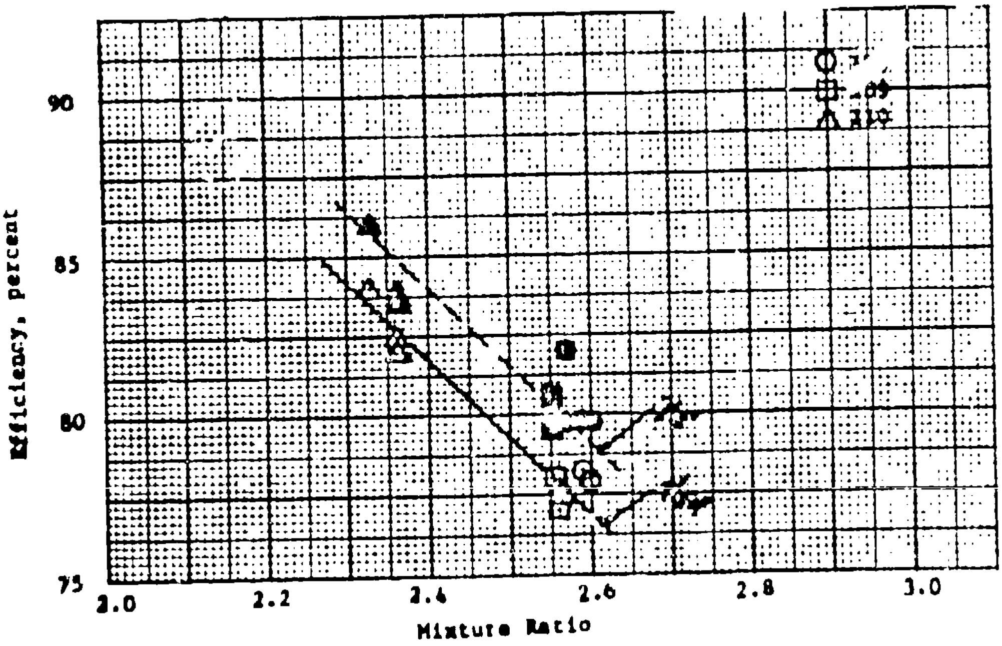

(C) Figure 3-65. Efficiency, Test Series 9 (U)

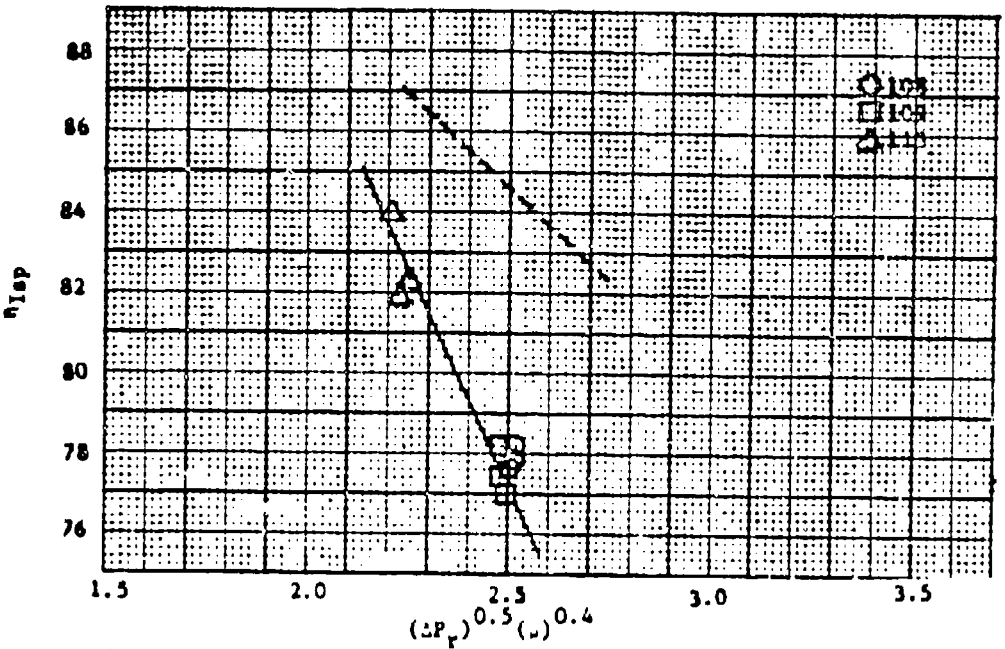

(C) Figure 3-66. Specific Impulse Efficiency, Test Series 9, Function of $(\Delta P_r)^{0.5}(\mu)^{0.4}$ (U)

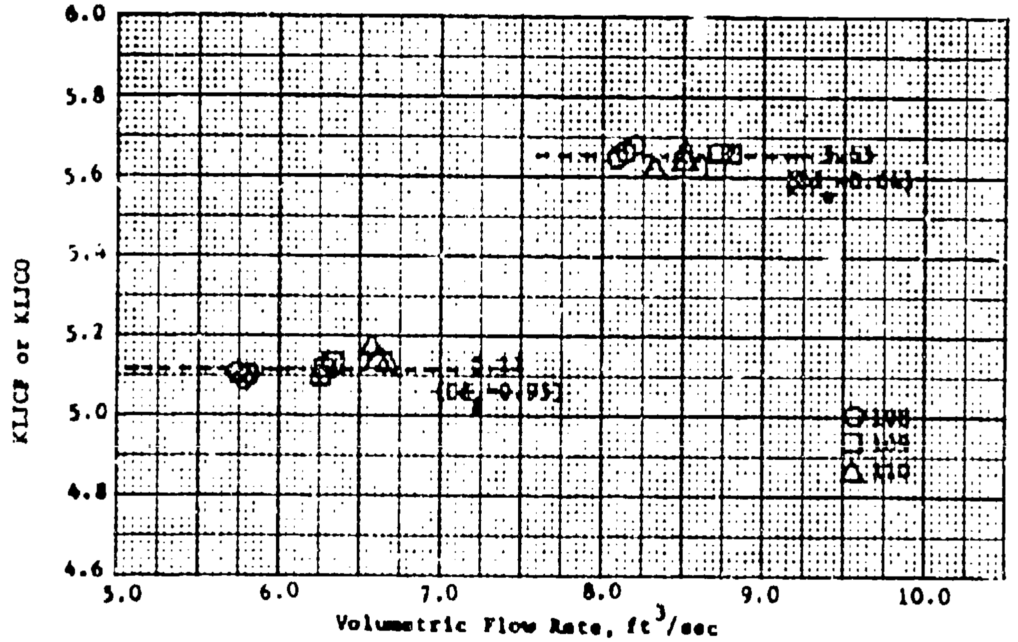

(U) Figure 3-67. Injector Conductance, Test Series 9 (U)

(C) Figure 3-68 shows the measured thrust as a function of nozzle stagnation pressure. The nozzle stagnation pressure Po, is the injector end pressure (PC-1) corrected for an $\epsilon_c = 2.25$ and a $\gamma = 1.235$. Figure 3-68 also shows the measured thrust as a function of nozzle stagnation pressure computed from PC-4 (nozzle entrance pressure) corrected for an $\epsilon_c = 2.25$ and a $\gamma = 1.235$. The data for firings 72-77 show good agreement with the data obtained with the 01B/F2 configuration. The average nozzle efficiency, shown in Figure 3-69, of 95.40 also is good agreement with the nominal value of 95.50.

(U) The computed specific impulse efficiency, $\eta_{I_{sp}}$ is shown in Figure 3-70 as a function of mixture ratio. The computed combustion efficiency, η_{C*}, for test firings 72-77 is shown in Figure 3-71 as a function of mixture ratio. Data for test series 5 is shown for comparative purposes. The data are widely scattered and are grouped according to nozzle stagnation pressure. The difference between test series 5 and this series is unexplained.

3.4.3.1.2 Injector Characteristics

(U) The fuel injector conductance, KIJCF, for test firings 72-77 is shown in Figure 3-72 as a function of the volumetric flow rate. The fuel side discharge coefficient computed from the average conductance is greater than 1.04 as compared with the Cd value of 0.885 computed for the same fuel injection area in test firings 30-46. In order to try and ascertain the cause of the very high discharge coefficient the various fuel feed system conductances were examined. Figure 3-73 shows the line conductance, based on (PLF)-(PC-1), for various volumetric flow rates. The average line conductance is about 7 percent greater than that previously measured during test firings 18-46. The internal fuel injector losses, (PIF-1)-(PIF-2) are shown in Figure 3-74. These conductances agree with the nominal value calculated for test firings 18-28 (internal losses were not measured on test firings 29-46). The low conductance for test firing 77 is unexplained.

(U) The oxidizer injector conductance, KIJCO, for test firings 72-77 is shown in Figure 3-75 as a function of the volumetric flow rate. The indicated oxidizer side discharge coefficient computed from the average conductance is about three percent less than the C_{do} computed for the 01B configuration employed on test firings 30-39, 43, and 46. The oxidizer line conductance (KLO) shows a much greater variation than would be expected.

3.4.3.2 Durability Firing = S/N 001 Injector

3.4.3.2.1 Performance Data

(U) The initial demonstration injector delivered to the AFRPL (S/N 001) was subjected to a 10 second duration firing to check the durability of the injector pintle tip. This injector was fired using the modified X403646-10 chamber (see Section 1.5.1.2) lined with a low-cost gypsum-phenolic insulation on test firing 78. This chamber is 6 inches shorter than the chamber employed in test firings 72-77 and has an L* of 108 inches.

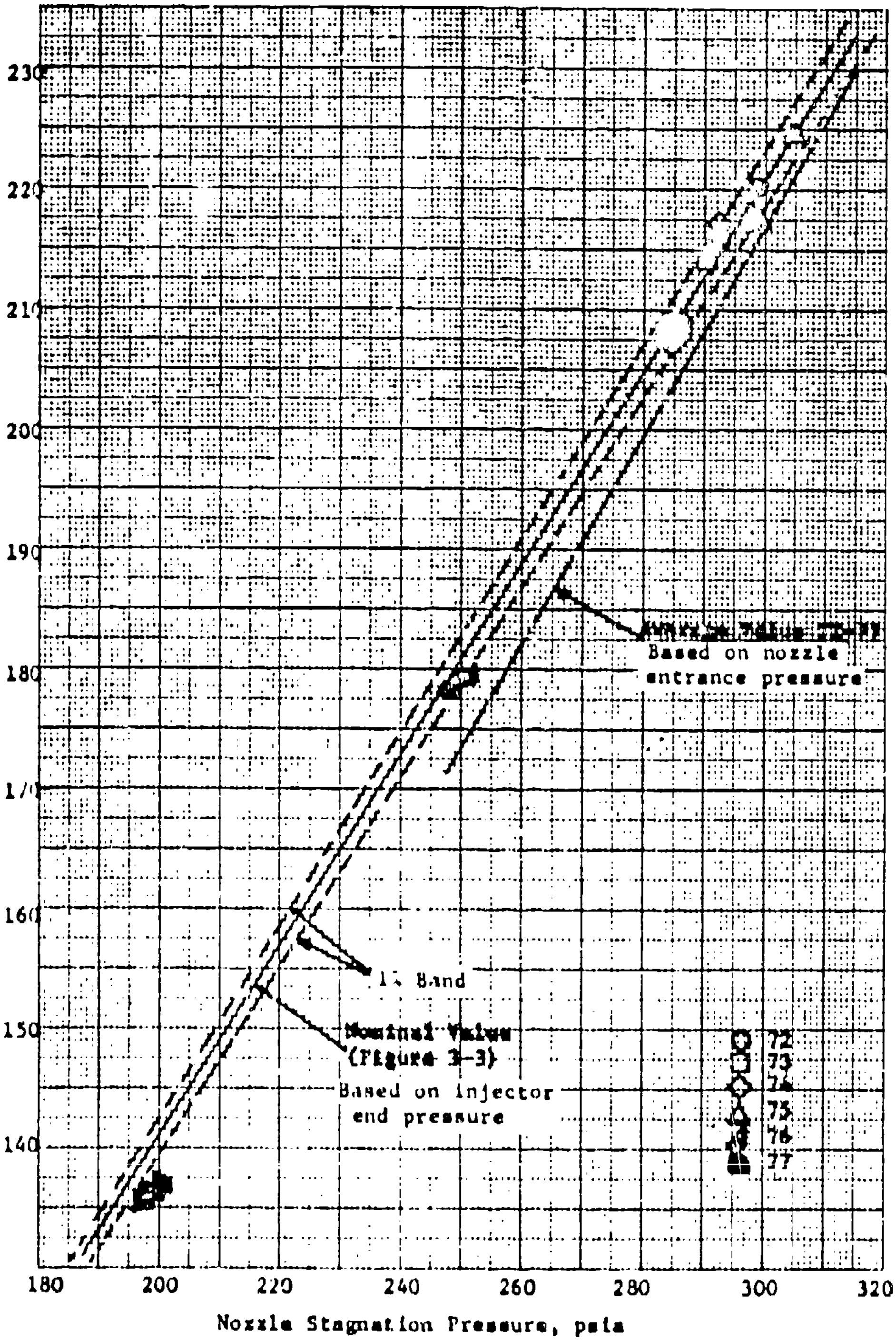

(C) Figure 3-68. Measured Thrust, Test Firings 72-77 (U)

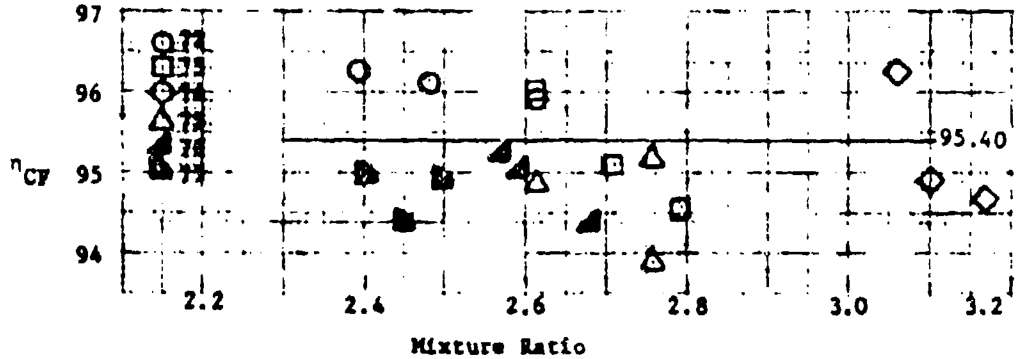

(C) Figure 3-69 Nozzle Efficiency, Test Firings 72-77 (U)

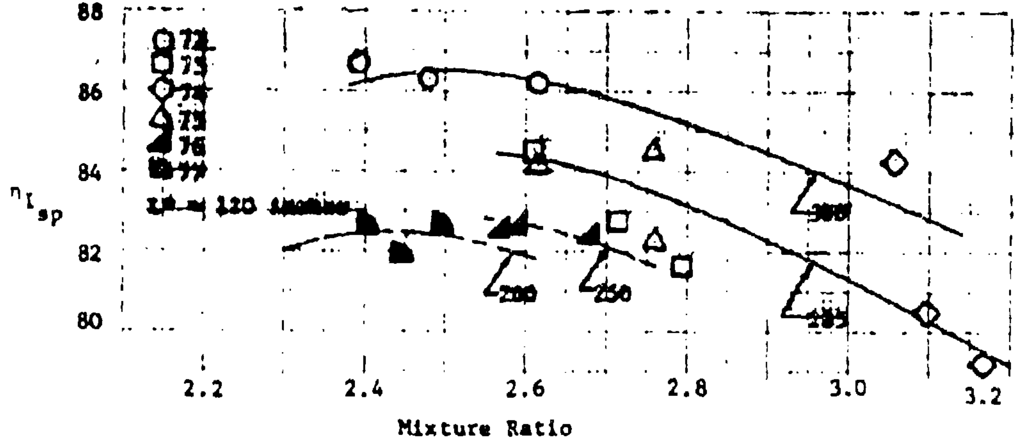

(C) Figure 3-70 Specific Impulse Efficiency, Test Firings 72-77 (U)

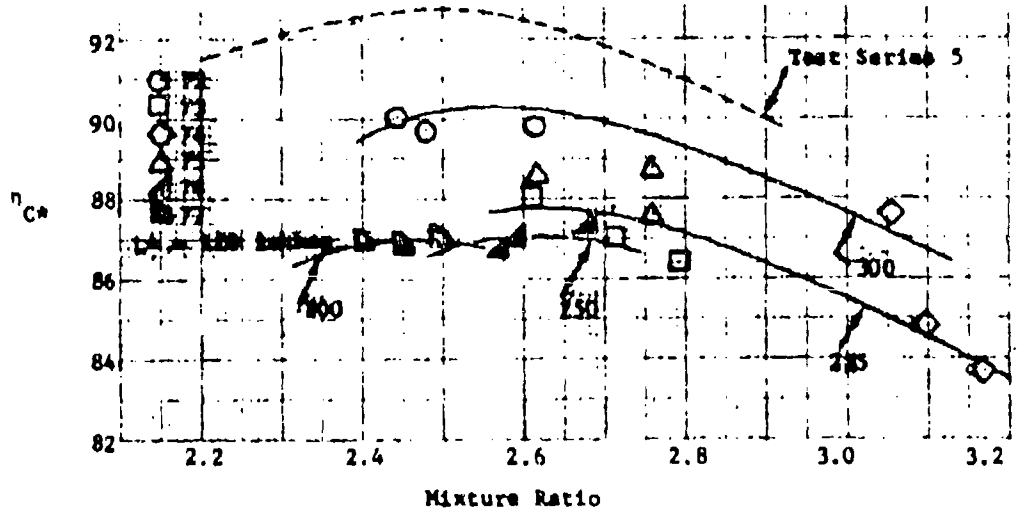

(C) Figure 3-71 Combustion Efficiency, Test Firings 72-77 (U)

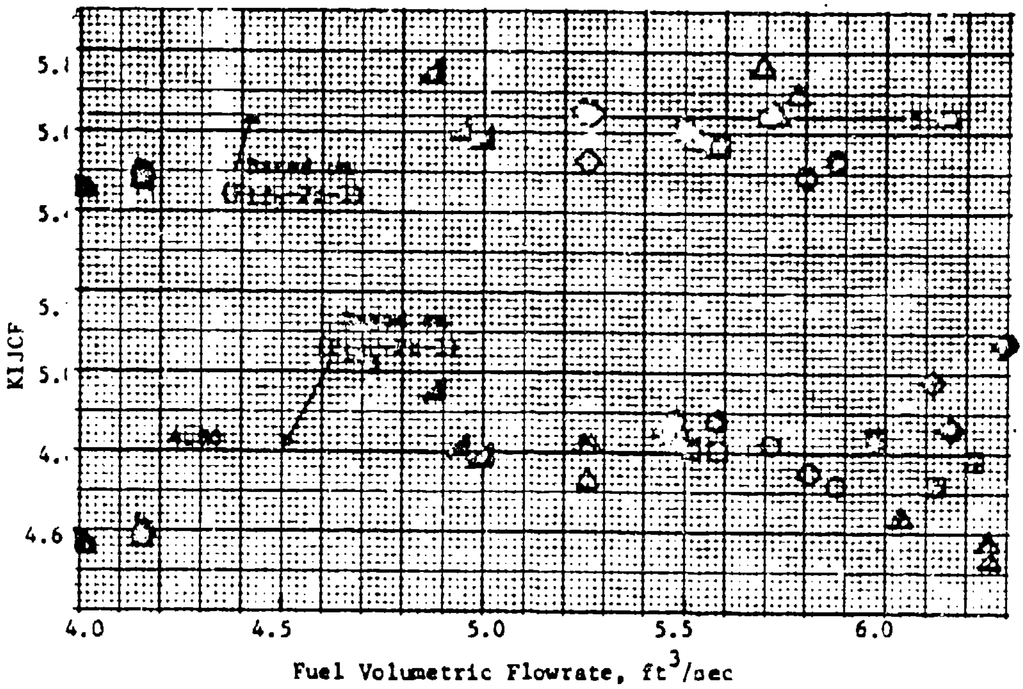

(U) Figure 3-72. Fuel Injector Conductance, Test Firings 72-77 (U)

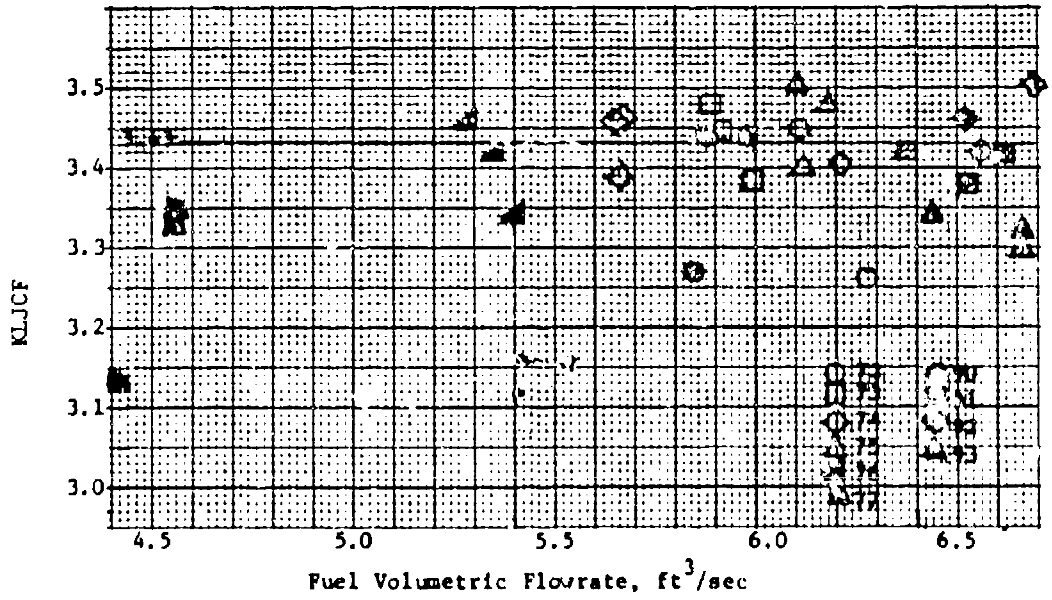

(U) Figure 3-73. Fuel Line Conductance, S/N 001 Injector (U)

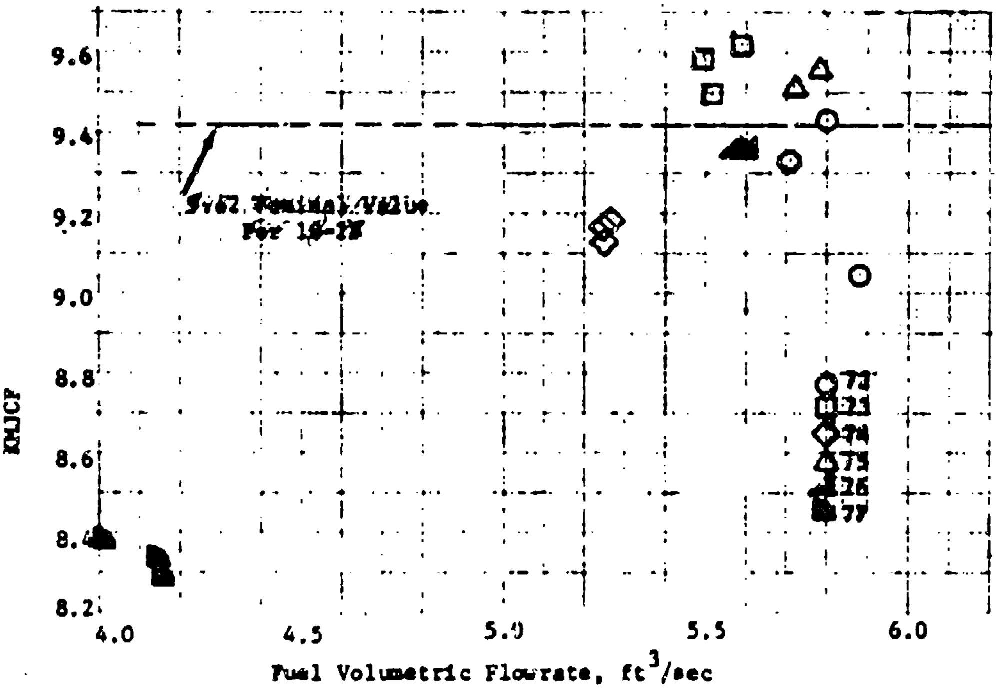

(U) Figure 3-74. Fuel Manifold Conductance, Test Firings 72-77 (U)

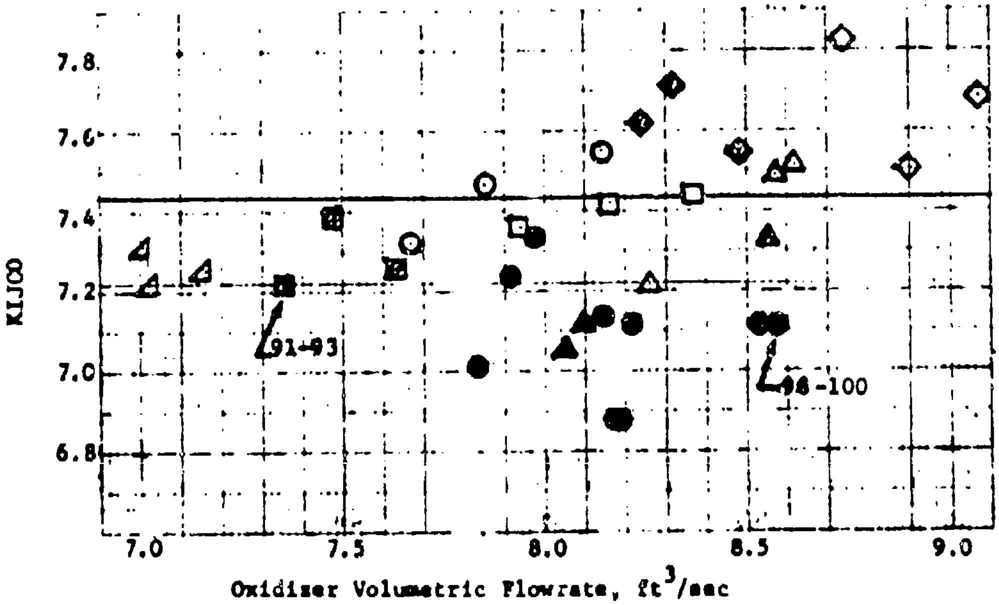

(U) Figure 3-75. Oxidizer Injector Conductance, Test Firings 72-77 (U)

(U) Figure 3-76 shows the computed specific impulse efficiency, $\eta_{I_{sp}}$, as a function of mixture ratio. The data from test firings 72-77 at 300 psi is shown for comparative purposes. It should be noted that the performance obtained on test firing 78 is about the same level as that obtained during firings 72-77 in a six inch longer chamber during the initial first second of the firing. However, the data for firing 78 also indicates a 2 percent performance increase with time.

3.4.3.2.2 Injector Characteristics

(U) The fuel injector conductance, KIJCF, for test firing 78 is shown in Figure 3-77 as a function of the volumetric flow rate. The fuel side conductance is 10 percent lower than that measured on the preceeding six firings and more in line with what was experienced on test firings 18-46. The line conductance KLJCF is also lower than that measured during firings 72-77. In addition, the internal fuel injector conductance, which is based on the pressure loss between PIF-1 and PIF-2, is considerably lower than that measured during firings 18-28 and confirmed during firings 72-76. The fuel side conductances for all three items, KIJCF, KLJCF, and KMJCF all show a time dependence during the approximate 10 second firing duration as shown in Figure 3-78.

(U) The oxidizer injection conductance, KIJCO is somewhat lower than measured during firings 72-77 as shown in Figure 3-75. The oxidizer injection conductance is time dependent in about the same manner as the fuel injection conductance. The PLO measurement was not available on test firing 78; therefore the line conductance could not be calculated.

3.4.3.3 Additional Firings - S/N 001 Injector

3.4.3.3.1 Performance Data

(U) The S/N 001 injector used in test firings 72-78 was test fired in conjunction with the X403646-14 thrust chamber configuration. This chamber configuration was identical to the X403646-11 thrust chamber, except for the addition of the turbulence ring (X404469-1).

(U) Figure 3-79 shows the measured thrust as a function of nozzle stagnation pressure, Po. The nozzle stagnation pressure is the nozzle entrance pressure (PC-4) corrected for an $\epsilon_c = 2.25$ and a $\gamma = 1.235$. The computed specific impulse efficiency, $\eta_{I_{sp}}$ is shown in Figure 3-80 as a function of mixture ratio. The data for test firings 72-77 is shown for comparative purposes on both Figures 3-79 and 3-80.

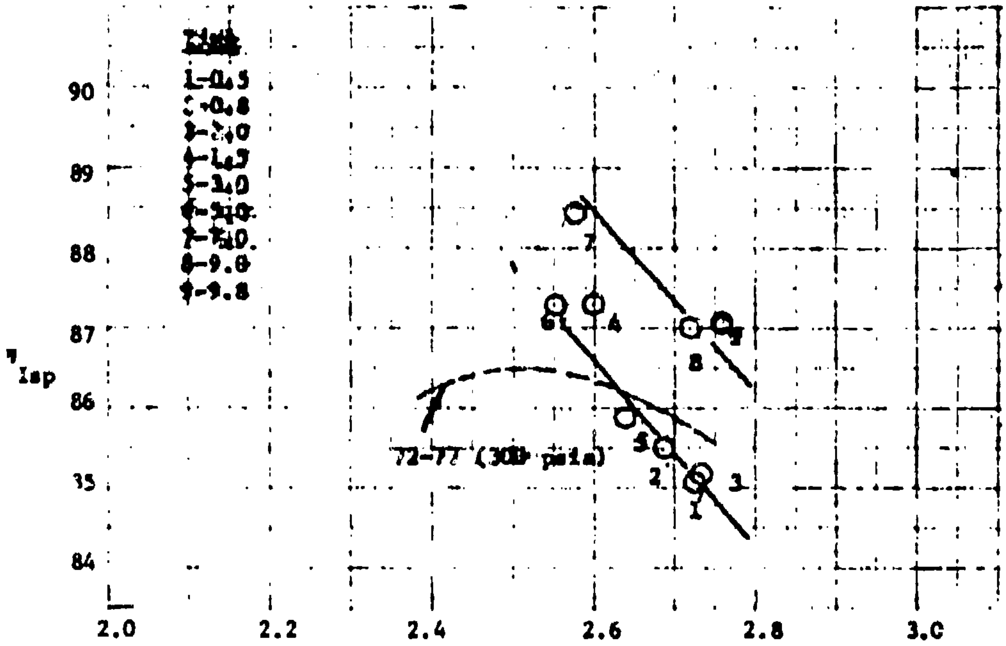

(C) Figure 3-76. Specific Impulse Efficiency-Durability Firing No. 78 (U)

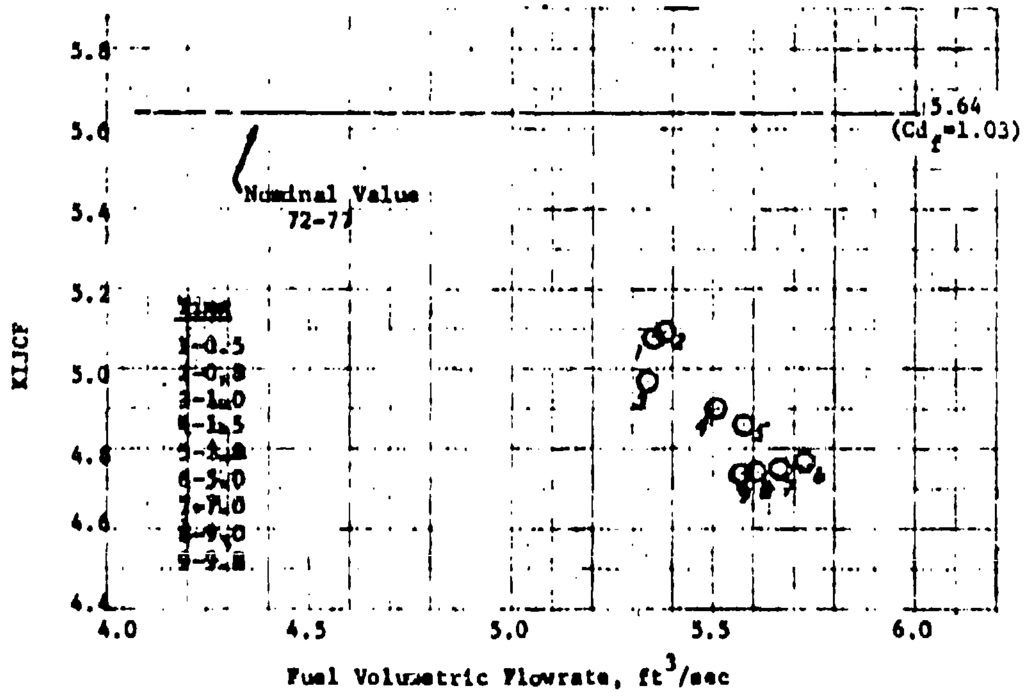

(C) Figure 3-77. Fuel Injector Conductance-Durability Firing No. 78 (U)

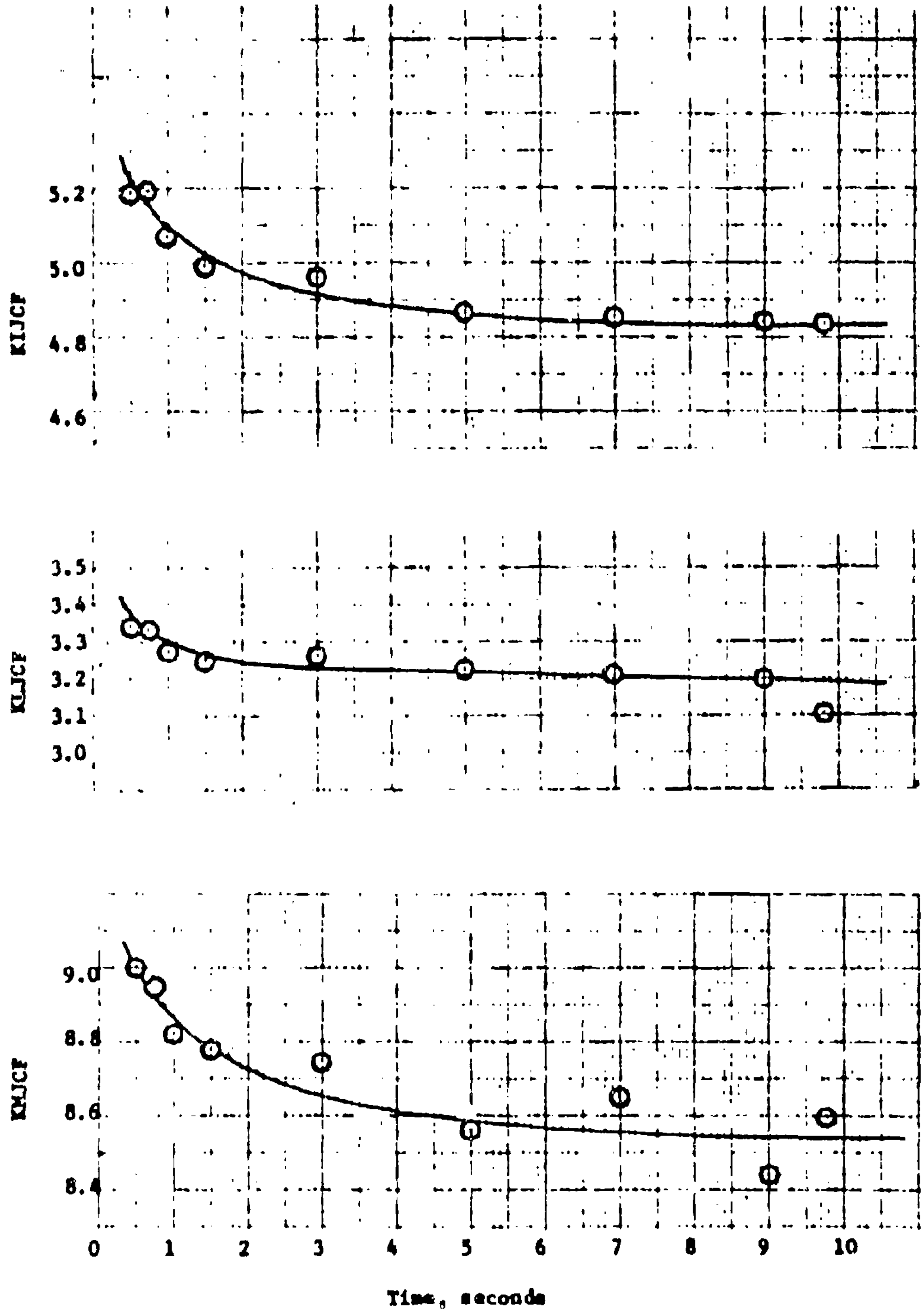

(U) Figure 3-78. Fuel Side Conductances as a Function of Time, Durability Firing No. 78 (U)

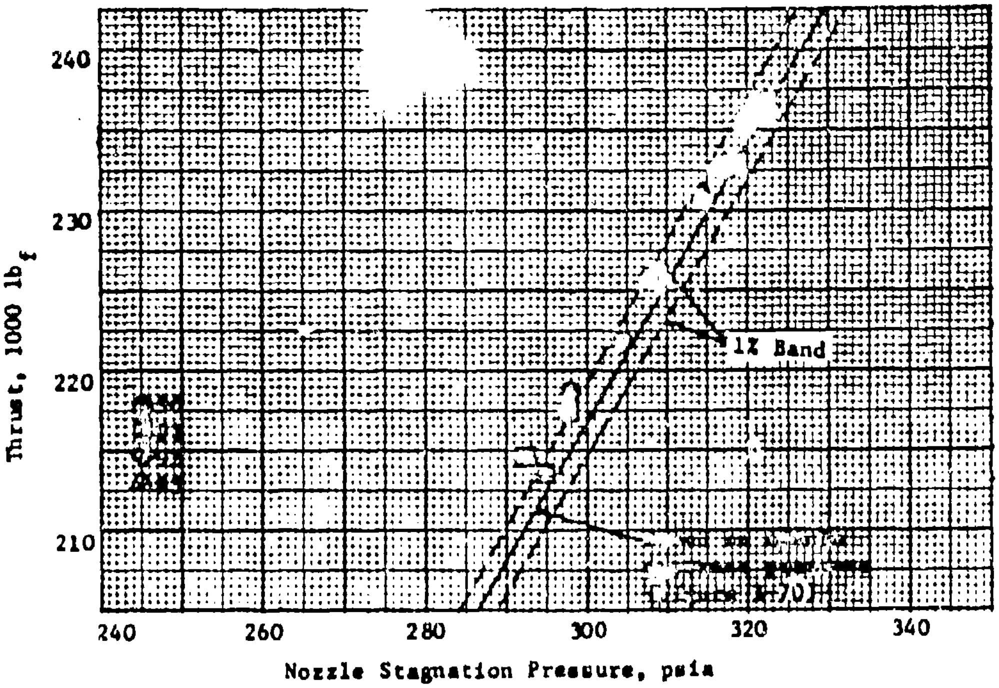

(C) Figure 3-79. Measured Thrust - Test Firings 90-93 (U)

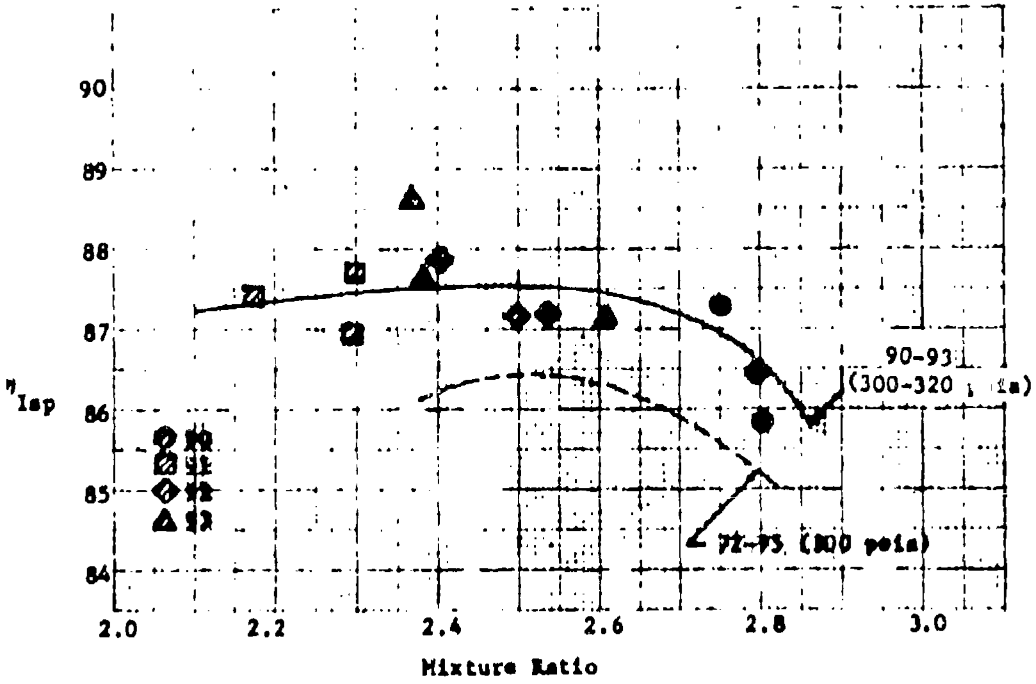

(C) Figure 3-80. Specific Impulse Efficiency, Test Firings 90-93 (U)

(C) The combustion efficiency for firings 90-93 is shown in Figure 3-81. These efficiencies are computed using PC-4, corrected to nozzle stagnation pressure. The data for test firings 72-75 and 98-100 (see Section 3.4.3.4.1) is shown for comparative purposes. Although the data for test firings 72-75 are badly scattered they show general agreement with the data obtained with the S/N 002 injector. It appears that the turbulence ring is responsible for about a one and one-half (1.5) percent increase in combustion efficiency.

3.4.3.3.2 Injector Characteristics

(U) The fuel injector conductance, KIJCF, for firings 90-93 is shown in Figure 3-78 as a function of the volumetric flow rate. The conductances shown are based on the pressure loss between the PIF-1' measurement and the PC-1 measurement. There was no PIF-2 measurement during this series and the PIF-1 transducer was located in the PIF-1' port which is on the toroidal manifold 180° removed from the PIF-1 port. The conductances for 90-93 show good agreement with the data of firings 72-77 when compared on the same basis. The line conductance, KLJCF, shows good agreement also with the data from firings 72-77.

(U) The oxidizer injection conductance, KIJCO, for test firings 91-93 is shown in Figure 3-79 as a function of the volumetric flow rate. The data shows a general agreement with that measured during firings 72-78 although the KIJCO for firing 90 is about 10 percent greater than the 72-78, 91-93 average.

3.4.3.4 Checkout Firings - S/N 002 Injector

3.4.3.4.1 Performance Data

(U) The S/N 002 injector was the only other demonstration injector checked out during Task I (test firings 98-100). The orifice configuration was nearly identical, in all respects, to the S/N 001 injector fired on tests 72-78 and 90-93. The S/N 002 injector was test fired using the X403646-11 thrust chamber configuration (without turbulence ring).

(C) Figure 3-82 shows the measured thrust as a function of nozzle stagnation pressure, P_o. The nozzle stagnation pressure is the injector end pressure (PC-1) or the average of PC-1/PC-1A corrected for an $\epsilon_c = 2.25$ and a $\gamma = 1.235$. Figure 3-83 shows an apparent 4 percent loss in thrust coefficient for test firings 98-100. This loss was not apparent in test firings 101-102 which used the same combustion chamber but used the development injector (01B/F2).

(U) Figure 3-84 shows the measured specific impulse efficiency as a function of mixture ratio. The S/N 002 injector performs as well as the 01B/F2 development injector configuration if the computed specific impulse efficiencies are corrected by the ratio of nozzle efficiencies shown in Figure 3-83. The combustion efficiency, η_{C*} for test firings 98-100, is shown in Figure 3-85 as a function of mixture ratio. The η_{C*} is based on a P_o computed from PC-1 or the average of PC-1/PC-1A corrected to nozzle stagnation for an $\epsilon_c = 2.25$ and a $\gamma = 1.235$. The combustion efficiency of the S/N 002 injector is about 2 percent greater than that measured with the S/N 001

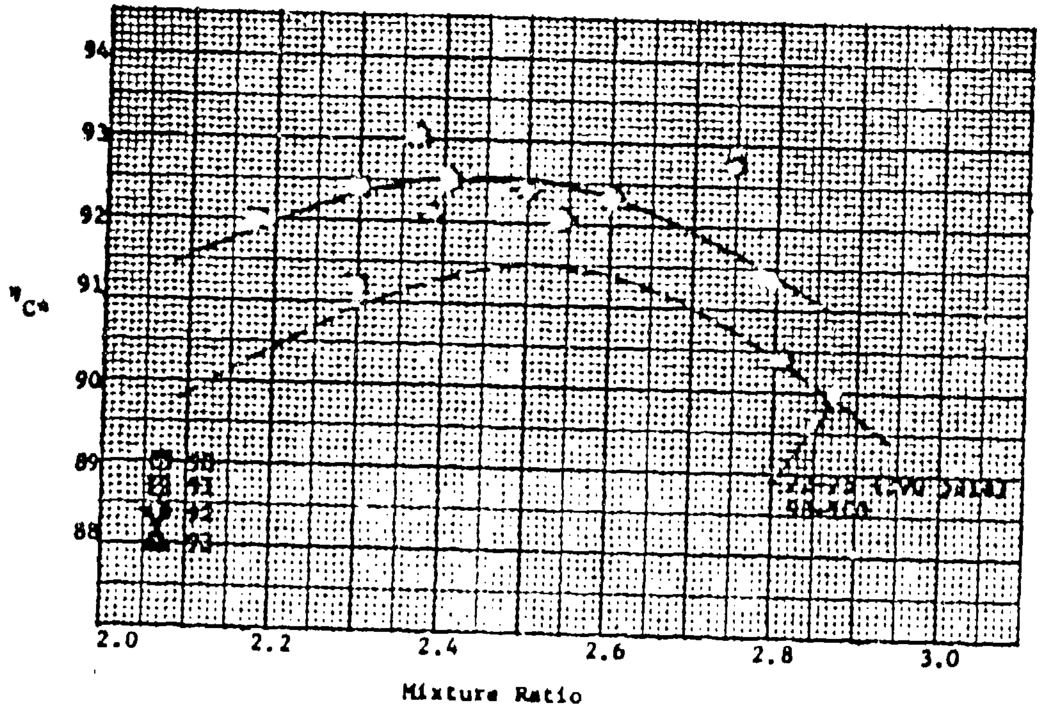

(C) Figure 3-81, Combustion Efficiency, Test Firings 90-93 (U)

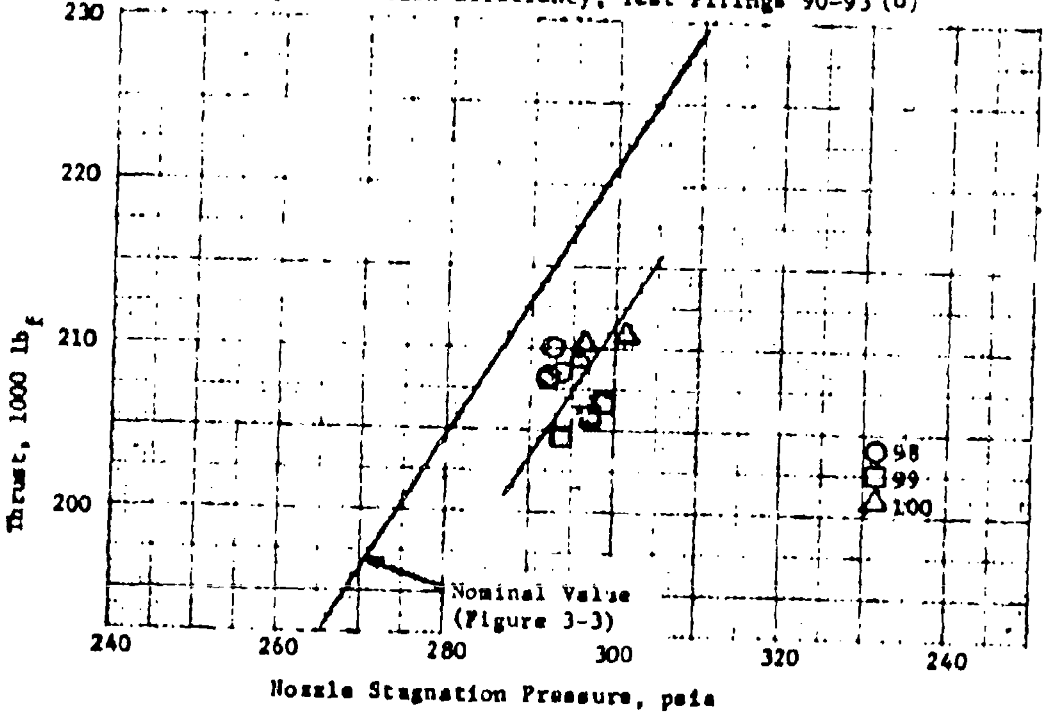

(C) Figure 3-82, Measured Thrust, Test Firings 98-100 (U)

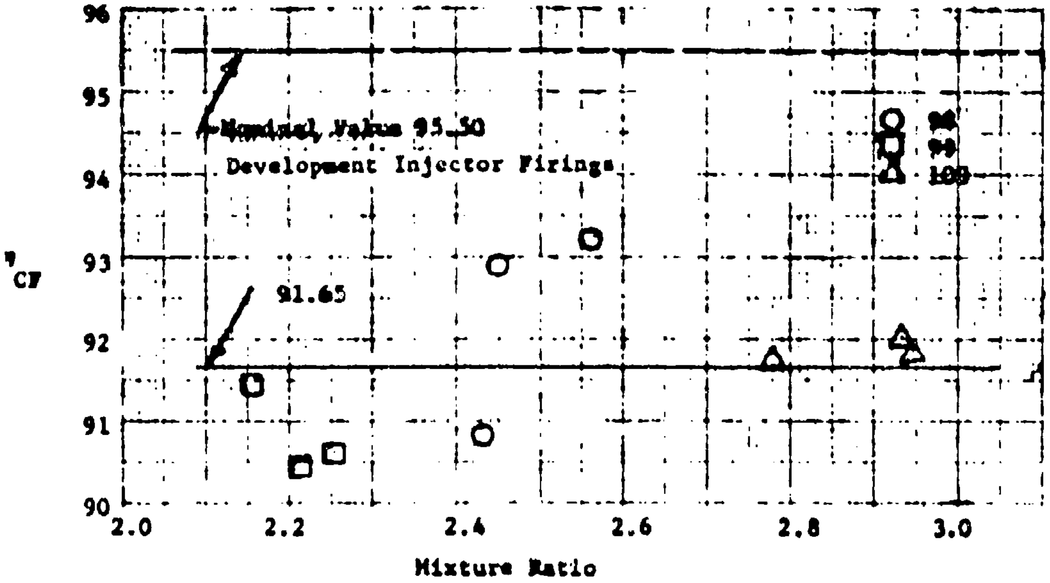

(C) Figure 3-83. Nozzle Efficiency, Test Firings 98-100 (U)

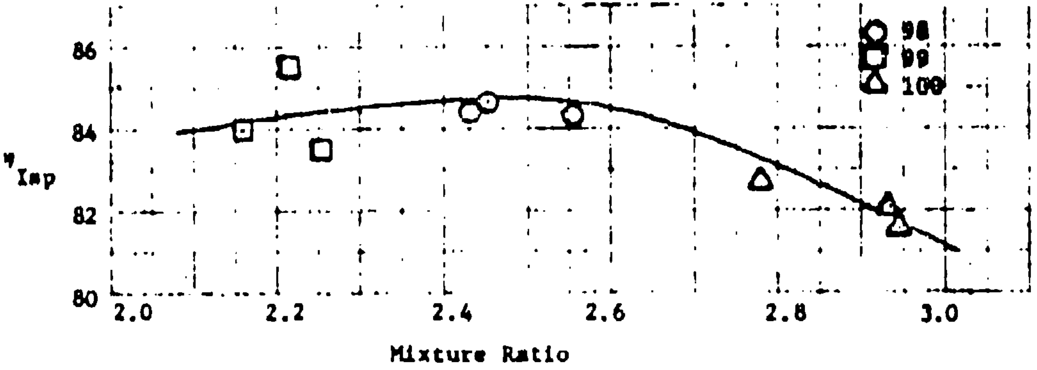

(C) Figure 3-84. Specific Impulse Efficiency Test Firings 98-100 (U)

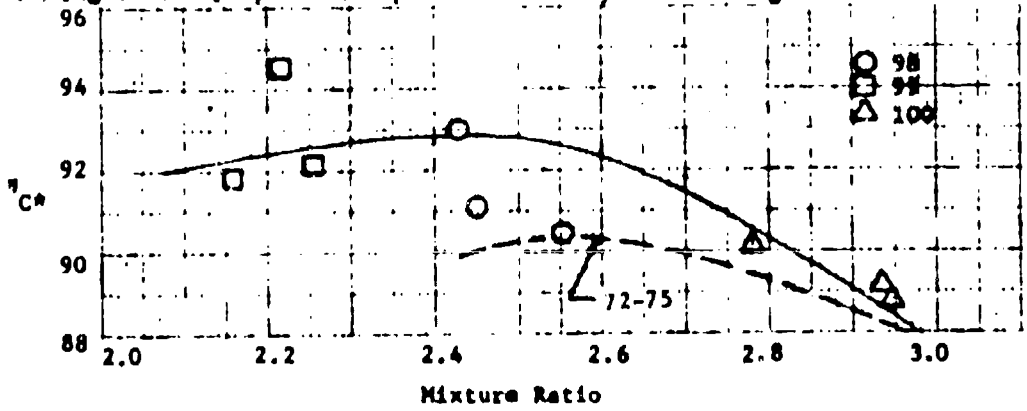

(C) Figure 3-85. Combustion Efficiency, Test Firings 98-100 (U)

(U) injector (shown as the dashed line), although the data from test firings 72-75 are so widely scattered that the comparison is somewhat clouded. The combustion efficiency of the S/N 002 injector essentially matches the performance obtained with the 01B/F2 injector configuration in firings 37-39, 43, and 46 (See Figure 3-45).

3.4.3.4.2 Injector Characteristics

(U) The fuel injector conductance, KIJCF, for test firings 98-100 is shown in Figure 3-86 as a function of the volumetric flow rate. The PIF-1 measurement (fuel inlet) listing in the General Performance Data was actually located on the PIF-2 port. The average KIJCF of 5.85 is approximately 4 percent greater than the KIJCF computed from the data on firings 72-77, and 90-93. The KLJCF measured averaged 3.47 which is in good agreement with the data taken during firings 72-77 and 90-93. Figure 3-87 shows the KLJCF for this test series. The oxidizer injector conductance, KIJCO for test firings 98-100 is shown in Figure 3-88. These measurements show general agreement with the data generated with the S/N 001 injector.

3.4.4 Injector Hydraulic Tests

(U) The three basic injector configurations used in the Task 1 test program were hydro-tested at the TRW Systems Capistrano Test Site following completion of the hot-firing tests. The three injectors water flowed included the X403666-1 (facility checkout injector), the X403829-16 (01B/F2) development injector, and the X404056-1 (S/N 002) demonstration injector.

3.4.4.1 Facility Checkout Injector

(U) Water-flow of the facility checkout injector was conducted at 100 percent of rated flow on the fuel side of the injector and 100, 90, 70 and 50 percent of rated flow on the oxidizer side of the injector. The experimentally determined discharge coefficients for these tests are essentially in agreement with those determined in August 1968 prior to shipment of the injector to the AFRPL (See Appendix A). The fuel side discharge coefficient at 100 percent of rated flow was 0.980 while the discharge coefficient on the oxidizer side of the injector was 0.725 which was in agreement with that measured earlier. The spray pattern produced by the oxidizer orifice appeared to be similar to that observed previously.

3.4.4.2 Development Injector

(U) Water-flow of the development injector assembly (01B/F2) was conducted at 100 percent of rated flow on the fuel side of the injector and at 100, 90, 70 and 50 percent of rated flow on the oxidizer side of the injector. The measured discharge coefficient on the fuel side was 0.875 which is in agreement with that observed during test firings 30-46. Water-flow of the oxidizer side of the development injector assembly disclosed a slight leakage between the threads of the orifice ring and the injector centerbody. Figure 3-89 is a photograph of the water-flow of the oxidizer orifice ring at 100 percent of rated flow. The injector pressure loss data for this water-flow test series is shown in Figure 3-90 as a function of the volumetric flow rate. The calculated discharge coefficient, C_{do}, for the water-flow was only slightly greater than that measured during test series 5.

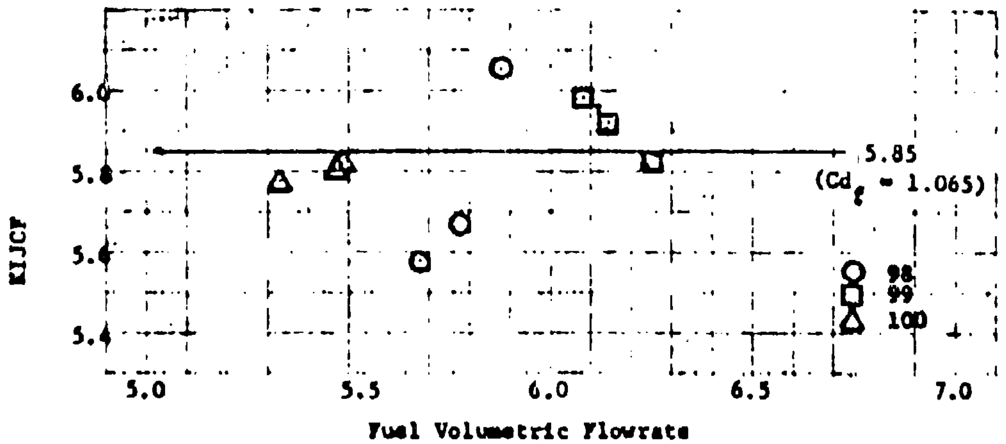

(U) Figure 3-86, Fuel Injector Conductance, Test Firings 98-100 (U)

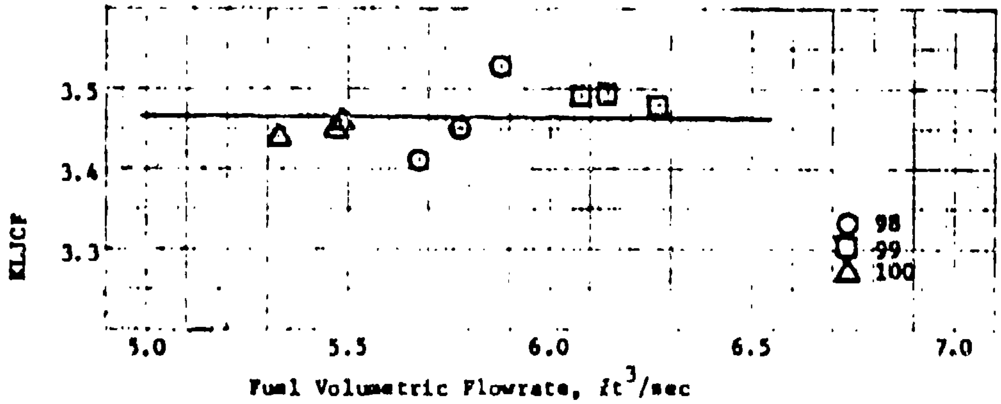

(U) Figure 3-87, Fuel Line Conductance, Test Firings 98-100 (U)

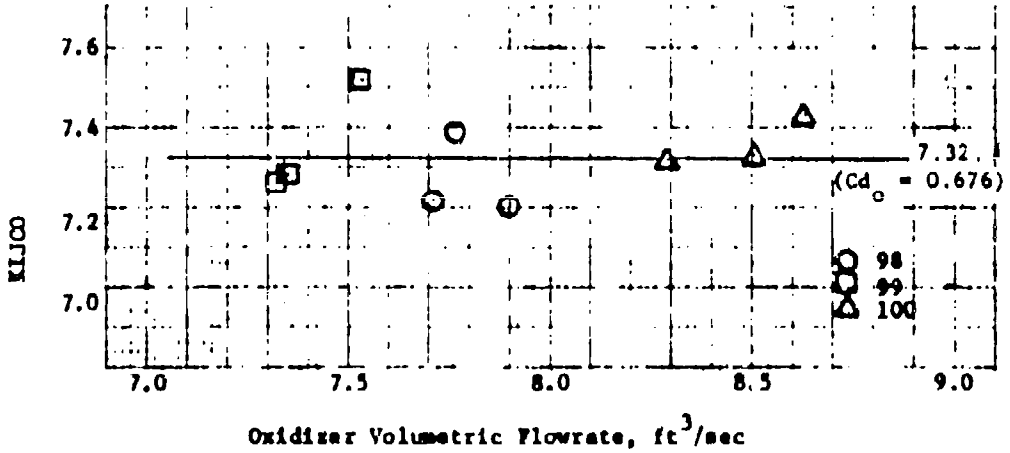

(U) Figure 3-88, Oxidizer Injector Conductance, Test Firings 98-100 (U)

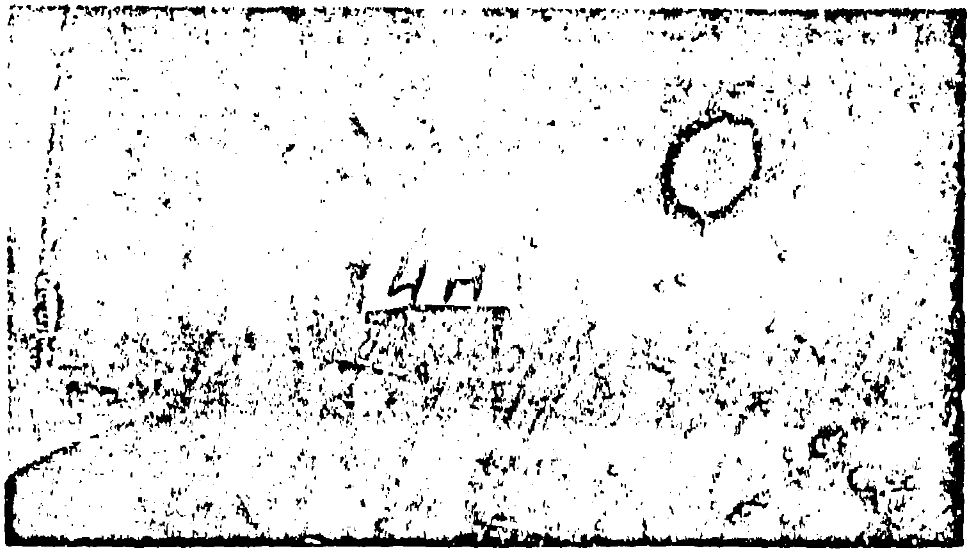

(U) Figure 3-89. Water Flow of Oxidizer Ring 01B @ 100% (U)

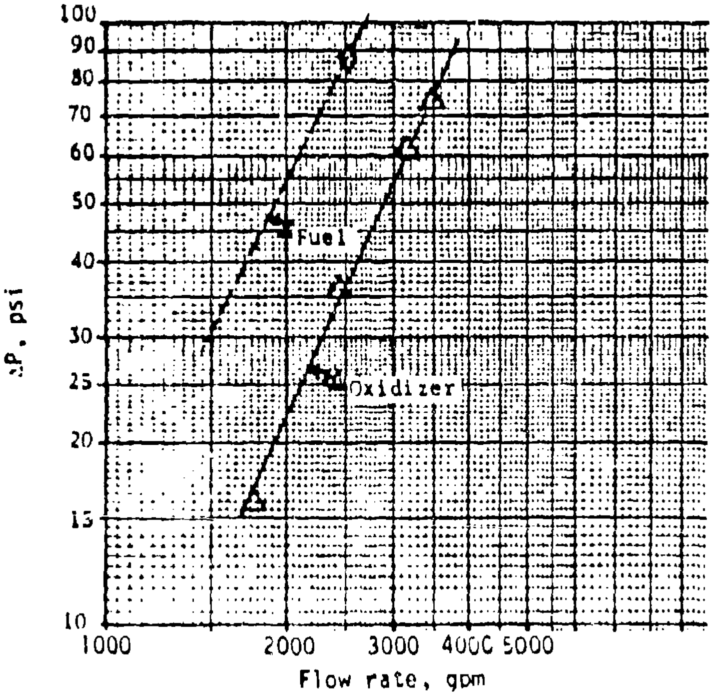

(U) Figure 3-90. Injection Pressure Loss, 01B/F2 (U)

The oxidizer leakage between the threads is assessed to be the probable cause of the low performance measured during test series 8 (101-102).

3.4.4.3 Demonstration Injector

(U) Water-flow of the S/N 002 demonstration injector was conducted at 100 and 22 percent of rated flow on the fuel side and at 100, 90, 70 and 50 percent of rated flow on the oxidizer side of the injector. Figure 3-91 shows the flow through the oxidizer orifices at 100 percent of rated flow. The individual streams appear to be somewhat broader across the top of the keyhole than the 01B injector configuration (See Figure 3-90). The fuel side coefficient was calculated to be 0.925 as compared to a value greater than 1.05 computed for the fuel side during firings 98-100. The oxidizer orifice discharge coefficient was nearly identical to that measured during firings 98-100. Figure 3-92 shows the injector pressure loss data as a function of the volumetric flow rate.

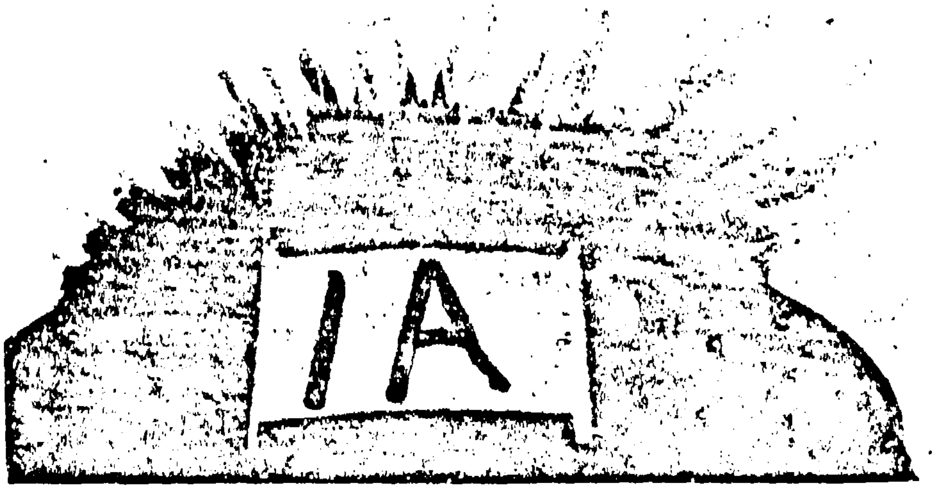

(U) Figure 3-91. Water Flow of Demonstration Injector S/N 002 @ 100% (U)

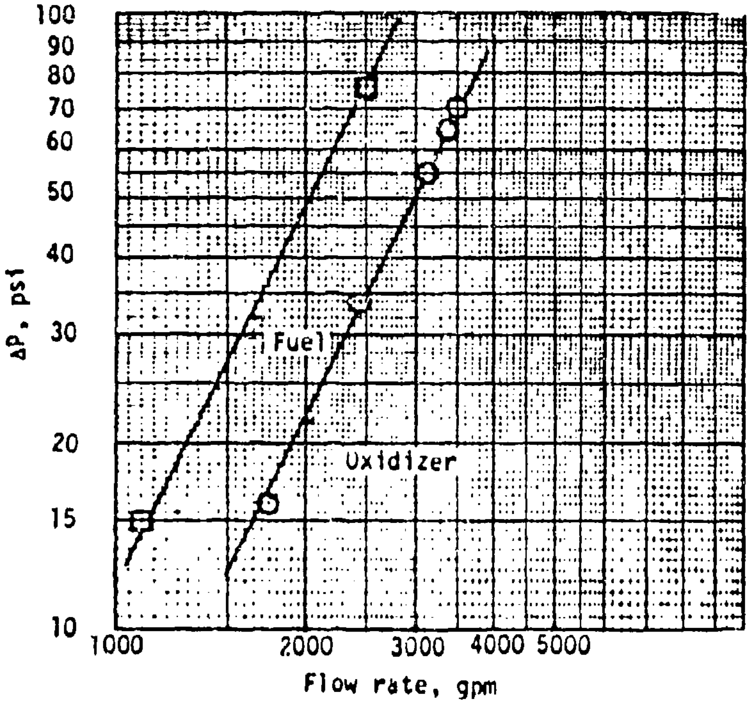

(U) Figure 3-92. Injection Pressure Loss, S/N 002 Demonstration Injector (U)

(U) Based on the hydraulic tests of the S/N 002 demonstration injector and subsequent long duration firing (See Volume II) it would appear that the high fuel injector conductance (KIJCF) and oxidizer injector conductance (KIJCO) and the low C_f efficiency is due, at least in part, to an erroneously high chamber pressure measurement.

4. SCALING

4.1 GENERAL

(U) The MCD Launch Vehicle concept is predicated on the ability to scale the engine designs over an approximate 100/1 thrust range, or from 50,000 lbf thrust to 5000K lbf thrust. Both the performance and combustion stability of the engine design must show the feasibility of being scaled over this thrust range. The TRW Systems approach to the scalable engine design is to maintain hydraulic similarity of the coaxial injector and geometric similarity of the combustion chamber using the scaling model which has been developed. Point designs of several size engines have been completed and various fabrication and performance parameters have been correlated with existing information and data.

4.2 SCALING VERIFICATION

4.2.1 Momentum Correlation

(U) The momentum correlating parameters, as modified after Reibling's correlation, indicates the maximum mixing efficiency for the range of the variable investigated. Insufficient data was taken to accurately predict peak values. Correlation of this parameter for various injector configurations (36 element versus 48 element, and for various percentage blockage) has been attempted but has not been completely successful. Mixing, or atomization, appears to be strongly dependent on not only the momentum ratio but also on the absolute injection pressure level as evidenced by the lowered performance when the flow rates were throttled back to give chamber pressures of 200 psia.

4.2.1.1 Effect of Number of Orifices

(C) Both 36 and 48 element oxidizer orifice rings were evaluated during the injector development task. The performance of the two configurations are within 1 percent of each other in the 60-inch long heat sink chamber (Figures 3-41 and 3-51). The 36 element oxidizer orifice ring had a 60 percent blockage to fuel while the 48 element oxidizer orifice ring had a 67 percent blockage to fuel. This factor probably has a greater effect on performance than the number of orifices (Section 4.2.1.3).

4.2.1.2 Location of Secondary Orifices

(U) The location of the secondary orifices does not appear to be a significant injector parameter, at least for the changes investigated in this program. Both the 01A and 01B oxidizer orifice rings performed identical and the only change between the two configurations was in the location of the secondary orifice. The 05 oxidizer orifice ring had a major relocation of the secondary orifice but also had a flow straightener ring added which precludes any evaluation of the effect of the location of the secondary orifice.

4.2.1.3 Spacing

(C) One of the more important injector parameters is the spacing between elements or blockage to fuel flow. Elements with blockage percentages of 50 percent to 67 percent were evaluated. For the orifice configurations employed in this program, the optimum percent blockage appears to be about 60 percent. Only two tests were run with the 03 oxidizer orifice ring (Test Series 6) and the performance of this configuration is inconclusive.

4.2.1.4 Shape

(U) The orifice shapes for all development injector configurations evaluated were essentially the same (keyhole), and had the same ring wall thickness. The facility checkout injector had an orifice wall thickness about 50 percent that of the development injector configurations and the injection spray pattern was obviously different. This aspect of the injector design requires further study.

4.2.2 Throttling

(C) Test data was taken for several configurations over the pressure range of 200 psia to 300 psia. For fixed area injectors this results in an injection ΔP decrease of roughly 50 percent (correcting for increased flow rate due to loss in performance). The best estimate of this performance loss is nearly 5 percent for a decrease in injection pressure by 50 percent.

(U) The mass median drop radius (see Section 2.1.3.2) would be expected to increase by 30 percent for this decrease in injection pressure. The one-dimensional vaporization rate-limited combustion efficiency analysis indicates that the expected loss in performance would be 5.5 percent for a decrease in chamber pressure from 300 psia to 200 psia. Thus, the injector ΔP can be seen to be a very important parameter in determining the engine performance.

4.2.3 Effect of Chamber Length

(C) The chamber length is probably the most important element in the determination of engine performance. The test data indicates that the overall process occurring in the combustion chamber is vaporization rate limited. The correlation of chamber length as a function of chamber diameter originally proposed and given by Equation 4-1

$$L_e = 1.45\, D_c \qquad \text{where} \qquad (4\text{-}1)$$

L_e = length between impingement plane and throat plane

appears valid for engines up to 250,000 lbf thrust.

(C) The use of a one-dimensional vaporization rate-limited combustion efficiency analysis (Section 2.1.3.2) indicates the use of the original length correlating parameter predicts a combustion efficiency for the 3000K lbf thrust engine that is 4 percent greater than that of the 250,000 lbf thrust engine. This suggests that the L_c/D_c parameter should vary with thrust level especially for thrust levels greater than 250,000 lbf thrust.

4.3 DESIGN AND FABRICATION

4.3.1 General

(C) Three point designs, Figures 4-1, 4-2, and 4-3 were configured. These designs are based on achieving a specific impulse efficiency of 90 percent (based on theoretical shifting equilibrium values) with the N_2O_4/UDMH propellant combination at a chamber pressure of 300 psia. A nominal mixture ratio (O/F) of 2.60 was selected. The chamber length was determined from the relation, $L_c/D_c = 1.63$. The ablative liners were sized for test durations of 120, 260 and [illegible] seconds for the stage one, stage two, stage three engines, respectively.

(.) Figure 4-4 shows approximate dimensions for combustion chambers in the 50,000 lbf to 5000K lbf thrust range as a function of thrust level. The various diameters and lengths (except for chamber length) are geometric scalings of the dimensions of the 250,000 lbf thrust (vacuum) demonstration hardware tested in this program. The chamber length is based upon results of a vaporization rate-limited analysis as discussed previously. The nozzle length is for a 15-degree half angle expansion cone.

(C) The fuel and oxidizer orifices are determined from the required injection velocities (ΔP's), spacing, pintle diameter as shown in the following example.

$$F = 3000\text{K at sea level, } \epsilon = 4/1,\ O/F = 2.6$$

$$W_t = \frac{3000\text{K}}{225\ (90\%)} = 13{,}300\ \text{lb}_m/\text{sec}$$

$$D_p = 0.4\sqrt{13{,}300} = \underline{46.2}\ \text{in.}$$

The fuel injection area may now be computed.

$$A_f = \frac{13{,}300}{(1 + O/F)\ 49.5\ V_f}$$

$$V_f = 96.30\ Cd_f\sqrt{60/49.5} \quad \text{for } \Delta P_{if} = 60\ \text{psi}$$

$$V_f = \underline{106}\ \text{ft/sec for } Cd_f = 1.0$$

$$A_f = \frac{13{,}300}{(3.6)\ 49.5\ (106)} = 0.705\ \text{ft}^2 \text{ or } 101.5\ \text{sq. in.}$$

$$A_f = \pi/4\left[D_{fm}^2 - D_p^2\right]$$

$$101.5 = \pi/4\left[D_{fm}^2 - 46.2^2\right]$$

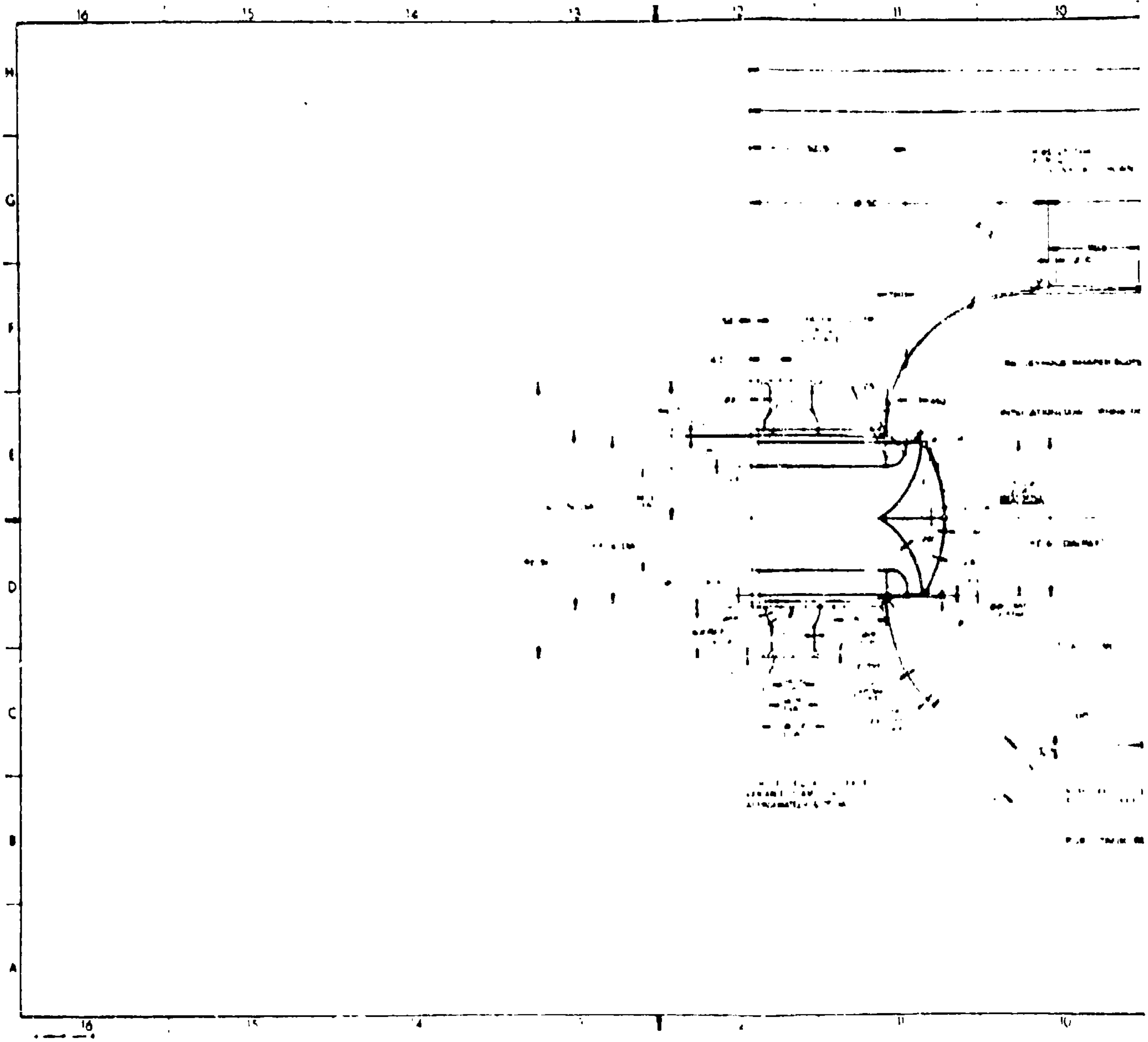
16
15
14
13
12
11
10
H
G
F
E
D
C
B
A

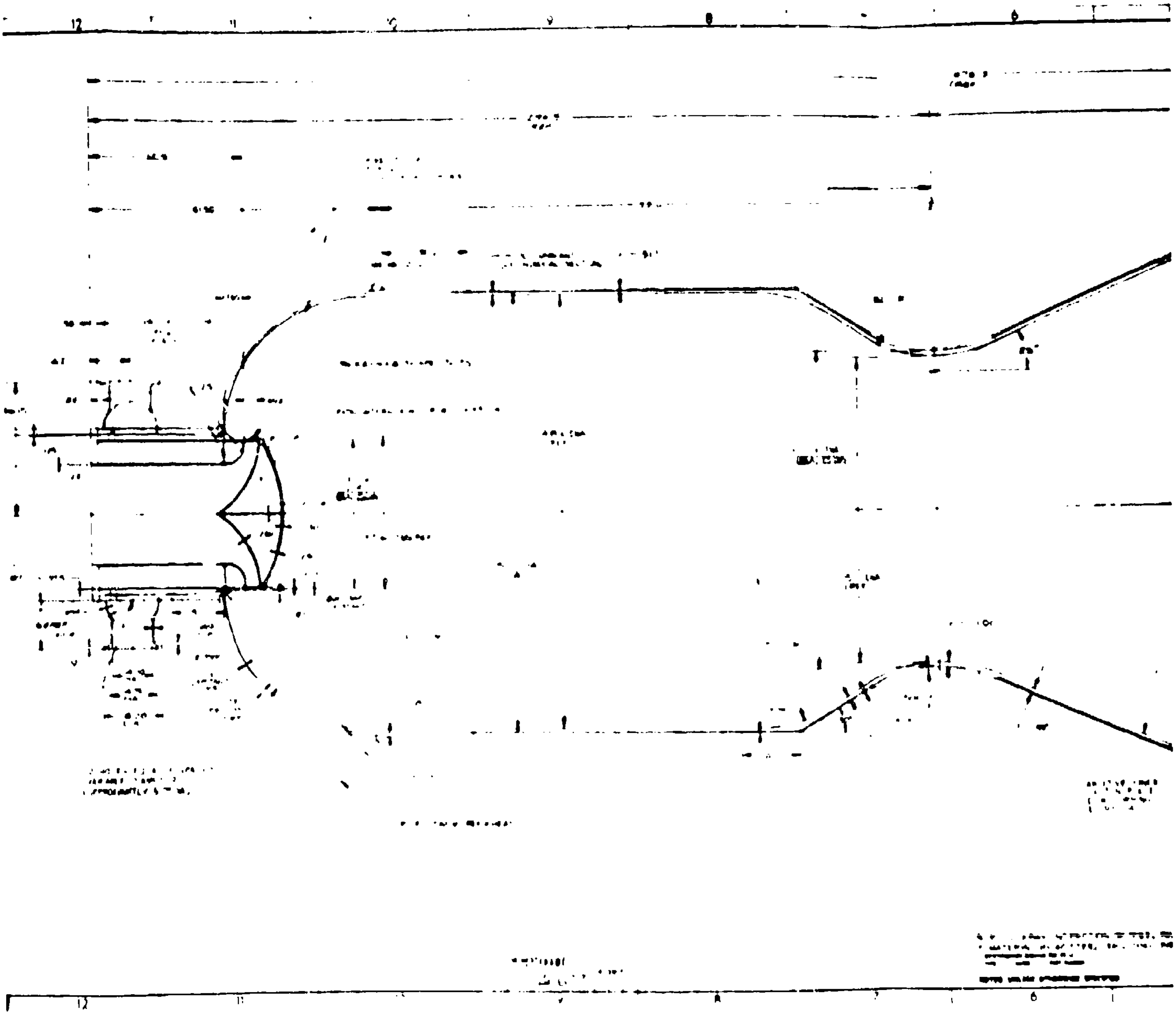

2

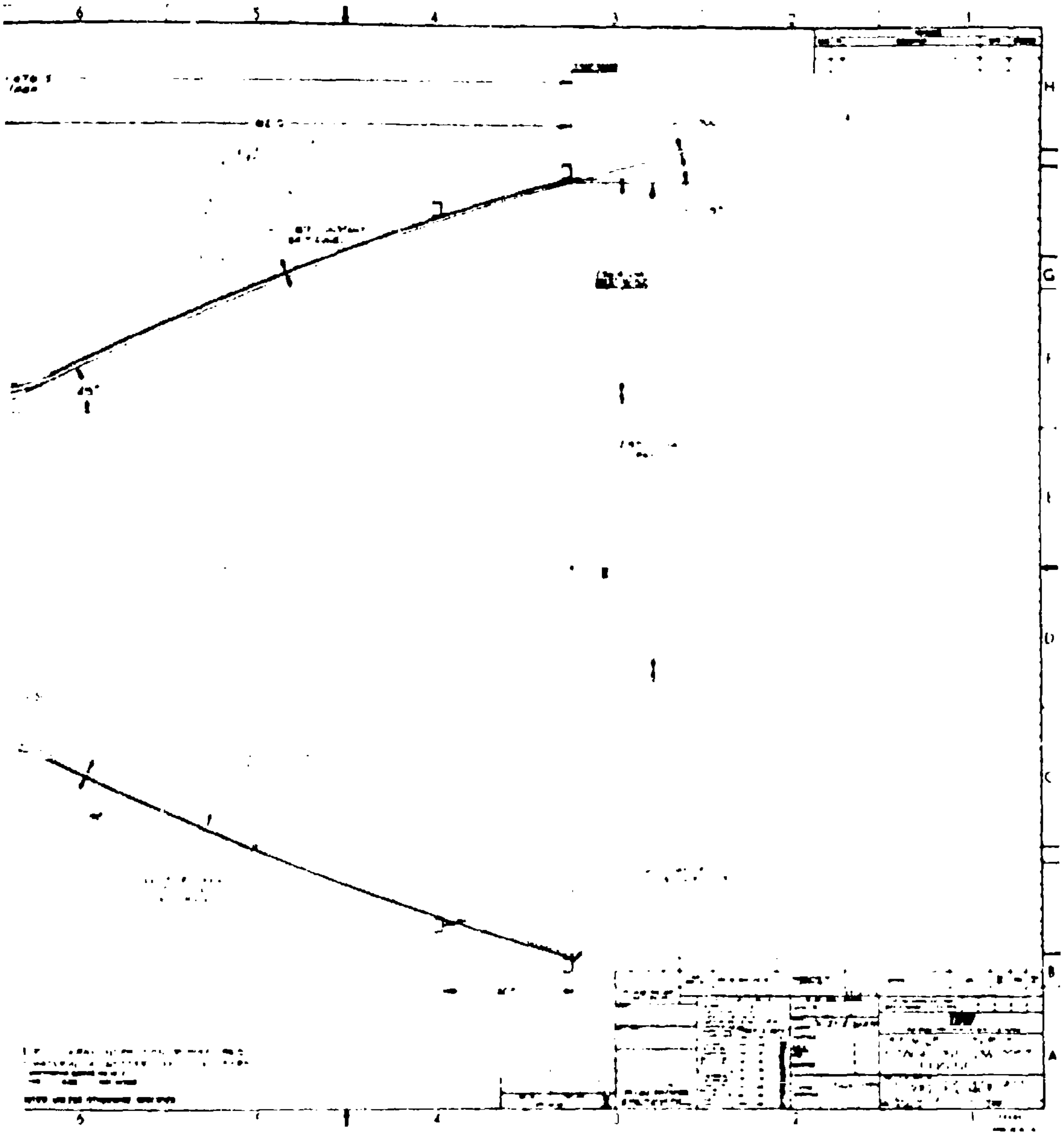
H
G
F
E
D
C
B
A
6
5
4
3
2
1

(C) Figure 4-1. Preliminary Design, 3500K lb_f Thrust (Sea Level) Engine (U)

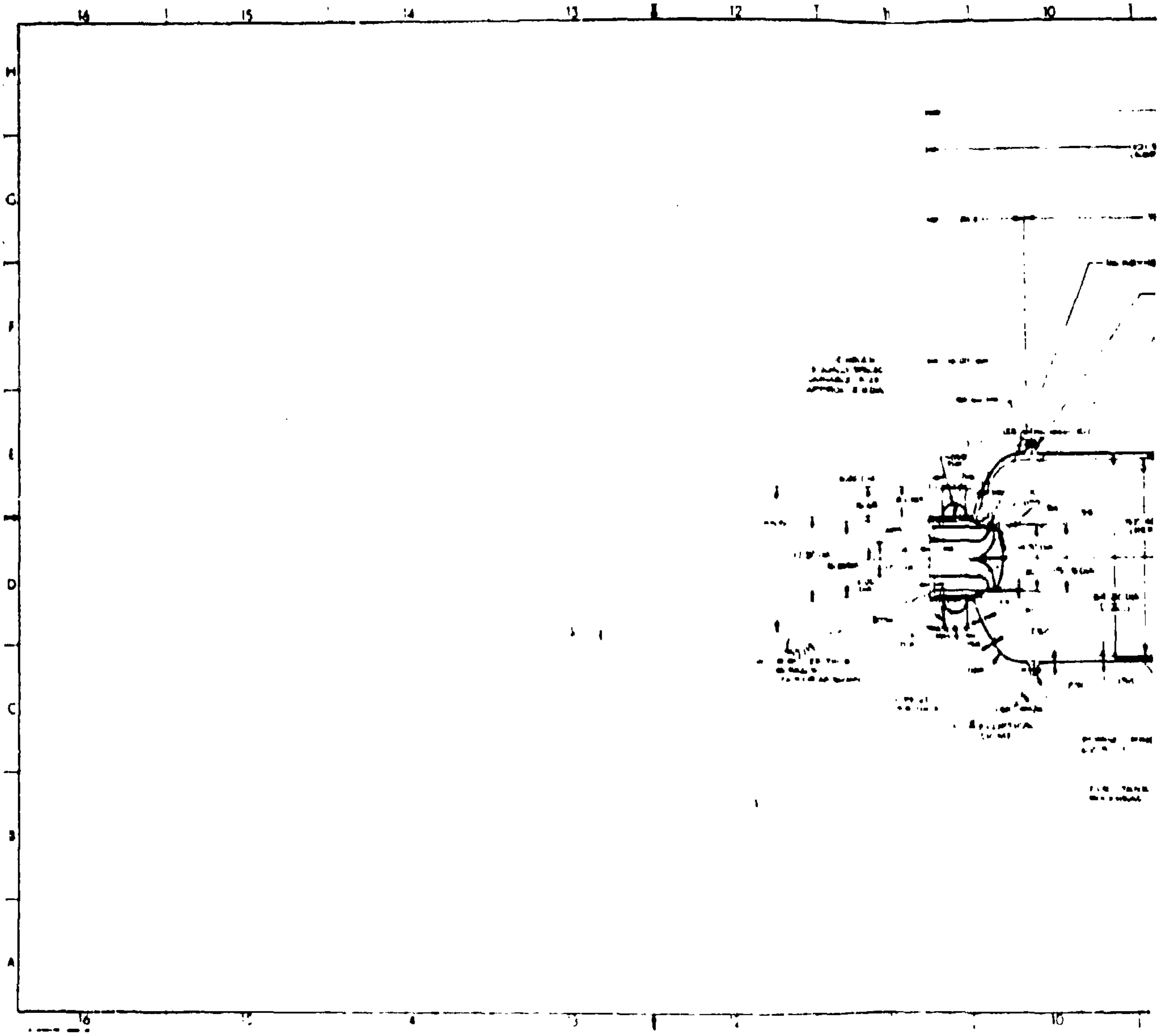
16
15
14
13
12
10
H
G
F
E
D
C
B
A

7

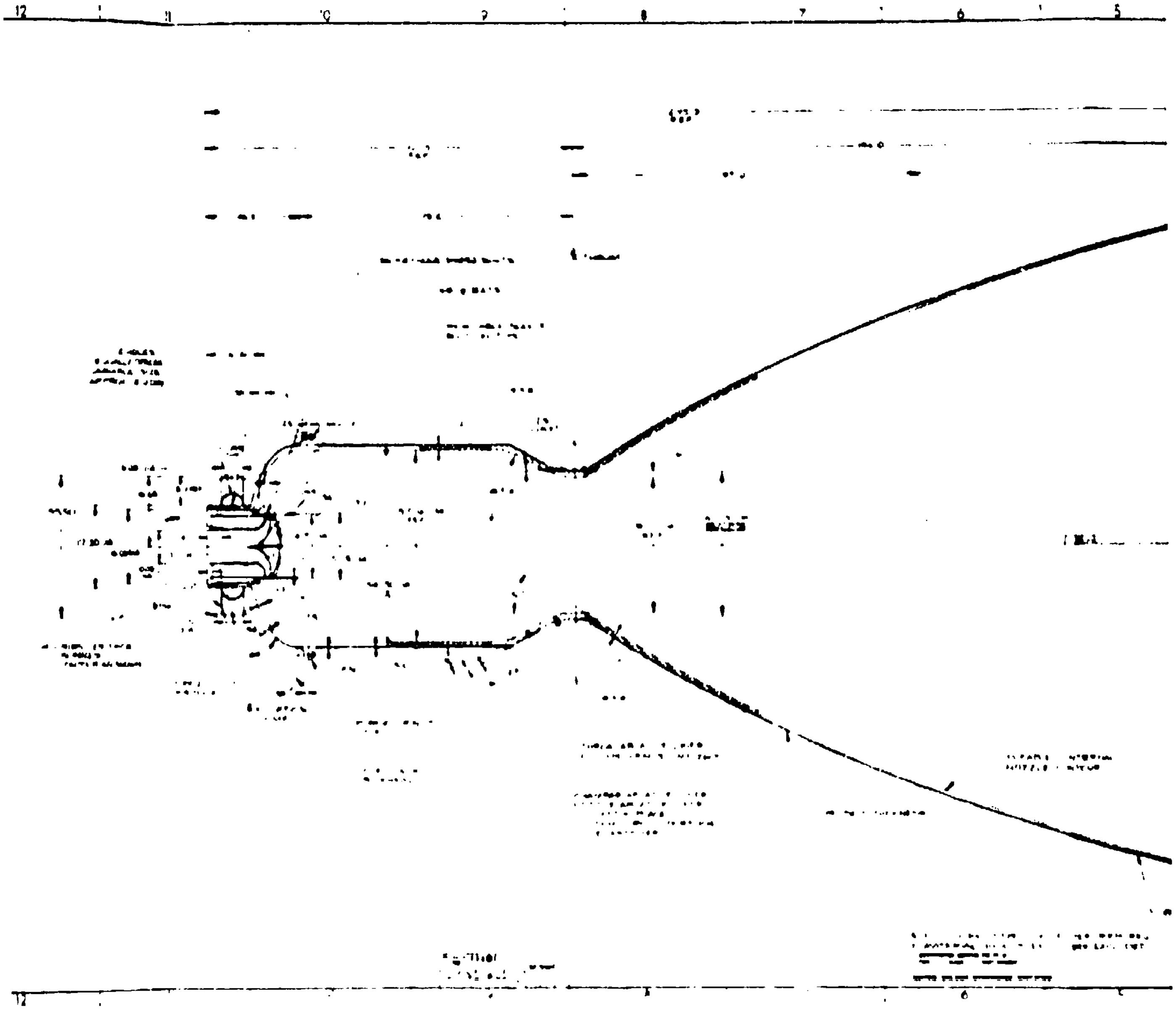
12
11
10
9
8
7
6
5

2

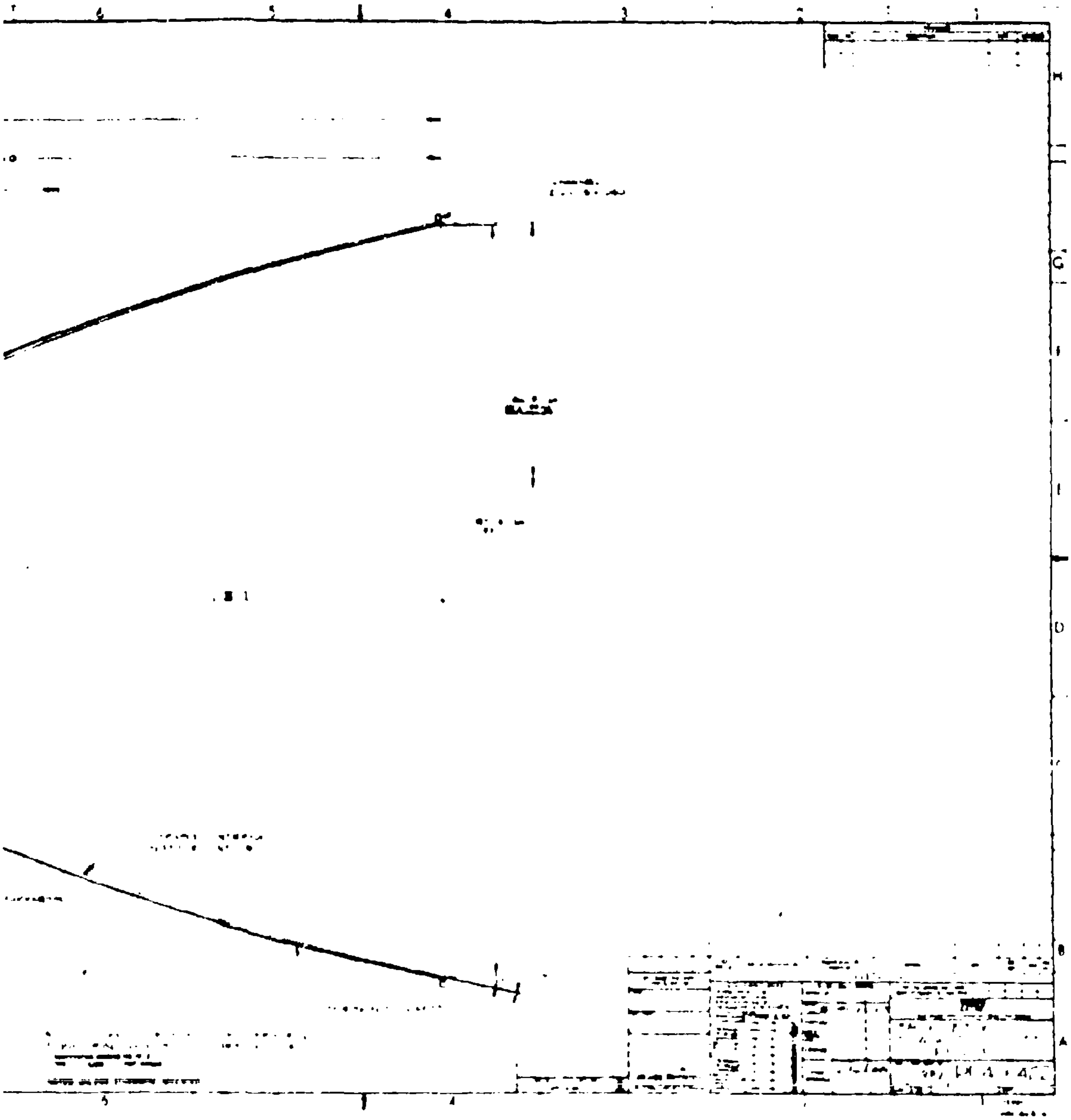

(C) Figure 4-2. Preliminary Design, 387K lb$_f$ Thrust (Vacuum) Engine (U)

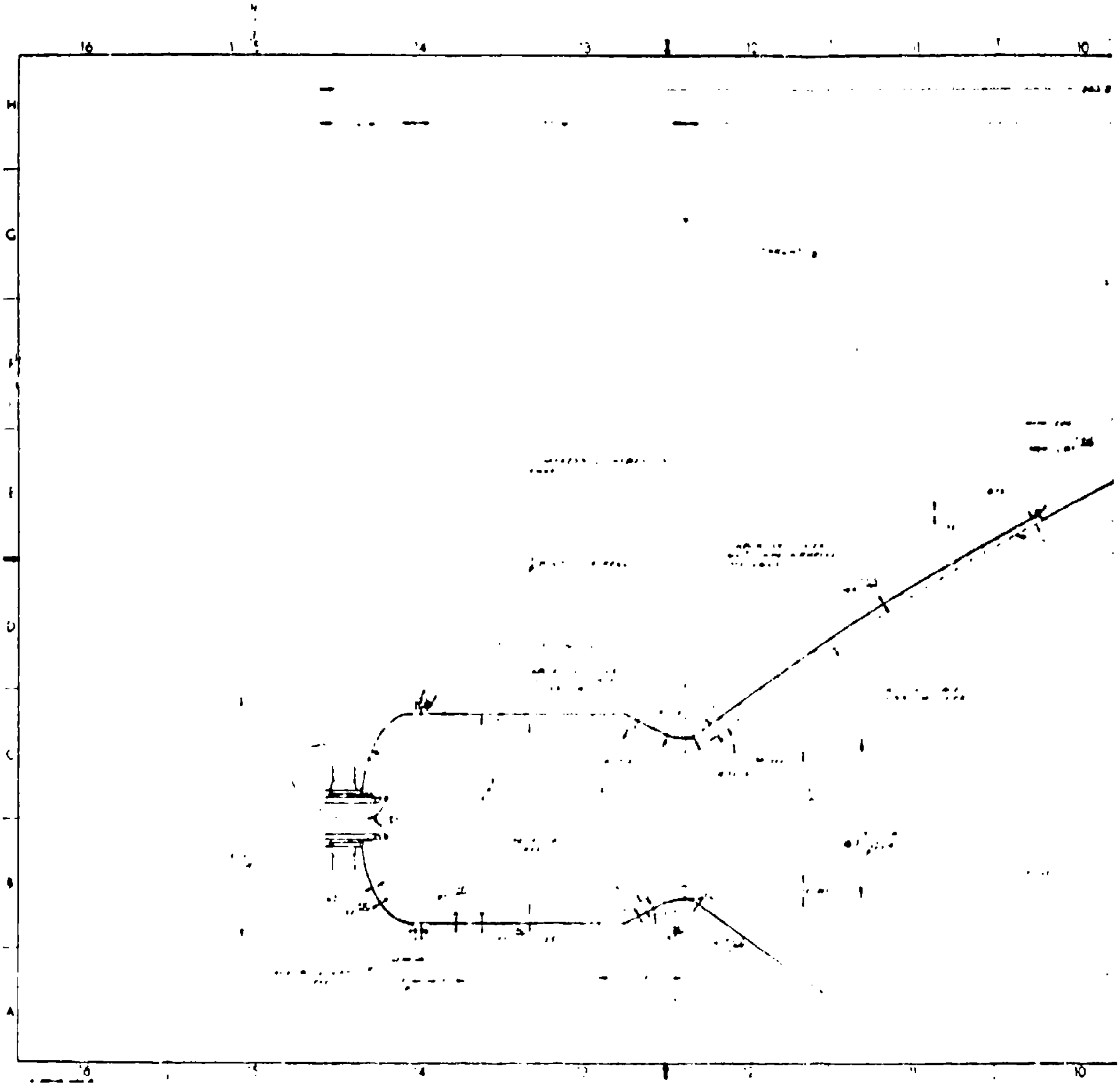
16
14
13
12
10
H
G
F
E
D
C
B
A

(C) Figure 4-3. Preliminary Design, 57.8K lb_f Thrust (Vacuum) Engine (")

-RB-00

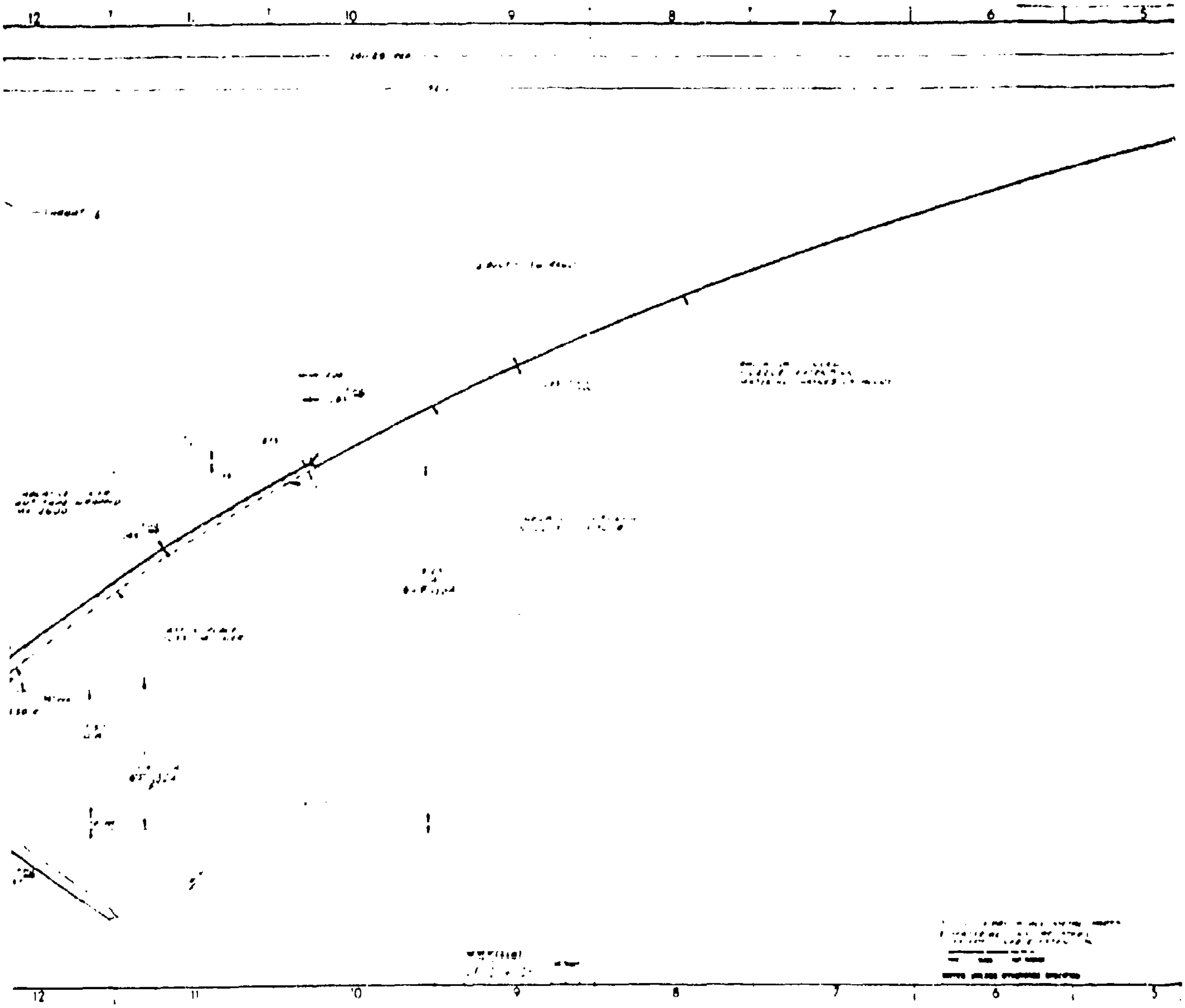

12
11
10
9
8
7
6
5

Design,
hrust
gine (U)

2

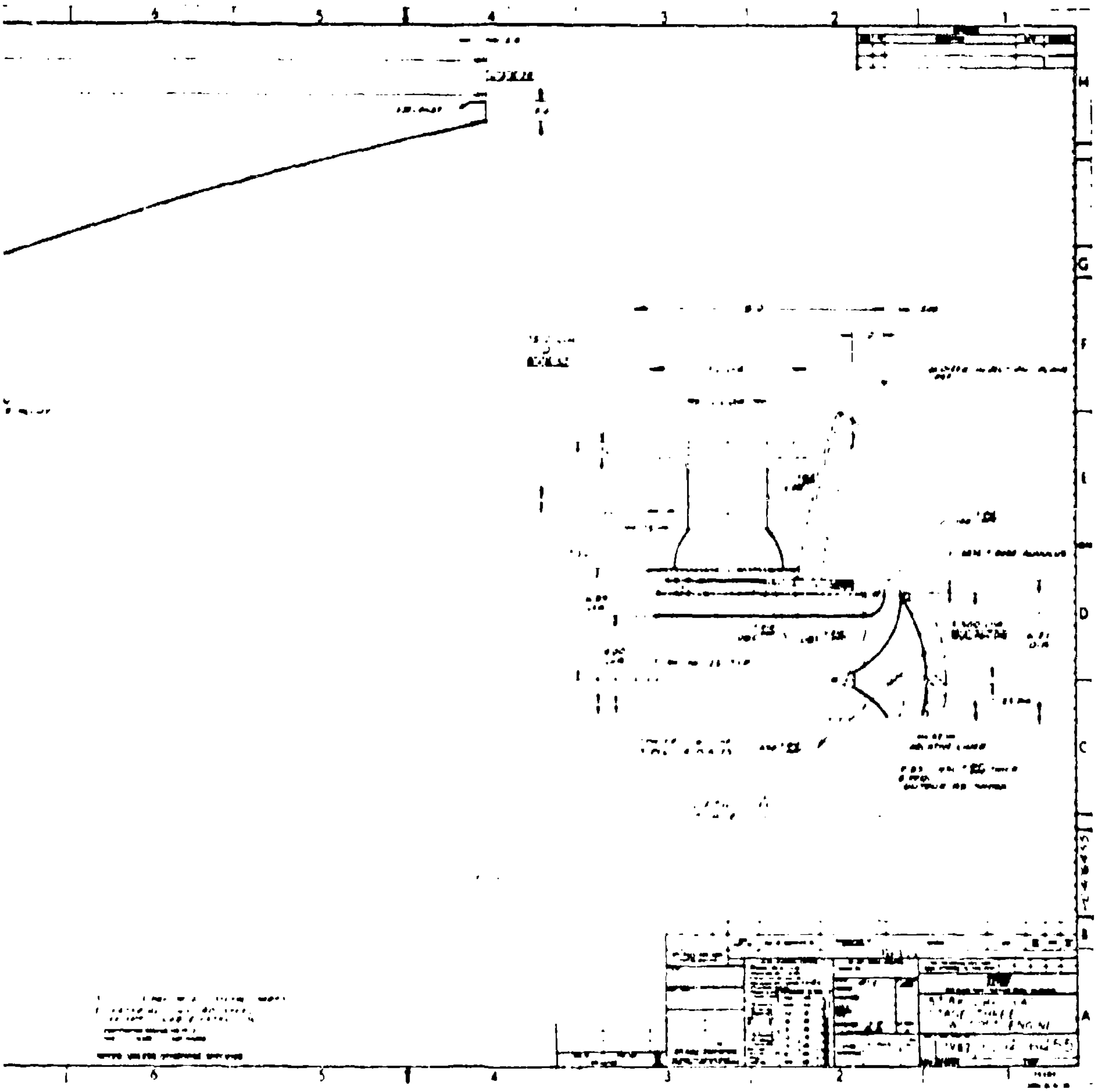
H
G
F
E
D
C
B
A
6
5
4
3
2
1

3

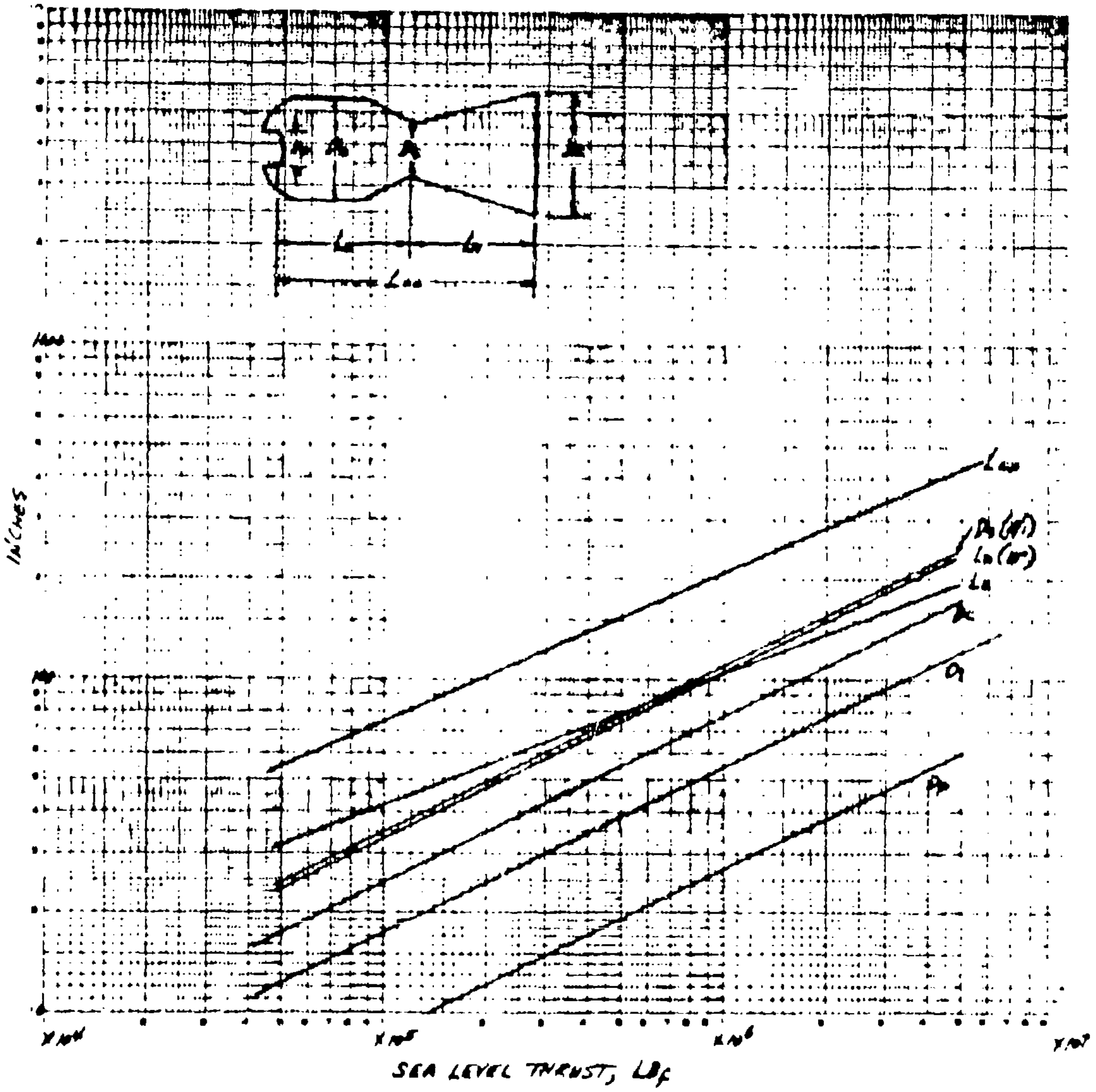

(C) Figure 4-4. Approximate Thrust Chamber Dimensions (U)

(C) $129.5 + 2130 = D_{fm}^{2}$

$$D_{fm} = \underline{47.6} \text{ in. or}$$

$$T_{fsh} = \frac{47.6 - 46.2}{2} = 0.7 \text{ in.}$$

The total oxidizer injection area is computed in the same manner assuming a ΔP_{io} of 120 psi and a C_{do} of 0.70.

$$V_o = 96.30 \times 0.7 \sqrt{120/91}$$

$$V_o = 77.8 \text{ ft/sec}$$

$$A_o = \frac{13,300}{(91)} \frac{1 - \frac{1}{1 + O/F}}{(77.8)} = 1.36 \text{ ft}^2 \text{ or } 196 \text{ sq. in.}$$

The primary oxidizer orifice area is selected as 90 percent of the total or 176.5 square inches

Assume that $L_p/W_{avg} = 2.0$

$$A_o = L_p W_{avg} = 2.0\, W_{avg}^{2}$$

$$\left(\frac{176.5}{36}\right)^{1/2} = 1.41\, W_{avg}$$

$$2.2/1.41 = W_{avg} = 1.56 \text{ in.}$$

$$L_p = 3.12 \text{ in.}$$

$$UW = \frac{\pi D_p}{36}$$

$$UW = \frac{\pi\, 46.2}{36} = 4.04 \text{ in.}$$

$$(W_p + W_s)/UW \cong 0.60$$

$$\therefore \quad W_p + W_s \cong 2.42$$

$$W_s = 0.36$$

$$\therefore \quad W_p = 2.06$$

(C) The primary oxidizer orifice is keyhole in shape with an area of 4.90 square inches. The W_p is 2.06 inches with an L_p of 3.12 inches. The W'_p is approximately 1.50 inches wide. The secondary oxidizer orifice is approximately 0.36 inches wide by 1.50 inches long.

4.3.2 Fabrication

4.3.2.1 Pressure Shells/Injectors

(U) The designs of large combustion chambers were submitted to various commercial fabricators to determine the feasibility of fabricating the large structures. It is concluded that the designs shown are practicable for a number of materials, including HY-140 and United States Steel T-1 steel alloy, using current commercial fabrication techniques. Sizes up to 3000K lbf thrust do not require any long material procurement lead times for special gage steel sheets nor does the handling or transportation of this engine size create any special problems.

4.3.2.2 Ablative Liners

(U) A number of ablative liner fabrication and installation methods have been studied for the various thrust size engines. For the 3000K lbf thrust engine size there are several methods which are feasible. The materials which appear applicable are the silica-phenolics (broadgoods, tape, molding compound, or castables), filled silicone-rubbers and in some applications, asbestos-phenolics. The fabrication methods applicable for each of the material classes are discussed in the following sections.

4.3.2.2.1 Silica-Phenolic Materials

(U) The silica-phenolic materials appear to be the only material acceptable as a throat insert for first stage engines (approximately 140 seconds burn time) smaller than 250,000 lbf thrust. These throat inserts could be tape-wrapped on a male mandrel, either autoclaved or hydroclaved cured, machined, and secondarily bonded into the pressure shell. The only limitation on throat insert size is the availability of wrapping and curing facilities. Presently, components for the 3000K engine size appear feasible.

(U) The broadgoods form of silica-phenolic materials appear advantageous in areas where the broadgoods can be installed using a hand lay-up technique, especially where the part can be cured insitu at low pressure.

4.3.2.2.2 Filled-Silicone Rubber

(U) The filled-silicone rubbers can be readily cast into the shell and bonded simultaneously or cast as segments and bonded into the shell after cure. The filled-silicone rubbers show promise as a throat insert, especially for first stage engine sizes larger than 250,000 lbf. The primary application of these materials will be in the exit cones where weight is very important and the contoured expansion section can be readily maintained.

(U) The silicone rubber bonds very well to both the pressure shell and other silicone rubber components. Neither the mixing or casting of large

(U) shells or segments appear to be insurmountable problems. Care must be taken to avoid entrapment of air during the casting process which is possible through the use of proper tooling.

4.3.2.2.3 Other Materials

(U) The castable silica-phenolic materials such as Ironsides Resin Co., Dp-5-161, can be fabricated into components in the same manner as the filled-silicone rubber. The ablative performance of this material is very good. However, the shrinkage and cracking problems associated with this material (see Volume II) must be resolved.

(U) Silica-phenolic materials are also available as molding compounds and as such could be molded into segments or "tiles" and bonded into place on site. Proper mold design and joint configuration would allow for net molding of the finished segments to provide a reliable joint in either the longitudinal or circumferential direction.

(U) Asbestos-phenolic materials, although showing relatively poor performance in this program may have future application because of their low-cost. Most asbestos-phenolic materials are available as molding compounds and could be fabricated in the same manner as the silica-phenolic molding compounds.

4.3.2.2.4 Adhesives

(U) A major concern in the secondary bonding of molded segments into the pressure shell is the choice of adhesive and out-of-roundness of the metal shell. With the use of relatively thin shells strain incompatibilities exist at the bond line and bond line thicknesses vary due to the out-of-roundness condition. It appears that use of secondary bonding technique will require special tooling and adhesive development.

4.4 COST AND WEIGHTS

(U) A weight and cost estimate has been made for each of the point design engine sizes and is given as Table 4-1. The major concern in the design of these engines is the material choice for the engine assuming that the engine size depends on whether it is a first, second, thrid or even fourth stage engine. The materials studied include USS T-1, HY-140 and a 200 grade maraging steel. The use of Haynes 25 as a radiation-cooled skirt was also investigated for the upper stage engine. The point design costs and weight are based on the use of HY-140 throughout, except for the radiation cooled nozzle extension (Haynes-25) in the 57,800 lbf thrust engine.

(U) It should be noted that the chamber length L_e, of the preliminary designs were all based on a L_e/D_c ratio of 1.63. As noted in Section 4.2.3, this value is greater than the original scaling length/diameter ratio which is also estimated to be too great for engine sizes larger than 250,000 lbf thrust.

(C) Table 4-1. Preliminary Cost and Weight Data for Three Point-Design Engine Sizes (U)

	Thrust Level, lb_f		
	3.5×10^6	387×10^3	57.8×10^3
Pressure, psia	300	200	125
Expansion Ratio, A_e/A_t	5	25	100
I_{sp}, lb_f-sec/lb_m	222 (s.l.)	295.5 (vac)	316 (vac)
Burn Time, seconds	118	260	355
Throat Diameter, inches	105	37.1	17.5
Chamber Length, inches	242	65.5	40.25
Contraction Ratio, A_c/A_t	2.0	2.0	2.0
Overall Length, inches	477	295.5	240.3
Weight$^{(1)}$, lbs	33,600	6,500	2,530
Cost$^{(2)}$, dollars	355,000	170,000	130,000
Cost/Weight, \$/lb_m	10.55	26.20	51.50
Cost/Thrust, \$/lb_f	0.10	0.44	2.25
Thrust/Weight, lb_f/lb_m	104	59.5	22.8

(1) Includes weight of injector, pressure shell, ablative, nozzle valves and engine mounts (does not include thrust vector control system).

(2) Cost includes material and fabrication costs, program management, QA, Reliability and all fixed costs (G&A, fee, etc.).

4.5 COMBUSTION PERFORMANCE

(C) The correlating data indicate mass median drop, radius, r_m of 207 microns for a proposed 3000K coaxial injector. The one-dimensional vaporization rate-limited combustion efficiency analysis of this droplet size in the 160-inch chamber ($L_c/D_c = 1.16$) indicate a combustion efficiency of 93 percent (89 percent I_{sp} efficiency) as shown in Figure 4-5. The vaporization rate-limited analysis does not consider increased vaporization due to secondary droplet breakup which would result in increased performance.

(C) The performance of the 3000K injector could be improved by (1) increased chamber length, (2) increased injection ΔP (100 psi was assumed for the baseline case, or (3) increased number of oxidizer injection orifices. Increasing the chamber length increases engine weight and cost (since the ablative cost is the largest single cost element of the engine). Increasing the injection ΔP's increases the stage weight and possibly the cost but appears to be more effective than increasing the chamber length.

(C) Increasing the injection ΔP for the oxidizer orifices to the 120 psi design injection ΔP decreased the mass median drop radius by the following relation.

$$r_m \sim \left(\frac{\dot{m}}{n}\right)^{1/4} \left(\frac{1}{\Delta P}\right)^{3/8} \quad \text{or} \qquad (4\text{-}1)$$

$$\frac{[r_{m\,2}]}{[r_{m\,1}]} \sim \left(\frac{\Delta P_1}{\Delta P_2}\right)^{3/8} \qquad \text{since the } (\dot{m}/n) \qquad (4\text{-}2)$$

remains constant. Thus, the r_m at a ΔP of 120 psi would be 93.4 percent of 207μ or 193μ which is equivalent to increasing the performance by one percent.

(C) Increasing the number of oxidizer orifices at the same time as increasing the injection ΔP from 100 psi to 120 psi (assuming mixing efficiency can be maintained) is also beneficial in increasing performance. The mass median drop radius is given by Equation 4- . This results in a ratio of $[r_m]_2/[r_m]_1$ for a 48 element oxidizer orifice as follows:

$$\frac{[r_m]_2}{[r_m]_1} = \left[\frac{n_1}{n_2}\right]^{1/4} \left[\frac{\Delta P_1}{\Delta P_2}\right]^{3/8} \qquad (4\text{-}3)$$

$$= [.931]\,[.934]$$

$$= 0.869$$

The r_m is therefore 180 microns and the predicted increase in performance is approximately two percent.

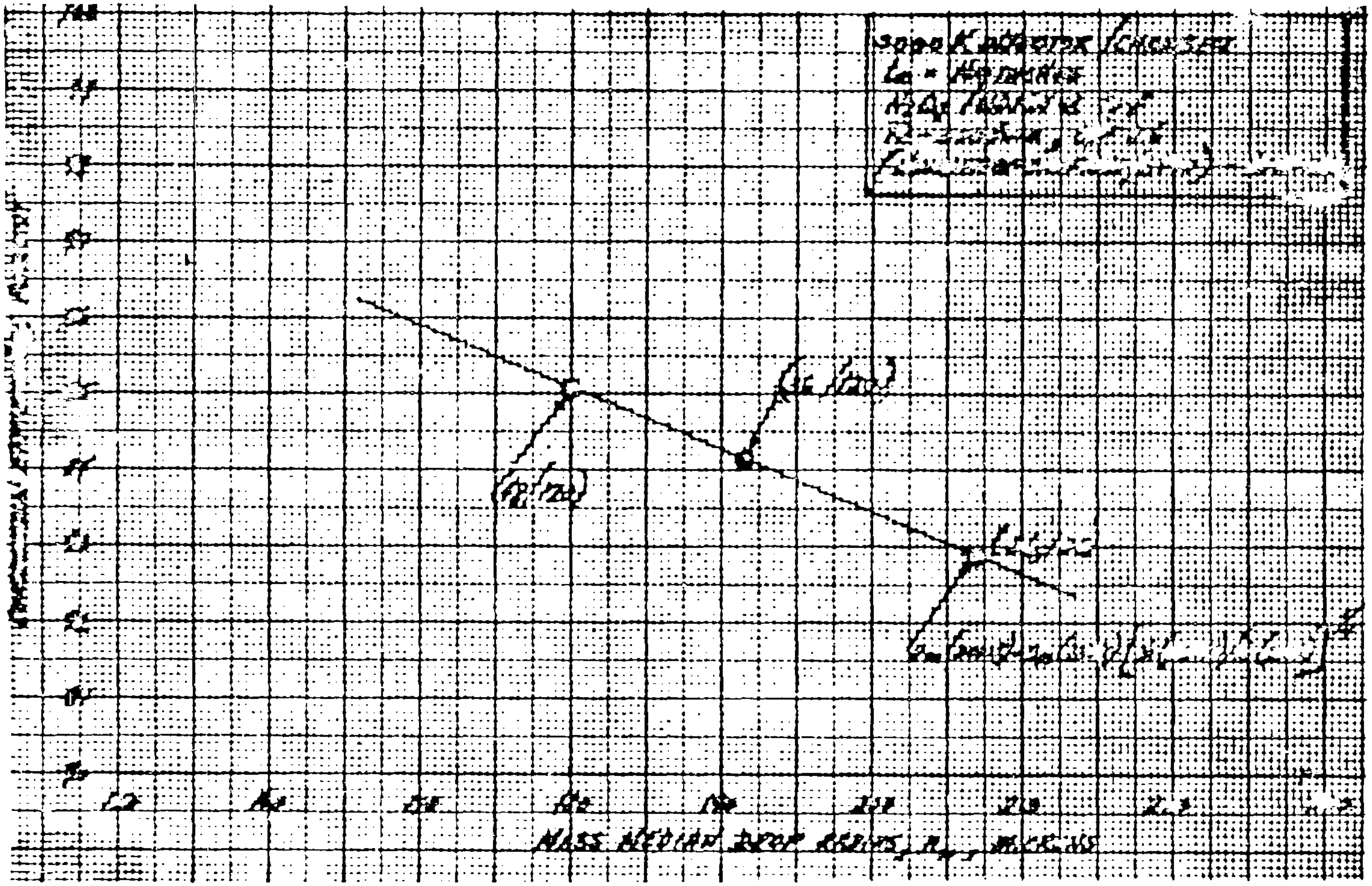

(C) Figure 4-5. Predicted Combustion Efficiency of 3000K Engine (U)

4.6 COMBUSTION STABILITY

(U) Minimization of engine development cost is strongly dependent on the inherent dynamic stability of the engine design which is to be scaled. As noted earlier, the centrally located coaxial injector design has been scaled over a 10,000-to-1 thrust range (25 lbf to 250,000 lbf) without a single occurrence of injector instability.

(U) During this program (250,000 lbf) the injector was subjected to 21 combustion stability rating tests with multiple disturbances being induced on a number of tests (Reference 7). There were no instances where the induced instability was not damped and it was concluded that the injector was dynamically stable.

(U) Analytical studies do not indicate any combustion instability problems when the engine is scaled to thrust levels in the 250,000 lbf thrust to 5000K lbf thrust range.

5. CONCLUSIONS

(U) This section presents TRW Systems conclusions based on results of design studies, on evaluation of fabrication methods, and on analyses of hardware performance during the Task I phase of the Injector/Chamber Scaling Feasibility Program.

(C) The coaxial injector concept demonstrated a test site specific impulse of 89 percent of theoretical (corresponding to 90 plus percent vacuum I_{sp}). The most significant engine design parameter with respect to engine performance was the chamber length. Increasing the length/diameter ratio from 0.935 to 1.54 (which is slightly greater than the 1.45 scaling factor) was responsible for an approximate four (4) percent increase in performance. The combustion process appears to be vaporization rate-limited and the performance at the various chamber lengths can be correlated through the use of a one-dimensional vaporization rate-limited combustion model.

(C) Both momentum ratio and absolute injection pressure level were shown to be important injection parameters. In the smaller L/D combustors the performance was very dependent on the momentum ratio (obtained by varying mixture ratio); the delivered performance became less dependent on momentum ratio as the combustor L/D was increased. The effect of absolute injection pressure was shown during tests in which the chamber pressure was decreased to approximately 200 psia (obtained by decreasing total flow rate through fixed injection orifices). There was an approximate 5 percent loss in I_{sp} efficiency as the injection pressures were reduced to about 50 percent of the design value.

(C) All artificially induced pressure disturbances, whether induced by pulse-guns or non-directional bombs damped within the required stability criteria of 40 milliseconds. There were no instances of spontaneous combustion instability even though the combustion chamber length was varied and the injector was operated over a wide range of mixture ratios and performance levels. There is no evidence to suggest that the coaxial injector will not be dynamically stable at the higher thrust levels.

(U) The design and fabrication of the development hardware (injector, replaceable orifices, and heat-sink combustion chambers) demonstrated that low-cost commercial fabrication techniques could produce acceptable hardware for the program. The use of an electrical discharge machining process for machining the oxidizer orifices resulted in uniform orifices with less than a 1-1/2 percent variation in total area for the three demonstration injectors which were fabricated.

(U) Some additional minimal injector development effort is indicated to minimize the propellant maldistribution which is caused by the single fuel inlet and fuel manifold. A resizing of the internal flow passages on the fuel side of the injector is indicated. The propellant maldistribution is manifested as unsymmetrical wall environments (higher recovery temperatures) in localized regions in addition to reduced performance due to MR variations.

(U) Further injector development is also needed to optimize injector performance, primarily in the area of the oxidizer orifice spacing (percent blockage), number of orifices and orifice shape.

6. REFERENCES

1. Priem, Richard J., and Heidman, Marcus F., "Propellant Vaporization as a Design Criteria for Rocket-Engine Combustion Chambers", NASA TR-R-67, Lewis Research Center, Cleveland, Ohio, 1959.

2. Elverum, G. W., Jr., and Staudhammer, P., "The Effect of Rapid Liquid Phase Reactions on Injector Design and Combustion in Rocket Motors", Progress Report No. 30-4, Jet Propulsion Laboratory, Pasadena, Calif., 1962.

3. Rupe, J., "On the Dynamic Characteristics of Free Liquid Jets and a Partial Correlation with Orifice Geometry", Technical Report No. 32-207, Jet Propulsion Laboratory, Pasadena, California, 1962.

4. Reibling, R., "Criteria for Optimum Propellant Mixing in Impinging-Jet Injection Elements", Pages 817-819, J. Spacecraft, June 1967.

5. Beltran, M. R., et. al, "Analysis of Liquid Rocket Engine Combustion Instability", AFRPL-TR-65-254, Dynamic Science, January 1966.

6. Breen, B. P., et.al, "Injection and Combustion of Hypergolic Propellants", AFRPL-TR-69-48, Dynamic Science, April 1969.

7. Bornhorst, B. R., et.al, "Injector/Chamber Scaling Evaluation, TRW Injector Development", AFRPL-TR-69-199, October 1969.

APPENDIX A

FACILITY CHECKOUT ENGINE DESIGN

1. ENGINE DESIGN

1.1 GENERAL

(U) In addition to the design and fabrication of the Task I development hardware TRW modified and delivered an existing 250,000 lb_f thrust engine for stand mock-up and checkout of the High Thrust Test Facility (1-56). The existing engine had been tested in 1967 at a chamber pressure of 60 psia and approximately 20 percent of rated flow (Ref. 1) under Air Force Contract AF04(611)-11382.

(U) Analysis and design of the engine was initiated at the start of the contract to determine the required modifications to the engine and allowable operating conditions. The objective of this effort was to provide a modified existing engine which was suitable for repeated short duration tests at rated conditions. These tests results would then provide some design criteria for the initial development injector configuration (prior to completion of fabrication of the initial development injector). However, tests of the modified thrust chamber assembly were not completed in time to allow any design changes to be incorporated into the development injector.

1.2 250,000 LB_F THRUST FACILITY CHECKOUT ENGINE DESIGN

(U) The 250,000 lb_f thrust engine is shown in Figure A-1 prior to testing at the TRW Capistrano Test Site in 1967. The engine consists of two components; the centrally located coaxial injector and the uncooled thrust chamber. The modifications required to each component to allow operation at rated conditions are discussed in the following sections.

1.2.1 Component Design - Injector

(U) The design of the modified injector (X403666-1) is shown as Figure A-2. The redesign was based on providing the nominal chamber pressure in the existing chamber which had a throat diameter of 27.0 inches. The propellant inlet interfaces were coordinated with AFRPL personnel prior to the modification. The single fuel inlet was retained; however, the 5 inch diameter, 150 lb ASA, slip-on flange was replaced with a 6 inch diameter, 300 lb ASA, welding neck flange and 6 inch schedule 80 pipe. The fuel manifold was replaced with a manifold constructed of 6 inch diameter, 90° elbows, of schedule 80 pipe. The maximum velocity in the annular inlet fuel manifold is 24 ft/sec at rated flow. The 8 inch diameter, 150 lb ASA oxidizer inlet flange was replaced with an 8 inch diameter, 300 lb ASA welding neck flange.

(U) The machined flanges for attaching the injector center body to the outer injector housing were changed from 1/2-inch to 1-inch in thickness. Twelve gusset stiffeners are welded between the oxidizer inlet flange and the machined flanges. The oxidizer diffuser plug was repositioned to provide a primary orifice opening of 0.88 inches. An ablative pintle tip of

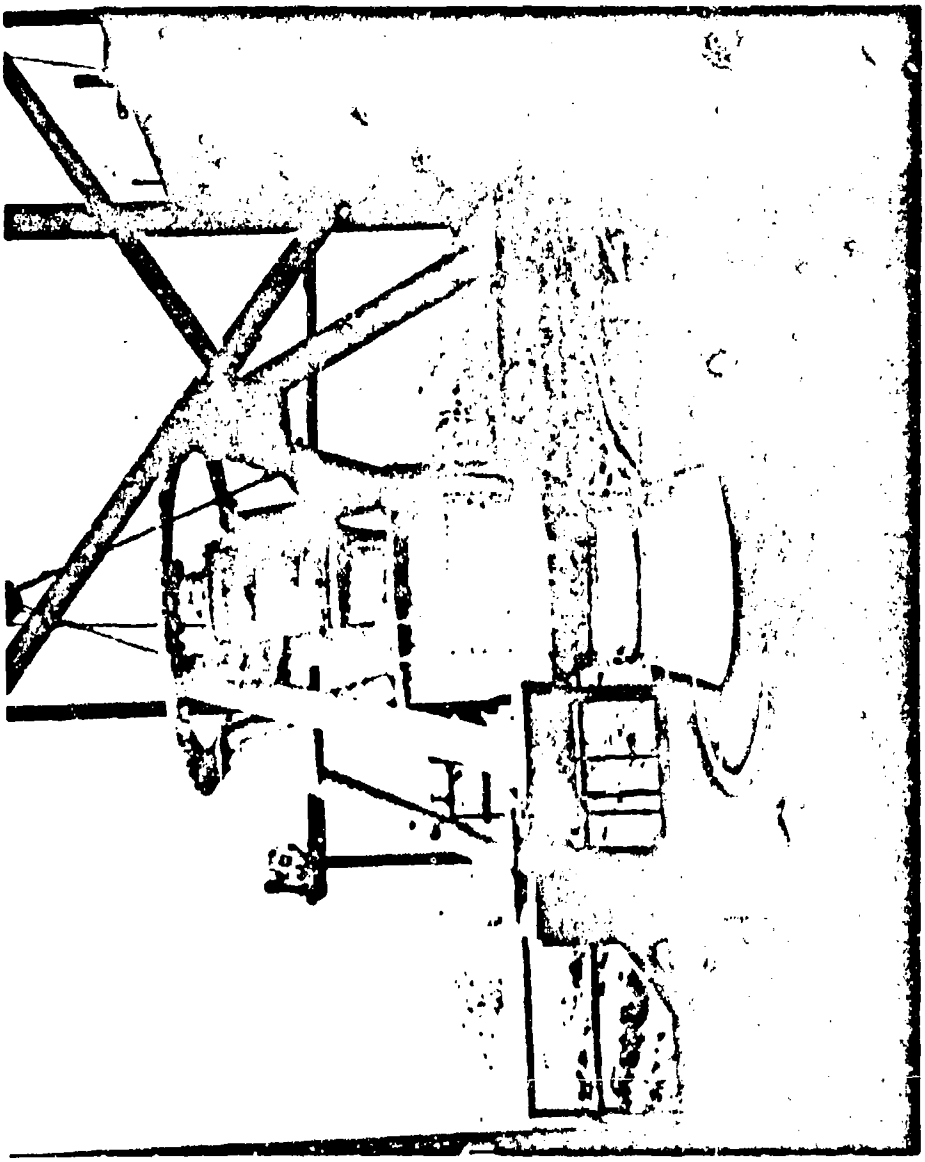

(U) Figure A-1. 250,000 lb_f Thrust Engine Prior to Tests at 50,000 lb_f Thrust (U)

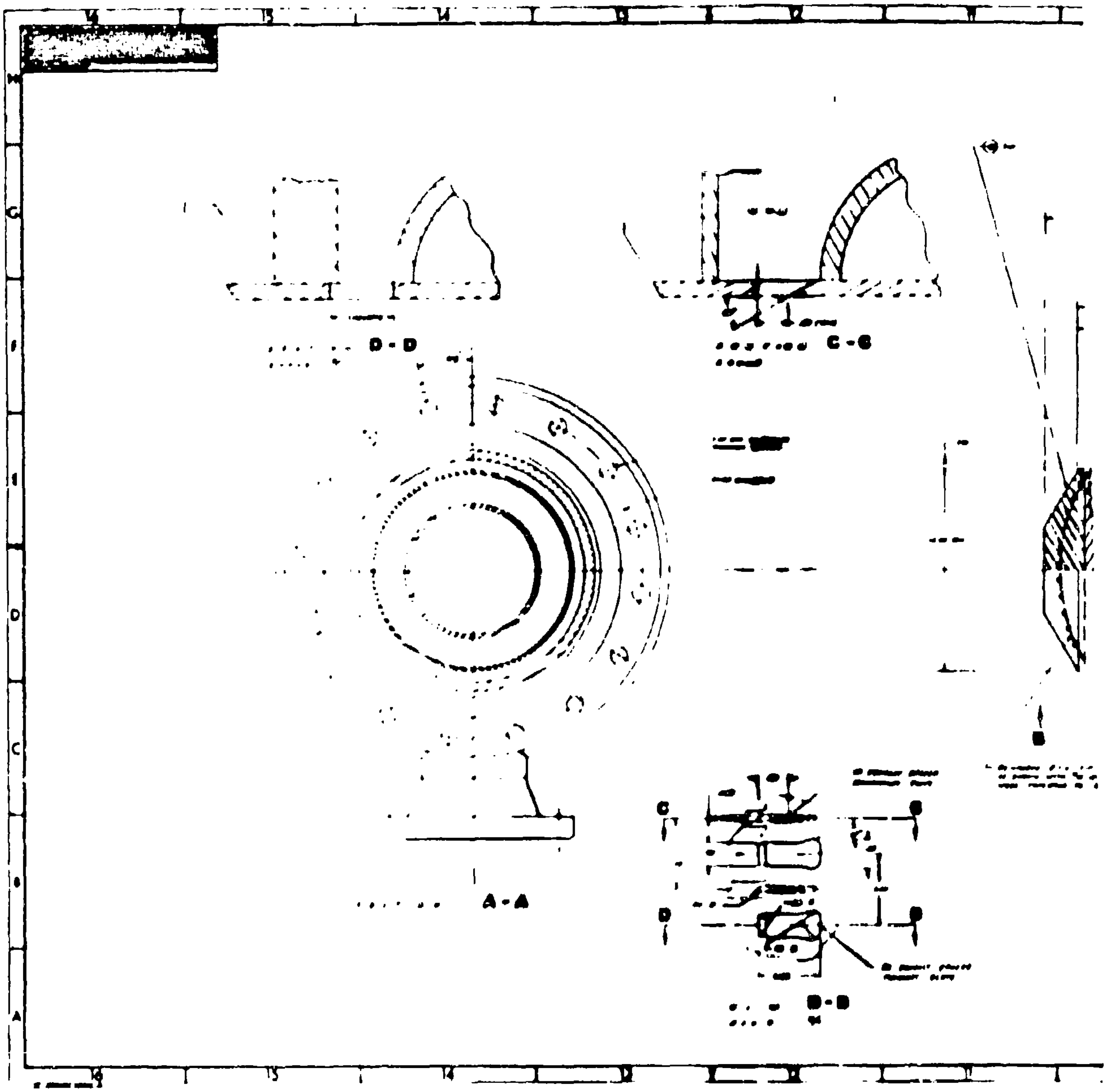
D - D
C - C
A - A
B - B
C
C
D
D
B
16
15
14
13
12
11
H
G
F
E
D
C
B
A

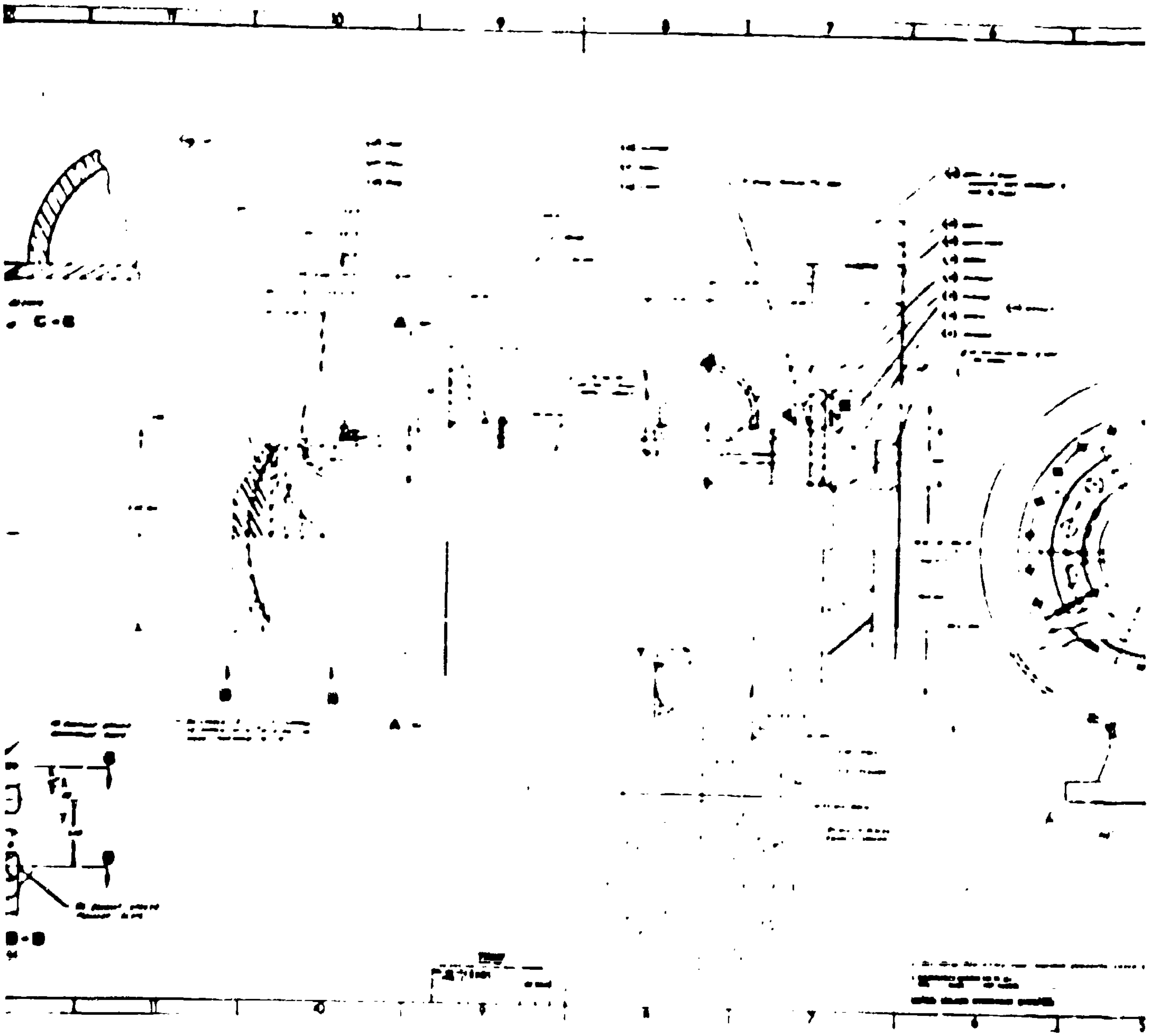

2

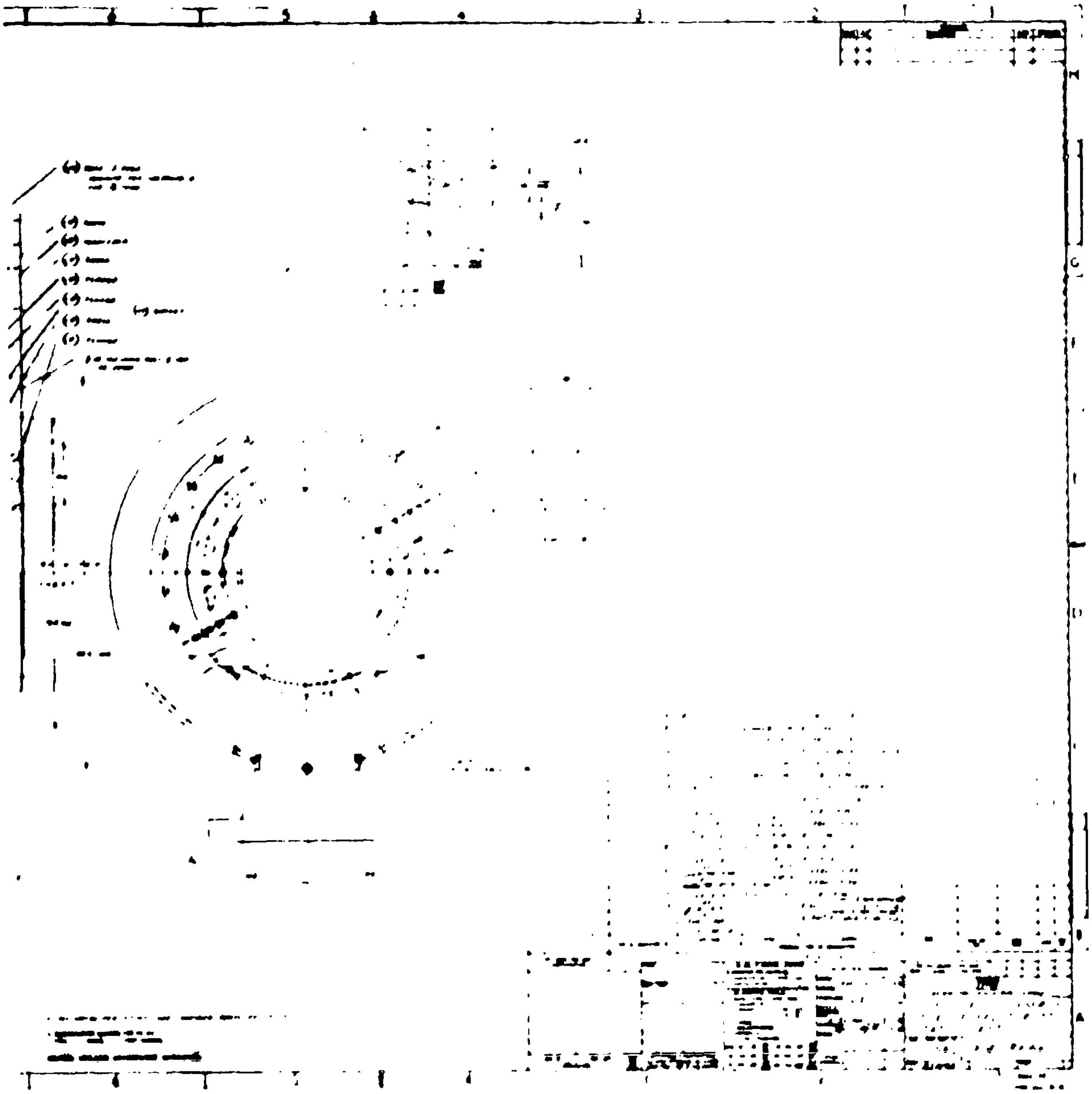

Figure A-2. [illegible] Injector Assembly [illegible] Fixed Thrust, Static [illegible]

(U) HAVEG 41F cement (asbestos-phenolic) was fabricated to protect the diffuser plug from the thermal environment. The reworked injector is shown in Figure A-3 prior to shipment to the AFRPL.

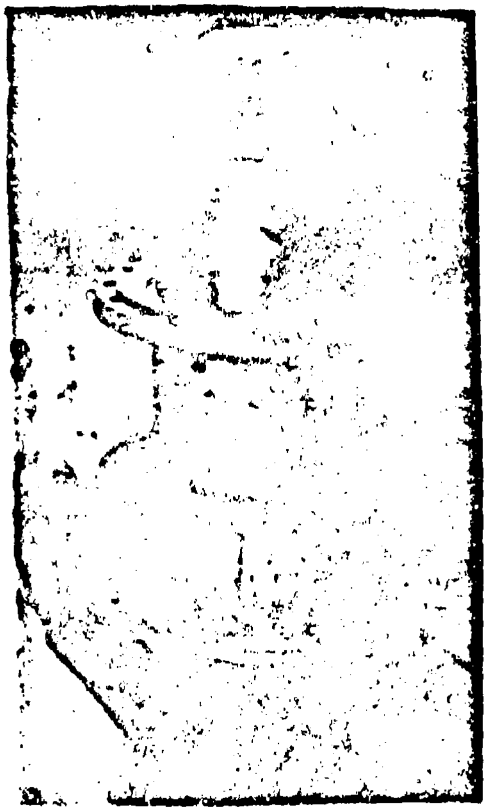

(U) Figure A-3. Reworked 250,000 lb_f Thrust Injector Prior to Shipment to AFRPL (Photo #6683-68)(U

1.2.1.1 Hydraulic Test-Injector

(U) A fixture for hydrostatically pressure checking the injector, fabricated from commercial pipe sections, was used to pressure check the injector at 415 psi. Blank flanges were used to seal both propellant inlets and the fixture was bolted to the injector-chamber mating flange which sealed the injection orifices.

(U) Water-flow tests were conducted at the Capistrano Test Site prior to shipment of the injector to the AFRPL. The injector was not water-flowed at the rated conditions because of facility limitations at the time of test. The injection pressure losses are presented in Figure A-4. The oxidizer injection orifice area is 13.29 sq. inches. The diffuser plug is welded into a position which covers 0.12 inches of the 1.00 inch primary orifice length. The fuel injection area is 10.75 sq. inches. The annular opening varies from 0.260 inches at the fuel inlet to 0.270 inches at 180 degrees from the fuel inlet. The experimentally determined values of the discharge coefficient for the injection orifices are 0.74 for the oxidizer element and 0.99 for the fuel orifice.

(U) A photograph of the injection spray pattern water flowing through both fuel and oxidizer orifices is shown in Figure A-5, at water flows equivalent to the throttled conditions. When the oxidizer side of the injector is water-flowed individually the secondary flow is shown to fan circumferentially after leaving the orifice (Figure A-6). The upstream regions of the primary orifices are not completely filled. In Figure A-5 the flow through the oxidizer orifices tends to fill the orifices and to spread circumferentially to form a uniform cone close to the injector.

1.2.2 Component Design - Thrust Chamber

(U) The existing TRW thrust chamber (X403668) shown in Figure A-7 was delivered to AFRPL on 18 July 1968 for modification. The chamber is constructed of 4130 steel. The only structural modification required to the thrust

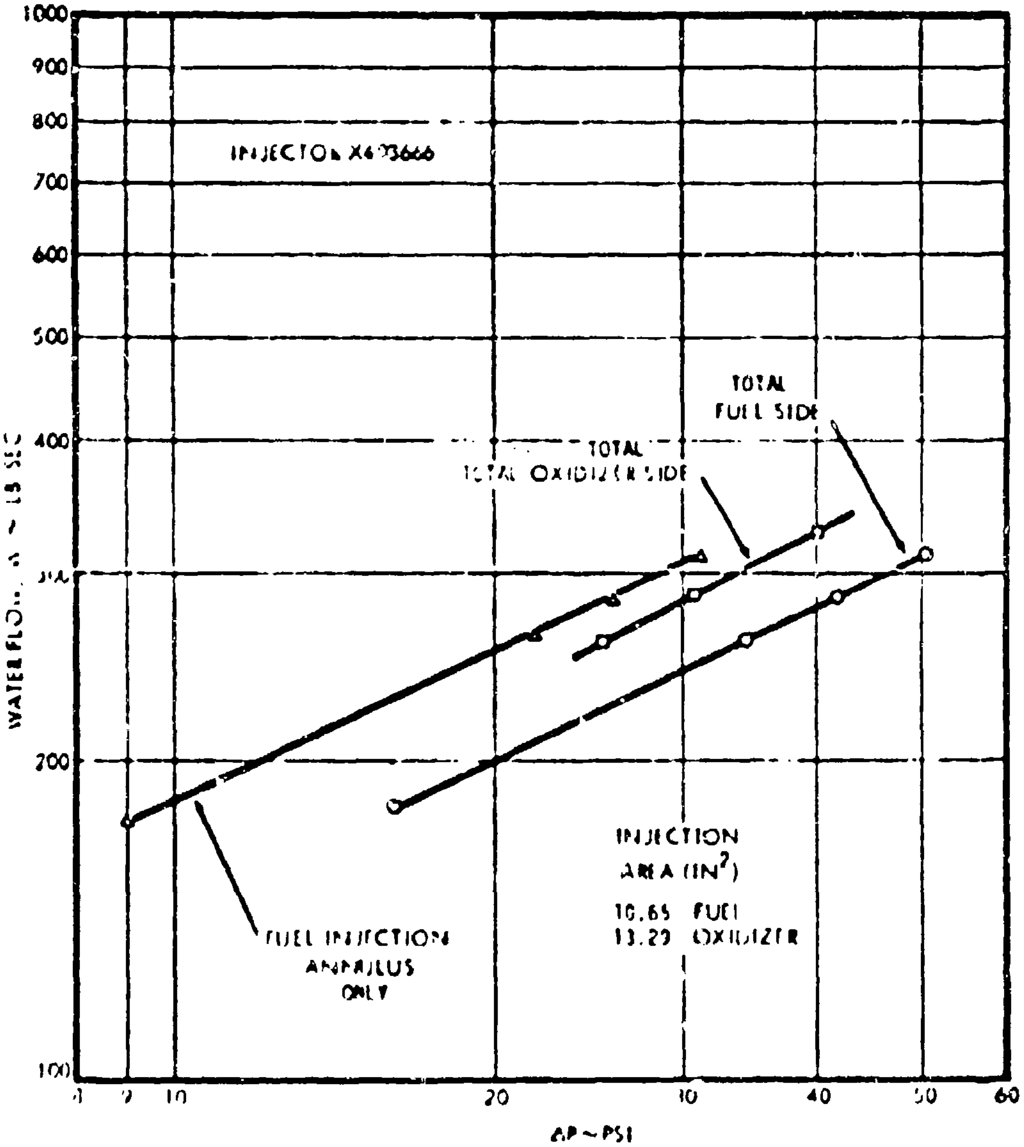

(U) Figure A-4. Predicted Injection Pressure Losses (U)

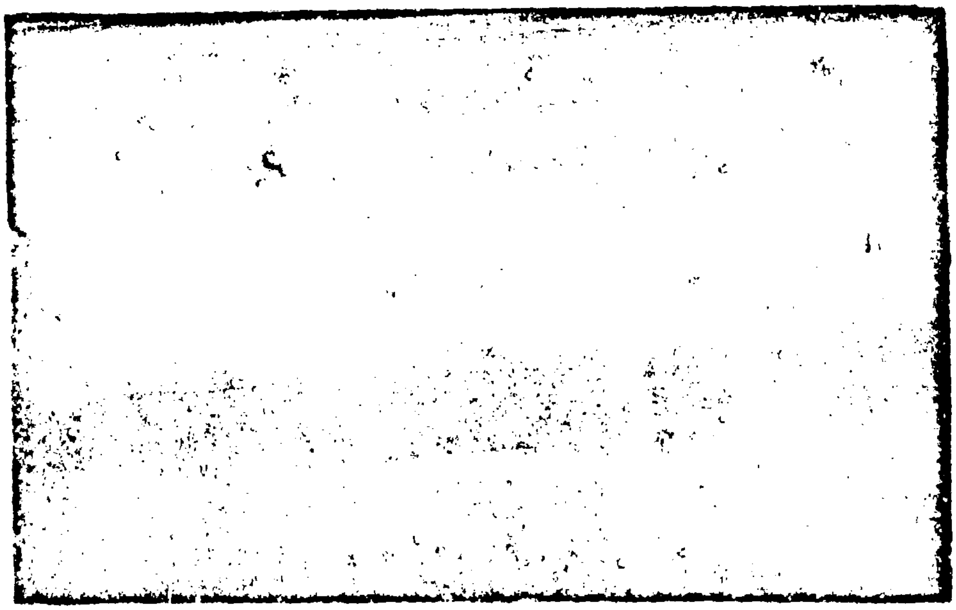

(U) Figure A-5. Water-Flow [illegible] New Feed [illegible] lbf
Thrust Injector At 5.2 (Photo 46654-68) (U)

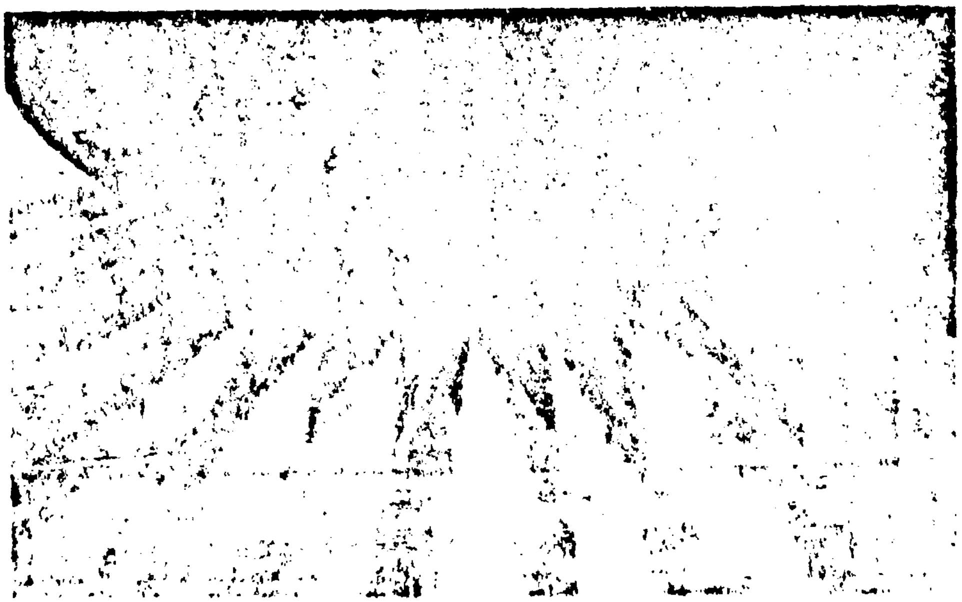

(U) Figure A-6. Water-Flow of Oxidizer Orifices
Reworked Injector (Photo 46648-68) (U)

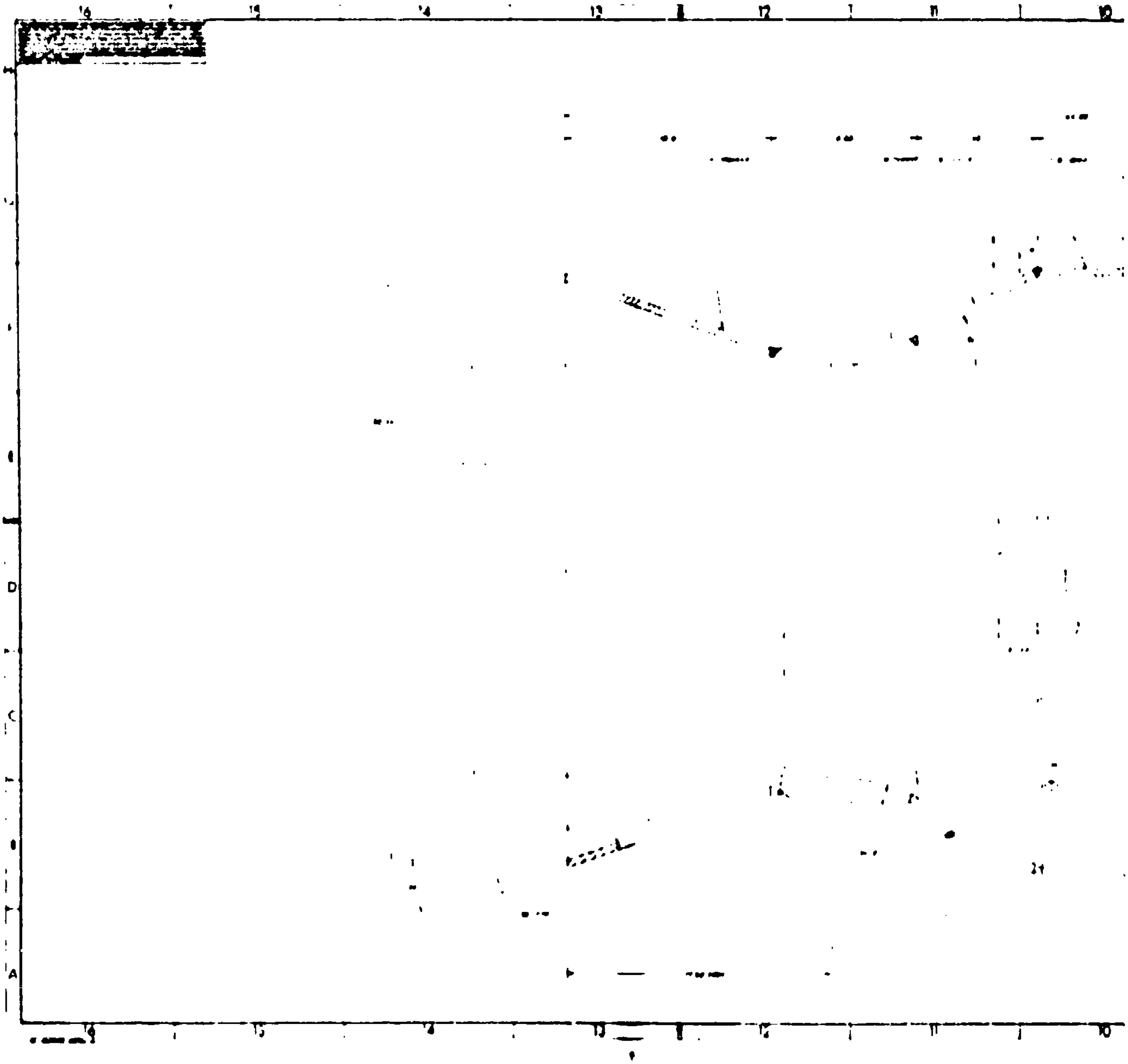
D
C
A

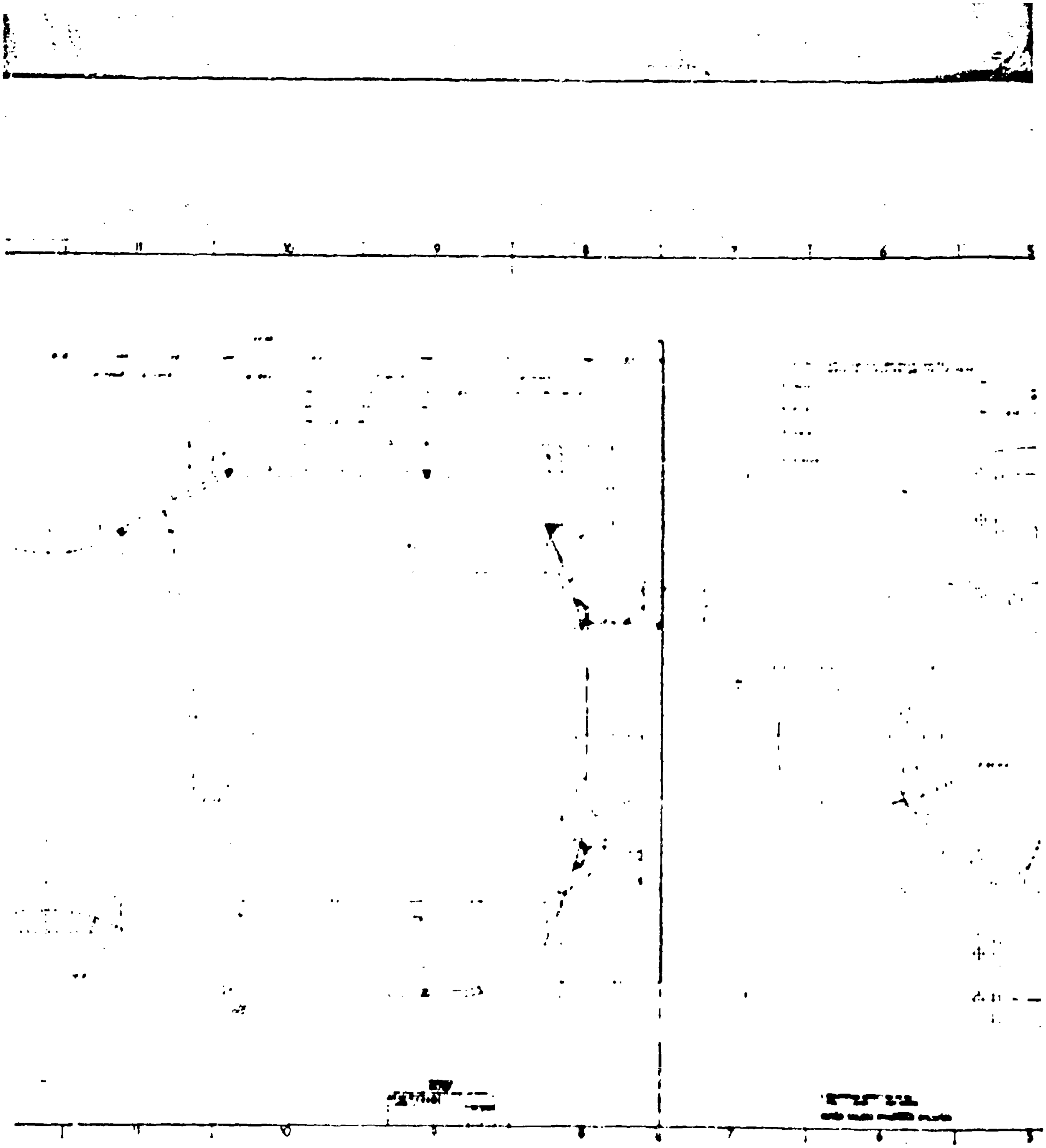

2

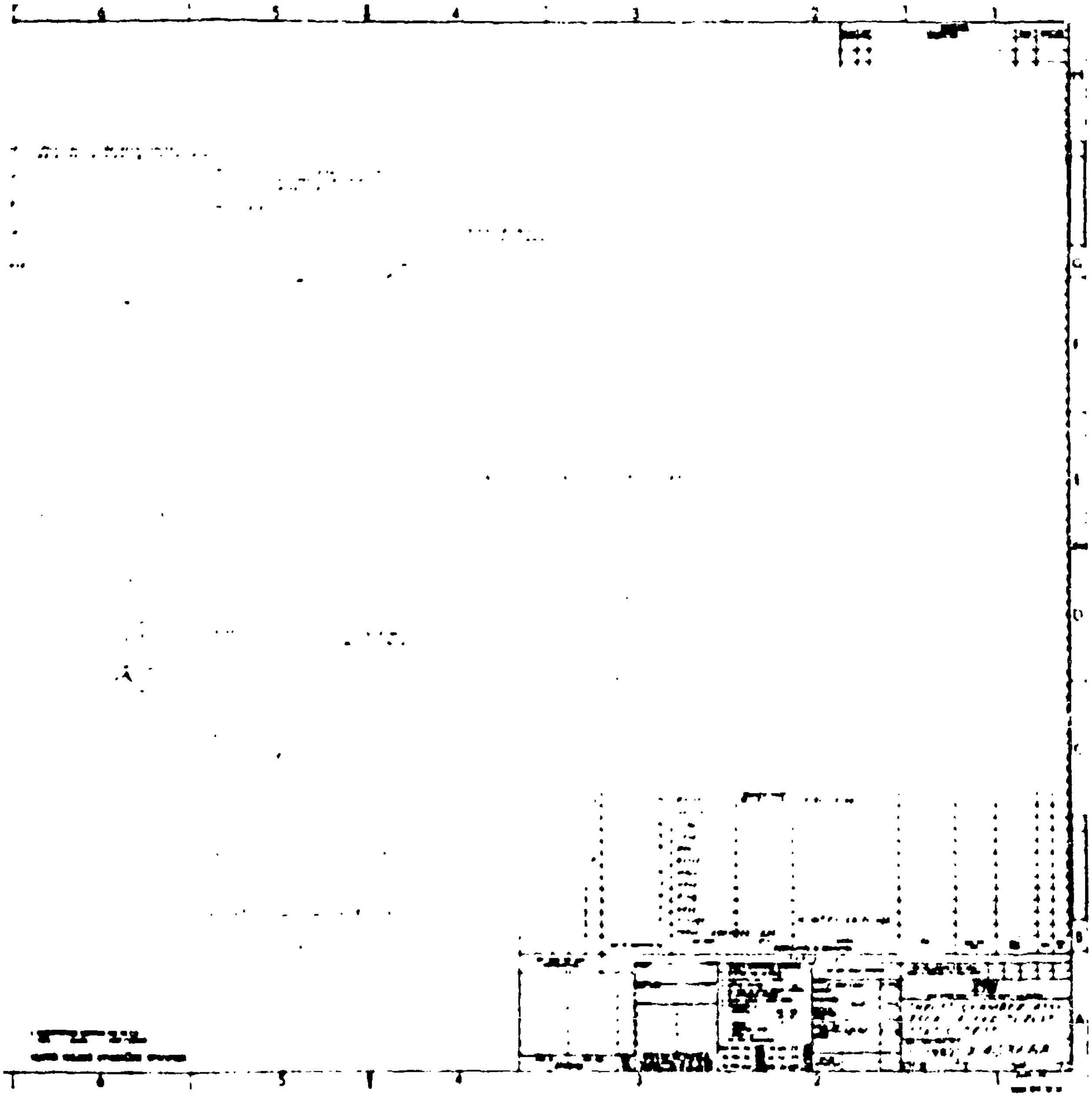

Figure A-7 X403668 Thrust Chamber Assembly, 250K - Fixed Thrust, Static Test (U)

(U) chamber, to enable operation at the rated conditions, consisted of the welding of gusset stiffeners (X403668-12) at the injector head as shown on TRW drawing X403668.

1.2.2.1 Modification 1 - Thrust Chamber

(U) After completion of the initial ten facility checkout firings the injector and thrust chamber were returned to TRW Systems. The thrust chamber (X403668) was reworked to be compatible with the development injector at the 16 inch flange attach point. The chamber was lengthened 12 inches in a manner similar to that employed for the heat-sink combustion chamber. The nozzle extension was lengthened (20° half-angle) to provide a 4/1 expansion ratio nozzle by adding a conical section with an exit diameter of 54.0 inches. This modified chamber was employed in test firings 33 and 34 only.

Reference:

1. AFRPL-TR-68-46, "Advancement of Injector and Thrust Chamber Technology," G. A. Voorhees, Jr., TRW Systems, December 1967, Confidential.

APPENDIX B

THERMAL ANALYSIS OF 250,000 LB_F THRUST HEAT-SINK ENGINE CONFIGURATION

1. PREDICTED HEAT TRANSFER COEFFICIENT AT NOZZLE THROAT

(U) The convective heat transfer coefficient along a thrust chamber wall can be calculated in many ways, using any number of currently available theoretical or empirical models, or modifications thereof, or it can be obtained by extrapolation from available test data. The following predicted value arbitrarily is based on the Bartz short form equation (Ref. 1) with the gas properties arbitrarily based on a film temperature, taken as the arithmetic average of the local static temperature and an average inside surface wall temperature. The local static temperature is calculated from an estimated recovery temperature which is based on test data obtained with the TRW coaxial injector. It should be pointed out that the effect of temperature on the calculated value of the heat transfer coefficient, h_g, for the UDMH/N_2O_4 propellant combination is of secondary importance. The predicted value of h_g is then compared to that corrected from available data obtained using a high performing coaxial injector at a chamber pressure of 300 psia.

$$h_g = \left[\frac{0.026}{D_t^{.2}} \left(\frac{\mu^{.2} C_p}{Pr^{.6}}\right)\left(\frac{P_c g}{C^*}\right)^{.8} \cdot \left(\frac{D_t}{r_c}\right)^{.1}\right]\left(\frac{A_t}{A}\right)^{.9} \sigma \qquad (1)$$

Theoretical performance and gas properties at a mixture ratio of 2.6 for N_2O_4/UDMH at 300 psia are

C^* = 5596 ft/sec (shifting)

T_c = 5930°R

C_p = 0.466 Btu/lb-°F (frozen)

Average molecular weight = 23.6 lb/lb mol

Primary gas constituents

	mol fraction
H_2O	.334
N_2	.285
CO	.129
CO_2	.086

Throat diameter = 26.1 in.

Throat radius = 11.5 in.

(U)

$$Pr = \frac{4\gamma}{9\gamma - 5} \qquad (2)$$

$$\gamma = \frac{1}{1 - R/JC_p} \qquad (3)$$

$$R = 1544/\text{mol. wt} = 1544/23.6 = 65.5 \; \frac{\text{ft-lb}}{\text{lb-°R}}$$

$$\gamma = \frac{1}{1 - 65.5/(778)(.466)} = 1.22$$

$$Pr = \frac{(4)(1.22)}{(9)(1.22) - 5} = 0.817$$

For a steel thrust chamber, the inside surface wall temperature during a 2 second firing is approximately 1000°F. The gas recovery temperature, based on test data obtained with the TRW coaxial injector, is approximately 4200°R. The gas static temperature at the throat is therefore

$$T_{static} = 4200 \left(\frac{T_{static}}{T_{total}} \text{ at } \gamma = 1.2 \right) = 4200 \times .90 = 3780°\text{R}$$

The film temperature is

$$T_f = \frac{T_w + T_{static}}{2} = \frac{1460 + 3780}{2} = 2620°\text{R}$$

The factor, σ, which accounts for gas density and viscosity variation across the boundary layer is determined from charts in Reference 1, for a ratio of wall temperature to recovery temperature of 0.386, and is approximately 1.25.

(U) The specific heat, C_p, is estimated to be 0.42 Btu/lb-°F at a film temperature of 2620°R. This value is estimated by noting that the effect temperature has on the gas constituents as temperature is decreased from 5930°R to 2620°R is approximately 10 percent. Therefore the C_p value of 0.466 Btu/lb-°F is decreased by 10 percent.

The viscosity, μ, is estimated from Reference 1.

$$\mu = (46.6 \times 10^{-10}) (\bar{m})^{1/2} (T_f)^{.6} \qquad (4)$$

$$= (46.6 \times 10^{-10}) (23.6)^{1/2} (2620)^{.6} = 0.254 \times 10^{-5} \text{ lb/in-sec}$$

(U) Substituting into Equation (1) for P_c = 300 psia and C* = 5230 ft/sec

$$h_g = \left\{ \frac{0.026}{(26.1)^{.2}} \left[\frac{(0.254 \times 10^{-5})^{.2}(0.42)}{(0.817)^{.6}} \right] \left[\frac{(300)(32.2)}{5230} \right]^{.8} \left(\frac{26.1}{11.5} \right)^{.1} \right\} (1)(1.25)$$

$$= \frac{(0.026)(0.076)(0.42)(1.632)(1.0855)(1.25)}{(1.92)\ (0.886)} = 1.08 \times 10^{-3} \frac{\text{BTU}}{\text{in}^2\text{-sec-°F}}$$

This calculated value is somewhat lower than experimentally determined values obtained with a TRW coaxial injector designed for a chamber pressure of 300 psia. Correcting the experimentally determined value by the ratio $D_t^{.2}$ for the chamber results in an estimated value of h_g of 1.58×10^{-3} $\frac{\text{Btu}}{\text{in}^2\text{-sec-°F}}$ for the 250K chamber. It is recommended that a value of approximately 1.58×10^{-3} $\frac{\text{Btu}}{\text{in}^2\text{-sec-°F}}$ be used for the 250K engine until further experimental data is obtained.

2. THERMAL ANALYSIS

(U) The results of an approximate thermal analysis of the 250,000 lb_f heat-sink combustion chamber are presented in the following paragraphs. The combustion chamber model and gas recovery temperature plot used in the analysis is shown in Figure B-1. Hot-side and cold-side wall temperatures were computed for varying wall thicknesses and gas recovery temperatures of 70, 85 and 100 percent of the theoretical maximum gas temperature in the throat and combustion chamber regions.

(U) A typical gas recovery temperature with the TRW coaxial injector is approximately 70 percent of theoretical maximum gas temperature, or 3810°F as determined from Figure B-1. The predicted hot-side and cold-side temperatures for the throat region and chamber region are shown in Figures B-2 and B-3, respectively. The analysis predicts an internal surface temperature of 1700°F is reached at the throat after two seconds of firing for wall thicknesses of 0.25 inches to 0.50 inches. Wall thickness has only a secondary affect on hot-side temperature.

(U) The predicted wall temperatures for an 85 percent gas recovery temperature are shown in Figures B-4 and B-5. The predicted internal surface temperature at the throat after two seconds of firing is approximately 2100°F. Figures B-6 and B-7 show the predicted wall temperatures for a 100 percent gas recovery temperature. The predicted internal surface temperature at the throat after two seconds of firing is approximately 2500°F.

(U) Definitive temperature limits for repeated short duration firings with T-1 steels are not available. It is recommended that test durations be limited to two seconds (or 1700°F) to minimize chemical attack by the propellants impinging on the hot combustion chamber wall. Thermocouples on the outside surface of the combustion chamber will not respond quickly enough to measure inner wall temperature. Therefore it is recommended that inside wall surface thermocouples (Nanmac's) be installed along the thrust chamber.

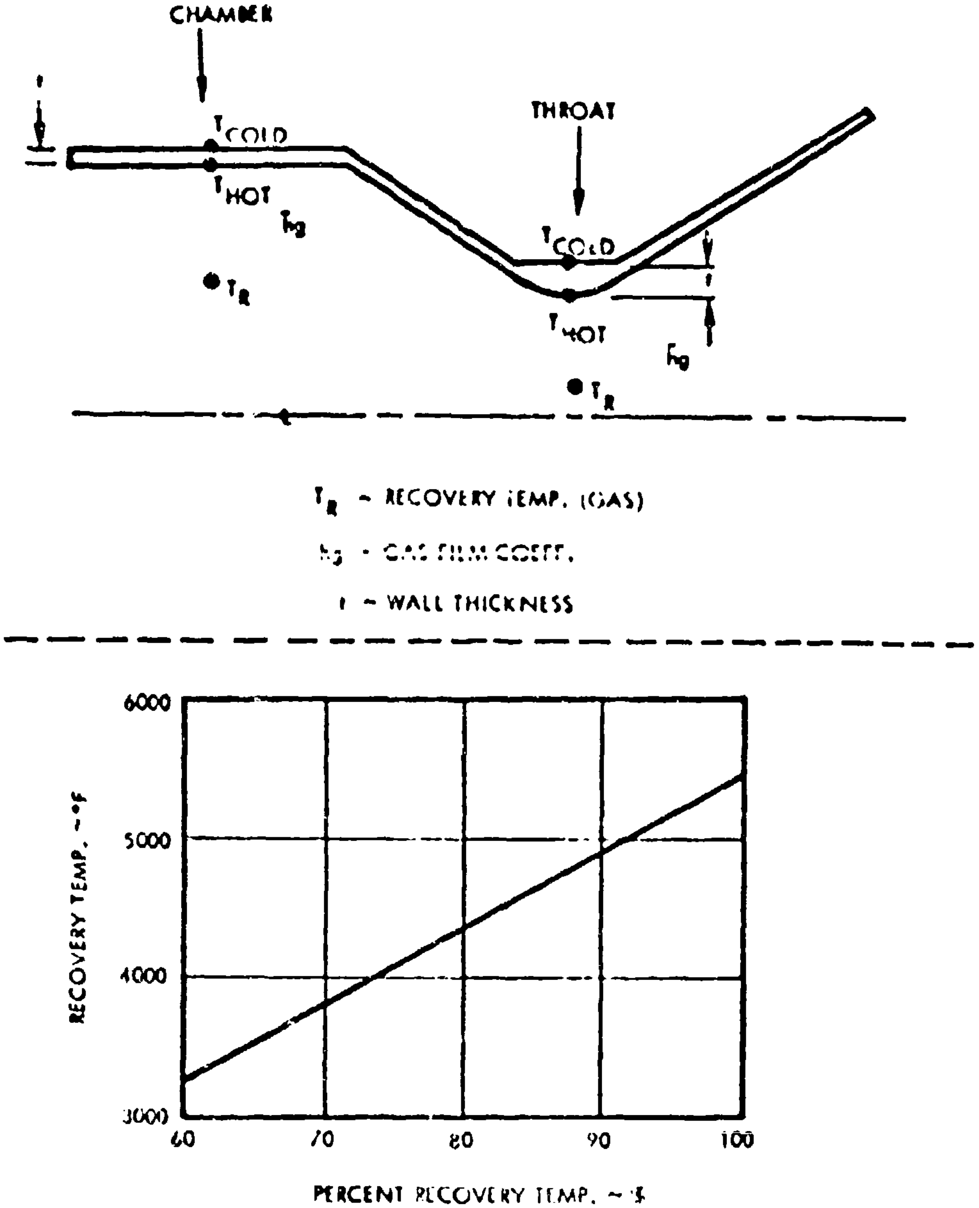

(U) Figure B-1. Parameters Used for Thermal Analysis (U)

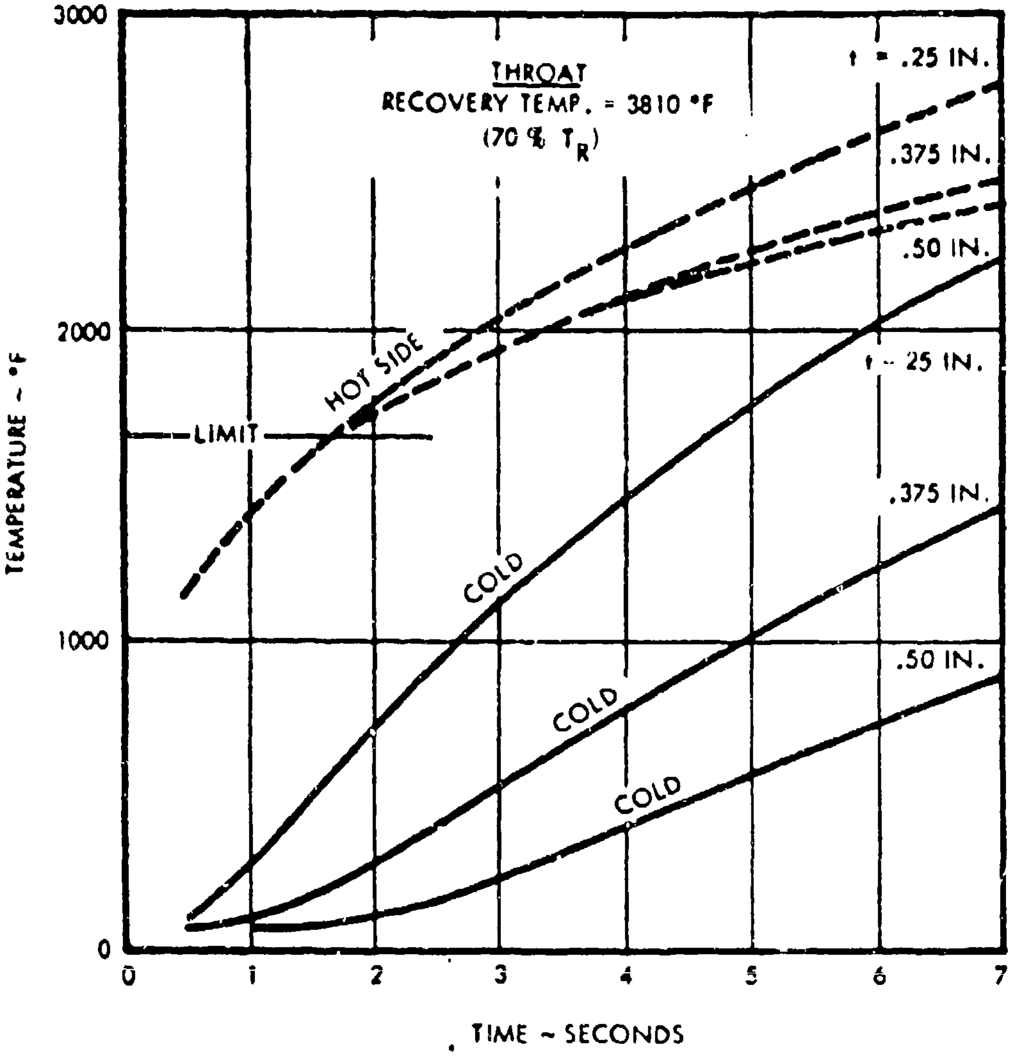

(U) Figure B-2. Predicted Nozzle Throat Wall Temperature for 70% Recovery Temperature (U)

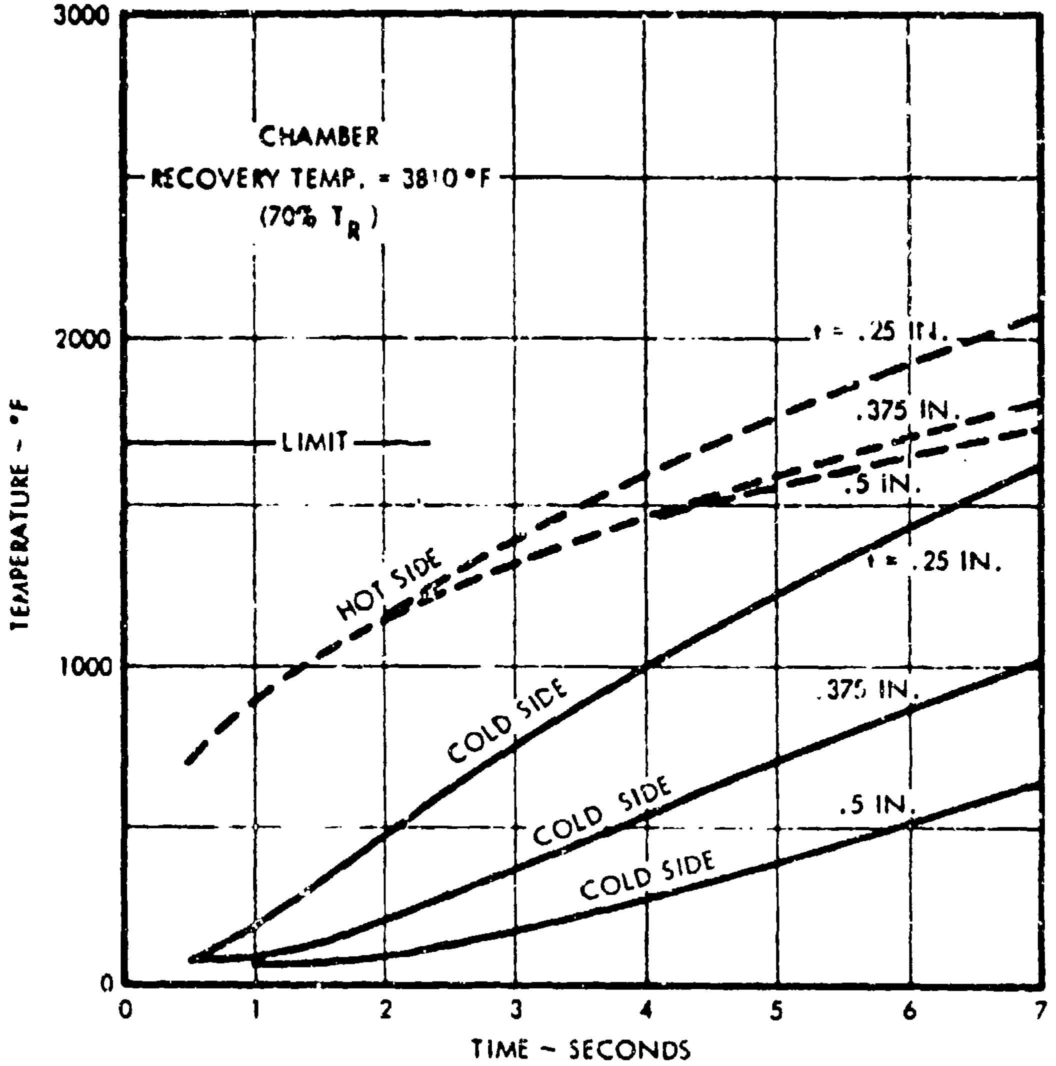

(U) Figure B-3. Predicted Chamber Wall Temperatures for 70% Recovery Temperature (U)

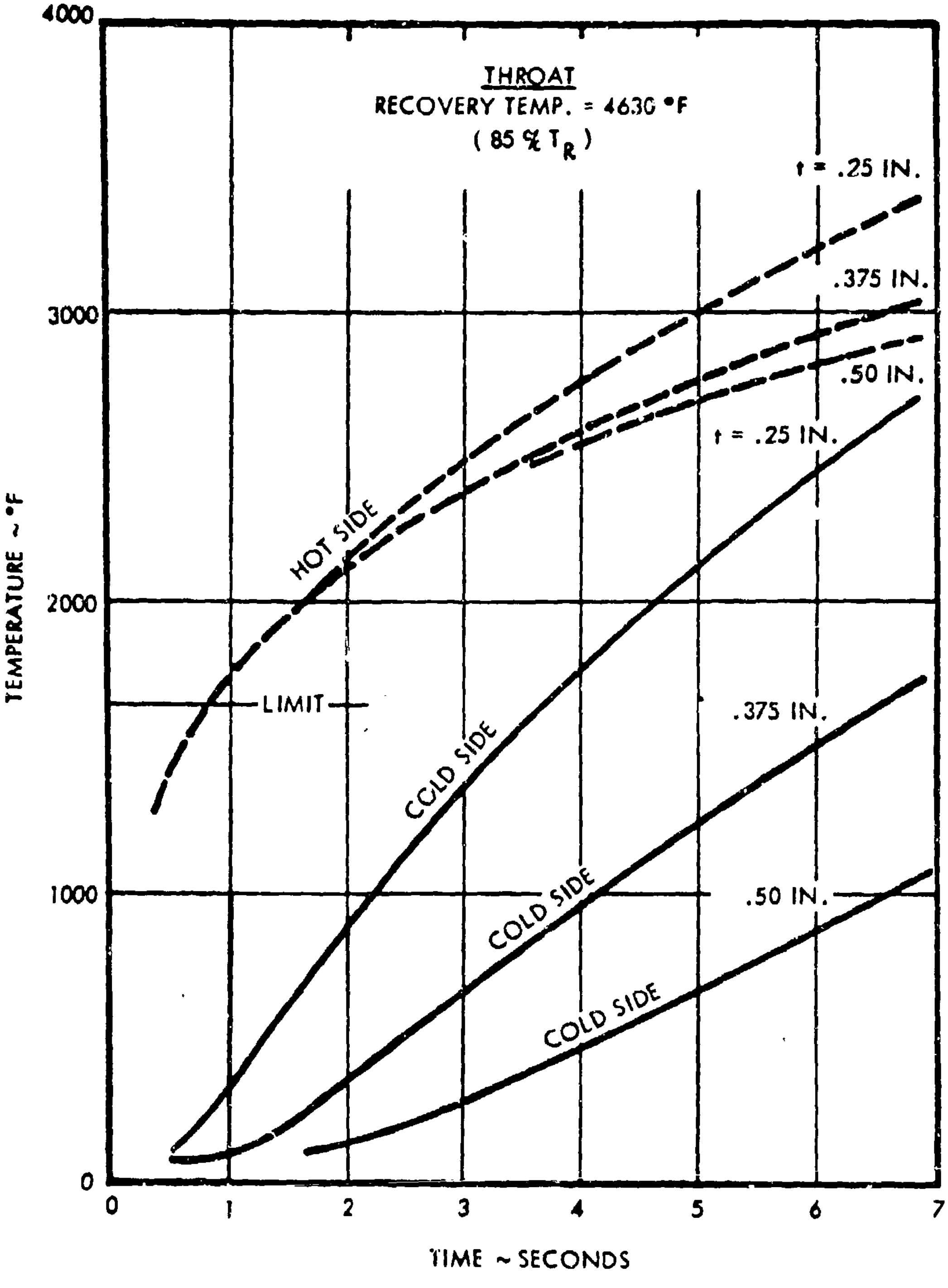

(U) Figure B-4. Predicted Nozzle Throat Wall Temperatures for 85% Recovery Temperature (U)

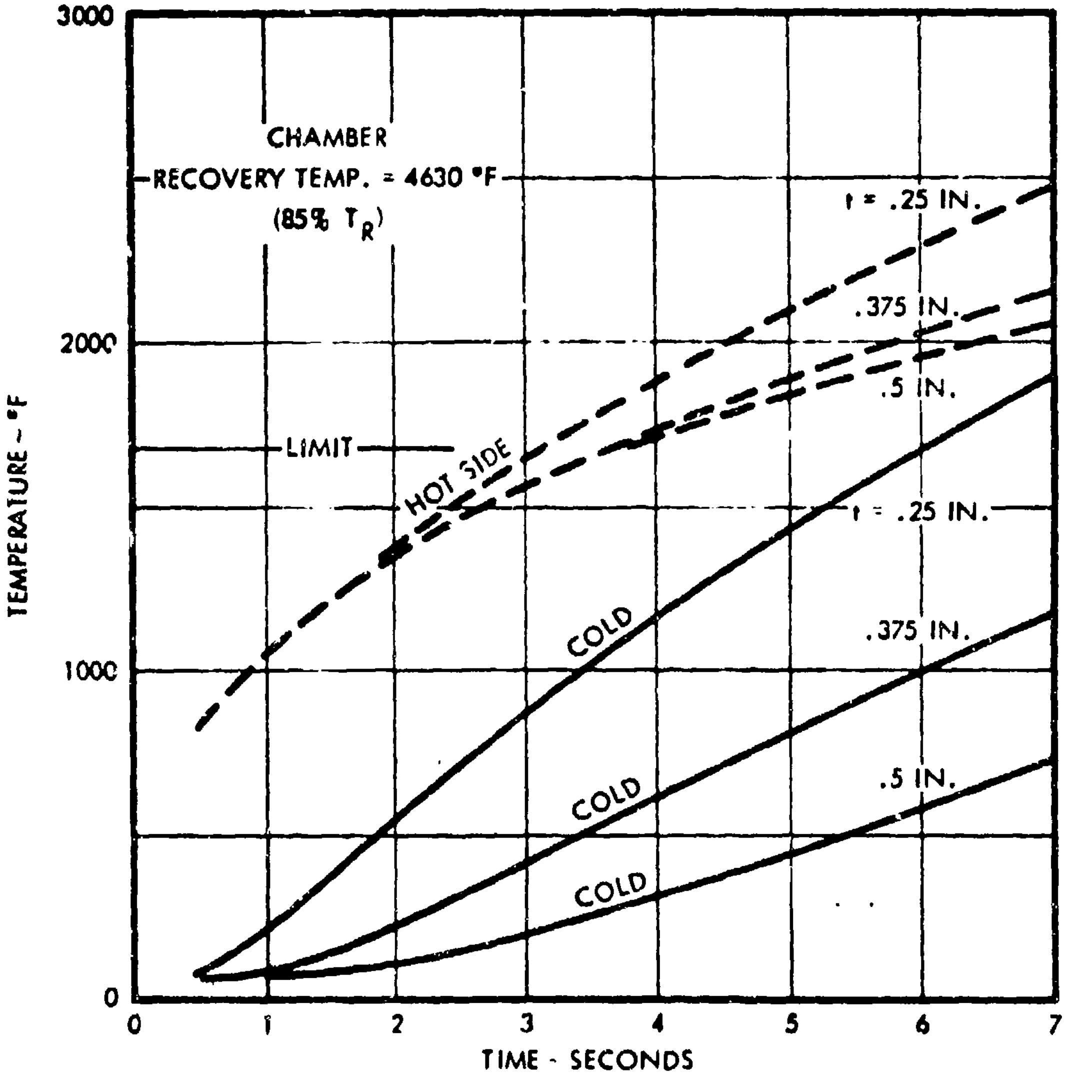

(U) Figure B-5. Predicted Chamber Wall Temperature for 85% Recovery Temperature (U)

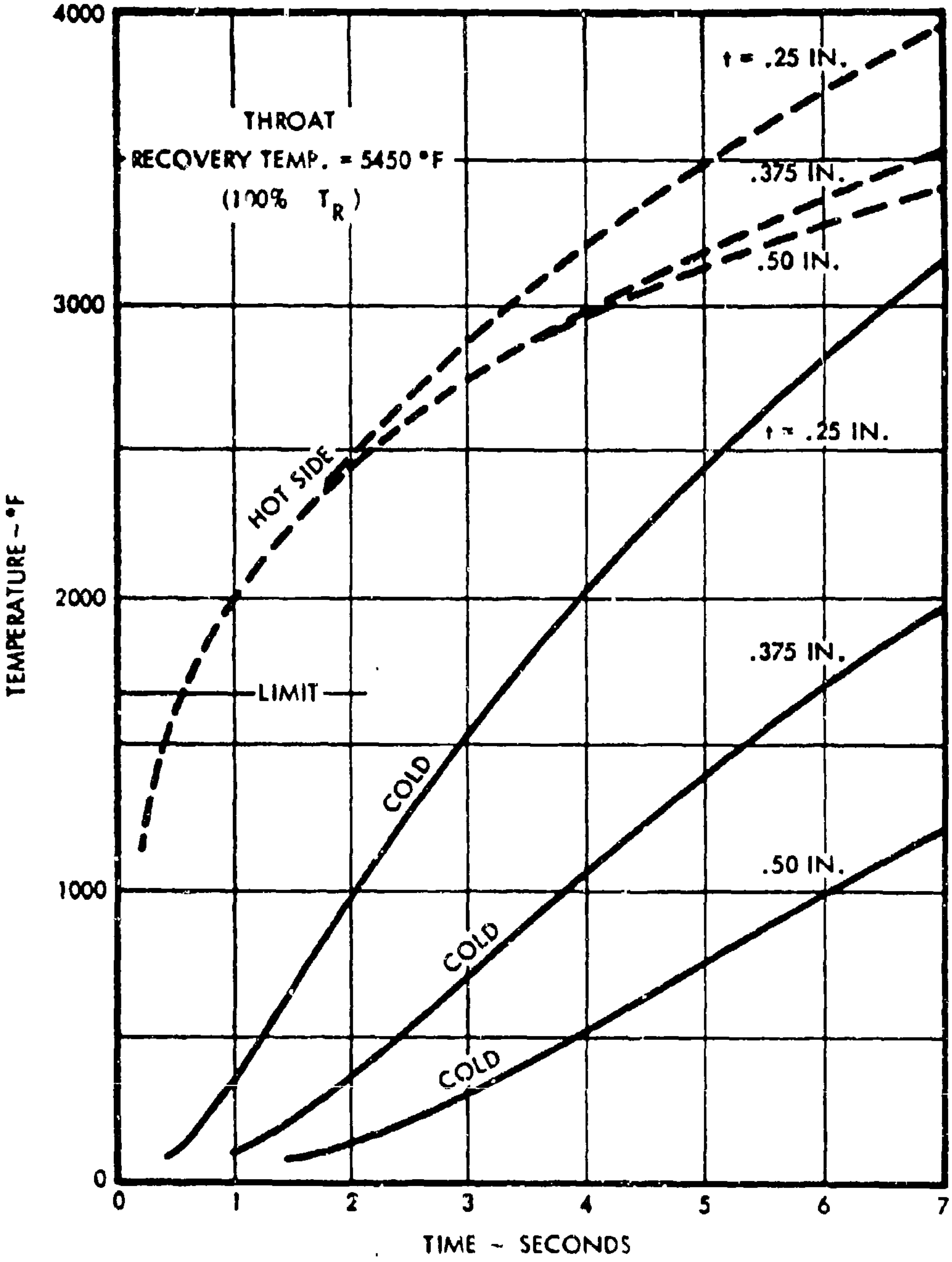

(U) Figure B-6. Predicted Nozzle Throat Wall Temperature for 100% Recovery Temperature (U)

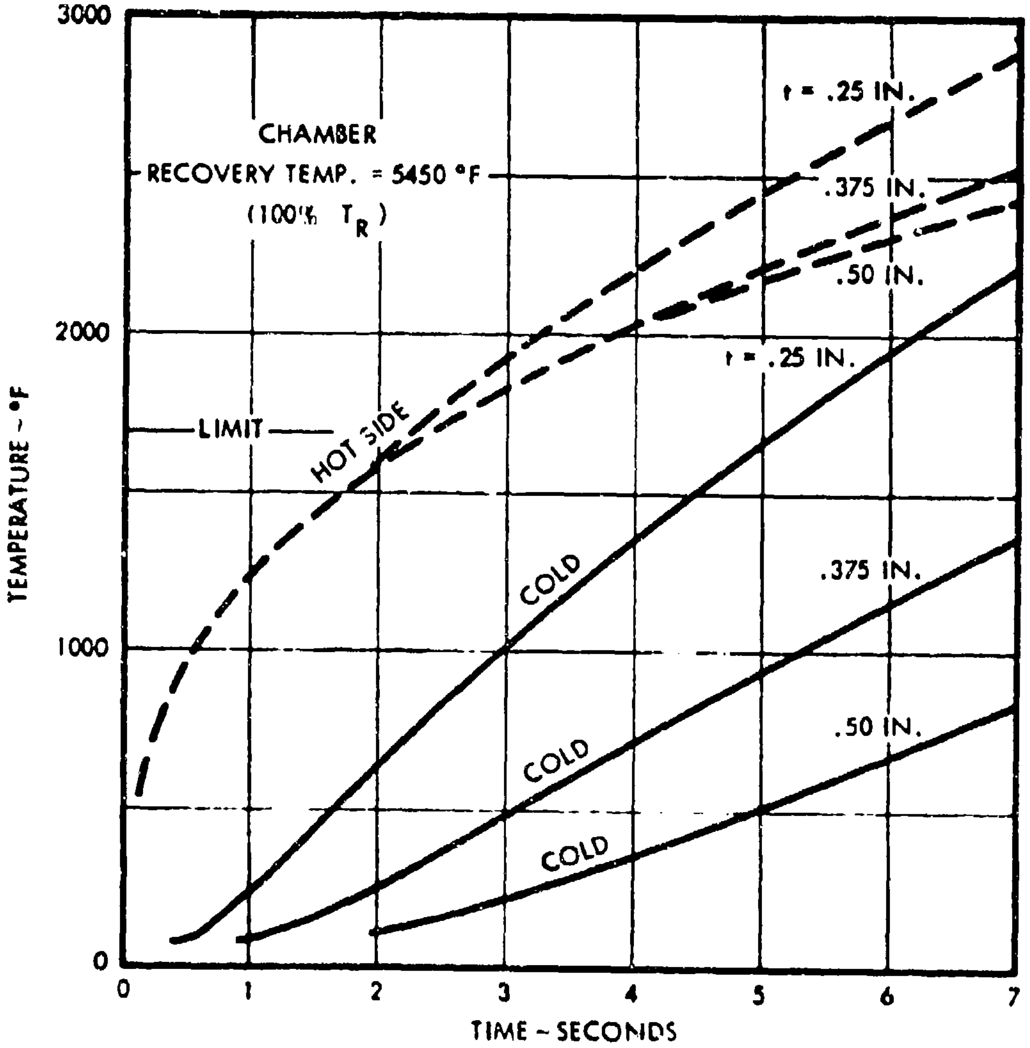

(U) Figure B-7. Predicted Chamber Wall Temperature for 100% Recovery Temperature (U)

Reference: (1) D. R. Bartz, "A Simple Equation for Rapid Estimation of Rocket Nozzle Convective Heat Transfer Coefficients," Jet Propulsion, January 1957. (U)

APPENDIX C

DATA REDUCTION PROCEDURES

1. GENERAL

(U) The test results presented herein are derived from computer printout data furnished TRW by the AFRPL. The AFRPL furnished TRW reduced performance data for test firings 2 through 17 and general performance data for test firings 18 through 46, 72-78, 90-93, 98-102, and 108-110. TRW Systems reduced the latter 45 firings; standard data reduction procedures were employed throughout. Details of the computational procedures and corrections which were applied are given in the following sections.

2. DELIVERED SPECIFIC IMPULSE AND THRUST COEFFICIENT

(U) The measured specific impulse is defined by the following equation

$$I_{sp}(\text{meas}) = \frac{F(\text{meas})}{\dot{W}_t} \qquad (1)$$

where:

F = (F1A + F1B)/2, outputs of dual bridge load cell, lb_f

$\dot{W}_t$ = $\dot{W}_o + \dot{W}_f$, weight flow, oxidizer and fuel, lb_m/sec

(U) The thrust coefficients were calculated from Equation (2) as follows:

$$C_{f(\text{meas})} = \frac{F(\text{meas})}{P_o\ A_t} \qquad (2)$$

where:

P_o = nozzle stagnation pressure, psia

A_t = throat area, in^2

(U) The nozzle stagnation pressure was obtained by two methods. The first method corrected the average of the two injector end pressure measurements for pressure loss to nozzle stagnation pressure using Figure C-1 (Reference 1). This method assumes that the gas velocity across the injector end pressure taps is zero and, therefore, they were reading injector end stagnation pressure. This was latter shown to be incorrect as measurements taken in the annular space between injector and chamber showed higher pressures. The second method used the nozzle entrance pressure, measured just upstream of the convergent section, which was corrected for static to stagnation pressure differences due to gas velocity. Both methods assume that combustion is complete at the nozzle entrance and flow in the nozzle is isentropic.

Reference 1. Altman, D., et al. Liquid Propellant Rockets, Princeton University Press, 1960.

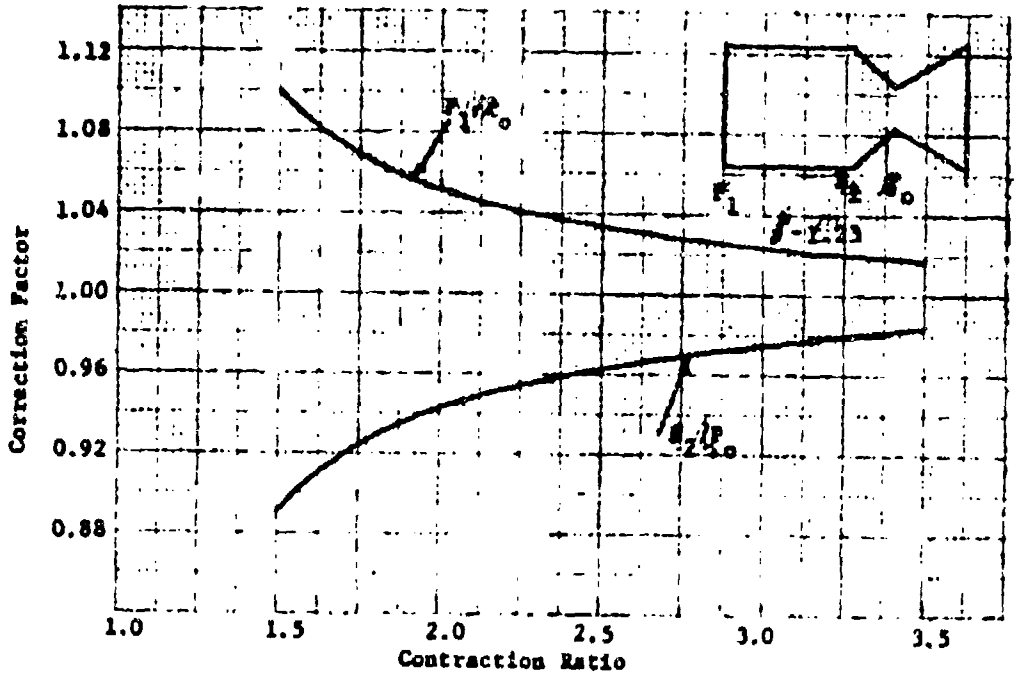

(U) Figure C-1. Correction Factors for Various Contraction Ratios (U)

2.1 SPECIFIC IMPULSE AND NOZZLE EFFICIENCY

(U) The theoretical I_{sp} and C* data for the pressure range of 200 psia to 300 psia and mixture ratios of 1.80 to 3.20 (O/F) were curve-fit and used in equation form to compute the theoretical I_{sp} and C*. The equations are as follows:

$$I_{sp}\ (pa = 13.2,\ \epsilon_n = 4.0) = -120.6491 + 379.7692\sqrt{\mu} - 123.4563\,\mu + 0.463773P - 0.00061575\,P^2 + 0.0017556P\sqrt{\mu} \qquad (3)$$

where: $\mu = \dot{W}_o/\dot{W}_f$

$$C^*_{(theo)} = 1496.4296 + 5838.8849\sqrt{\mu} - 2072.959\,\mu - 0.21772P - 0.0003875P^2 + 0.379418P\sqrt{\mu} \qquad (4)$$

(U) The specific impulse efficiency was computed as follows

$$\eta I_{sp} = \frac{F(meas.)}{\dot{W}_t\ I_{sp(theo.)}} \qquad (5)$$

with the theoretical I_{sp} being computed from equation (3).

(U) The nozzle efficiency was determined from the following:

$$\eta_{CF} = \frac{\eta_{Isp}}{\eta_{C*}} \qquad (6)$$

2.2 EXPECTED NOZZLE EFFICIENCY

(U) The expected η_{CF} for the 2/1 expansion ratio, 20 degree half-angle conical nozzle was 0.955. In the 4/1 expansion ratio configuration the expected η_{CF} was 0.965. Theoretical calculations were made for the various losses (kinetic, divergence and friction) in the 4/1 expansion ratio, 15 degree half-angle conical nozzle. These computations indicate a nozzle efficiency of 0.980 at a mixture ratio of 2.60 (O/F). Theoretical calculations for mixture ratios of 0.5 to 10.0 (O/F) show less than 0.3 percent variation in the theoretical thrust coefficient.

3. MEASURED CHARACTERISTIC VELOCITY EFFICIENCY

(U) The characteristic velocity was calculated as follows:

$$C^* = \frac{P_o A_t g_o}{\dot{W}_t} \qquad (7)$$

where:

P_o = nozzle stagnation pressure, psia
A_t = throat area, in^2
g = 32.2 lb_m-ft^2/lb_f-ft-sec^2
$\dot{W}_t$ = $\dot{W}_o + \dot{W}_f$, lb_m/sec

(U) During the facility checkout firings (1-10) the characteristic velocity also was computed using the following equation:

$$C^* = \frac{(PC\text{-}1)\ \beta\ A_t g}{\dot{W}T} \qquad (8)$$

where:

$$\beta = \frac{PC\text{-}3}{PC\text{-}1} \quad \text{(Correction Factor } P_1/P_o\text{)}$$

The correction factor for P_1/P_o is obtained from Figure C-1 and the ratio of PC-3/PC-1 for firings 9-17 was 1.071; this results in a β term value of 0.982.

(U) The flow rates used in both the measured I_{sp} and C* equations were obtained from single turbine flowmeters using water flow calibrations. Propellant temperatures were measured in the propellant tanks and lines and at the injector. Densities for both propellants were computed from AFRPL derived equations given as Equations (9) and (10).

$$\rho_f = 51.777139 - 0.0350405\ (T_f) \tag{9}$$

$$\rho_o = 95.8447 - 0.078033\ (T_o) \tag{10}$$

(U) The combustion efficiency was computed from the following equation:

$$\eta_{C*} = \frac{C^*\ (\text{measured})}{C^*\ (\text{theo.})} \tag{9}$$

where the theoretical C* is determined from equation (4).

4. INJECTION PARAMETERS

(U) The injector and system flow conductances were determined using the following general equation

$$K = \dot{Q}\sqrt{\rho/\Delta P} \tag{12}$$

where:,

Q = volumetric flow rate, ft^3/sec
ρ = propellant density, lb_m/ft^3
ΔP = measured pressure loss, psi

(U) The fuel injection pressure loss was measured between the entrance to the orifice (PIF-2) and the injector end chamber pressure (PC-1 or PC-2). The oxidizer injection pressure (PIO-1) was used to determine the ΔP_{io}. Injector conductance was calculated from the following equations.

$$KIJCF = \dot{Q}_f\ \sqrt{\rho f/\Delta P_{if}} \tag{13}$$

$$KIJCO = \dot{Q}_o\ \sqrt{\rho o/\Delta P_{io}} \tag{14}$$

(U) The orifice discharge coefficient is related to the injector conductance by the following equation:

$$C_{do} = 1.495\ \frac{KIJCO}{A_{io}} \tag{15}$$

$$Cd_f = 1.495\ \frac{KIJCF}{A_{if}} \tag{16}$$

APPENDIX D

TASK I INJECTOR/CHAMBER
DESIGN CRITERIA

1. DESIGN REQUIREMENTS/GOALS

(C) The injector and uncooled thrust chamber designs are based upon:

Nominal Thrust	~250,000 lb_f (vacuum)
Nominal Chamber Pressure	~300 psia
Exit Area Ratio	~4.0/1
Chamber Length	~36.5 inches
Propellants	~N_2O_4/UDMH
Nominal Mixture Ratio	~2.6
Mixture Ratio Range	~2.3 to 2.9
Specific Impulse Efficiency (Goal)	~90% (based on shifting equilibrium)
Thrust Range	~2.0/1
Chamber Pressure Range	~300 psia to 150 psia

2. TECHNICAL APPROACH

(U) The injector is a centrally located single element coaxial type in which throttling is accomplished by varying the propellant supply pressures. The combustion chamber and injector are designed for a factor of safety of 2 at ambient temperature and 100 percent over pressure. Standard 300 lb. ASA flanges are used on the injector and chamber where applicable. The run duration is limited by the capability of the uncooled heat-sink thrust chamber; this duration is sufficiently long to reach steady-state flows, chamber pressure and thrust so that engine performance can be documented.

(U) The coaxial injector incorporates replaceable fuel and oxidizer injection orifices to provide rapid change of the injector configuration with minimum down-time between tests. The design guideline for the injector is to maximize use of commercially available pipe components (flanges, elbows, tubing), using commonly available steels, with minimum modification.

(U) The fabrication process for the injectors and chambers specifies that welds be made in accordance with the ASME code for unfired pressure vessels. This eliminates some stress analysis which might otherwise be required. To reduce costs, fabrication will be conducted outside the normal aerospace industry. Only the critical dimensions will be inspected closely by aerospace standards and only industrial cleanliness standards are required.

3. GENERAL CHARACTERISTICS

3.1 Injector

(C) The initial development injector oxidizer orifice configuration is identical to that employed in the TRW Systems 1967 test program. The required flow rates are calculated as follows.

(C)

$$\dot{W}_t = \frac{250,000}{0.90 x 283.3} = 980 \text{ lb}_m/\text{sec}$$

$$\dot{W}_f = \frac{980}{1+2.6} = 272 \text{ lb}_m/\text{sec}$$

$$\dot{W}_o = 980 \left(1 - \frac{1}{3.6}\right) = 708 \text{ lb}_m/\text{sec}$$

3.1.1 Fuel Injection Orifice

(C) The initial fuel injection ΔP and oxidizer injection ΔP are chosen as 35 psi and 140 psi, respectively. The required fuel injection area for the design condition is calculated from the following equation.

$$A_f = \frac{Q_f \sqrt{\rho_f}}{96.30 \; C_d \sqrt{\Delta P_f}}$$

$$A_f = \frac{272}{49.5} \times \frac{\sqrt{49.5}}{96.30 \; C_d \sqrt{35}}$$

$$A_f = 10.05 \text{ in}^2$$

The fuel sheet thickness is calculated assuming that the clean-up diameter (D_p) on the oxidizer pintle assembly is 12.65 inches.

$$A_f = \pi/4 \left(D_{fm}^2 - D_p^2\right)$$

$$10.0 = \pi/4 \left(D_{fm}^2 - 160\right)$$

$$D_{fm}^2 = 160 + 12.8 = 172.8$$

$$D_{fm} = 13.15$$

$$t_{fsh} = \frac{13.15 - 12.65}{2} = 0.25 \text{ in.}$$

A tolerance of ± 0.010 inches in the fuel sheet thickness results in an area variaton of ± 4 percent and a pressure loss variation of ± 8 percent at the nominal mixture ratio.

3.1.2 Oxidizer Injection Orifices

(C) Thirty-six elements (primary orifice and secondary orifice) are equally spaced on the 12.65 in. pintle diameter. The required oxidizer injection area for the design condition is

(c)
$$A_o = \frac{Q_o\sqrt{\rho_o}}{96.30\ C_d\sqrt{\Delta P_o}}$$

$$A_o = \frac{708}{91} \times \frac{\sqrt{91}}{96.30\ C_d\sqrt{140}}$$

$$A_o = 13.40\ \text{in}^2$$

Nominally, 10 percent of the oxidizer flow is injected through the secondary orifices. Therefore, the area of the 36 primary orifices is

$$A_{op} = 0.9 \times 13.40 = 12.05\ \text{in}^2$$

(C) The unit spacing, UW, for 36 oxidizer elements on the 12.65 inch pintle diameter is

$$UW = \frac{12.65\pi}{36} = 1.105\ \text{inch}$$

The width of the primary orifice W_p, is selected as 0.45 inch; the width of the primary orifice plus the width of the secondary orifice W_s is given by the following relation

$$(W_p + W_s)/UW \cong 0.50$$

The width of the secondary orifice is

$$W_s = 0.50\ UW - 0.45\ \text{or}$$

$$W_s = 0.553 - 0.45 \cong 0.100$$

(C) The oxidizer injection pressure loss for the mixture ratio range of 2.3 to 2.9 is expected to vary from -8 percent to +6 percent assuming constant total flow rate over the mixture ratio range.

3.1.3 Internal Velocities and Pressure Drops

(C) The velocity through the 6-inch diameter fuel inlet pipe (schedule 80) is

$$V = \frac{\dot{W}\ (@\ O/F = 2.3)}{\rho A}$$

$$= \frac{288}{49.2}\left(\frac{144}{25.9}\right) = 32.6\ \text{ft/sec}$$

The pressure loss from the fuel inlet into the fuel manifold is

(C) $$\Delta P = \frac{K V^2 \rho}{2g}$$

where K = 1.5

$$\Delta P = \frac{1.5 \times (32.6)^2 \times 49.2}{64.4 \times 144}$$

$$\Delta P = 8.5 \text{ psi}$$

The pressure loss through the eight, 3-inch diameter holes is approximately

$$\Delta P = \frac{K V^2 \rho}{2g}$$

where $K = \left(\frac{1}{C_d}\right)^2 = \left(\frac{1}{.65}\right)^2 = 2.37$ and the velocity is given by

$$V = \frac{288}{49.2}\left(\frac{144}{56.5}\right) = 14.95 \text{ ft/sec}$$

$$\Delta P = \frac{2.37(14.95)^2 49.2}{64.4 \times 144} = 2.8 \text{ psi}$$

The expansion loss from the internal fuel annulus, based on nominal dimensions is

$$\Delta P = \frac{1.0(37)^2 49.2}{64.4 \times 144} = 7.3 \text{ psi}$$

(C) The remaining turning and contraction losses should be negligible because of the large areas and smooth inlets. The total fuel side pressure loss (excluding injection orifice) is approximately 20 psi.

(C) The velocity in the 8-inch diameter oxidizer tube (schedule 40) is

$$V = \frac{\dot{W}\ (@\ O/F = 2.9)}{\rho A}$$

$$V = \frac{729}{89.5} \times \left(\frac{144}{50.2}\right) = 23.4 \text{ ft/sec}$$

The friction loss and turning loss to the injection orifices is included in the oxidizer discharge coefficient which is determined experimentally.

3.2 Combustion Chamber

(C) The design point conditions are used to size the thrust chamber for a nozzle stagnation pressure, P_o, of 300 psia. The throat diameter is calculated from Equation 1 assuming a 94 percent C* efficiency.

(C)

$$D_t = \left[\frac{4\eta_{c*}\, C^*\, \dot{W}_t}{\pi\, P_o\, g_o}\right]^{1/2} \qquad (1)$$

$$D_t = \left[\frac{4 \times 0.94 \times 5596 \times 980}{\pi \times 300 \times 32.17}\right]^{1/2}$$

$$D_t = 26.10 \text{ in.}$$

The chamber diameter (39.0 in.) and length of chamber from impingement plane to throat (36.5 in.) are identical to the chamber tested in 1967.

4. STRESS ANALYSIS

(U) The structural elements of the engine were analyzed for a static pressure loading of 600 psi at ambient temperature with a minimum required margin of safety of one against pressure loading. The use of 300 lb ASA flanges were recommended for the injector inlets and chamber attach points. The margin of safety of three is defined for this design; therefore a margin of safety of one is derived for the 600 psi loading in the injector.

(U) The methods used in this analysis applied both membrane and discontinuity principles set forth by Timoshenko and Hetenyi. Thermal stresses and thermal shock (chamber-throat temperature of approximately 1000-1500°F inner surface and ambient temperature outer surface for 2-3 second firing) from temperature and temperature gradients might be of importance but were not considered except in the support structure.

(U) The analytical calculations are given in the following pages.

PREPARED P Y HSIEH

CHECKED

MODEL

REPORT NO.

CONFIDENTIAL

SECTION 1.2.6.3. CHAMBER HEAD

$p = 600$ PSI.

T = AMBIENT TEMP

MAT'L. T-1 STEEL A-181-II STEEL

$f_{tu} = 135000$ PSI. $f_{tu} = 70000$ PSI.

$f_{ty} = 100000$ PSI $f_{ty} = 36000$ PSI.

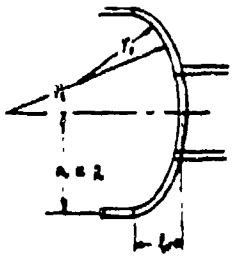

AT CENTER OF HEAD (WITHOUT NOZZLE)

$$\sigma_1 = \sigma_2 = \frac{p a^2}{2 h t}$$

$$= \frac{600 \cdot 19.75^2}{2 \cdot 9.875 \cdot 0.5}$$

$$= 23700 \text{ PSI.}$$

AT EQUATOR

$$\sigma_1 = 2.172 \frac{pR}{2t}$$

$$= 2.172 \cdot \frac{600 \cdot 19.75}{2 \cdot 0.5}$$

$$= 2.172 \cdot 11850$$

$$= 25700 \text{ PSI.}$$

$$\sigma_1 = 1.128 \frac{pR}{t}$$

$$= 1.128 \cdot 23700$$

$$= 26700 \text{ PSI.}$$

$$\text{M.S.} = \frac{135000}{26700} - 1 = 4.05$$

HEAD AT NOZZLE

$$\frac{a}{h} = 2$$

$$\frac{\text{NOZZLE RADIUS}}{a} = 0.4$$

$$\frac{r_2}{a} = 1.875$$

$$r_2 = 1.875 \cdot 19.75 = 37$$

$$\frac{r_1}{a} = 1.15$$

$$r_1 = 1.15 \cdot 19.75 = 32.4 \quad \text{USE } 37$$

CONFIDENTIAL
(This page is unclassified)

PREPARED D Y HSIEH
CHECKED
MODEL
REPORT NO.

UNCLASSIFIED

$\sin\alpha = \frac{r}{r_1} = \frac{8.75}{37} = 0.236$

$\alpha = 13.7°$

$\cot\alpha = 4.102$

$P = \frac{pr}{2}$

$= \frac{600 \cdot 8.75}{2}$

$= 2630$ LB/IN

$\beta = \sqrt[4]{3(1-\nu^2)\left(\frac{r_1}{t_H}\right)^2}$

$= \sqrt[4]{3(.91)\left(\frac{37}{0.5}\right)^2}$

$= 11.06$

$\beta^2 = 122$

$\beta^3 = 1350$

$K_1 = 1 - \frac{1-2\nu}{2\beta}\cot\alpha$

$= 1 - \frac{.4}{2 \cdot 11.06} 4.102$

$= .926$

$K_2 = 1 - \frac{1+2\nu}{2\beta}\cot\alpha$

$= 1 - \frac{1.6}{2 \cdot 11.06} 4.102$

$= .702$

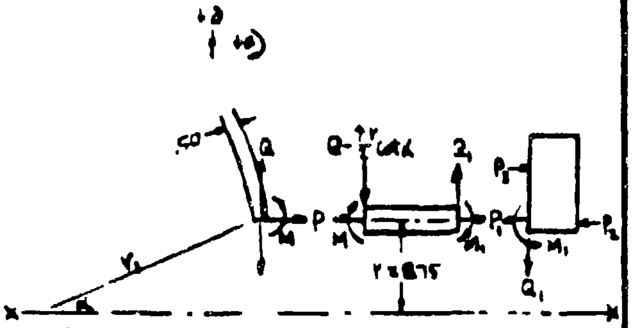
+δ
+θ
.50
Q
Q − pr/2 cot α
Q₁
P₃
P
M
M
P₁
M₁
M₁
P₂
Q₁
r = 8.75
r₁
α

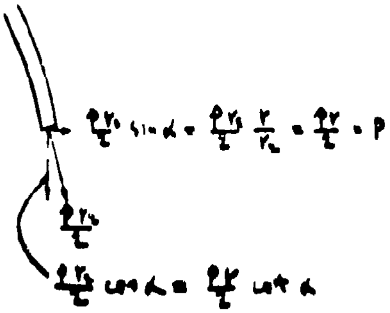
$\frac{pr_1}{2}\sin\alpha = \frac{pr_1}{2}\frac{r}{r_1} = \frac{pr}{2} = P$
$\frac{pr_1}{2}$
$\frac{pr_1}{2}\cos\alpha = \frac{pr}{2}\cot\alpha$

UNCLASSIFIED

PREPARED P. Y. HSIEH
CHECKED
MODEL
REPORT NO.

UNCLASSIFIED

$$\delta_H = \frac{P r_1^2}{2 E t_H}(1-\nu)\sin\alpha + \frac{M}{E t_H}\left(\frac{2\beta^2 \sin\alpha}{K_1}\right) + \frac{Q}{E t_H}\,\beta r_1 \sin^2\alpha\left(K_2 + \frac{1}{K_1}\right)$$

$$= \frac{600 \cdot 37^2}{2 \cdot 30 \cdot 10^6 \cdot 0.5}(.70)\,.276 + \frac{M}{30 \cdot 10^6 \cdot 0.5}\left(\frac{2 \cdot 122 \cdot .276}{.926}\right) + \frac{Q}{30 \cdot 10^6 \cdot 0.5}\,4.06 \cdot 37\,(.276)^2\left(.702 + \frac{1}{.926}\right)$$

$$= 10^{-6}(4520 + 4.15M + 7.7Q)$$

$$\theta_H = -\frac{M}{E t_H}\left(\frac{4\beta^3}{r_1 K_1}\right) - \frac{Q}{E t_H}(2\beta^2 \sin\alpha)\left(\frac{1}{K_1}\right)$$

$$= -\frac{M}{30 \cdot 10^6 \cdot .25}\left(\frac{4 \cdot 1350}{37 \cdot 0.926}\right) - \frac{Q}{30 \cdot 10^6 \cdot 0.5}(2 \cdot 122 \cdot .276)\left(\frac{1}{.926}\right)$$

$$= 10^{-6}(-10.5M - 4.15Q)$$

FOR NOZZLE

$$D = \frac{E t_n^3}{12(1-\nu^2)}$$

$$= \frac{30 \cdot 10^6 \cdot 1.5^3}{12(1-.09)}$$

$$= 9.28 \cdot 10^6$$

$$\lambda = \sqrt[4]{\frac{3(1-\nu^2)}{r^2 t_n^2}}$$

$$= \sqrt[4]{\frac{3(1-.09)}{8.75^2 \cdot 1.5^2}}$$

$$= .355$$

$$\lambda^2 = .126$$

$$\lambda^3 = .0448$$

$$\lambda \ell = .355 \cdot 4 = 1.42$$

$$\frac{r}{t_n} = \frac{8.75}{1.5} = 5.84$$

WITH $\lambda\ell = 1.42$ & $\frac{r}{t_n} = 5.84$,
THIS NOZZLE SECTION IS CONSIDERED AS RIGID RING

UNCLASSIFIED

PREPARED T. T. HSIEH
CHECKED
MODEL
REPORT NO.

$$M_T = M - \left(Q - \frac{2P}{\pi}\cot\alpha\right) 2.0 + M_1 - Q_1 \cdot 2.0$$

$$= M + M_1 - 2Q - 2Q_1 + 2630 \cdot 4.102$$

$$= M + M_1 - 2Q \cdot 2Q_1 + 10560$$

$$I_y = \frac{1}{12}\, 1.5 \cdot 4^3$$

$$= 8.0 \text{ IN}^4$$

$$\theta_n = \frac{M_T\, r^2}{E\, I_y}$$

$$= \frac{8.75^2}{30\cdot 10^6 \cdot 8}\left(M + M_1 - 2Q - 2Q_1 + 10560\right)$$

$$= 10^{-6}\left(0.319\, M + 0.319\, M_1 - 0.638\, Q - 0.638\, Q_1 + 3400\right)$$

NOZZLE DISPLACEMENT AT HEAD

$$(\delta_n)_H = \frac{\Delta P r^2}{A E} + 2.0\, \theta_n$$

$$= \frac{\left[600\cdot 4 - (Q - 2630\cdot 4.102) + Q_1\right] 8.75^2}{1.5\cdot 4\cdot 30\cdot 10^6} + 2\cdot 10^{-6}\left(0.319\, M + 0.319\, M_1 - 0.638\, Q - 0.638\, Q_1 + 3400\right)$$

$$= 10^{-6}\left(1020 - 0.425\, Q + 4600 + 0.425\, Q_1\right) + 10^{-6}\left(0.638\, M + 0.638\, M_1 - 1.276\, Q - 1.276\, Q_1 + 6800\right)$$

$$= 10^{-6}\left(0.638\, M + 0.638\, M_1 - 1.701\, Q - 0.851\, Q_1 + 12320\right)$$

NOZZLE DISPLACEMENT AT FLANGE RING

$$(\delta_n)_R = \frac{\Delta P r^2}{A E} - 2.0\, \theta_n$$

$$= 10^{-6}\left(1020 - 0.425\, Q + 4600 + 0.425\, Q_1\right) - 10^{-6}\left(0.638\, M + 0.638\, M_1 - 1.276\, Q - 1.276\, Q_1 + 6800\right)$$

$$= 10^{-6}\left(-0.638\, M - 0.638\, M_1 + 0.851\, Q + 1.701\, Q_1 - 1180\right)$$

PREPARED P Y HSIEH
CHECKED
MODEL
REPORT NO.

UNCLASSIFIED

FLANGE RING

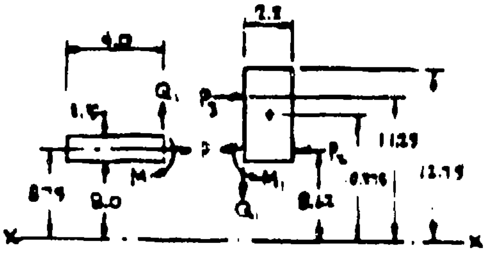

$Y_{cg} = 10.775$

$P_1 = \frac{600 \cdot 8.75}{2}$

$= 2630$ LB/IN

$P_2 = (9.25 - 8)\,3000$

$= 3750$ LB/IN

$P_3 = \frac{1}{11.25}\,(3750 \cdot 8.62 + 2630 \cdot 8.75)$

$= 4920$ LB/IN

FOR 20 - $1\frac{1}{4}$ ⌀ BOLTS $A_{bolt} = 20 \cdot .893 = 17.86\ \text{in}^2$

BOLT STRESS $\sigma_t = \frac{4920 \cdot 2\pi \cdot 11.25}{17.86}$

$= 19500$ psi.

$M_y = \frac{1}{Y_{cg}}\left[\,Y\,(1.625\,P_1 - M_1 - 1.1\,Q_1) + Y_2\,(1.75\,P_2) + Y_3\,(.875\,P_3)\right]$

$= \frac{1}{10.775}\left[\,8.75\,(1.625 \cdot 2630 - M_1 - 1.1\,Q_1) + 8.62\,(1.75 \cdot 3750) + 11.25\,(.875 \cdot 4920)\right]$

$= 3600 - 0.842\,M_1 - 0.928\,Q_1 + 5480 + 4660$

$= -0.842\,M_1 - 0.928\,Q_1 + 13740$

$I_y = \frac{1}{12}\,4.75 \cdot 2.2^3$

$= 4.2\ \text{in}^4$

UNCLASSIFIED

PREPARED P Y HSIEH
CHECKED
MODEL

UNCLASSIFIED

$$\theta_R = \frac{M_P r_{cg}^2}{E I_y}$$

$$= \frac{10.375^2}{30\cdot10^6\cdot4.2}(-0.842 M_1 - 0.928 Q_1 + 13740)$$

$$= 10^{-6}(-0.72 M_1 - 0.794 Q_1 + 11750)$$

$$\delta_R = \frac{\Sigma P r r_{cg}}{AE} + 1.1\,\theta_R$$

$$= \frac{(605\cdot2.2\cdot8.0 - Q\cdot9.75)10.375}{2.2\cdot4.79\cdot30\cdot10^6} + 1.1(-0.72 M_1 - 0.794 Q_1 + 11750)10^{-6}$$

$$= 10^{-6}(350 - 0.29 Q) + 10^{-6}(-0.793 M_1 - 0.873 Q_1 + 12950)$$

$$= 10^{-6}(-0.793 M_1 - 1.163 Q_1 + 13300)$$

$$\delta_M = (\delta_u)_M$$

$$10^{-6}(4520 + 4.15 M + 2.7 Q) = 10^{-6}(0.678 M + 0.678 M_1 - 1.701 Q - 0.851 Q_1 + 12320)$$

$$3.512 M + 4.401 Q - 0.678 M_1 + 0.851 Q_1 = 1800 \qquad (1)$$

$$\theta_M = \theta_u$$

$$10^{-6}(-10.5 M - 4.15 Q) = 10^{-6}(0.314 M + 0.314 M_1 - 0.678 Q - 0.678 Q_1 + 3400)$$

$$-10.819 M - 3.512 Q - 0.314 M_1 + 0.678 Q_1 = 3400 \qquad (2)$$

$$(\delta_u)_R = \delta_R$$

$$10^{-6}(-0.678 M - 0.678 M_1 + 0.851 Q + 1.701 Q_1 - 1280) = 10^{-6}(-0.793 M_1 - 1.163 Q_1 + 13300)$$

$$-0.678 M + 0.851 Q + 0.155 M_1 + 2.864 Q_1 = 14580 \qquad (3)$$

$$\theta_u = \theta_R$$

$$10^{-6}(0.319 M + 0.314 M_1 - 0.678 Q - 0.678 Q_1 + 1400) = 10^{-6}(-0.72 M_1 - 0.794 Q_1 + 11750)$$

$$0.319 M - 0.678 Q - 1.039 M_1 + 0.156 Q_1 = 10350 \qquad (4)$$

UNCLASSIFIED

$-3.512\,M - 1.140\,Q - 0.1036\,M_1 + 0.2015\,Q_1 = 1105$ (4)

(1)+(4) $3.261\,Q - 0.7446\,M_1 + 1.0585\,Q_1 = 8905$ (5)

$-0.615\,M - 0.207\,Q - 0.0188\,M_1 + 0.0376\,Q_1 = 200$ (2)

(1)-(2) $1.098\,Q + 0.1738\,M_1 + 2.8274\,Q_1 = 14380$ (6)

$-0.319\,M + 0.478\,Q + 0.077\,M_1 + 1.472\,Q_1 = 7290$ (3)

(3)+(4) $-0.217\,Q + 1.078\,M_1 + 1.588\,Q_1 = 15640$ (7)

$1.098\,Q - 0.260\,M_1 + 0.343\,Q_1 = 2885$ (5)

(5)-(6) $-0.4178\,M_1 - 2.4844\,Q_1 = -11495$ (8)

$0.217\,Q + 0.073\,M_1 + 0.570\,Q_1 = 2895$ (6)

(6)+(7) $1.151\,M_1 + 2.158\,Q_1 = 18535$ (9)

$0.4178\,M_1 + 0.775\,Q_1 = 6660$

(8)+(9) $-1.7094\,Q_1 = -4835$

$Q_1 = 2830$ LB/IN

FROM (9) $M_1 = \dfrac{18535 - 2.158(2830)}{1.151}$

$= 10800$ IN-LB/IN

FROM (5) $Q = \dfrac{8905 - 1.0585(2830) + 0.7446(10800)}{3.261}$

$= 4260$ LB/IN

FROM (6) $M = \dfrac{3150 - 0.156(2830) - 1.079(10800) + 0.418(4260)}{0.319}$

$= -1815$ IN-LB/IN

PREPARED I Y HSIEH
CHECKED
MODEL
REPORT NO.

UNCLASSIFIED

STRESSES IN HEAD

$$\sigma_1 = \frac{p r_1}{2 t_h} \pm \frac{6M}{t_h^2} + \frac{Q \cos\alpha}{t_h}$$

$$= \frac{600 \cdot 37}{2 \cdot 0.5} \pm \frac{6(-1819)}{0.5^2} + \frac{4260 \cdot 0.972}{0.5}$$

$$= 22200 \pm 43500 + 8270$$

$$= 73970 \text{ psi. MAX. OUTER SURFACE}$$

$$\sigma_2 = p\left(r_2 - \frac{r_2^2}{2 r_1}\right)\frac{1}{t_h} + \frac{Q}{t_h}\left(\frac{1}{K_1} + \frac{K_1 + K_2}{2}\right)\beta \sin\alpha + \frac{M}{t_h r_1}\left(\frac{2\beta^2}{K_1}\right) \pm \nu \frac{6M}{t_h^2}$$

$$= 600\left(37 - \frac{37^2}{2 \cdot 37}\right)\frac{1}{0.5} + \frac{4260}{0.5}\left(\frac{1}{.926} + \frac{.926 + .978}{2}\right) 11.06 \cdot 0.236 - \frac{1815}{0.5 \cdot 37}\left(\frac{2 \cdot .172}{.926}\right) \pm 0.3(43500)$$

$$= 11100 + 42100 - 25800 \pm 13000$$

$$= 40400 \text{ psi. MAX.}$$

STRESSES IN NOZZLE

$$M_T = M + M_1 - 2Q - 2Q_1 + 10560$$

$$= -1819 + 10900 - 2 \cdot 4260 - 2 \cdot 2830 + 10560$$

$$= 5365$$

$$\sigma_b = \frac{M_T r \alpha'}{I_T}$$

$$= \frac{5365 \cdot 8.75 (\pm 2.0)}{8.0}$$

$$= \pm 11{,}720 \text{ psi.}$$

$$\sigma_t = \frac{\Sigma P r}{2A}$$

$$= \frac{[600 \cdot 4 - (4260 - 10560) + 2830]\, 8.75}{2 \cdot 1.5 \cdot 4}$$

$$= 8400 \text{ psi.}$$

$$\sigma_{TOTAL} = 11720 + 8400 = 20120 \text{ psi. AT HEAD END}$$

$$= -11720 + 8400 = -3320 \text{ psi. AT FLANGE END}$$

UNCLASSIFIED

PREPARED P Y HSIEH

CHECKED

MODEL

REPORT NO.

UNCLASSIFIED

STRESSES IN FLANGE

$M_T = -0.842\, M_1 - 0.928\, Q_1 + 13740$

$= -0842(10800) - 0928(2830) + 13740$

$= 2020$

$\sigma_b = \dfrac{M_T\, Y_{cg}\, x'}{I_y}$

$= \dfrac{2020 \cdot 10.375 \cdot 1.1}{42}$

$= 5490$ psi.

$\sigma_t = \dfrac{1\, p\, r}{2\, A}$

$= \dfrac{600 \cdot 22.1}{2 \cdot 16} - \dfrac{2830 \cdot .875}{4.75}$

$= -680$ psi.

$\sigma_{TOTAL} = 5490 - 680$

$= 4800$ psi

UNCLASSIFIED

SYSTEMS 1441 REV. 8-67

PREPARED P Y HSIEH
CHECKED
MODEL
REPORT NO.

UNCLASSIFIED

TO SIZE THE ASA FLANGE, ANALYZING THE 300 LB LONG WELD NECK WITH FULL NOZZLE LENGTH

$$\theta_H = \frac{M_1}{\lambda D} - \frac{Q_1}{2D\lambda^2}$$

$$= \frac{M_1}{.155 \cdot 938 \cdot 10^6} - \frac{Q_1}{2.938\ 10^6 \cdot 0.024}$$

$$= 10^{-6}(0.314\ M_1 - 0.428\ Q_1)$$

$$\delta_H = \frac{pr^2}{Et_n}\left(1 - \frac{\nu}{2}\right) - \frac{M_1}{2D\lambda^2} + \frac{Q_1}{2D\lambda^3}$$

$$= \frac{400 \cdot 4.75^2}{30 \cdot 10^6 \cdot .19}\left(1 - \frac{.3}{2}\right) - \frac{M_1}{2.938 \cdot 10^6 \cdot 0.026} + \frac{Q_1}{2.938 \cdot 10^6\ 0.0048}$$

$$= 10^{-6}(866 - 0.428\ M_1 + 1.2\ Q_1)$$

SETTING $\theta_B = \theta_H$ AND $\delta_B = \delta_H$

$$10^{-6}(-0.72\ M_1 - 0.744\ Q_1 + 11750) = 10^{-6}(0.314\ M_1 - 0.428\ Q_1)$$

$$1.034\ M_1 + 0.366\ Q_1 = 11750$$

$$10^{-6}(-0.743\ M_1 - 1.167\ Q_1 + 13700) = 10^{-6}(866 - 0.428\ M_1 + 1.2\ Q_1)$$

$$-0.366\ M_1 - 2.367\ Q_1 = -12834$$

$$1.034\ M_1 - 6.68\ Q_1 = -35200$$

$$-6.314\ Q_1 = -23450$$

$$Q_1 = 3720 \text{ LB/IN}$$

$$M_1 = \frac{11750 - 0.366(3720)}{1.034}$$

$$= 10050 \text{ IN-LB/IN}$$

UNCLASSIFIED

PREPARED P Y HSIEH

CHECKED

MODEL

REPORT NO.

UNCLASSIFIED

STRESSES IN NOZZLE

$$\sigma_1 = \frac{pr}{2t_n} \pm \frac{6M_1}{t_n^2}$$

$$= \frac{600 \cdot 9.75}{2 \cdot 1.5} \pm \frac{6(10050)}{1.5^2}$$

$$= 1750 \pm 26800$$

$= 28550$ PSI MAX, OUTER SURFACE

$$\sigma_2 = \frac{pr}{t_n} + \frac{2Q_1}{t_n}\lambda r - \frac{2M}{t_n}\lambda^2 r \pm \nu \frac{6M_1}{t_n^2}$$

$$= 3500 + \frac{2(7720)}{1.5} 0.155 \cdot 9.75 - \frac{2(10050)}{1.5} 0.116 \cdot 9.75 \pm 0.3(26800)$$

$$= 3500 + 15400 - 14800 \pm 8040$$

$= 12140$ PSI MAX.

STRESSES IN FLANGE RING

$$M_r = -0.842\ M_1 - 0.928\ Q_1 + 17740$$

$$= -0.842(10050) - 0.928(7720) + 19940$$

$$= 1820$$

$$\sigma_b = \frac{M_r\ r_{cur}\ x'}{I_y}$$

$$= \frac{1820 \cdot 10.775 \cdot 1.1}{42}$$

$= 4950$ PSI

$$\sigma_t = \frac{\Sigma P r}{2A}$$

$$= \frac{600 \cdot 22 \cdot 8 - 7720 \cdot 9.75}{2 \cdot 22 \cdot 4.75}$$

$= -1050$ PSI.

$$\sigma_{TOTAL} = 4950 - 1050$$

$= 3900$ PSI

UNCLASSIFIED

PREPARED P Y HSIEH
CHECKED
MODEL
REPORT NO.

UNCLASSIFIED

CHAMBER HEAD - WITH WELD BUILT-UP AT NOZZLE

$\sin\alpha = \frac{r}{r_1} = \frac{8.75}{37} = 0.236$

$\alpha = 13.7°$

$\cot\alpha = 4.102$

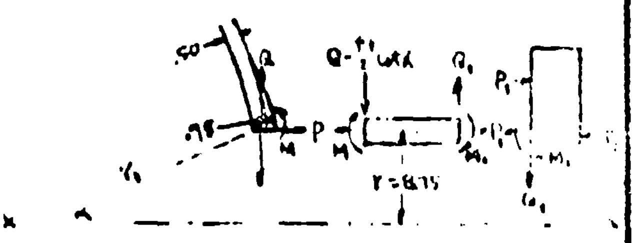
.50
Q
.75
M
P
M
$Q - \frac{pr}{2}\cot\alpha$
Q_1
P_1
M_1
$r = 8.75$
r_1
α
Q_1

$P = \frac{pr}{2}$

$= [illegible] \cdot 8.75$

$= 2630$ lb/in

$\beta = \sqrt[4]{3(1-\nu^2)\left(\frac{r_1}{t_n}\right)^2}$

$= \sqrt[4]{3(.91)\left(\frac{37}{.75}\right)^2}$

$= ~~[illegible]~~\ 9.02$

$\beta^2 = ~~[illegible]~~\ 81.4$

$\beta^3 = ~~[illegible]~~\ 735$

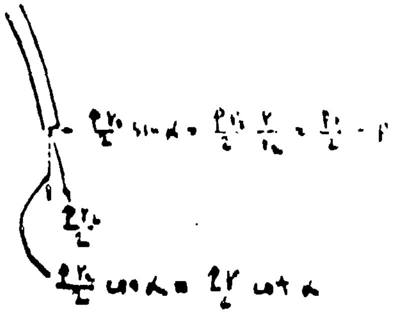
$\frac{pr_1}{2}\sin\alpha = \frac{pr_1}{2}\frac{r}{r_1} = \frac{pr}{2} = P$
$\frac{pr_1}{2}$
$\frac{pr_1}{2}\cos\alpha = \frac{pr}{2}\cot\alpha$

$K_1 = 1 - \frac{1-2\nu}{2\beta}\cot\alpha$

$= 1 - \frac{.4}{2 \cdot 9.02} 4.102$

$= ~~[illegible]~~\ .909$

$K_2 = 1 - \frac{1+2\nu}{2\beta}\cot\alpha$

$= 1 - \frac{1.6}{2 \cdot 9.02} 4.102$

$= ~~.762~~\ .636$

UNCLASSIFIED

PREPARED D Y HSIEH
CHECKED
MODEL
REPORT NO.

$$\delta_H = \frac{p r_1^2}{2E t_H}(1-\nu)\sin\alpha + \frac{M}{E t_H}\left(\frac{2\beta^2 \sin\alpha}{K_1}\right) + \frac{Q}{E t_H}\beta r_1 \sin^2\alpha\left(K_2+\frac{1}{K_1}\right)$$

$$= \frac{620\cdot 37^2}{2\cdot 10\cdot 10^6\cdot \underset{0.75}{\cancel{\cdots}}}(.70)\,0.236 + \frac{M}{30\cdot 10^6\cdot\underset{0.75}{\cancel{\cdots}}}\left(\frac{2\cdot\overset{969}{\cancel{\cdots}}\cdot 0.236}{\underset{.909}{\cancel{\cdots}}}\right) + \frac{Q}{30\cdot 10^6\cdot\underset{0.75}{\cancel{\cdots}}}\overset{9.02}{\cancel{\cdots}}\cdot 37(.236)^2\left(\frac{.616}{\cancel{\cdots}}+\frac{1}{\underset{.909}{\cancel{\cdots}}}\right)$$

$$= 10^{-6}\left(\underset{3020}{\cancel{\cdots}} + \underset{1.88}{\cancel{\cdots}}M + \underset{1.44}{\cancel{\cdots}}Q\right)$$

$$\theta_H = -\frac{M}{E t_H}\left(\frac{4\beta^3}{r_1 K_1}\right) - \frac{Q}{E t_H}(2\beta^2\sin\alpha)\left(\frac{1}{K_1}\right)$$

$$= -\frac{M}{30\cdot 10^6\cdot\underset{0.75}{\cancel{\cdots}}}\left(\frac{4\cdot\overset{915}{\cancel{\cdots}}}{37\cdot\underset{0.909}{\cancel{\cdots}}}\right) - \frac{Q}{30\cdot 10^6\cdot\underset{0.75}{\cancel{\cdots}}}\left(2\cdot\overset{81.6}{\cancel{\cdots}}\cdot 0.236\right)\left(\frac{1}{\underset{.909}{\cancel{\cdots}}}\right)$$

$$= 10^{-6}\left(-\underset{7.91}{\cancel{\cdots}}M - \underset{1.88}{\cancel{\cdots}}Q\right)$$

~~END NOZZLE~~

~~[illegible]~~

~~[illegible]~~

~~[illegible]~~

~~[illegible]~~

~~[illegible]~~

~~[illegible]~~

~~[illegible]~~

~~[illegible]~~

~~[illegible]~~

~~[illegible]~~ ,

~~THIS NOZZLE SECTION IS CONSIDERED AS [illegible]~~

PREPARED P Y Hsieh
CHECKED
MODEL
REPORT NO.

UNCLASSIFIED

~~[illegible]~~

~~[illegible]~~

$\partial_H = (\partial_u)_H$

$10^{-4}(\overset{3020}{\cancel{\;}} + \overset{1.88}{\cancel{\;}}M + \overset{1.64}{\cancel{\;}}Q) = 10^{-4}(0.638\,M + 0.638\,M_1 - 1.701\,Q - 0.851\,Q_1 + 12330)$

$\overset{1.242}{\cancel{\;}}M + \overset{3.141}{\cancel{\;}}Q - 0.638\,M_1 + 0.851\,Q_1 = \cancel{\;}\,9700$ (1)

$\theta_H = \theta_u$

$10^{-4}(-\overset{389}{\cancel{\;}}M - \overset{1.88}{\cancel{\;}}Q) = 10^{-4}(0.319\,M + 0.319\,M_1 - 0.638\,Q - 0.638\,Q_1 + 3400)$

$\overset{4.209}{\cancel{\;}}M - \overset{1.242}{\cancel{\;}}Q - 0.319\,M_1 + 0.638\,Q_1 = 3400$ (2)

$(\partial_u)_a = \partial_H$

$10^{-4}(-0.638\,M - 0.638\,M_1 + 0.851\,Q + 1.701\,Q_1 - 1120) = 10^{-4}(-0.793\,M_1 - 1.163\,Q_1 + 13700)$

$-0.638\,M + 0.851\,Q + 0.155\,M_1 + 2.864\,Q_1 = 14580$ (3)

$\theta_H = \theta_a$

$10^{-4}(0.319\,M + 0.319\,M_1 - 0.638\,Q - 0.638\,Q_1 + 3400) = 10^{-4}(-0.72\,M_1 - 0.794\,Q_1 + 11750)$

$0.319\,M - 0.638\,Q + 1.039\,M_1 + 0.156\,Q_1 = 8350$ (4)

UNCLASSIFIED

$-\overset{1.298}{\cancel{3.544}} M - \overset{0.366}{\cancel{\text{[illegible]}}} Q - \overset{0.094}{\cancel{\text{[illegible]}}} M_1 + \overset{0.188}{\cancel{0.2025}} Q_1 = \overset{1003}{\cancel{1405}}$ (4)

(1)+(2) $\overset{2.775}{\cancel{3.044}} Q - \overset{0.731}{\cancel{\text{[illegible]}}} M_1 + \overset{1.019}{\cancel{1.0584}} Q_1 = \overset{10303}{\cancel{9405}}$ (5)

$-0.678 M - \overset{0.189}{\cancel{0.207}} Q - \overset{0.0483}{\cancel{\text{[illegible]}}} M_1 + \overset{0.499}{\cancel{\text{[illegible]}}} Q_1 = \overset{519}{\cancel{\text{[illegible]}}}$ (2)

(1)-(2) $\overset{1.039}{\cancel{\text{[illegible]}}} Q + \overset{0.2033}{\cancel{\text{[illegible]}}} M_1 + \overset{2.267}{\cancel{\text{[illegible]}}} Q_1 = \overset{14065}{\cancel{\text{[illegible]}}}$ (6)

$-0.319 M + 0.435 Q + 0077 M_1 + 1.472 Q_1 = 7290$ (3)

(3)+(4) $-0.213 Q + 1.16 M_1 + 1.588 Q_1 = 15640$ (7)

$\overset{1.039}{\cancel{\text{[illegible]}}} Q - \overset{0.774}{\cancel{\text{[illegible]}}} M_1 + \overset{0.39}{\cancel{\text{[illegible]}}} Q_1 = \overset{3960}{\cancel{\text{[illegible]}}}$ (5)

(5)-(6) $-\overset{0.4773}{\cancel{\text{[illegible]}}} M_1 - \overset{2.377}{\cancel{\text{[illegible]}}} Q_1 = -\overset{10205}{\cancel{\text{[illegible]}}}$ (8)

$0.213 Q + \overset{1.0416}{\cancel{\text{[illegible]}}} M_1 + \overset{0.368}{\cancel{\text{[illegible]}}} Q_1 = \overset{2880}{\cancel{\text{[illegible]}}}$ (6)

(6)+(7) $\overset{1.1590}{\cancel{\text{[illegible]}}} M_1 + \overset{2.156}{\cancel{\text{[illegible]}}} Q_1 = \overset{18520}{\cancel{\text{[illegible]}}}$ (9)

$\overset{0.4773}{\cancel{0.4498}} M_1 + \overset{0.933}{\cancel{\text{[illegible]}}} Q_1 = \overset{7640}{\cancel{\text{[illegible]}}}$

(8)+(9) $-\overset{1.489}{\cancel{\text{[illegible]}}} Q_1 = -\overset{2565}{\cancel{\text{[illegible]}}}$

$Q_1 = \overset{1725}{\cancel{2730}}$ LB/IN

FROM (9) $M_1 = \dfrac{\overset{18520}{\cancel{\text{[illegible]}}} - \overset{2.156}{\cancel{\text{[illegible]}}}\left(\overset{1725}{\cancel{\text{[illegible]}}}\right)}{\overset{1.1590}{}}$

$= \overset{12800}{\cancel{\text{[illegible]}}}$ IN-LB/IN

FROM (5) $Q = \dfrac{\overset{10303}{\cancel{\text{[illegible]}}} - \overset{1.039}{\cancel{\text{[illegible]}}}\left(\overset{1725}{\cancel{\text{[illegible]}}}\right) + \overset{0.731}{\cancel{\text{[illegible]}}}\left(\overset{12800}{\cancel{\text{[illegible]}}}\right)}{\overset{2.775}{\cancel{\text{[illegible]}}}}$

$= \overset{6440}{\cancel{\text{[illegible]}}}$ LB/IN

FROM (6) $M = \dfrac{3357 - 0.156\left(\overset{1725}{\cancel{\text{[illegible]}}}\right) - 1.039\left(\overset{12800}{\cancel{\text{[illegible]}}}\right) + 0.435\left(\overset{6440}{\cancel{\text{[illegible]}}}\right)}{0.319}$

$= -\overset{3230}{\cancel{1645}}$ IN-LB/IN

PREPARED P Y HSIEH
CHECKED
MODEL
REPORT NO.

UNCLASSIFIED

STRESSES IN HEAD

$$\sigma_1 = \frac{pr_1}{2t_n} \mp \frac{6M}{t_n^2} + \frac{Q\cos\alpha}{t_n}$$

$$= \frac{600\cdot 33}{2\cdot 0.75} \mp \frac{6(-\overset{3235}{\cancel{\ }})}{0.75^2} + \frac{\overset{6440}{\cancel{4440}}\cdot 0.472}{0.75}$$

$$= \overset{14800}{\cancel{\ }} \pm \overset{34600}{\cancel{\ }} + \overset{3950}{\cancel{\ }}$$

$$= \overset{57850}{\cancel{74470}} \text{ psi. MAX. OUTER SURFACE} \qquad M.S. = \frac{175000}{74470} - 1 = 1.35$$

$$\sigma_2 = p\left(r_2 - \frac{r_2^2}{2r_1}\right)\frac{1}{t_n} + \frac{Q}{t_n}\left(\frac{1}{K_1} + \frac{K_1+K_2}{2}\right)\beta\sin\alpha + \frac{M}{t_n r_1}\left(\frac{2\beta^2}{K_1}\right) \mp \nu\frac{6M}{t_n^2}$$

$$= 600\left(33 - \frac{33^2}{2\cdot 17}\right)\frac{1}{0.75} + \frac{\overset{6440}{\cancel{4440}}}{0.75}\left(\frac{1}{.126} + \frac{.126+0.70}{2}\right)11.06\cdot 0.236 - \frac{\overset{3235}{\cancel{\ }}}{0.75\cdot 17}\left(\frac{2\cdot .122}{.126}\right) \pm 0.3\left(\overset{34600}{\cancel{\ }}\right)$$

$$= \overset{7400}{\cancel{11100}} + \overset{41900}{\cancel{42100}} - \overset{30600}{\cancel{35000}} \pm \overset{10300}{\cancel{13000}}$$

$$= \overset{29600}{\cancel{40400}} \text{ psi. MAX.}$$

STRESSES IN NOZZLE

$$M_T = M + M_1 - 2Q - 2Q_1 + 10560$$

$$= -\overset{3230}{\cancel{\ }} + \overset{12800}{\cancel{10900}} - 2\cdot\overset{6440}{\cancel{4440}} - 2\cdot\overset{1775}{\cancel{2030}} + 10560$$

$$= \cancel{5765}\ 3800$$

$$\sigma_b = \frac{M_T r \alpha'}{I_1}$$

$$= \frac{\overset{3800}{\cancel{\ }}\cdot 8.75(\pm 2.0)}{8.0}$$

$$= \pm\overset{8300}{\cancel{\ }} \text{ psi.}$$

$$\sigma_\phi = \frac{\Sigma P r}{2A}$$

$$= \frac{\left[600\cdot 4 - \left(\overset{6440}{\cancel{4440}} - 10560\right) + \overset{1775}{\cancel{2030}}\right]8.75}{2\cdot 1.5\cdot 4}$$

$$= \overset{6000}{\cancel{8400}} \text{ psi.}$$

$$\sigma_{TOTAL} = \overset{8300}{\cancel{\ }} + \overset{6000}{\cancel{8400}} = \overset{14300}{\cancel{\ }} \text{ psi. AT HEAD END} \qquad M.S. = \frac{70000}{14300} - 1 = 3.90$$

$$= -\overset{8300}{\cancel{\ }} + \overset{6000}{\cancel{8400}} = -\overset{2300}{\cancel{\ }} \text{ psi. AT FLANGE END}$$

UNCLASSIFIED

PREPARED B Y HSIEH

CHECKED

MODEL

REPORT NO.

UNCLASSIFIED

STRESSES IN FLANGE

$$M_Y = -0.842\,M_1 - 0.928\,Q_1 + 13740$$

$$= -0.842\left(\overset{12900}{\cancel{+0800}}\right) - 0.928\left(\overset{14775}{\cancel{+840}}\right) + 13740$$

$$= \cancel{9040}\ 1740$$

$$\sigma_b = \frac{M_Y\,Y_{cg}\,K'}{I_Y}$$

$$= \frac{\overset{1740}{\cancel{3020}} \cdot 10.375 \cdot 1.1}{4.2}$$

$$= \overset{3640}{\cancel{6000}}\ \text{psi.}$$

$$\sigma_t = \frac{\ell\,p\,r}{2A}$$

$$= \frac{600 \cdot 22 \cdot 8 - \overset{1725}{\cancel{2040}} \cdot 5.75}{2 \cdot 12 \cdot 4.75}$$

$$= -\overset{110}{\cancel{600}}\ \text{psi.}$$

$$\sigma_{TOTAL} = \overset{3640}{\cancel{5400}} - \overset{110}{\cancel{600}}$$

$$= \overset{3530}{\cancel{4800}}\ \text{psi.}$$

UNCLASSIFIED

PREPARED ________________

CHECKED ________________

MODEL ________________

REPORT NO.

UNCLASSIFIED

SECTION 4 CHAMBER-CONE

$p = 600$ psi

T = AMBIENT TEMP

MATL T-1 STEEL

$f_{tu} = 115000$ psi.

$f_{ty} = 100000$ psi.

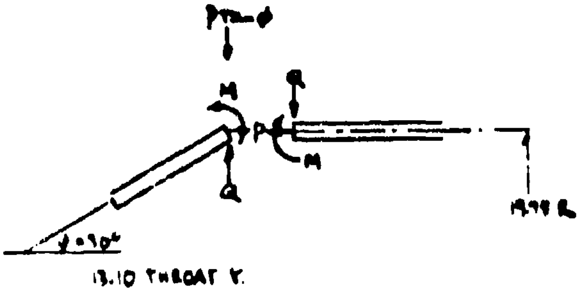
$P\tan\phi$
M
Q
P
M
Q
19.75 R
$\phi = 30°$
13.10 THROAT r.

CONE

$$P = \frac{p\pi(R^2 - r^2)}{2\pi R}$$

$$= \frac{600(19.75^2 - 13.10^2)}{2 \cdot 19.75}$$

$$= 3310 \text{ LB/IN}$$

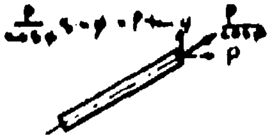
$\frac{P}{\cos\phi}\sin\phi = P\tan\phi$
$\frac{P}{\cos\phi}$
P

$$R_2 = \frac{R}{\cos\phi} = \frac{19.75}{\cos 30°} = 22.8$$

$$\beta = \sqrt[4]{3(1-\nu^2)\left(\frac{R_2}{t}\right)^2}$$

$$= \sqrt[4]{3(1-.3^2)\left(\frac{22.8}{.5}\right)^2}$$

$$= 8.68$$

β^2 75.2

$\beta^3 = 653$

$$K_1 = 1 - \frac{1-2\nu}{2\beta}\cot\phi$$

$$= 1 - \frac{1-.6}{2 \cdot 8.68} 1.732$$

$$= 0.96$$

$$K_2 = 1 - \frac{1+2\nu}{2\beta}\cot\phi$$

$$= 1 - \frac{1+.6}{2 \cdot 8.68} 1.732$$

$$= 0.84$$

UNCLASSIFIED

PREPARED P Y HSIEH
CHECKED
MODEL
REPORT NO.

MEMBRANE STRESSES

$$\sigma_1' = \frac{P}{t\cos\phi}$$

$$= \frac{3310}{0.5\cos 30^\circ}$$

$$= 7640 \text{ psi.}$$

$$\sigma_2' = \frac{pR}{t\cos\phi}$$

$$= \frac{600\cdot 1975}{0.5\cos 30^\circ}$$

$$= 27400 \text{ psi.}$$

$$\delta_c = \frac{R}{E}(\sigma_2' - \nu\sigma_1') + \frac{M}{Et}\left(\frac{2\beta^2\sin\phi}{K_1}\right) + (Q - P\tan\phi)\frac{\beta R_2\sin^2\phi}{Et}\left(K_2 + \frac{1}{K_1}\right)$$

$$= \frac{1975}{30\cdot10^6}(27400 - 0.3\,7640) + \frac{M}{30\cdot10^6\cdot .85}\left(\frac{2\cdot 15.2\cdot .85}{.946}\right) + (Q - 3310\cdot 0.578)\frac{3.08\cdot 22.8\cdot .85^2}{30\cdot10^6\cdot .85}\left(0.64 + \frac{1}{.96}\right)$$

$$= 10^{-6}(16500 + 5.22\,M + 6.2\,Q - 11850)$$

$$= 10^{-6}(5.22\,M + 6.2\,Q + 4650)$$

$$\theta_c = -\frac{2pR\sin\phi(1 - \frac{1}{2}\nu)}{Et} - \frac{M}{Et}\left(\frac{4\beta^3}{R_2 K_1}\right) - (Q - P\tan\phi)\frac{2\beta^2\sin\phi}{Et}\left(\frac{1}{K_1}\right)$$

$$= -\frac{2\cdot 600\cdot 1975\;0.5\,(.85)}{30\cdot10^6\cdot 0.5} - \frac{M}{30\cdot10^6\;0.5}\left(\frac{4\cdot 651}{22.8\;0.96}\right) - (Q - 3310\cdot .578)\frac{2\cdot 15.2\;0.5}{30\,10^6\cdot 0.5}\left(\frac{1}{.96}\right)$$

$$= 10^{-6}(-670 - 7.98\,M - 5.22\,Q + 9980)$$

$$= 10^{-6}(-7.98\,M - 5.22\,Q + 9310)$$

CHAMBER SHELL

$$D = \frac{Et^3}{12(1-\nu^2)}$$

$$= \frac{30 \cdot 10^6 \cdot .65^3}{12(1-.3^2)}$$

$$= 0.744 \cdot 10^6$$

$$\lambda = \sqrt[4]{\frac{3(1-\nu^2)}{R^2 t^2}}$$

$$= \sqrt[4]{\frac{3(1-.3^2)}{11.75^2 \cdot .65^2}}$$

$$= .409$$

$$\lambda^2 = .1675$$

$$\lambda^3 = .0685$$

MEMBRANE STRESSES

$$\sigma_1' = \frac{P}{t}$$

$$= \frac{4310}{.65}$$

$$= 6620 \text{ PSI}$$

$$\sigma_2' = \frac{pR}{t}$$

$$= \frac{1400 \cdot 11''}{.65}$$

$$= 23700 \text{ PSI}$$

$$D_s = \frac{R^2}{Et}(\sigma_2 - \nu\sigma_1) + \frac{M}{2D\lambda^2} - \frac{Q}{2D\lambda^3}$$

$$= \frac{1975}{30 \cdot 10^6}(23700 - .3 \cdot 6620) + \frac{M}{2 \cdot 0.744 \cdot 10^6 \cdot .1675} - \frac{Q}{2 \cdot 0.744 \cdot 10^6 \cdot .0685}$$

$$= 10^{-6}(16300 + 8.7M - 21.2Q)$$

$$\theta_0 = \frac{M}{\lambda D} - \frac{Q}{2D\lambda^2}$$

$$= \frac{M}{.409 \cdot 0.744 \cdot 10^6} - \frac{Q}{2 \cdot 0.744 \cdot 10^6 \cdot .1675}$$

$$= 10^{-6}(7.1M - 8.7Q)$$

PREPARED D Y HSIEH
CHECKED
MODEL
REPORT NO.

SETTING $\delta_6 = \delta_5$, $\theta_6 = \theta_5$

$$10^{-6}(5.22\,M + 6.2\,Q + 6650) = 10^{-6}(8.1\,M - 21.2\,Q + 16300)$$

$$-2.88\,M + 27.4\,Q = 9650$$

$$10^{-6}(-7.98\,M - 5.22\,Q + 9310) = 10^{-6}(7.1\,M - 8.7\,Q)$$

$$15.08\,M - 3.48\,Q = 9310$$

$$3.48\,M - 8.905\,Q = 2150$$

$$26.317\,Q = 11800$$

$$Q = 447 \text{ LB/IN}$$

$$M = \frac{9310 + 3.48(447)}{15.08}$$

$$= 720 \text{ IN-LB/IN}$$

PREPARED P Y HSIEH
CHECKED
MODEL
REPORT NO.

UNCLASSIFIED

STRESSES IN CHAMBER SHELL

$\sigma_1 = \frac{P}{t} \mp \frac{6M}{t^2}$

$= \frac{3310}{0.5} \mp \frac{6(720)}{0.5^2}$

$= 6620 \mp 17300$

$= 23920$ PSI MAX INNER SURFACE

$\sigma_2 = \frac{pR}{t} - \frac{2Q}{t}\lambda\gamma + \frac{2M}{t}\lambda^2\gamma \mp \nu\frac{6M}{t^2}$

$= \frac{1007 \cdot 13.75}{0.5} - \frac{2(449)}{0.5} 0.409 \cdot 19.78 + \frac{2(720)}{0.5} 0.1675 \cdot 13.75 \mp 0.3(17300)$

$= 27700 - 14450 + 5500 \mp 5190$

$= 23940$ PSI MAX

STRESSES IN CONE

$\sigma_1 = \frac{P}{t\cos\phi} \mp \frac{6M}{t^2} + (Q - P\tan\phi)\frac{\cos\phi}{t}$

$= 7040 \mp 17300 + (449 - 3310 \cdot 0.978)\frac{.566}{.50}$

$= 7040 \mp 17300 - 2540$

$= 21800$ PSI MAX. INNER SURFACE

$\sigma_2 = \frac{pR}{t\cos\phi} + (Q - P\tan\phi)\frac{1}{t}\left(\frac{1}{K_1} + \frac{K_1 + K_2}{2}\right)\beta\sin\phi + \frac{M}{tR_2}\left(\frac{2\beta^2}{K_1}\right) \mp \nu\frac{6M}{t^2}$

$= 27400 - \frac{1467}{0.5}\left(\frac{1}{.96} + \frac{0.964 + 0.984}{2}\right)5.66 \cdot 0.5 + \frac{720}{0.5 \cdot 22.8}\left(\frac{2 \cdot 7.53}{.96}\right) \mp 0.3(17300)$

$= 27400 - 24700 + 9900 \mp 5190$

$= 17790$ PSI MAX.

27400 PSI MEMBRANE STRESS MAX $\quad$ $MS = \frac{135000}{27400} - 1 = 3.93$

UNCLASSIFIED

PREPARED P Y HSIEH
CHECKED
MODEL
REPORT NO.

UNCLASSIFIED

SECTION 5. THROAT

$p = 170 \cdot 2 = 340$ psi.

T = AMBIENT TEMP.

MAT'L. T-1 STEEL

$f_{tu} = 135000$ psi.
$f_{ty} = 100000$ psi.

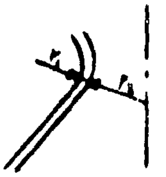

THROAT

$N_\phi = \frac{p r_2}{2}$

$\frac{N_\phi}{-r_1} + \frac{N_\theta}{r_2} = p$

$N_\theta = p r_2 \left(1 + \frac{r_2}{2 r_1}\right)$

$r_2 = 13.1$
$r_1 = 11.5$
$t = 0.50$

$$\sigma_1 = \frac{N_\phi}{t} = \frac{p r_2}{2 \cdot t} = \frac{340 \cdot 13.1}{2 \cdot 0.50} = 4450 \text{ psi}$$

$$\sigma_2 = \frac{N_\theta}{t} = \frac{p r_2}{t}\left(1 + \frac{r_2}{2 r_1}\right) = \frac{340 \cdot 13.1}{.50}\left(1 + \frac{13.1}{2 \cdot 11.5}\right) = 14000 \text{ psi.}$$

$$M.S. = \frac{135000}{14000} - 1 = 8.65$$

NOZZLE RADIUS 13.1 TO 26.2

CRITICAL COMPRESSIVE LOAD $= (.606)\, 2\pi E t^2 \cos^2\alpha$
$= .606 \cdot 2\pi \cdot 30 \cdot 10^6 \cdot 0.50^2 \cos^2 15°$
$= 26.8 \cdot 10^6$ LBS.

CRITICAL EXTERNAL PRESSURE $= \frac{0.92 E}{\frac{L}{r}\left(\frac{r}{t}\right)^{5/2}}$
$= \frac{.92 \cdot 30 \cdot 10^6}{\frac{20}{19.64}\left(\frac{19.64}{.38}\right)^{5/2}}$
$= 1120$ psi.

UNCLASSIFIED

PREPARED P Y HSIEH
CHECKED
MODEL
REPORT NO.

UNCLASSIFIED

SECTION 6.7. SUPPORT STRUCTURE

$p = 600$ psi

$T = 3720(20-r)^2 + 70$

MAT'L. T-1 STEEL $f_{tu} = 135000$ psi.
$f_{ty} = 100000$ psi

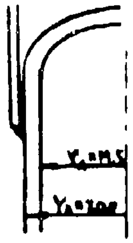

CHAMBER DISPLACEMENT

$$u = (1+\nu)\frac{\alpha}{r}\int_{r_i}^{r} Tr\,dr + C_1 r + \frac{C_2}{r}$$

$$\sigma_r = -\alpha E\frac{1}{r^2}\int_{r_i}^{r} Tr\,dr + \frac{E}{1-\nu^2}\left(C_1(1+\nu) - C_2(1-\nu)\frac{1}{r^2}\right]$$

$$\sigma_\theta = \alpha E\frac{1}{r^2}\int_{r_i}^{r} Tr\,dr - \alpha TE + \frac{E}{1-\nu^2}\left(C_1(1+\nu) + C_2(1-\nu)\frac{1}{r^2}\right)$$

AT $r = r_i$ $\sigma_r = -p_i$
$r = r_o$ $\sigma_r = -p_o$

FROM σ_r EQUATION

$$-p_i = \frac{E}{1-\nu^2}\left(C_1(1+\nu) - C_1(1-\nu)\frac{1}{r_i^2}\right]$$

$$-p_o = -\alpha E\frac{1}{r_o^2}\int_{r_i}^{r_o} Tr\,dr + \frac{E}{1-\nu^2}\left[C_1(1+\nu) - C_2(1-\nu)\frac{1}{r_o^2}\right]$$

$$-p_i\frac{1-\nu^2}{E} + C_2(1-\nu)\frac{1}{r_i^2} = -p_o\frac{1-\nu^2}{E} + \frac{\alpha(1-\nu^2)}{r_o^2}\int_{r_i}^{r_o} Tr\,dr + C_2(1-\nu)\frac{1}{r_o^2}$$

$$C_2(1-\nu)\left(\frac{1}{r_i^2} - \frac{1}{r_o^2}\right) = \frac{1-\nu^2}{E}(p_i - p_o) + \frac{\alpha(1-\nu^2)}{r_o^2}\int_{r_i}^{r_o} Tr\,dr$$

$$C_2\left(\frac{1}{r_i^2} - \frac{1}{r_o^2}\right) = \frac{1+\nu}{E}(p_i - p_o) + \frac{\alpha}{r_o^2}(1+\nu)\int_{r_i}^{r_o} Tr\,dr$$

$$C_2 = \frac{r_o^2 r_i^2(1+\nu)}{(r_o^2 - r_i^2)E}(p_i - p_o) + \frac{r_i^2\alpha}{r_o^2 - r_i^2}(1+\nu)\int_{r_i}^{r_o} Tr\,dr$$

USING $k = \frac{r_o}{r_i}$

$$C_2 = \frac{1+\nu}{E}\left[\frac{r_o^2}{k^2-1}(p_i - p_o) + \frac{r_i^2}{r_o^2 - r_i^2}E\alpha\int_{r_i}^{r_o} Tr\,dr\right]$$

$$C_1(1+\nu) = -p_i\frac{1-\nu^2}{E} + C_2(1-\nu)\frac{1}{r_i^2}$$

$$C_1 = -p_i\frac{1-\nu}{E} + \frac{1-\nu}{(1+\nu)r_i^2}\left(\frac{r_o^2 r_i^2(1+\nu)}{(r_o^2 - r_i^2)E}(p_i - p_o) + \frac{r_i^2\alpha}{r_o^2 - r_i^2}(1+\nu)\int_{r_i}^{r_o} Tr\,dr\right]$$

$$= -p_i\frac{1-\nu}{E} + \frac{(1-\nu)r_o^2}{(r_o^2 - r_i^2)E}(p_i - p_o) + \frac{(1-\nu)\alpha}{r_o^2 - r_i^2}\int_{r_i}^{r_o} Tr\,dr$$

UNCLASSIFIED

PREPARED P Y HSIEH
CHECKED
MODEL
REPORT NO.

$$= \frac{1-\nu}{E} p_i \left(\frac{r_i^2}{r_o^2-r_i^2} - 1 \right) - \frac{(1-\nu) r_o^2}{(r_o^2-r_i^2)E} p_o + \frac{(1-\nu)\alpha}{r_o^2-r_i^2} \int_{r_i}^{r_o} T r\,dr$$

$$= \frac{1-\nu}{E} \left(\frac{p_i}{k^2-1} - \frac{k^2 p_o}{k^2-1} + \frac{E\alpha}{r_o^2-r_i^2} \int_{r_i}^{r_o} T r\,dr \right)$$

$$\delta = (1+\nu)\frac{\alpha}{r}\int_{r_i}^{r} T r\,dr + \frac{(1-\nu)r}{E}\left[\frac{p_i}{k^2-1} - \frac{k^2 p_o}{k^2-1} + \frac{E\alpha}{r_o^2-r_i^2}\int_{r_i}^{r_o} T r\,dr \right]$$
$$+ \frac{1+\nu}{Er}\left[\frac{r_o^2}{k^2-1}(p_i - p_o) + \frac{r_i^2}{r_o^2-r_i^2} E\alpha \int_{r_i}^{r_o} T r\,dr \right]$$
$$= \frac{p_i}{k^2-1}\left[\frac{(1-\nu) r}{E} + \frac{(1+\nu) r_o^2}{E r} \right] - \frac{p_o}{k^2-1}\left[\frac{(1-\nu) r k^2}{E} + \frac{(1+\nu) r_o^2}{E r} \right]$$
$$+ \frac{\alpha r}{(r_o^2-r_i^2)}\left[(1-\nu) + (1+\nu)\frac{r_i^2}{r^2} \right]\int_{r_i}^{r_o} T r\,dr + (1+\nu)\frac{\alpha}{r}\int_{r_i}^{r} T r\,dr$$

FOR THIN SHELL & $p_o = 0$

$r_o \cong r_i$

$$k^2 - 1 = \frac{r_o^2 - r_i^2}{r_i^2} = \frac{(r_o + r_i)(r_o - r_i)}{r_i^2} \simeq \frac{2rt}{r^2} = \frac{2t}{r}$$

$$r_o^2 - r_i^2 \simeq 2rt$$

$$\delta = \frac{p_i r^2}{E t} + \frac{\alpha}{t}\int_{r_i}^{r_o} T r\,dr + (1+\nu)\frac{\alpha}{r}\int_{r_i}^{r} T r\,dr$$

$$\int_{r_i}^{r_o} T r\,dr = \int_{r_i}^{r_o} \left[3720(400 - 40r + r^2) + 70 \right] r\,dr$$
$$= \left[3720(400)\tfrac{1}{2} r^2 - 3720(40)\tfrac{1}{3} r^3 + 3720 \tfrac{1}{4} r^4 + 70 \tfrac{1}{2} r^2 \right]_{19.5}^{20}$$
$$= \left[(744035 - 49600 r + 930 r^2) r^2 \right]_{19.5}^{20}$$
$$= 3924$$

$$\delta_o = \frac{600 \cdot 20^2}{30 \cdot 10^6 \cdot 0.5} + \left[\frac{7.74 \cdot 10^{-6}}{0.5} + (1+0.3)\frac{7.74 \cdot 10^{-6}}{20} \right](3924)$$
$$= 10^{-6}(1600 + 62700)$$
$$= 10^{-6}(64300)$$

$$\delta_i = \frac{600 \cdot 19.5^2}{30 \cdot 10^6 \cdot 0.5} + \left[\frac{7.74 \cdot 10^{-6}}{0.5} \right](3924)$$
$$= 10^{-6}(1520 + 61800)$$
$$= 10^{-6}(63320)$$

PREPARED P Y HSIEH
CHECKED
MODEL
REPORT NO.

UNCLASSIFIED

SUPPORT SKIRT

$$D = \frac{Et^3}{12(1-\nu^2)}$$

$$= \frac{30\cdot10^6\ 0.33^3}{12(1-0.3^2)}$$

$$= 0.139\cdot10^6$$

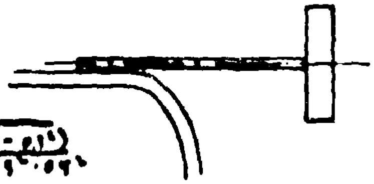

$$\lambda = \sqrt[4]{\frac{3(1-\nu^2)}{r^2 t^2}}$$

$$= \sqrt[4]{\frac{3(1-0.3^2)}{30.19^2\cdot0.33^2}}$$

$$= 0.47$$

$$\lambda_{CHAMBER} = \sqrt[4]{\frac{3(1-0.3^2)}{19.95^2\cdot0.5^2}}$$

$$= 0.409$$

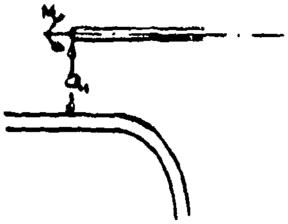

$$\lambda^2 = 0.221$$

$$\lambda^3 = 0.104$$

$\delta_{SKIRT} + \delta_{CHAMBER} = \delta_0$ AT WELD

$$-\frac{M_1}{2D\lambda^2} + \frac{Q_1}{2D\lambda^3} + \frac{Q_1(R^2\lambda)_{CHAMBER}}{2E\,t_{CHAMBER}} = 10^{-6}(64300)$$

$$-\frac{M_1}{2\cdot0.139\cdot10^6\cdot0.221} + \frac{Q_1}{2\cdot0.139\cdot10^6\cdot0.104} + \frac{Q_1\cdot19.93^2\cdot0.409}{2\cdot30\cdot10^6\cdot0.5} = 10^{-6}(64300)$$

$$10^{-6}(-16.3M_1 + 34.6Q_1 + 5.1Q_1) = 10^{-6}(64300)$$

$$-16.3M_1 + 39.9Q_1 = 64300$$

$\theta_{SKIRT} = 0$ AT WELD

$$-\frac{M_1}{\lambda D} + \frac{Q_1}{2D\lambda^2} = 0$$

$$-\frac{M_1}{.47\cdot0.139\cdot10^6} + \frac{Q_1}{2\cdot0.139\cdot10^6\cdot0.221} = 0$$

$$10^{-6}(-15.3M_1 + 16.3Q_1) = 0$$

$$16.3M_1 - 17.36Q_1 = 0$$

$$22.54Q_1 = 64300$$

$$Q_1 = 2850 \text{ LB/IN}$$

$$M_1 = \frac{16.3\cdot2850}{15.3} = 3030 \text{ IN-LB/IN}$$

UNCLASSIFIED

PREPARED P Y HSIEH
CHECKED
MODEL
REPORT NO.

UNCLASSIFIED

STRESSES IN SKIRT

$\lambda L = 0.47 \cdot 10 = 4.7$

MOMENT AND SHEAR FORCE EFFECTS ON SUPPORT RING END NOT EFFECTING THIS END

$$\sigma_1 = \pm \frac{6M_1}{t^2} - \frac{P}{t}$$

$$= \pm \frac{6(3030)}{.37^2} - \frac{3950}{0.37}$$

$$= \pm 133000 - 10700$$

$$= +122300 \text{ psi OUTER SURFACE}$$

$$-143700 \text{ psi INNER SURFACE}$$

(APPROX −135000 IF 0.38 t USED)

$$M.S. = \frac{135000}{135000} - 1 = 0$$

$$\sigma_2 = \frac{2Q_1}{t}\lambda r - \frac{2M_1}{t}\lambda^2 r \pm \nu \frac{6M}{t^2}$$

$$= \frac{2 \cdot 2850}{.37} 0.47 \; 20.19 - \frac{2 \cdot 3030}{.37} 0.221 \cdot 20.19 \pm 0.3(133000)$$

$$= 146000 - 73000 \pm 40000$$

$$= 113000 \text{ psi MAX}$$

STRESSES IN CHAMBER

$$\sigma_1 \text{ MAX} = -\frac{3Q_1}{2(\lambda t)t^2}$$

$$= -\frac{3 \cdot 2850}{2 \cdot 0.409 \cdot 0.5^2}$$

$$= -41800 \text{ psi}$$

$$\sigma_2 \text{ MAX} = -\frac{Q_1 R \lambda}{2t}$$

$$= -\frac{2850 \cdot 19.95 \cdot 0.409}{2 \cdot 0.5}$$

$$= -23000 \text{ psi.}$$

UNCLASSIFIED

PREPARED P Y HSIEH

CHECKED

MODEL

REPORT NO.

UNCLASSIFIED

$P = 250{,}000 \cdot 2 / 2\pi \cdot 20.19$
$= 3950$ LB/IN

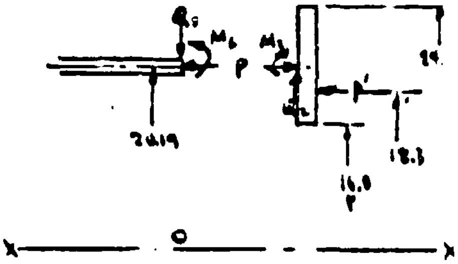

RING

$A = 1.0 \cdot 8 = 8 \text{ in}^2$

$I_y = \frac{1}{12} 8.0 \cdot 1.0^3 = 0.66 \text{ in}^4$

$M_T = 3950 (20.19 - 18.3) + M_2 + 0.5\,Q_2$
$= 7460 + M_2 + 0.5\,Q_2$

$\theta_A = \frac{M_T r_c^2}{E I_y}$

$= \frac{20.19^2}{30 \cdot 10^6 \cdot 0.66} (7460 + M_2 + 0.5\,Q_2)$

$= 10^{-6} (153800 + 20.6\,M_2 + 10.3\,Q_2)$

$\delta_A = \frac{Q_2 r^2}{AE} + 0.5\,\theta_A$

$= \frac{Q_2 \cdot 20.19^2}{8 \cdot 30 \cdot 10^6} + 10^{-6} (76900 + 10.3\,M_2 + 5.15\,Q_2)$

$= 10^{-6} (76900 + 103\,M_2 + 6.85\,Q_2)$

$\theta_A = 10^{-6} (153800 + 20.6\,M_2 + 10.3\,Q_2) = 10^{-6} (-15.3\,M_2 + 16.3\,Q_2)$

$35.9\,M_2 - 6.0\,Q_2 = -153{,}800$

$\delta_A = 10^{-6} (76900 + 103\,M_2 + 6.85\,Q_2) = 10^{-6} (16.3\,M_2 - 34.6\,Q_2)$

$-6.0\,M_2 + 41.45\,Q_2 = -76{,}900$

$-35.9\,M_2 + 248\,Q_2 = -460{,}000$

$242\,Q_2 = -613{,}800$

$Q_2 = -2540$ LB/IN

$M_2 = \frac{-153{,}800 + 6(-2540)}{35.9} = -4700$ IN·LB/IN

UNCLASSIFIED

PREPARED P Y HSIEH
CHECKED
MODEL
REPORT NO.

UNCLASSIFIED

INCLUDING THE MATING SUPPORT RING FOR STIFFNESS

$P = 250000 \cdot 2 / 2\pi \cdot 20.19$
$= 3950$ LB/IN

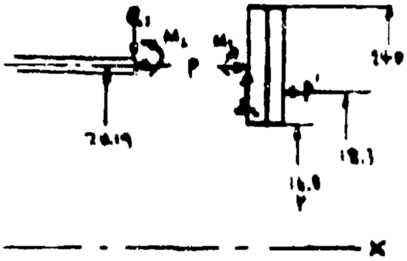

RING
$A = 2.0 \cdot 8 = 16$ IN^2
$I_y = \frac{1}{12} 8.0 \; 2.0^3 = 5.33$ IN^4

$M_T = 3950(20.19 - 18.3) + M_2 + 1.0\,Q_2$
$= 7460 + M_2 + 1.0\,Q_2$

$\theta_A = \frac{M_T r_m^2}{E I_y}$
$= \frac{20.19^2}{30 \cdot 10^6 \cdot 5.33}(7460 + M_2 + 1.0\,Q_2)$
$= 10^{-6}(19000 + 2.54 M_2 + 2.54 Q_2)$

$\delta_A = \frac{Q_2 r^2}{A E} + 1.0\,\theta_A$
$= \frac{Q_2 \cdot 20.19^2}{16 \cdot 30 \cdot 10^6} + 10^{-6}(19000 + 2.54 M_2 + 2.54 Q_2)$
$= 10^{-6}(19000 + 2.54 M_2 + 3.39 Q_2)$

$\theta_A = 10^{-6}(19000 + 2.54 M_2 + 2.54 Q_2) = 10^{-6}(-15.3 M_2 + 16.3 Q_2)$
$17.84 M_2 - 13.76 Q_2 = -19000$

$\delta_A = 10^{-6}(19000 + 2.54 M_2 + 3.39 Q_2) = 10^{-6}(16.3 M_2 - 34.6 Q_2)$
$-13.76 M_2 + 37.99 Q_2 = -19000$
$-17.84 M_2 + 49.2 Q_2 = -24600$

$35.44 Q_2 = -43600$
$Q_2 = -1230$ LB/IN
$M_2 = \frac{-19000 + 13.76(-1230)}{17.84} = -2010$ IN·LB/IN

UNCLASSIFIED

PREPARED P Y HSIEH
REPORT NO.
CHECKED
MODEL

STRESSES IN SUPPORT SKIRT

$$\sigma_1 = \mp \frac{6M}{t^2} - \frac{P}{t}$$

$$= \mp \frac{6(-2010)}{.37^2} - \frac{3950}{.37}$$

$$= \pm 88000 - 10700$$

$$= -98700 \text{ PSI}$$ INNER SURFACE MAX.

$$M.S. = \frac{134000}{98700} - 1 = 0.35$$

$$\sigma_2 = \frac{2M}{t} \lambda^2 r - \frac{2Q}{t} \lambda r \mp \nu \frac{6M}{t^2}$$

$$= \frac{2(-2010)}{.37} 2.21 \cdot 20.19 - \frac{2(-1330)}{.37} 0.47 \cdot 20.19 \pm .3(88000)$$

$$= \cdot 50000 + -3000 \pm 26400$$

$$= 39400 \text{ PSI MAX.}$$

STRESSES IN RING

$$M_r = 7660 - 2010 - 1330$$

$$= 4320$$

$$\sigma_b = \frac{M_r r c}{I_y}$$

$$= \frac{4320 \cdot 20.19 \; 1.0}{5.44}$$

$$= 16000 \text{ PSI}$$

$$\sigma_h = \frac{\Delta P r}{2A}$$

$$= \frac{-1330 \; 20.19}{2 \cdot 16}$$

$$= -780 \text{ PSI}$$

$$\sigma_{TOTAL} = 16000 - 780$$

$$= 15220 \text{ PSI}$$

PREPARED
CHECKED
MODEL

UNCLASSIFIED

SECTION 8. PINTLE TIP

$p = 600$ psi

T = AMBIENT TEMP

MAT'L. A-212-B STEEL
$f_{tu} = 70000$ psi.
$f_{ty} = 62000$ psi.

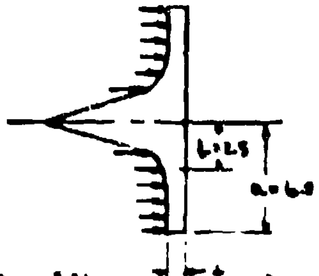

AT b, FOR 1.00 t

$$\text{MAX. } \sigma_r = \frac{3p}{4t^2}\left[\frac{4a^2b^2(m+1)\log\frac{a}{b} - a^4(3m+1) + a^2b^2(5m-1)}{a^2(m+1)+b^2(m-1)} - b^2\right]$$

$$= \frac{3\cdot 600}{4\cdot 1^2}\left[\frac{4\cdot 6^2\cdot 2.5^2(3.3+1)\log 6/2.5 - 6^4(3\cdot 3.3+1) + 6^2\cdot 2.5^2(5\cdot 3.3+1)}{6^2(3.3+1)+2.5^2(3.3-1)} - 2.5^2\right]$$

$$= 450\left[\frac{3400-14100+3490}{155+14.4} - 6.25\right]$$

$$= 450\left[-40-6.25\right]$$

$= 20800$ psi NONE RIGID EDGE

$$\sigma_r = \frac{3p}{4t^2}\left[(a^2+b^2) - \frac{4a^2b^2}{a^2-b^2}\left(\log\frac{a}{b}\right)\right]$$

$$= 450\left[(6^2+2.5^2) - \frac{4\cdot 6^2\cdot 2.5^2}{6^2-2.5^2}\log\frac{6}{2.5}\right]$$

$$= 450\left[42.25 - 26.5\right]$$

$= +7100$ psi RIGID EDGE

AT a, FOR 1.00 t

$\sigma_r = 0$ NONE RIGID EDGE

$$\text{MIN. } \sigma_r = \frac{3p}{4t^2}\left[(a^2-3b^2) + \frac{4b^4}{a^2-b^2}\left(\log\frac{a}{b}\right)\right]$$

$$= 450\left[(6^2-3\cdot 2.5^2) + \frac{4\cdot 2.5^4}{6^2-2.5^2}\log\frac{6}{2.5}\right]$$

$$= 450\left[17.25 + 4.6\right]$$

$= 9850$ psi RIGID EDGE

UNCLASSIFIED

REPORT NO.

PREPARED

CHECKED

MODEL

UNCLASSIFIED

PINTLE TIP, t REDUCED TO 0.75 IN.

P = 600 PSI

T = AMBIENT TEMP

MAT'L. A-181-II STEEL

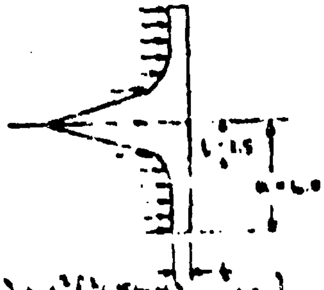

AT b, FOR $\frac{0.75}{\cancel{1.00}}$ t

$$\text{MAX. } \sigma_r = \frac{3p}{4t^2}\left[\frac{4a^2b^2(m+1)\log\frac{a}{b} - a^4(3m-1) + a^2b^2(5m+1)}{a^2(m+1) + b^2(m-1)} - b^2\right]$$

$$= \frac{3\cdot 600}{4\cdot 0.75^2}\left[\frac{4\cdot 6^2\cdot 2.5^2(3.33+1)\log 6/2.5 - 6^4(3\cdot 3.33-1) + 6^2\cdot 2.5^2(5\cdot 3.33+1)}{6^2(3.33+1) + 2.5^2(3.33-1)} - 2.5^2\right]$$

$$= \frac{800}{\cancel{450}}\left[\frac{\;-\;+2242}{155+14.6} - 6.25\right]$$

$$= \frac{800}{\cancel{450}}\left[-40 - 6.25\right]$$

= −37000 ~~[illegible]~~ psi NONE RIGID EDGE

$$\sigma_r = \frac{3p}{4t^2}\left[(a^2+b^2) - \frac{4a^2b^2}{a^2-b^2}\left(\log\frac{a}{b}\right)\right]$$

$$= \frac{800}{\cancel{450}}\left[(6^2+2.5^2) - \frac{4\cdot 6^2\cdot 2.5^2}{6^2-2.5^2}\log\frac{6}{2.5}\right]$$

$$= \frac{800}{\cancel{450}}\left[42.25 - 26.9\right]$$

= +12600 ~~[illegible]~~ PSI RIGID EDGE

$$M.S. = \frac{78000}{.8(38000+12600)} - 1$$
$= 1.96$

AT a, FOR $\frac{0.75}{\cancel{1.00}}$ t

$\sigma_r = 0$ . . . RIGID EDGE

$$\text{MAX. } \sigma_r = \frac{3p}{4t^2}\left[(a^2-3b^2) + \frac{4b^4}{a^2-b^2}\left(\log\frac{a}{b}\right)\right]$$

$$= \frac{800}{\cancel{450}}\left[(6^2-3\cdot 2.5^2) + \frac{4\cdot 2.5^4}{6^2-2.5^2}\log\frac{6}{2.5}\right]$$

$$= \frac{800}{\cancel{450}}\left[17.25 + 4.6\right]$$

= 17500 ~~[illegible]~~ psi RIGID EDGE

UNCLASSIFIED

SYSTEMS 1101 REV. [illegible]

TRW
... PARK • REDONDO BEACH, CALIFORNIA

PREPARED P Y HSIEH
CHECKED
MODEL
REPORT NO.

UNCLASSIFIED

SECTION 15. PINTLE SHELL

$P_{ext} = 600$ psi.

T = AMBIENT TEMP.

MAT'L. A106-B STEEL

$f_{tu} = 60000$ psi
$f_{ty} = 36000$ psi.

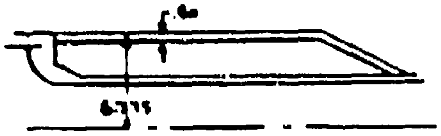

REFER TO
ELASTIC STABILITY OF THIN SHELL
BY PAUL SEIDE

$$Z = \sqrt{1-\nu^2}\,\frac{L^2}{rt}$$
$$= \sqrt{1-0.3^2}\,\frac{20^2}{6.17 \cdot 0.4}$$
$$= 162 > 100$$

CRITICAL BUCKLING PRESSURE $P_{cr} = \dfrac{0.92E}{\frac{L}{r}\left(\frac{r}{t}\right)^{5/2}} = \dfrac{0.92 \cdot 30 \cdot 10^6}{\frac{20}{6.17}\left(\frac{6.17}{0.4}\right)^{5/2}} = 9100$ psi

$$\sigma_1 = -\frac{pr}{2t}$$
$$= -\frac{600 \cdot 6.17}{2 \cdot 0.4}$$
$$= -4630 \text{ psi.}$$

$$\sigma_2 = -9260 \text{ psi}$$

DISCONTINUITY STRESS
REFER TO PRESSURE VESSEL & PIPING DESIGN, ASME COLLECTED PAPERS, P. 258

$$\frac{d}{t} = \frac{12.34}{.40} = 31$$

$$\frac{T}{t} = \frac{1.5}{.40} = 3.75$$

MAX. STRESS RATIO = 3.26

MAX. STRESS $\sigma = $ [illegible]$\left(-\frac{pr}{t}\right)$
= 3[illegible]260)
= −30[illegible] psi.

$$\text{M.S.} = \frac{60000}{30000} - 1 = 1.0$$

UNCLASSIFIED

PREPARED P Y Wong
CHECKED
MODEL
REPORT NO.

[redacted] UNCLASSIFIED

THREAD

SHEAR AREA $= \pi \cdot 117 \cdot 0.4$
$= 147 \text{ IN}^2$

FORCE $= \pi \cdot 6^2 \cdot 600$
$= 67800$ LBS

SHEAR STRESS $\sigma_s = \dfrac{67800}{147}$
$= 460$ psi.

[redacted] UNCLASSIFIED

Unclassified [redacted]
Security C [redacted]

[redacted]

DOCUMENT CONTROL DATA - R & D

(Security classification of title, body of abstract and indexing annotation must be entered when the overall report is classified)

1. ORIGINATING ACTIVITY (Corporate author)
TRW Systems Group
One Space Park
Redondo Beach, California

2a. REPORT SECURITY CLASSIFICATION
[redacted] l

2b. GROUP
Group 4

3. REPORT TITLE
Injector/Chamber Scaling Feasibility F[illegible] J),
Design and Short Duration Testing
Volume 1

4. DESCRIPTIVE NOTES (Type of report and inclusive dates)
Final Report, Covering Period of 8 July 1968 to 1 September 1969

5. AUTHOR(S) (First name, middle initial, last name)
Voorhees, G. A., Jr.
Morton, B. G.

6. REPORT DATE
July 1970

7a. TOTAL NO. OF PAGES
212

7b. NO. OF REFS
7

8a. CONTRACT OR GRANT NO.
F04611-68-C-0085

b. PROJECT NO.

c.

d.

9a. ORIGINATOR'S REPORT NUMBER(S)
Vol I - TRW 11199-6006-R8-00

9b. OTHER REPORT NO(S) (Any other numbers that may be assigned this report)
AFRPL-TR-86-Vol I

10. DISTRIBUTION STATEMENT
[redacted]

11. SUPPLEMENTARY NOTES

12. SPONSORING MILITARY ACTIVITY
Air Force Rocket Propulsion Laboratory
Air Force Systems Command, USAF
Edwards CA 93523

13. ABSTRACT

(U) The results of the Task I phase of an injector/chamber scaling feasibility program are presented. During the fourteen month program, covering the period from 8 July 1968 to 1 September 1969, the feasibility of scaling the TRW Systems coaxial injector design to the 250,000 lb_f thrust level was demonstrated. A total of forty-one injector development test firings were made using eight injector configurations. Three chamber lengths were evaluated with a single injector configuration. Satisfactory performance was achieved with the longest chamber tested. Injector dynamic stability was demonstrated in numerous stability rating tests employing both pulse-guns and non-directional bombs. Three demonstration injectors were designed and fabricated and two of these injectors were subjected to check-out firings in preparation for Task II testing.

[redacted]

[redacted]

DD FORM 1 NOV 65 1473

Unclassified
Security Classification

[redacted] Security Classification

14. KEY WORDS	LINK A		LINK B		LINK C	
	ROLE	WT	ROLE	WT	ROLE	WT
Low-[redacted]r						
Performance						
Stability						
N_2O_4/UDMH						
Scaling						
250,000 lb_f						
Low-Cost Thrust Chamber						
Ablative Liners						
Silica-Phenolic Ablatives						
Silicone Rubber Ablators						

[redacted]

[redacted]sified
[redacted]rity Classification